UNIVERSITY OF CALIFORNIA

Los Angeles

Role of Flagellar Motility in *Trypanosoma brucei* Pathogenesis

A dissertation submitted in partial satisfaction of the requirements for the degree Doctor of Philosophy in Microbiology, Immunology and Molecular Genetics

By

Neville Kielau Kisalu

2013

ABSTRACT OF THE DISSERTATION

Role of Flagellar Motility in *Trypanosoma brucei* Pathogenesis

By

Neville Kielau Kisalu

Doctor of Philosophy in Microbiology, Immunology, and Molecular Genetics

University of California, Los Angeles, 2013

Professor Kent L. Hill, Chair

The flagellum of *Trypanosoma brucei* is an essential and multifunctional organelle that drives parasite motility and is receiving increased attention as a potential drug target. Parasite motility is suspected to contribute to infection and disease pathogenesis in the mammalian host. However, it has not been possible to test this hypothesis owing to lack of motility mutants that are viable in the bloodstream life cycle stage that infects the mammalian host. In the first part of my dissertation we identified a viable bloodstream-form motility mutant in 427-derived *T. brucei* and by adapting published approaches we set up mouse infection models of African trypanosomiasis. To assess the impact of trypanosome motility on infection in mice we these mutants in a mouse infection model and showed that disrupting parasite motility has no

discernible effect on *T. brucei* bloodstream infection. This presents the first ever investigation of the influence of parasite motility on infection of the mammalian host. Mutant cells used were derived from the laboratory-adapted strain 427-BSSM that causes an acute infection that progress rapidly in mice. This quick disease progression limits any reliable assessment of the CNS penetration, which commonly takes more than 14 days. To allow direct investigation of the requirement of parasite motility in the central nervous system (CNS) invasion, we have generated motility mutants in *T. brucei* strains that cause chronic infection in mice. Identification of motility mutants in pleomorphic BSF *T. brucei* that causes chronic infection will now make it possible for the first time to test if parasite motility is required for CNS penetration.

Traditionally, assessment of *T. brucei* infection is based upon examining parasitemia in blood and limited use of histochemistry to determine parasite presence in chemically-treated tissues. We have developed an advanced live-cell imaging approach using fluorescent *T. brucei* that will facilitate detailed dynamic studies of infection. This system enabled visualization of *T. brucei ex vivo* in mouse tissues as well as *in vivo* in whole live zebrafish embryos. Further validation of mCherry parasites at a microscale level revealed trypanosomes at single-cell resolution in *ex vivo* mouse tissues and in blood vessels of live fish. Hence, these systems have the potential for uncovering novel features of host-parasite interactions that could lead to drug, vaccine and diagnostics development, all of which is expected to ameliorate patient management in sleeping sickness.

A major roadblock to the study of the flagellum is a lack of facile methods for systematic mutational analysis of flagellar genes. We recently established systems for structure-function analysis of proteins in *T. brucei*, which has emerged as an excellent model to study the

eukaryotic flagellum. Several flagellar proteins have been identified but there is scant information on molecular mechanisms underlying these proteins functions, individually or collectively. For instance, key amino acids and domains required for these proteins are for the most part unknown. To exploit the flagellum as a drug target it is crucial that we deepen understanding of molecular mechanisms of flagellum protein function. To start bridging this gap, we applied our structure-function system to define amino acids required for IFT88 and trypanin protein function in flagellum assembly and motility. Our studies tested amino acids that correspond to IFT88 mutations observed in human patients with defective cilia and showed which of these mutations are loss of function mutations versus polymorphisms. We have also uncovered key domains essential for the assembly and function of the dynein regulatory protein trypanin.

Altogether, these investigations broadly contribute to understanding *T. brucei* pathogenesis mechanisms and expand our knowledge of flagellum motility functions in trypanosomes, which are directly applicable to other flagellated protozoan parasites. In humans, the flagellum, also called a cilium, is required for normal development and physiology and genetic changes in flagellar genes cause many human heritable diseases. Thus, our studies are also relevant to eukaryotic cell biology in connection to human health and disease.

The dissertation of Neville Kielau Kisalu is approved

_____
Peter J. Bradley, Committee Member

_____
Patricia J. Johnson, Committee Member

_____
Shimon Weiss, Committee Member

_____
Kent L. Hill, Committee Chair

University of California, Los Angeles

2013

DEDICATION

To

my loving and supporting wife Jeanne Kisalu

my lovely children Sion, David, Marie-Grace, Sharron-Rose, and Thamar

my mother Marie Mengi

my late father Jean Nlombi

my brother Emmanuel Toko

I dedicate this dissertation to you.

TABLE OF CONTENTS

LIST OF FIGURES AND TABLES

Chapter 1

Chapter 2

Chapter 3

Chapter 4

Chapter 5

Chapter 6

Chapter 7

Appendix 1

Appendix 2

ACKNOWLEDGMENTS

First and foremost my deepest appreciation is for my Supervisor and Committee Chair Professor Kent L. Hill, for overseeing the research described in this dissertation from the beginning to the end. Not only has Dr. Hill shared insights about the needs to develop a strategy to fight African sleeping sickness, but also helped me define my academic goals and provided the necessary support to complete my research in a timely manner. I would like to also thank the other members of my dissertation committee: Professor Peter J. Bradley, Professor Patricia J. Johnson and Professor Shimon Weiss.

I extend my gratefulness to the following experts for their comments and advice: Dr. Katherine Ralston provided technical assistance in generating the *T. brucei* bloodstream form motility mutants; Professor Shimon Weiss and Dr. Laurent Bentolila shared their mouse and fish imaging expertise; Gerasimos Langousis assisted me with the mouse infections and generation of the fluorescent mCherry *T. brucei*; Dr. Michelle Shimogawa and Dr. Josh Beck critically reviewed and provided valuable comments for chapters 4, 6, and 7 and chapter 5 respectively. I am particularly indebted to Dr. John Mokili for his continual support and mentorship. Dr. Anne W. Rimoin and Dr. Barney S. Graham have been behind the scenes providing invaluable support over the years leading to and throughout my Ph.D. studies.

I thank Oxford University Press, Annual Review of Microbiology and Elsevier for permission to reproduce Figures 1, 3, 4, 5, and 6 displayed in Chapter 1. I am also grateful to the United States Proceedings of the National Academy of Sciences and American Society for Microbiology for permission to include my previously published papers (Proc Natl Acad Sci

USA. 106(46): p.19322-7 and Eukaryotic Cell. 10(7): p. 884-94) as part of this dissertation (Appendices 1 and 2).

Financial support for the research undertaken for this dissertation was supplied by grants to Professor Kent L. Hill from the Burroughs Wellcome Fund and the National Institutes of Health (NIH-NIAID, grant AI052348) as well as by my awards from the Shapiro Fellowship (2010-11) and a UCLA Graduate Division Dissertation Year Fellowship (2012-2013).

VITA

Education

University of California, Los Angeles (UCLA) 2007 - Present
PhD Candidate, Microbiology, Immunology, and Molecular Genetics, Expected by 10/2013

Institut Superieur des Techniques Medicales, University of Kinshasa, the Democratic Republic of the Congo
B.S, Biological Sciences-Medical Laboratory Technology, 2005

Professional Experience

07/2012	Teaching Assistant, "Biology of Parasitism" Summer Research Course Marine Biological Laboratory, Woods Hole, MA
2008- 2010	Teaching Assistant, Department of Microbiology, Immunology, and Molecular Genetics, UCLA, Los Angeles, CA.
09/2004-08/2007:	Monkeypox Project, University of North Carolina (UNC)-Democratic Republic of Congo (DRC) Program and Kinshasa School of Public Health, Kinshasa, D.R. Congo Project Manager
08/2006-08/2007:	Viral Pathogenesis Laboratory, Vaccine Research Center, National Institutes of Health (NIH), Bethesda, MD Consultant Scientist
07/2003-11/2003	Vaccine Research Center, NIH, Bethesda, MD Visiting Scientist
11/2003-12/2003:	Los Alamos National Laboratory, Los Alamos, NM Visiting Scientist
01/2002-02/2002:	Institute of Tropical Medicine, Antwerp, Belgium. Visiting Scientist
07/1989-08/2004:	Congo AIDS Program (ex. Projet SIDA), Kinshasa, the Democratic Republic of the Congo Scientist

Honors, Awards, and Fellowships

2012-2013	Dissertation Year Fellowship, UCLA Graduate Division, UCLA, Los Angeles, CA
2012	Travel Grant, Biology of Host-Parasite Interactions, Gordon Research Conferences, Newport, RI
2010-2011	Shapiro Fellowship, College of Letters and Science, UCLA

2010	Burroughs Wellcome Fund Tuition Scholarship "*Biology of Parasitism*" Research Course Scholarship, Marine Biological Laboratory, Woods Hole, MA (2010)
2010	Travel Award, Graduate Committee, Department of Microbiology, Immunology, and Molecular Genetics, UCLA

Other achievements

2013	Invited Speaker Vaccine Research Center, National Institute for Allergies and Infectious Diseases, National Institutes of **Error! Reference source not found.** Bethesda, MD
2008	"*Planet In Peril*" documentary with CNN icons Anderson Cooper and Sanjay Gupta, Kinshasa, Democratic Republic of the Congo

Publications

1. **Neville K. Kisalu,** Gerasimos Langousis, Laurent A. Bentolila, Katherine S. Ralston, Shimon Weiss, and Kent L. Hill. *Mouse infection and pathogenesis by Trypanosoma brucei motility mutants* (Submitted).

2. Thomassen, H. A., Fuller, T., Asefi-Najafabady, S., Shiplacoff, J. A., Mulembakani, P. M., Blumberg, S., Johnston, S. C., **Kisalu, N. K.**, et al. (2013), *Pathogen-host associations and predicted range shifts of human monkeypox in response to climate change in central Africa.* PLoS One **8**(7): e66071.

3. Katherine S. Ralston, **Neville K. Kisalu** and Kent L. Hill (2011), *Structure-Function Analysis of Dynein Light Chain 1 Identifies Viable Motility Mutants in Bloodstream-Form Trypanosoma brucei.* Eukaryotic Cell. 10(7): p. 884-94.

4. Fuller, T., Thomassen H.A, Mulembakani P.M, Sara C. Johnston S.C., **Kisalu N.K**, et al., (2010), *Using Remote Sensing to Map the Risk of Human Monkeypox Virus in the Congo Basin.* Ecohealth 8, 14–25.

5. Rimoin, A.W., Mulembakani P.M., Johnston S., Smith, J.O., **Kisalu, N.K.**, et al. (2010), *Major increase in human monkeypox incidence 30 years after smallpox vaccination campaigns cease in the Democratic Republic of Congo*. Proc Natl Acad Sci USA. v107, p16262-16267.

6. Jose A. Rodríguez, Miguel A. Lopez, Michelle C. Thayer, Yunzhe Zhao, Michael Oberholzer, Donald D. Chang, **Neville K. Kisalu**, Manuel L. Penichet, Gustavo Helguera, Robijn Bruinsma, Kent L. Hill, and Jianwei Miao (2009), *Propulsion of African trypanosomes is driven by bihelical waves with alternating chirality separated by kinks.* Proc Natl Acad Sci USA. 106(46): p.19322-7.

7. Rimoin, A. W., **Kisalu, N**., Kebela-Ilunga, B., Mukaba, T., Wright, L. L., Formenty, P., Wolfe, N. D., Shongo, R. L., Tshioko, F., Okitolonda, E., Muyembe, J. J., Ryder, R. W., and Meyer, H. (2007) *Endemic human monkeypox, Democratic Republic of Congo*, 2001-2004. *Emerg Infect Dis* v13, p934-937.

8. **Neville K. Kisalu** et al. "Live-cell imaging of *Trypanosoma brucei* in ex vivo mouse tissues and in live zebrafish." (In Preparation).

9. **Neville K. Kisalu** et al. "Identification of a residue required for IFT88 function in *Trypanosoma brucei*." (In Preparation).

Chapter 1

Introduction

African sleeping sickness

Epidemiology, risk factors, prevention and control

African trypanosomes including *Trypanosoma brucei* and related species, are kinetoplastid protozoan parasites responsible for the neglected disease African sleeping sickness, also known as human African trypanosomiasis (HAT) and related diseases in domestic and wild animals. These parasites cause important human mortality and hinder economic development in sub-Saharan Africa (Figure 1). About 60 million people are at risk of HAT across sub-Saharan Africa and approximately 10,000 cases are reported annually, although this number is likely a significant underestimate of the total cases [Simarro et al., 2008]. Two subspecies of *T. brucei,* found in different geographic regions of Africa, cause sleeping sickness. *T. b. gambiense*, the causal agent of West African sleeping sickness, is mainly found in central Africa and in some zones of West Africa and is the source of the majority of sleeping sickness cases in Africa. *T. b. rhodesiense* causes East African sleeping sickness. This parasite is found in focal locations of eastern and southeastern Africa. Which specific subspecies is involved influences clinical manifestations of the disease, although both are fatal if untreated. *T. b. gambiense* causes a chronic disease, lasting months to a year or more, while *T. b. rhodesiense* causes a more acute form of the disease that progresses rapidly, generally within several weeks, to lethal outcome [Jelinek et al., 2002; Blum et al., 2006]. For *T. b. rhodesiense*, domestic and wild animals constitute the principal infection reservoir and are a major factor in the transmission cycle, while *T. b. gambiense* is spread almost exclusively through human-tsetse-human transmission. On average one sleeping sickness case per year is diagnosed in the US, mostly in travelers who were

on safari in East Africa [Moore et al., 2002; Urech et al., 2011]. Trypanosome infection is transmitted by the bite of the tsetse fly (*Glossina* species), but other modes of transmission including blood transfusion, congenital and sexual [Rocha et al., 2004] are theoretically possible. With no vaccine, control of sleeping sickness rests soley on diagnosis and treatment of infected patients as well as on vector control and reservoir management.

Disease

Trypanosome infection of a mammalian host proceeds in several steps. Following transmission *via* the bite of an infected tsetse fly, the parasites reside and replicate extracellularly in the bloodstream and tissue fluids of their mammalian host despite being regularly exposed to the host immune system. *T. brucei* has evolved several sophiscated strategies it uses to escape the host immune system and cause disease. For instance, antigenic variation of the cell surface coat and active removal of host immunoglobulin attached to the parasite surface allows the trypanosome population to escape immune killing and remain in the bloodstream limitlessly [Barry and McCulloch 2001; Borst 2002; Pays 2005].

Bloodstream infection constitutes the first stage of sleeping sickness and is clinically characterized by as flu-like symptoms with intermittent waves of fever and emergence of lymphadenopathy [Stich et al., 2002; Rodgers 2010]. After several weeks *T. brucei* traverses the blood vessel endothelium and penetrates the central nervous system (CNS) [Stich et al., 2002; Rodgers 2010], introducing the second stage the disease. During this stage, patients have chronic meningoencephalitis accompanied by headaches and neurological disruptions that

unyieldingly perturb sleep. Leaving the disease untreated leads to coma and death [Stich et al., 2002; Rodgers 2010]. Although African sleeping sickness has been recognized for centuries several features of disease pathogenesis, such as the cause of death, are not understood.

Laboratory diagnosis

Sleeping sickness diagnosis and stage determination are difficult and should not be interpreted based on clinical signs [Lejon and Buscher 2005]. Since clinical manifestations of trypanosome infection are insufficiently specific, the diagnosis relies mainly on microscopy examination of body fluid or tissue in order to identify the parasite. Trypanosomes can be found in blood, lymph node aspirate, or biopsy of a chancre. Accurate diagnosis is based on microscopic observation of the parasite (Figure 2). Although highly specific, microscopic examination has low sensitivity. Serological tests such as the card agglutination test for trypanosomiasis (CATT) [Magnus et al., 1978; Vervoort et al., 1978; Lejon et al., 2002; Buscher et al., 2013] exist but these tests are mostly used for screening purposes and are prone to false positive results [Truc et al., 2002]. To compensate the limitations of microscopic examination and serological methods, molecular tests such as PCR have been introduced but these methods have their own drawbacks including lack of reproducibility due to the genome sequence used as probe, uncertain specificity, limited sensitivity, expensive, and require extensive training [Chappuis et al., 2005; Koffi et al., 2006; Deborggraeve and Buscher 2010; Jamonneau et al., 2010]. As such, the diagnosis is frequently missed initially leading hospitalization of some patients in psychiatric clinics. Moreover, diagnosis outside endemic regions is repeatedly missed or delayed in Africans resulting in cases with advanced stages of the disease. Because the choice

of drugs for treatment is critically dependent on correct disease staging, it is recommended that all patients diagnosed with sleeping sickness undergo a cerebrospinal fluid (CSF) examination to determine whether parasites have invaded the central nervous system. A white blood cell count of more than 5 per microliter and an increased protein concentration in CSF suggests central nervous system (CNS) involvement according to WHO recommendations. Given the limited means for diagnosis and in particular, for staging, improved diagnostic approaches and paradigms are sorely needed for human trypanosomiasis management.

Treatment

The choice of drugs used to treat sleeping sickness depends on the stage [Mumba Ngoyi et al., 2013] of disease and type of infection. Pentamidine (introduced in 1939) is the pillar drug recommended for first stage of disease (bloodstream infection) by *T. b. gambiense*, whereas Suramin (introduced in 1916) is used for *T. b rhodesiense* disease [Brun et al., 2010]. Early diagnosis, which is often missed because of non- specificity of the initial symptoms, is critical for the success of treatment in stage 1 of the disease. Stages 2 of the disease is difficult to manage since existing drugs lack ease of administration and are associated with serious adverse events such as permanent neurologic damage and death [Chappuis 2007]. Drugs used to treat stage 2 of sleeping sickness must be able cross the blood brain barrier. The two frontline drugs for stage two are melarsoprol (an arsenic derivative, introduced in 1946), and eflornithine (introduced in 1977) and each has severe limitations [Nok 2003; Bisser et al., 2007; Lejon et al., 2013]. In 2009, combined therapy with eflornithine and nifurtimox was also introduced,

although, as is the case for eflornithine alone, the treatment is only effective against *T. b. gambiense*. Nifurtimox is also used for Chagas disease or American trypanosomiasis treatment. Melarsoprol is the drug most frequently used drug for CNS infection. However this drug is highly toxic, killing up to 10% of patients [Kennedy 2004], and therapeutic failures have been reported in my home country, the Democratic Republic of Congo [Legros et al., 2002]. Drug-resistant trypanosomes have emerged in several regions of Africa. In order to mitigate treatment failures due to resistance as well as reduce dosages and adverse reactions, Nifurtimox and eflornithine combination therapy (NECT) was recently evaluated and introduced [Legros et al., 2002]. Other combinations such as nifurtimox with melarsoprol or melarsoprol with nifurtimox have also been assessed [Bouteille et al., 2003]. The difficulty to administer and high toxicity of these drugs, together with the emergence of drug-resistant trypanosomes makes it imperative to develop safer, more effective, and easy to administer drugs, in order to facilitate clinical management of sleeping sickness cases.

T. brucei **life cycle**

The whole life cycle of *T. brucei* is defined by extracellular stages within the tsetse fly and mammalian hosts. An infected tsetse fly injects infectious metacyclic trypomastigotes into the mammalian host during a blood meal. Parasites develop into bloodstream trypomastigotes within the mammalian host and enter the bloodstream where they divide by binary division as long slender trypomastigotes (Figure 3A). The doubling time is estimated to be 6 hours [[Seed 1978]]. Antigenic variation of the parasite surface coat and active clearance of host antibody

bound to the parasite surface allows trypanosomes to evade immune destruction and persist in the bloodstream indefinitely [Barry and McCulloch 2001; Borst 2002; Pays 2005]]. *T. brucei* exhibits waves of parasitemia in the bloodstream, corresponding to recurring cycles of growth, clearance by the immune response and then recrudescence owing to emergence of new surface antigen variants. Over time, long slender forms differentiate into non-dividing short, stumpy (Figure 3A) form trypomastigotes. Ultimately, the stumpy forms constitute the majority of the parasite population in the bloodstream [MacGregor et al., 2011] and these are the only forms that are able to continue the life cycle in the tse tse fly [MacGregor et al., 2012].

The tsetse fly (Figure 3B) is infected with bloodstream trypanosomes during a blood meal on an infected mammalian host. Within the tsetse, parasites travel through specific host tissues and undergo extensive morphological and metabolic differentiation, culminating in production of human-infectious forms in the salivary gland (Figure 3A) [Vickerman 1985; van den Abbeele et al., 1995; Sharma et al., 2009]. Stumpy trypanosomes differentiate into procyclic trypanosomes in the posterior part of the fly's midgut (Figure 3C) and enter the ectoperitrophic space by penetrating the preitrophic membrane, which separates the blood meal from the midgut epithelium. Parasites in the ectoperitrophic space are more elongated than their predecessors in the midgut. Trypanosomes become even more elongated as they move to the proventriculus,(Figure 3C) where they undergo asymmetric division to produce one long and one short epimastigote [Vickerman 1985; van den Abbeele et al., 1995; Sharma et al., 2009]. Proventricular trypanosomes (Fifure 3A) migrate to the salivary glands where they attach to the gland epithelium and then complete their differentiation into mature metacyclic trypanosomes that are uniquely adapted for life within the mammalian host. These are the forms that will be injected into the mammalian host during a tse tse fly blood meal [Vickerman 1985]. The entire

cycle in the tse tse fly takes about 3 weeks.

The *T. brucei* flagellum

T. brucei flagellum is an essential [Kohl et al., 2003] and defining feature of the trypanosome cell and plays crucial roles in cell motility, cell morphogenesis, cell division, host parasite interaction, and presumably sensing [Ralston et al., 2009]. It represents the sole means of locomotion and contributes directly to the development and pathogenic capacity of *T. brucei*.

Flagellum structure

The *T. brucei* flagellum emerges from the basal body near the cell posterior end and is laterally connected to the rest of the cell body (Figure 4A). This flagellum possesses a canonical "9 + 2" axoneme, as well as an extra-axonemal filament, called the paraflagellar rod that runs alongside the axoneme. (Figure 4B-C) [Ralston et al., 2009]. In the cytoplasm the axoneme is anchored via the basal body at the parasite posterior's end. The basal body is a barrel-like structure including 9 outer triplet microtubules with no central pair. As triplet microtubules of the basal body extend outward, they become microtubule doublets in order to form a "9 + 0" axoneme transition zone that then becomes the "9 + 2" axoneme.

The flagellum emerges from the cytoplasm through the flagellar pocket, a unique invagination of the plasma membrane. The flagellar pocket is the sole site for endocytosis and

exocytosis, making it a critical feature for host-parasite interactions [Gull 2003; Field and Carrington 2009]. The flagellar membrane, the flagellar pocket and plasma membranes have lipid and protein composition that differ from each other [Balber 1990; Fridberg et al., 2007; Maric et al., 2010]. How the trypanosome sorts proteins differentially to these different domains is not known and is a topic of much interest. The *T. brucei* flagellum runs alongside of the cell body and is connected to the cell body flagellum attachment zone or FAZ (Figure 4C).

Flagellum composition

The Axoneme

The "9+2" axoneme encompasses 9 peripheral microtubule doublets symmetrically distributed around a central pair of microtubule singlets and is the fundamental unit of flagellum motility (Figure 4B-C) [Satir 1995]. Each outer doublet microtubule is composed of an A-tubule and a B-tubule. Dynein motors attached to outer doublets drive flagellum beating. Radial spokes point inward from individual outer doublets toward the central pair apparatus (Figure 4C). The nexin-dynein regulatory complex (NDRC) connects neighboring microtubule doublets and restrict microtubule sliding in order to promote bending of the axoneme [Summers and Gibbons 1971; Satir 2007]. While dyneins provide power for motility, radial spokes, the central pair and the NDRC function in dynein regulation [Lindemann 2004]. Individual structures on the outer doublets are arranged together in a repeating unit with a periodicity of 96 nm [Nicastro et al., 2006; Hughes et al., 2012] [Nicastro et al., ; Hughes et al.,]. Although the fundamental structure of this repeating unit is conserved across eukaryotes that assemble motile cilia, some differences

exist and in *T. brucei* the axonemal repeating unit consist of the NDRC, three radial spokes, four outer arm dyneins, and inner arm dyneins [Nicastro et al., 2006; Hughes et al., 2012]. Additionally, compared to *Chlamydomonas reinhardtii*, the prototype eukaryotic organism for axoneme structure, the central pair microtubules are in a fixed orientation in relation to outer doublet microtubules [Ralston et al., 2009].

Dyneins and Nexin-dynein regulation complex (NDRC)

Dyneins are ATP-driven, microtubule-based molecular motors that furnish the driving force for flagellar motility. Outer arm and inner arm dyneins protrude from outer doublet A-tubules toward the adjacent doublet (Figure 4C). Dynein motors consist of several affiliated light, intermediate and light-intermediate chains, and 1-3 heavy chains [King 2003]. The dynein heavy chains possess ATPase catalytic activity and constitute the motor domains. Despite the eminent role of flagellar motility to *T. brucei* biology, the identity of *T. brucei* axonemal dynein subunits has not been determined and very little is known about specific dyneins and their contributions to axonemal motility in these parasites. Nonetheless, genomic studies have shown that the *T. brucei* genome encodes two predicted outer dynein heavy chains and seven inner dynein heavy chains [Wickstead and Gull 2007]. Outer dynein subunits IC78 [Baron et al., 2007] and LC1 [Baron et al., 2007] are required for outer arm dyneins assembly and for controlling beat directionality in *T. brucei*. Depletion of either protein by RNAi reverses the tip-to-base beat, a prominent feature of *T. brucei* flagellum, to base-to-tip beating. LC1 is essential in bloodstream form *T. brucei* [Ralston et al., 2011]. Mechanisms underlying flagellar protein functions are almost unknown. Identification of domains and residues required for flagellar

protein functions is the topic of Chapters 6 and 7.

For a proper spread of flagellar waveforms along the axoneme, thousands of dyneins must be coordinately regulated spatially and temporally [Baron et al., 2007]. Molecular mechanisms underlying dynein regulation are poorly understood. It has been proposed that dynein regulation involves mechanical and chemical signals [Lindemann and Kanous 1997; Porter and Sale 2000; Smith and Yang 2004; Lindemann and Lesich 2010]. NDRC (also known as DRC) is as a key regulator of axonemal dyneins in several organisms including *T. brucei* [Piperno et al., 1992; Gardner et al., 1994; Howard et al., 1994; Ralston et al., 2006; Colantonio et al., 2009; Heuser et al., 2009]. This complex was originally identified through mutant screens that identified extragenic suppressors of flagellar paralysis in radial spoke and central pair mutants in the flagellated green algae *Chlamydomonas reinhardtii* [Huang et al., 1982]. NDRC acts as a reversible inhibitor of axonemal dyneins. The current model suggests that NDRC transmits mechanochemical signals from the central pair apparatus and radial spokes, releasing inhibition of dyneins at precisely the right time and place along the axoneme [Huang et al., 1982; Piperno et al., 1992; Gardner et al., 1994; Omoto et al., 1999; Porter and Sale 2000; Hutchings et al., 2002; Rupp and Porter 2003; Ralston et al., 2006].

The NDRC is a megadalton complex of several polypeptides. A few NDRC subunits are known in *T. brucei* including trypanin, trypanin related protein (TRP) and component of motile flagella (CMF) 70 [Ralston et al., 2006; Kabututu et al., 2010]; K.L.H. (in preparation)], and the DRC candidate CMF22 [Bower et al., 2013; Nguyen 2013]. Additional studies in *Chlamydomonas* have expanded the inventory of the DRC subunits to include an estimated 11 proteins, with 6 of these being genes (trypanin, CMF22, CMF44, CMF46, CMF70, Tb927.5.550 and Tb927.7.130) that are conserved in *T. brucei* [Baron et al., 2007; Lin et al., 2011; Bower et

al., 2013]. The NDRC subunit trypanin, homologous to the *C. reinhardtii* PF2 protein, is necessary for normal motility in *T. brucei* [Hutchings et al., 2002; Ralston et al., 2006] and is broadly conserved among organisms that assemble motile flagella but is absent in organisms that do not assemble motile flagella [Ralston et al., 2006; Baron et al., 2007]. The NDRC has been demonstrated to be required for ciliary motility and inner ear development in vertebrates [Colantonio et al., 2009] and defects in drc genes cause primary ciliary dyskinesia, a human disease that causes infertility, respiratory malfunction and left-right axis defects [Wirschell et al., 2013]. Unfortunately, despite these advances additional NDRC members, member interactions and molecular mechanisms such as domains or residues required for the DRC function remain to be determined. Identification of trypanin domains required for function and targeting will be the topic of Chapter 7.

Paraflagellar Rod (PFR)

The PFR is a unique flagellum feature limited to kinetoplastids and a few related organisms. The PFR is a large lattice-like filament connected to microtubule doublets 4-7 and expands alongside the axoneme (Figure 4C). In cross section the PFR displays three defined structural regions that include the proximal, intermediate and distal determined by their positions relative to the axoneme [Cosson et al., 1988]. Although the precise structure and function of the PFR is unclear, it is believed to play structural and regulatory roles. PFR is required for normal motility in both *T. brucei* [Bastin et al., 1998] and is essential in the bloodstream life cycle stage [Branche et al., 2006; Broadhead et al., 2006]. Three-dimensional observations of the *T. brucei* PFR by Hughes and colleagues suggests that the PFR causes structural constraints on flagellar

beating and operates as a biomechanical spring to receive and transmit energy generated by flagellum twisting and beating [Hughes et al., 2012]. Although many PFR proteins have been identified [Santrich et al., 1997; Bastin et al., 1998; Ridgley et al., 2000; Portman et al., 2009] the functions these proteins are unknown. Additional studies are needed to identify domains and residues essential for function of PFR proteins. The role played by the flagellum and flagellar motility in *T. brucei* biology makes the PFR an ideal target for therapeutic intervention, especially since this complex is not found in the human host.

In summary, the flagellum is estimated to contain more than 600 [Ralston et al., 2009]. Recent genomics and proteomics investigations have immensely extended the inventory of proteins that compose the flagellum [Avidor-Reiss et al., 2004; Li et al., 2004; Pazour et al., 2005; Broadhead et al., 2006; Baron et al., 2007; Oberholzer et al., 2011]] . However, our understanding of how these proteins contribute to flagellar function individually or collectively is very limited. For example, specific domains or amino acids of important flagellar proteins are for the most unknown. To bridge this important gap, we have developed, in the course of my dissertation, facile systems for mutational analysis of flagellar proteins in *T. brucei* (Appendix 2) (Ralston et al. 2011) and chapter 4. These approaches allow quick discovery of domains or amino acids required for flagellar protein functions in *T. brucei* (Appendix 2). Application of our structure-function approach to the study of LC1 led to rapid idenification of LC1 residues required for motility in *T. brucei* (Appendix 2) [Ralston et al., 2011]. Since the flagellum is essential in *T. brucei*, residues or domains restricted to these pathogens represent potential drug targets, whereas conserved aspects of flagellar proteins should increase our understanding of human biology and disease.

Flagellum assembly

The majority of eukaryotic organisms assemble their flagella by addition of new building blocks to the tip of the growing flagellum. This is mediate by **i**ntra**f**lagellar **t**ransport (IFT), a bidirectional movement system that delivers proteins from the cytoplasm to the flagellum and return proteins from the flagellum to the cytoplasm [Rosenbaum and Witman 2002]. This transport system is dependent on kinesin and cytoplasmic dynein motor proteins. The IFT machinery is conserved and functions in *T. brucei* [Kohl et al., 2003; Davidge et al., 2006; Absalon et al., 2008]. In chapter 6 we exploit the tools we've developed in *T. brucei* to conduct structure-function analysis of the IFT protein IFT88.

Flagellum biogenesis is essential for cell division and is one of the earliest stages of cell cycle in *T. brucei*. The new flagellum emerges from the probasal body in G1 and extend parallel to the old flagellum until it reaches about halfway along the old flagellum at which point it pauses growing. The flagellar connector (FC) is a cytoskeletal structure of unknown composition that links the tip of the new flagellum the old flagellum and mediates the new flagellum's tracking of the old flagellum's path [Moreira-Leite et al., 2001; Briggs et al., 2004]. The flagellum connector is not detected in bloodstream form *T. brucei* or in other trypanosomatids, suggesting the FC is specific to the procyclic form. The reason for this apparent specificity is unknown. Cytokinesis that splits the two cell bodies proceeds along a helical path between the nascent and old flagella [Sherwin and Gull 1989; Moreira-Leite et al., 2001].

Flagellum functions

Role in motility

The dominant role of the flagellum on trypanosome biology is demonstrated even in initial descriptions of these organisms, which centered on their particular, helical cell movement as observed in blood samples from infected frogs [Gruby 1843]. In those studies the parasite's auger-like locomotion, twisting and rotating around its long axis as it moved forward, led to the genus name "*Trypanosoma*", which combines the Greek words *trypanon* (auger) and *soma* (body). Seminal work by Walker [Walker 1961] demonstrated that motility in *T. brucei* is driven by a flexible flagellar beat that initiates at the tip of the flagellum and propagates to the flagellum base, differing from what is seen in most other eukaryotic flagella.

T. brucei rapidly navigates at velocities of 3 - 20 um s^{-1} in three dimension and displays bacterial run-and-tumble actions [Hutchings et al., 2002; Hill] allowing the parasite to reorient [Branche et al., 2006]. The complex, rapid, and energetic locomotion of *T. brucei* has limited quantitative measurement of flagellar beating, although recent studies have begun to overcome this limitations [Rodriguez et al., 2009; Uppaluri et al., 2011; Heddergott et al., 2012; Weisse et al., 2012]. Axoneme RNAi has demonstrated a requirement for the PFR, central pair apparatus, radial spokes, outer doublets, NDRC, and dynein motors in normal motility. Unfortunately, as discussed above, molecular mechanisms underlying the structure and function most of flagellar proteins are unkon. Additionally, proteins that mediate trypanosome-specific features have not been defined, in part due to the lack of quantitative description of flagellar beating.

Role of flagellum motility in disease transmission and pathogenesis

T. brucei is extracellular at all stages of infection and depends on its own flagellum for navigation within the host. Within the tsetse, the parasite must undergo a series of directional movementss in precise tissues from the midgut through the salivary glands to complete differention into mammalian infectious forms. While migrating within the tse tse fly, the parasite encounters several tissue obstacles to invade such as the peritrophic matrix and proventriculus, presaging a requirement for active motility. The flagellum mediates attachment to the salivary gland epithelium (Figure 5A), which induces the terminal stage of development into mature mammalian infectious metacyclic forms [Vickerman 1969; Borst et al., 1985]. As such, transmission depends on parasite motility. However, a requirement for trypanosome motility in tse tse transmission is still to be demonstrated.

The contribution of parasite motility to infection and pathogenesis is a long-standing problem. Parasite motility is generally considered to be important for infection and pathogenesis in the mammalian host and motility roles of *T. brucei* flagellum are receiving a particular attention as potential drug targets [Broadhead et al., 2006; Ralston and Hill 2006; Ginger et al., 2008; Ralston et al., 2009]. Precise requirements for motility in the mammalian host are unclear, but motility is believed to participate in parasite immune evasion and for penetration of extravascular tissues including the blood brain barrier . For example, parasite forward locomotion has been suggested to drive displacement of surface-bound immunoglobulin to the posterior end of the cell, where it is internalized, thereby allowing the parasite to resist opsonization and immune destruction [Engstler et al., 2007]. As an extracellular pathogen, *T.*

brucei probably depends on its own motility for traversal of the blood vessels and entry into the CNS. Recent studies have even evoked that *T. brucei* motility is adapted specifically to the bloodstream environment [Heddergott et al., 2012]. Unfortunately, direct examintion of a requirement for flagellar motility in any facet of host infection has not been achieved, because of the lack of viable motility mutants in the *T. brucei* mammalian infectious life stages [Ginger et al., 2008; Ralston and Hill 2008].

Studies of the flagellum and motility in the bloodstream-form of *T. brucei* are limited by two major factors. First: no-one has been able to generate a viable bloodstream-form motility mutant, so it has not been possible to test the role of motility *in vivo*. Second: it is not known how flagellar proteins actually work, because all studies to date have used RNAi, which can determine if a protein is required for motility, but does not give information about mechanisms. The trypanosome flagellum has emerged as a potential drug target in sleeping sickness, but without knowledge of molecular mechanisms, or motility mutant models to test *in vivo*, there is a major gap in our understanding of this critical feature of trypanosome biology and pathogenesis. Most *T. brucei* motility mutants have been generated by RNAi knockdown of specific flagellar proteins and these knockdowns were lethal in bloodstream form cells, leading to the suggestion that disrupting motility is lethal [Branche et al., 2006; Broadhead et al., 2006; Ralston and Hill 2006; Ralston and Hill 2008]. However, most if not all, *T. brucei* flagellar protein knockdowns have known or suspected structural defects, including some that are far more substantial than just loss of the targeted protein [Ralston and Hill 2008]. Thus, it is not possible with RNAi alone to distinguish between phenotypes arising from defective motility versus pleotropic consequences of ablating target gene expression. To bridge this gap, we established an approach for systematic

structure-function analysis of flagellar proteins in *T. brucei.* This system allowed us to overcome both barriers described above. First: it allows us to replace any endogenous gene with a mutant copy, carrying any mutation(s) we choose. The mutated protein still assembles, but does not function, allowing us to separate phenotypes caused by loss of function versus gross structural defects. Second, this strategy allowed discovery of amino acids in the LC1 subunit of outer arm dynein that are required for motility (Appendix 2) [Ralston et al., 2011]. Third, and most importantly: using this system, we identified two independent motility mutants that are viable in the bloodstream-form life cycle stage (Appendix 2) [Ralston et al., 2011]. We have now capitalized on these advances to test the impact of motility on trypanosome infection. These studies are the focus of Chapter 3.

In addition to its role in driving parasite motility, the *T. brucei* flagellum has important roles in directing cell division and cell morphogenesis and has emerged as an important host-pathogen interface that functions in parasite virulence [Borst et al., 1985]. Furthermore, cilia or flagella are essential for human development [Ralston and Hill 2008; Vincensini et al., 2011] since flagellum defects underlie several genetic diseases in humans [Fliegauf et al., 2007]. The availability in this parasite of a battery of molecular genetic tools including a robust RNAi system and a fully annotated and completed genome [Oberholzer et al., 2009] make *T. brucei* as a superior system to study the eukaryotic cilium or flagellum. Therefore, studies of the *T. brucei* flagellum are broadly applicable to other flagellated protozoa and are suitable for understanding the roles of the eukaryotic flagellum in human biology and disease (Figure 6).

The main goal of my dissertation has been to examine a requirement for flagellar motility for infection and pathogenesis of in African trypanosomiasis. The trypanosome flagellum has emerged as a potential drug target in sleeping sickness and *T. brucei* is an excellent system to study the eukaryotic flagellum. However, without knowledge of molecular mechanisms or motility mutant models to test *in vivo*, there is a major gap in our understanding of this critical feature of trypanosome biology and pathogenesis.

In the first part of my dissertation studies, we developed facile methods for systematic mutation analysis of flagellar proteins in *T. brucei*. Application of these approaches allowed identification of amino acids required for the function of the axonemal dynein regulatory LC1 protein and more importantly led to the generation of the first-ever viable motility mutants in mammalian infectious, bloodstream form ("BSF") trypanosomes (Appendix 2) [Ralston et al., 2011]. We do not know if disrupting motility blocks infection and testing this with our BSF motility mutants is the topic of chapters 2 - 4.

By adapting published approaches, I have set up a mouse infection model of *T. brucei* in our laboratory (Chapter 2). In collaboration of Dr. Jianwei Miao's laboratory from the Physics Department here at UCLA, we have already used this infection model to describe a new model for trypanosome forward motility and new theoretical considerations for movement of microbial pathogens. My work shows that this new model of parasite locomotion also operates in blood from infected mice (Appendix 1) [Rodriguez et al., 2009]. The availability of bloodstream form motility mutants combined to the mouse infection system I have set up allowed me to directly determine the role of motility in *T. brucei* infection and pathogenesis. This topic is the subject of Chapter 3. We surprisingly found that parasite motility is dispensable for bloodstream infection (Kisalu et al., submitted) (Chapter 3). To assess the contribution of parasite motility for the

CNS penetration, I have been collaborating with Dr. Keith Matthews (Edinburgh University), generating motility mutants in *T. brucei* strains that cause chronic infection and are able to invade the CNS and this is the topic of chapter 4. In order to better characterize infection dynamics and host-parasite interations during infection, I have developed imaging modalities using fluorescent parasites in mouse and fish infection systems in collaboration with Dr. Shimon Weiss laboratory at UCLA. This subject id the topic of Chapter 5 (Kisalu et al. manuscript in preparation).

In addition to investigating the contribution of flagellar motility to infection and pathogenesis, I have also capitalized on our systems for structure-function analysis to define amino acids required for function and or trafficking of proteins required for flagellum assembly (IFT88, chapter 6) and motility (trypanin, chapter 7). My studies in Chapter 6 tested amino acids that correspond to IFT88 mutations observed in human patients with defective cilia identified by our collaborator, Dr. Heymut Omran in Germany, and showed which of these mutations are loss of function mutations versus polymorphisms (Kisalu et al. manuscript in preparation). Identification of trypanin domains required for function is the topic of Chapter 7.

Overall, these studies represent an important contribution to understanding *T. brucei* pathogenesis mechanisms and should help efforts to develop effective therapies for sleeping sickness. Imaging studies and further developments also have potential broad application for therapeutics and diagnostics development, as well as patient management in sleeping sickness. Finally, studies of flagellum protein structure/function have broad relevance for understanding biology of the eukaryotic flagellum, which is of central importance to several human pathogens and required for normal human development and physiology. As such, my investigations

contribute to deepen our knowledge of flagellum motility functions in trypanosomes, with direct relevance to other flagellated protozoa, as well as toward fundamental aspects of eukaryotic cell biology as it relates to human health and disease.

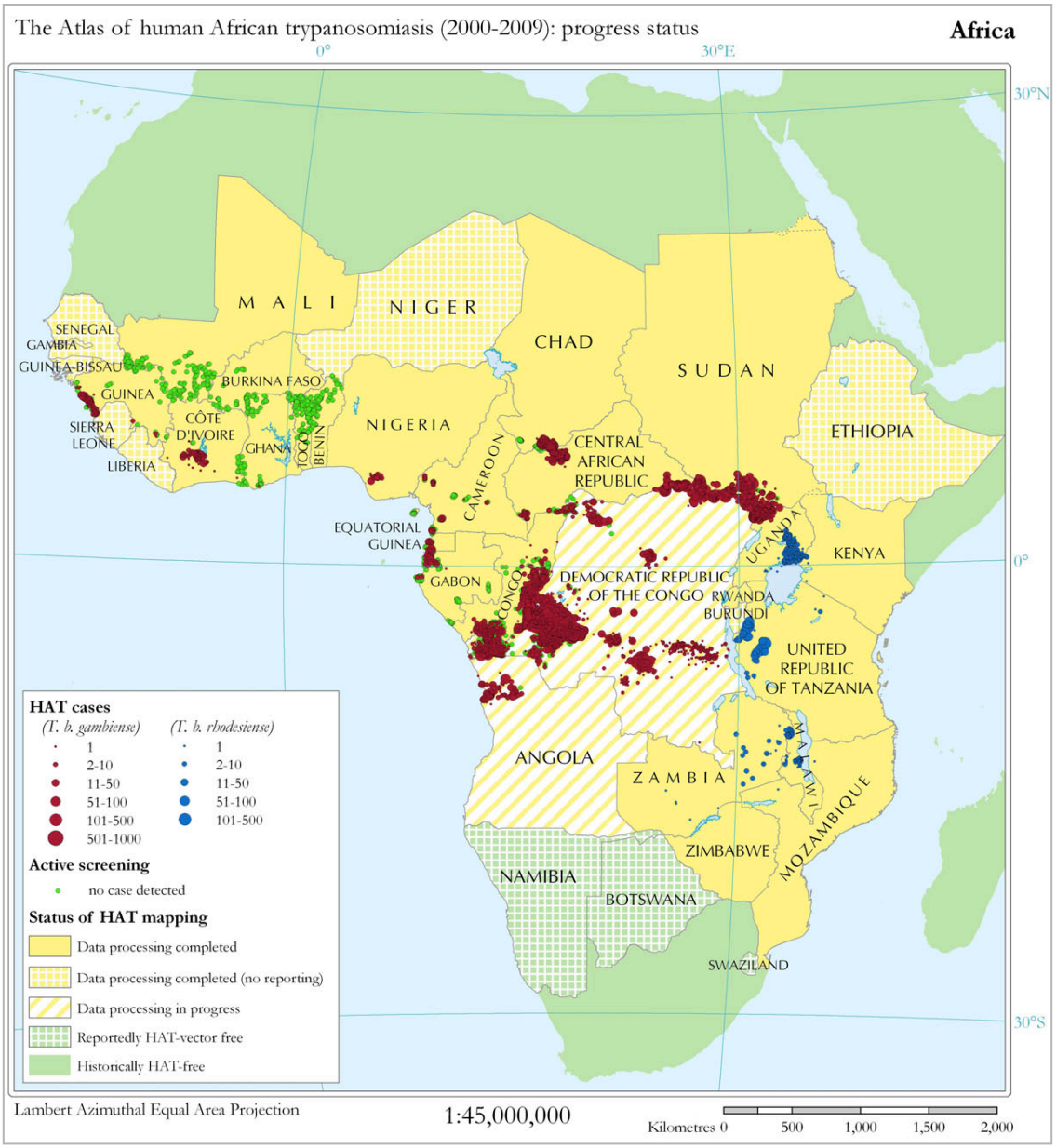

Figure 1. Recent atlas of African sleeping sickness. Map represents geographic distribution of the disease and for each country the number of cases reported is indicated for the period 2000-2009. From [Simarro et al., 2010].

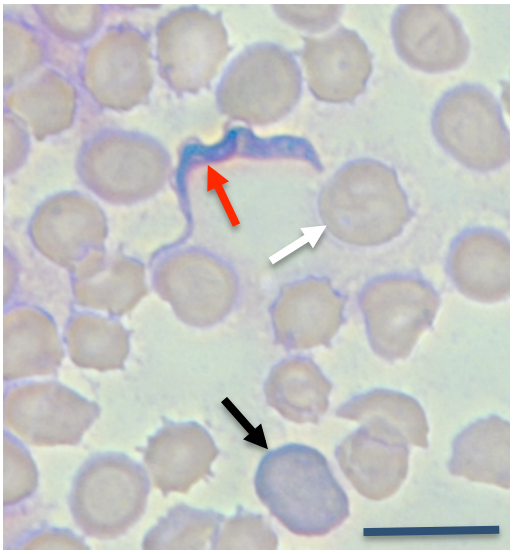

Figure 2. Observation of trypanosome in blood by microscopic examination. Giemsa stain showing a trypanosome (*T. b. brucei* strain 667) in blood taken from an infected mouse at five days post-infection. Arrows point to trypanosome (red arrow), young (black arrow) or old (white arrow) erythrocytes. Scale bar is 12.5 μm.

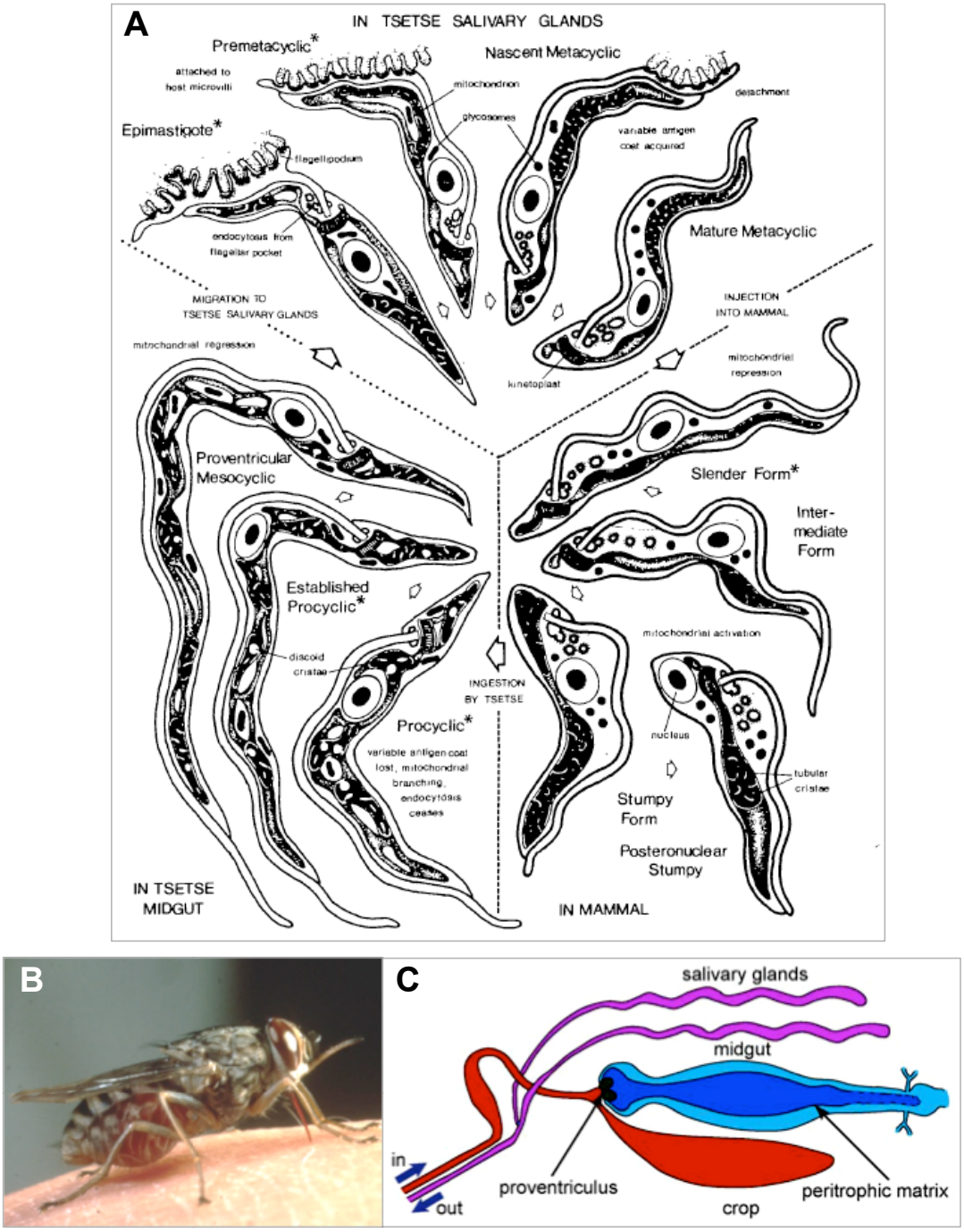

Figure 3. ***T. brucei*** **life cycle**. (A) The diagram depicts various transformations African trypanosomes undergo throughout their life cycle both in the tse tse fly and mammalian host.

Changes shown include relative size of different stages, cell surface, mitochondrion, glycosomes and receptor-mediated endocytosis. Bloodstream stages are placed to the right while insect stages to the left and top. An example of a stumpy form with a posterior nucleus (bottom right) is shown. An asterix (*) indicates cell division occurs in these stages. (B) A tse tse fly vector during blood meal on a human host. (C) Sketch of tse tse fly viscera. Trypanosomes taken up by the tse tse fly are fist found in the endoperitrophic space of the midgut before they penetrate the peritrophic space. Following anterograte movements toward the proventriculus, parasites continue to differentiate into epimatigote forms before their maturation into mammalian-infectious metacyclics in the salivary glands. Panel A is from [Vickerman 1985], panel B is from [Sharma et al., 2009], all reproduced with permission.

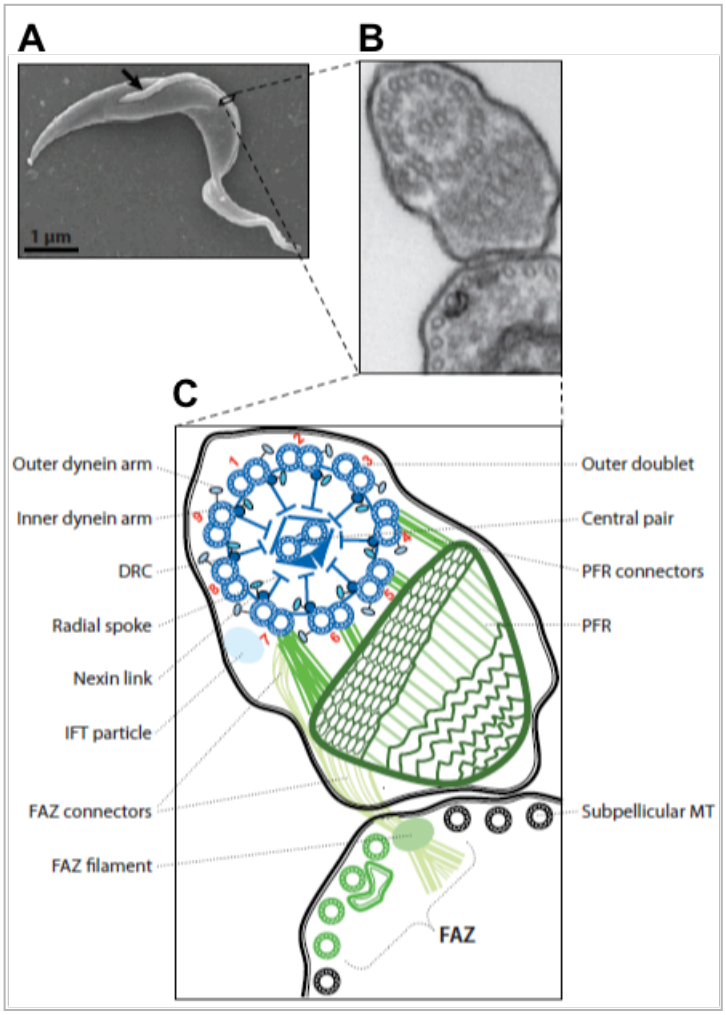

Figure 4. Structure of *T. brucei* flagellum. (A) Scanning electron micrograph of the insect stage trypanosome. The arrow points to the unique flagellum. (B) Transmission electron micrograph displaying a cross-section of the flagellum attached to the cell body as observed when viewing from posterior toward anterior. (C) Cartoon of the micrograph presented in panel B. Important structures of the flagellum are indicated. Doublet microtubules are conventionally numbered. Conserved structures of the eukaryotic flagellum are in blue, whereas shown in green are structures restricted to trypanosomes and closely related organisms. PFR, paraflagellar rod; MT, microtubule; IFT, intraflagellar transport; FAZ, flagellum attachment zone; DRC, dynein

regulatory complex. Adapted from [Ralston et al., 2009], with permission.

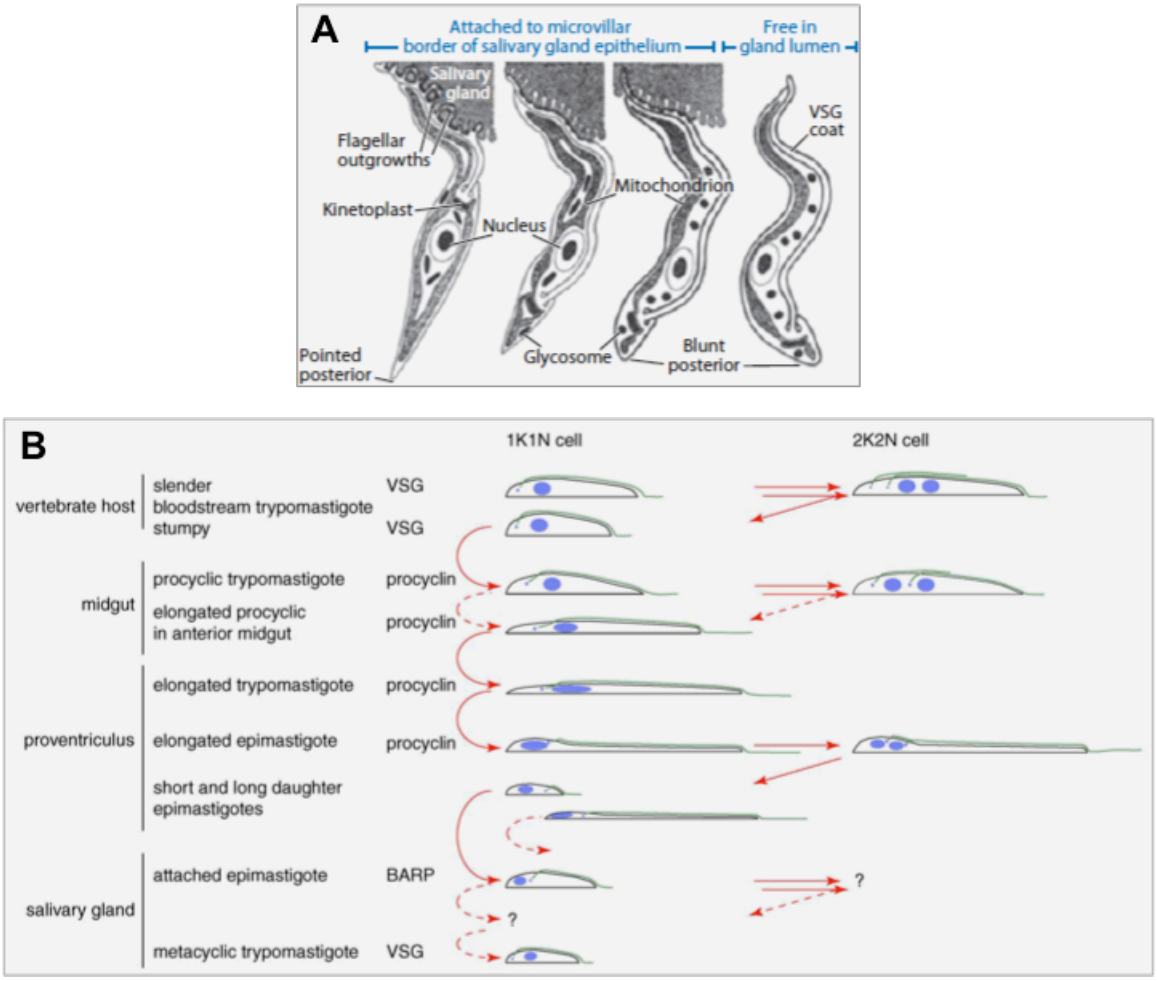

Figure 5. The flagellum regulates attachment to the tsetse fly salivary gland and influences cell morphogenesis. (A) Schematic representation of the developmental transformations the parasite endergoes while attached to the salivary gland epithelium. Cells are displayed from left to right as epimastigote, premetacyclic, nascent metacyclic, and metacyclic forms. VSG stands for variant surface glycoprotein. Adapted from [Ralston et al., 2009], with permission. (B) Morphotypes found in a tsetse fly, and a comparison with replicating bloodstream form parasites of the mammalian host. Distinct morphotypes throughout the life cycle undergo an ordered series of changes that encompass reorganization of internal substructures as well as

transformation of cell shape. Solid lines indicate well characterized transitions whereas dashed lines are for uncharacterized or alternative steps. Question mark represents unfairly described morphologies. Among several transitions that occur in the tse tse vector, differentiation of bloodstream to procyclics and the asymmetric division that gives rise to epimastigotes have been studied extensively. Procyclics in the midgut, salivary glad attached epimastigotes, and mammalian bloodstream forms undergo multiple rounds of cell division to sustain these populations. In contrast, although they can divide proventricular epimastigotes undergo a single asymmetric division and are not self-sustaining populations. Cellular arrangement of the kinetoplast and nucleus is shown for 1K1N and 2K2N cells before cytokinesis. Adapted from [Sharma et al., 2009], with permission.

Figure 6. Using *T. brucei* as a model organism to study the eukaryotic flagellum. This drawing represents the trypanosome axoneme. In order to exemplify the evolutionarily conserved nature of the 9 + 2 flagellar axoneme, various ciliated organisms are displayed as the radial spokes. (Clockwise from top: *Ciona intestinalis, Danio rerio, Drosophila melanogaster, Gallus gallus, Chlamydomonas reinhardtii, Homo sapiens, Caenorhabditis elegans, Mus musculus, and Asterias forbesi*.) The paraflagellar rod is not shown because this substructure is restricted to trypanosomes. Adapted from [Ralston et al., 2009], with permission.

CHAPTER 1 REFERENCES

Absalon, S., Blisnick, T., Kohl, L., Toutirais, G., Dore, G., Julkowska, D. et al. (2008). "Intraflagellar transport and functional analysis of genes required for flagellum formation in trypanosomes." Mol Biol Cell 19(3): 929-944.

Avidor-Reiss, T., Maer, A. M., Koundakjian, E., Polyanovsky, A., Keil, T., Subramaniam, S. and Zuker, C. S. (2004). "Decoding cilia function: defining specialized genes required for compartmentalized cilia biogenesis." Cell 117(4): 527-539.

Balber, A. E. (1990). "The pellicle and the membrane of the flagellum, flagellar adhesion zone, and flagellar pocket: functionally discrete surface domains of the bloodstream form of African trypanosomes." Crit Rev Immunol 10(3): 177-201.

Baron, D. M., Kabututu, Z. P. and Hill, K. L. (2007). "Stuck in reverse: loss of LC1 in Trypanosoma brucei disrupts outer dynein arms and leads to reverse flagellar beat and backward movement." J Cell Sci 120(Pt 9): 1513-1520.

Baron, D. M., Ralston, K. S., Kabututu, Z. P. and Hill, K. L. (2007). "Functional genomics in Trypanosoma brucei identifies evolutionarily conserved components of motile flagella." J Cell Sci 120(Pt 3): 478-491.

Barry, J. D. and McCulloch, R. (2001). "Antigenic variation in trypanosomes: enhanced phenotypic variation in a eukaryotic parasite." Adv Parasitol 49: 1-70.

Bastin, P., Sherwin, T. and Gull, K. (1998). "Paraflagellar rod is vital for trypanosome motility." Nature 391(6667): 548.

Bisser, S., N'Siesi, F. X., Lejon, V., Preux, P. M., Van Nieuwenhove, S., Miaka Mia Bilenge, C. and Buscher, P. (2007). "Equivalence trial of melarsoprol and nifurtimox monotherapy and combination therapy for the treatment of second-stage Trypanosoma brucei gambiense sleeping sickness." J Infect Dis 195(3): 322-329.

Blum, J., Schmid, C. and Burri, C. (2006). "Clinical aspects of 2541 patients with second stage human African trypanosomiasis." Acta Trop 97(1): 55-64.

Borst, P. (2002). "Antigenic variation and allelic exclusion." Cell 109(1): 5-8.

Borst, P., Fase-Fowler, F., Weijers, P. J., Barry, J. D., Tetley, L. and Vickerman, K. (1985). "Kinetoplast DNA from Trypanosoma vivax and T. congolense." Mol Biochem Parasitol 15(2): 129-142.

Bouteille, B., Oukem, O., Bisser, S. and Dumas, M. (2003). "Treatment perspectives for human African trypanosomiasis." Fundam Clin Pharmacol 17(2): 171-181.

Bower, R., Tritschler, D., Vanderwaal, K., Perrone, C. A., Mueller, J., Fox, L. et al. (2013). "The N-DRC forms a conserved biochemical complex that maintains outer doublet alignment and limits microtubule sliding in motile axonemes." Mol Biol Cell 24(8): 1134-1152.

Branche, C., Kohl, L., Toutirais, G., Buisson, J., Cosson, J. and Bastin, P. (2006). "Conserved and specific functions of axoneme components in trypanosome motility." J Cell Sci 119(Pt 16): 3443-3455.

Briggs, L. J., Davidge, J. A., Wickstead, B., Ginger, M. L. and Gull, K. (2004). "More than one way to build a flagellum: comparative genomics of parasitic protozoa." Curr Biol 14(15): R611-612.

Broadhead, R., Dawe, H. R., Farr, H., Griffiths, S., Hart, S. R., Portman, N. et al. (2006). "Flagellar motility is required for the viability of the bloodstream trypanosome." Nature 440(7081): 224-227.

Brun, R., Blum, J., Chappuis, F. and Burri, C. (2010). "Human African trypanosomiasis." Lancet 375(9709): 148-159.

Buscher, P., Gilleman, Q. and Lejon, V. (2013). "Rapid diagnostic test for sleeping sickness." N Engl J Med 368(11): 1069-1070.

Chappuis, F. (2007). "Melarsoprol-free drug combinations for second-stage Gambian sleeping sickness: the way to go." Clin Infect Dis 45(11): 1443-1445.

Chappuis, F., Loutan, L., Simarro, P., Lejon, V. and Buscher, P. (2005). "Options for field diagnosis of human african trypanosomiasis." Clin Microbiol Rev 18(1): 133-146.

Colantonio, J. R., Vermot, J., Wu, D., Langenbacher, A. D., Fraser, S., Chen, J. N. and Hill, K. L. (2009). "The dynein regulatory complex is required for ciliary motility and otolith biogenesis in the inner ear." Nature 457(7226): 205-209.

Cosson, J., Cachon, M., Cachon, J. and Cosson, M. P. (1988). "Swimming behaviour of the unicellular biflagellate Oxyrrhis marina: in vivo and in vitro movement of the two flagella." Biol Cell 63(2): 117-126.

Davidge, J. A., Chambers, E., Dickinson, H. A., Towers, K., Ginger, M. L., McKean, P. G. and Gull, K. (2006). "Trypanosome IFT mutants provide insight into the motor location for mobility of the flagella connector and flagellar membrane formation." J Cell Sci 119(Pt 19): 3935-3943.

Deborggraeve, S. and Buscher, P. (2010). "Molecular diagnostics for sleeping sickness: what is the benefit for the patient?" Lancet Infect Dis 10(6): 433-439.

Engstler, M., Pfohl, T., Herminghaus, S., Boshart, M., Wiegertjes, G., Heddergott, N. and Overath, P. (2007). "Hydrodynamic flow-mediated protein sorting on the cell surface of trypanosomes." Cell 131(3): 505-515.

Field, M. C. and Carrington, M. (2009). "The trypanosome flagellar pocket." Nat Rev Microbiol 7(11): 775-786.

Fliegauf, M., Benzing, T. and Omran, H. (2007). "When cilia go bad: cilia defects and ciliopathies." Nat Rev Mol Cell Biol 8(11): 880-893.

Fridberg, A., Buchanan, K. T. and Engman, D. M. (2007). "Flagellar membrane trafficking in kinetoplastids." Parasitol Res 100(2): 205-212.

Gardner, L. C., O'Toole, E., Perrone, C. A., Giddings, T. and Porter, M. E. (1994). "Components of a "dynein regulatory complex" are located at the junction between the radial spokes and the dynein arms in Chlamydomonas flagella." J Cell Biol 127(5): 1311-1325.

Ginger, M. L., Portman, N. and McKean, P. G. (2008). "Swimming with protists: perception, motility and flagellum assembly." Nat Rev Microbiol 6(11): 838-850.

Gruby, M. (1843). "Analysis and observation of a novel hematozoan species, *Trypanosoma sanguinis*." C R Hebd Seqnces Acad Sci 17:: 1134-1136.

Gull, K. (2003). "Host-parasite interactions and trypanosome morphogenesis: a flagellar pocketful of goodies." Curr Opin Microbiol 6(4): 365-370.

Heddergott, N., Kruger, T., Babu, S. B., Wei, A., Stellamanns, E., Uppaluri, S. et al. (2012). "Trypanosome motion represents an adaptation to the crowded environment of the vertebrate bloodstream." PLoS Pathog 8(11): e1003023.

Heuser, T., Raytchev, M., Krell, J., Porter, M. E. and Nicastro, D. (2009). "The dynein regulatory complex is the nexin link and a major regulatory node in cilia and flagella." J Cell Biol 187(6): 921-933.

Hill, K. L. (2003). "Biology and mechanism of trypanosome cell motility." Eukaryot Cell 2(2): 200-208.

Howard, D. R., Habermacher, G., Glass, D. B., Smith, E. F. and Sale, W. S. (1994). "Regulation of Chlamydomonas flagellar dynein by an axonemal protein kinase." J Cell Biol 127(6 Pt 1): 1683-1692.

Huang, B., Ramanis, Z. and Luck, D. J. (1982). "Suppressor mutations in Chlamydomonas reveal a regulatory mechanism for Flagellar function." Cell 28(1): 115-124.

Hughes, L. C., Ralston, K. S., Hill, K. L. and Zhou, Z. H. (2012). "Three-dimensional structure of the Trypanosome flagellum suggests that the paraflagellar rod functions as a biomechanical spring." PLoS One 7(1): e25700.

Hutchings, N. R., Donelson, J. E. and Hill, K. L. (2002). "Trypanin is a cytoskeletal linker protein and is required for cell motility in African trypanosomes." J Cell Biol 156(5): 867-877.

Jamonneau, V., Bucheton, B., Kabore, J., Ilboudo, H., Camara, O., Courtin, F. et al. (2010). "Revisiting the immune trypanolysis test to optimise epidemiological surveillance and control of sleeping sickness in West Africa." PLoS Negl Trop Dis 4(12): e917.

Jelinek, T., Bisoffi, Z., Bonazzi, L., van Thiel, P., Bronner, U., de Frey, A. et al. (2002). "Cluster of African trypanosomiasis in travelers to Tanzanian national parks." Emerg Infect Dis 8(6): 634-635.

Kabututu, Z. P., Thayer, M., Melehani, J. H. and Hill, K. L. (2010). "CMF70 is a subunit of the dynein regulatory complex." J Cell Sci 123(Pt 20): 3587-3595.

Kennedy, P. G. (2004). "Human African trypanosomiasis of the CNS: current issues and challenges." J Clin Invest 113(4): 496-504.

King, S. M. (2003). "Organization and regulation of the dynein microtubule motor." Cell Biol Int 27(3): 213-215.

Koffi, M., Solano, P., Denizot, M., Courtin, D., Garcia, A., Lejon, V. et al. (2006). "Aparasitemic serological suspects in Trypanosoma brucei gambiense human African trypanosomiasis: a potential human reservoir of parasites?" Acta Trop 98(2): 183-188.

Kohl, L., Robinson, D. and Bastin, P. (2003). "Novel roles for the flagellum in cell morphogenesis and cytokinesis of trypanosomes." EMBO J 22(20): 5336-5346.

Legros, D., Ollivier, G., Gastellu-Etchegorry, M., Paquet, C., Burri, C., Jannin, J. and Buscher, P. (2002). "Treatment of human African trypanosomiasis--present situation and needs for research and development." Lancet Infect Dis 2(7): 437-440.

Lejon, V., Bentivoglio, M. and Franco, J. R. (2013). "Human African trypanosomiasis." Handb Clin Neurol 114: 169-181.

Lejon, V. and Buscher, P. (2005). "Review Article: cerebrospinal fluid in human African trypanosomiasis: a key to diagnosis, therapeutic decision and post-treatment follow-up." Trop Med Int Health 10(5): 395-403.

Lejon, V., Legros, D., Richer, M., Ruiz, J. A., Jamonneau, V., Truc, P. et al. (2002). "IgM quantification in the cerebrospinal fluid of sleeping sickness patients by a latex card agglutination test." Trop Med Int Health 7(8): 685-692.

Li, J. B., Gerdes, J. M., Haycraft, C. J., Fan, Y., Teslovich, T. M., May-Simera, H. et al. (2004). "Comparative genomics identifies a flagellar and basal body proteome that includes the BBS5 human disease gene." Cell 117(4): 541-552.

Lin, J., Tritschler, D., Song, K., Barber, C. F., Cobb, J. S., Porter, M. E. and Nicastro, D. (2011). "Building blocks of the nexin-dynein regulatory complex in Chlamydomonas flagella." J Biol Chem 286(33): 29175-29191.

Lindemann, C. B. (2004). "Testing the geometric clutch hypothesis." Biol Cell 96(9): 681-690.

Lindemann, C. B. and Kanous, K. S. (1997). "A model for flagellar motility." Int Rev Cytol 173: 1-72.

Lindemann, C. B. and Lesich, K. A. (2010). "Flagellar and ciliary beating: the proven and the possible." J Cell Sci 123(Pt 4): 519-528.

MacGregor, P., Savill, N. J., Hall, D. and Matthews, K. R. (2011). "Transmission stages dominate trypanosome within-host dynamics during chronic infections." Cell Host Microbe 9(4): 310-318.

MacGregor, P., Szoor, B., Savill, N. J. and Matthews, K. R. (2012). "Trypanosomal immune evasion, chronicity and transmission: an elegant balancing act." Nat Rev Microbiol 10(6): 431-438.

Magnus, E., Vervoort, T. and Van Meirvenne, N. (1978). "A card-agglutination test with stained trypanosomes (C.A.T.T.) for the serological diagnosis of T. B. gambiense trypanosomiasis." Ann Soc Belg Med Trop 58(3): 169-176.

Maric, D., Epting, C. L. and Engman, D. M. (2010). "Composition and sensory function of the trypanosome flagellar membrane." Curr Opin Microbiol 13(4): 466-472.

Moore, D. A., Edwards, M., Escombe, R., Agranoff, D., Bailey, J. W., Squire, S. B. and Chiodini, P. L. (2002). "African trypanosomiasis in travelers returning to the United Kingdom." Emerg Infect Dis 8(1): 74-76.

Moreira-Leite, F. F., Sherwin, T., Kohl, L. and Gull, K. (2001). "A trypanosome structure involved in transmitting cytoplasmic information during cell division." Science 294(5542): 610-612.

Mumba Ngoyi, D., Menten, J., Pyana, P. P., Buscher, P. and Lejon, V. (2013). "Stage determination in sleeping sickness: comparison of two cell counting and two parasite detection techniques." Trop Med Int Health 18(6): 778-782.

Nguyen, H. K., Sandhu, J. S., Langousis, G. & Hill, K. (2013). "CMF22 is a broadly conserved axonemal protein and is required for propulsive motility in Trypanosoma brucei." Euk Cell In Press.

Nicastro, D., Schwartz, C., Pierson, J., Gaudette, R., Porter, M. E. and McIntosh, J. R. (2006). "The molecular architecture of axonemes revealed by cryoelectron tomography." Science 313(5789): 944-948.

Nok, A. J. (2003). "Arsenicals (melarsoprol), pentamidine and suramin in the treatment of human African trypanosomiasis." Parasitol Res 90(1): 71-79.

Oberholzer, M., Langousis, G., Nguyen, H. T., Saada, E. A., Shimogawa, M. M., Jonsson, Z. O. et al. (2011). "Independent analysis of the flagellum surface and matrix proteomes provides insight into flagellum signaling in mammalian-infectious Trypanosoma brucei." Mol Cell Proteomics 10(10): M111 010538.

Oberholzer, M., Lopez, M. A., Ralston, K. S. and Hill, K. L. (2009). "Approaches for functional analysis of flagellar proteins in African trypanosomes." Methods Cell Biol 93: 21-57.

Omoto, C. K., Gibbons, I. R., Kamiya, R., Shingyoji, C., Takahashi, K. and Witman, G. B. (1999). "Rotation of the central pair microtubules in eukaryotic flagella." Mol Biol Cell 10(1): 1-4.

Pays, E. (2005). "Regulation of antigen gene expression in Trypanosoma brucei." Trends Parasitol 21(11): 517-520.

Pazour, G. J., Agrin, N., Leszyk, J. and Witman, G. B. (2005). "Proteomic analysis of a eukaryotic cilium." J Cell Biol 170(1): 103-113.

Piperno, G., Mead, K. and Shestak, W. (1992). "The inner dynein arms I2 interact with a "dynein regulatory complex" in Chlamydomonas flagella." J Cell Biol 118(6): 1455-1463.

Porter, M. E. and Sale, W. S. (2000). "The 9 + 2 axoneme anchors multiple inner arm dyneins and a network of kinases and phosphatases that control motility." J Cell Biol 151(5): F37-42.

Portman, N., Lacomble, S., Thomas, B., McKean, P. G. and Gull, K. (2009). "Combining RNA interference mutants and comparative proteomics to identify protein components and dependences in a eukaryotic flagellum." J Biol Chem 284(9): 5610-5619.

Ralston, K. S. and Hill, K. L. (2006). "Trypanin, a component of the flagellar Dynein regulatory complex, is essential in bloodstream form African trypanosomes." PLoS Pathog 2(9): e101.

Ralston, K. S. and Hill, K. L. (2008). "The flagellum of Trypanosoma brucei: new tricks from an old dog." Int J Parasitol 38(8-9): 869-884.

Ralston, K. S., Kabututu, Z. P., Melehani, J. H., Oberholzer, M. and Hill, K. L. (2009). "The Trypanosoma brucei flagellum: moving parasites in new directions." Annu Rev Microbiol 63: 335-362.

Ralston, K. S., Kisalu, N. K. and Hill, K. L. (2011). "Structure-function analysis of dynein light chain 1 identifies viable motility mutants in bloodstream-form Trypanosoma brucei." Eukaryot Cell 10(7): 884-894.

Ralston, K. S., Lerner, A. G., Diener, D. R. and Hill, K. L. (2006). "Flagellar motility contributes to cytokinesis in Trypanosoma brucei and is modulated by an evolutionarily conserved dynein regulatory system." Eukaryot Cell 5(4): 696-711.

Ridgley, E., Webster, P., Patton, C. and Ruben, L. (2000). "Calmodulin-binding properties of the paraflagellar rod complex from Trypanosoma brucei." Mol Biochem Parasitol 109(2): 195-201.

Rocha, G., Martins, A., Gama, G., Brandao, F. and Atouguia, J. (2004). "Possible cases of sexual and congenital transmission of sleeping sickness." Lancet 363(9404): 247.

Rodgers, J. (2010). "Trypanosomiasis and the brain." Parasitology 137(14): 1995-2006.

Rodriguez, J. A., Lopez, M. A., Thayer, M. C., Zhao, Y., Oberholzer, M., Chang, D. D. et al. (2009). "Propulsion of African trypanosomes is driven by bihelical waves with alternating chirality separated by kinks." Proc Natl Acad Sci U S A 106(46): 19322-19327.

Rosenbaum, J. L. and Witman, G. B. (2002). "Intraflagellar transport." Nat Rev Mol Cell Biol 3(11): 813-825.

Rupp, G. and Porter, M. E. (2003). "A subunit of the dynein regulatory complex in Chlamydomonas is a homologue of a growth arrest-specific gene product." J Cell Biol 162(1): 47-57.

Santrich, C., Moore, L., Sherwin, T., Bastin, P., Brokaw, C., Gull, K. and LeBowitz, J. H. (1997). "A motility function for the paraflagellar rod of Leishmania parasites revealed by PFR-2 gene knockouts." Mol Biochem Parasitol 90(1): 95-109.

Satir, P. (1995). "Landmarks in cilia research from Leeuwenhoek to us." Cell Motil Cytoskeleton 32(2): 90-94.

Satir, P. (2007). "Cilia biology: stop overeating now!" Curr Biol 17(22): R963-965.

Seed, J. R. (1978). "Competition among serologically different clones of Trypanosoma brucei gambiense in vivo." J Protozool 25(4): 526-529.

Sharma, R., Gluenz, E., Peacock, L., Gibson, W., Gull, K. and Carrington, M. (2009). "The heart of darkness: growth and form of Trypanosoma brucei in the tsetse fly." Trends Parasitol 25(11): 517-524.

Sherwin, T. and Gull, K. (1989). "The cell division cycle of Trypanosoma brucei brucei: timing of event markers and cytoskeletal modulations." Philos Trans R Soc Lond B Biol Sci 323(1218): 573-588.

Simarro, P. P., Cecchi, G., Paone, M., Franco, J. R., Diarra, A., Ruiz, J. A. et al. (2010). "The Atlas of human African trypanosomiasis: a contribution to global mapping of neglected tropical diseases." Int J Health Geogr 9: 57.

Simarro, P. P., Jannin, J. and Cattand, P. (2008). "Eliminating human African trypanosomiasis: where do we stand and what comes next?" PLoS Med 5(2): e55.

Smith, E. F. and Yang, P. (2004). "The radial spokes and central apparatus: mechano-chemical transducers that regulate flagellar motility." Cell Motil Cytoskeleton 57(1): 8-17.

Stich, A., Abel, P. M. and Krishna, S. (2002). "Human African trypanosomiasis." BMJ 325(7357): 203-206.

Summers, K. E. and Gibbons, I. R. (1971). "Adenosine triphosphate-induced sliding of tubules in trypsin-treated flagella of sea-urchin sperm." Proc Natl Acad Sci U S A 68(12): 3092-3096.

Truc, P., Lejon, V., Magnus, E., Jamonneau, V., Nangouma, A., Verloo, D. et al. (2002). "Evaluation of the micro-CATT, CATT/Trypanosoma brucei gambiense, and LATEX/T b gambiense methods for serodiagnosis and surveillance of human African trypanosomiasis in West and Central Africa." Bull World Health Organ 80(11): 882-886.

Uppaluri, S., Nagler, J., Stellamanns, E., Heddergott, N., Herminghaus, S., Engstler, M. and Pfohl, T. (2011). "Impact of microscopic motility on the swimming behavior of parasites: straighter trypanosomes are more directional." PLoS Comput Biol 7(6): e1002058.

Urech, K., Neumayr, A. and Blum, J. (2011). "Sleeping sickness in travelers - do they really sleep?" PLoS Negl Trop Dis 5(11): e1358.

van den Abbeele, J., Rolin, S., Claes, Y., Le Ray, D., Pays, E. and Coosemans, M. (1995). "Trypanosoma brucei: stimulation of adenylate cyclase by proventriculus and esophagus tissue of the tsetse fly, Glossina morsitans morsitans." Exp Parasitol 81(4): 618-620.

Vervoort, T., Magnus, E. and Van Meirvenne, N. (1978). "Enzyme-linked immunosorbent assay (ELISA) with variable antigen for serodiagnosis of T. B. gambiense trypanosomiasis." Ann Soc Belg Med Trop 58(3): 177-183.

Vickerman, K. (1969). "On the surface coat and flagellar adhesion in trypanosomes." J Cell Sci 5(1): 163-193.

Vickerman, K. (1985). "Developmental cycles and biology of pathogenic trypanosomes." Br Med Bull 41(2): 105-114.

Walker, P. J. (1961). "Organization of function in trypanosome flagella." Nature 189: 1017-1018.

Weisse, S., Heddergott, N., Heydt, M., Pflasterer, D., Maier, T., Haraszti, T. et al. (2012). "A quantitative 3D motility analysis of Trypanosoma brucei by use of digital in-line holographic microscopy." PLoS One 7(5): e37296.

Wickstead, B. and Gull, K. (2007). "Dyneins across eukaryotes: a comparative genomic analysis." Traffic 8(12): 1708-1721.

Wirschell, M., Olbrich, H., Werner, C., Tritschler, D., Bower, R., Sale, W. S. et al. (2013). "The nexin-dynein regulatory complex subunit DRC1 is essential for motile cilia function in algae and humans." Nat Genet 45(3): 262-268.

Chapter 2

Setting up mouse infection for analysis of *Trypanosoma brucei* host-parasite interaction

Abstract

Mice are a powerful tool to dissect critical pathogenesis mechansims for infectious diseases including for African trypanosomiasis. For many pathogens, mice present an artificial model, but African trypanosomes infect mice naturally and indeed, have proven to be valuable for understanding many features of African trypanosomiasis, as well as characterization of staging biomarkers and evaluation of novel drug therapies have been achieved in murine models of trypanosomiasis. Despite these advances, several aspects of trypanosomiasis infection and pathogenesis remain to be unraveled. For example, a role of trypanosome flagellum-mediated motility has been suggested in infection and pathogenesis of African sleeping sickness, but this hypothesis has never been tested. We recently generated motility mutants that are viable in the bloodstream form life cycle stage, which is the life cycle stage that infects mammals [Ralston et al., 2011]. In order to capitalize on that advance, we have set up mouse infection models using monomorphic and pleomorphic *Trypanosoma brucei*. These parasites cause acute and chronic infections, respectively. We specifically have established multiplicity of infection necessary for reproducible infection, determined parasitemia dynamics, time to lethal outcome and effectiveness of chemotherapy using standard therapeutics to assess brain invasion by *T. brucei*. This mouse infection system has been used to examine trypanosome motility *ex vivo* in blood from infected mice, leading to a new model in which bihelical waves of alternate handedness drive parasite forward movement (Appendix 2) [Rodriguez et al., 2009]. These mouse infection systems also enable studies of pathogenesis mechanisms including direct analysis of the impact of parasite motility on infection and pathogenesis, which is a topic of Chapters 3-5.

Introduction

African trypanosomes, i.e. *Trypanosoma brucei* and related sub-species, are protozoan parasites that cause sleeping sickness in humans and related diseases in animals. The disease is always lethal if left untreated [Ralston et al., 2009]. There is no vaccine against trypanosomes and existing drugs are toxic and associated with drug resistance. These parasites cause devastating health and economic consequences and endanger more than 60 million people in 36 countries in Sub-Saharan Africa [WHO 2010]. The disease advances through two mains stages. During the first stage of the disease, parasites actively multiply in the bloodstream and the lymphatics following transmission by the bite of an infected tse tse fly. Clinical manifestations of stage one of the disease are benign and non-specific, resembling to flu-like symptoms accompanied by fever and lymphoadenopathy. In contrast, the second stage of the disease, also known as the meningoencephalitic phase, manifests several weeks after infection when parasites invade connective tissues including the central nervous system. This stage involves a chronic meninoencephalitis associated with headaches and sleep disorder. Stage two culminates in death if the disease is left untreated [Stich et al., 2002; Rodgers 2010]. Two subspecies of *T. brucei* are incriminated for trypanosomiasis pathologies in humans. *T. b. gambiense* is responsible for a mild and chronic disease that remains several months to years, whereas the disease caused by *T. b. rhodesiense* is more acute and advances the host to death quickly within several weeks [Jelinek et al., 2002; Blum et al., 2006].

African sleeping sickness has been known for hundreds of years [Gruby 1843]. However, clinical management of African sleeping sickness patients is still challenging in part because there is a lack of reliable biomarkers to unequivocally determine progression from stage one to

stage 2 of the disease. Additionally, treatment of African sleeping sickness is dangerous since current drugs, are toxic and old. Once *T. brucei* invades the CNS the number of drugs available for treatment is reduced because the parasites are no longer accessible to drugs that do not penetrate the blood brain barrier. Invasion of the CNS is therefore a crucial step in the pathogenesis of sleeping sickness. Because of ethical issues and the difficulty to manage human patients, several aspects of trypanosomiasis pathogenesis cannot be tested in humans. Thus, much of our understanding for this disease comes from animal models of infection.

Animals including mice, rats, cattle, rabbits, dogs, and non-human primates such as monkeys have been used in experimental African trypanosomiasis [Gray 1960; Schindler and Sachs 1970; Schindler et al., 1970]; [Kennedy 2007]. It is increasingly recognized that mice evolved as an important tool to dissect critical pathogenesis processes in trypanosomiasis [Foote et al., 2005; Antoine-Moussiaux et al., 2008; Morrison and MacLeod 2011]. Notably, known clinical features of human African trypanosomiasis including the meningo-encephalitic stage of the disease have been accomplished in rodent models [Gray 1960; Bentivoglio et al., 1994; Antoine-Moussiaux et al., 2008; Masocha et al., 2008]. Moreover, murine models of trypanosomiasis have been used to test not only novel therapies but also to test combination chemotherapy of known or new drugs for potential human applications [Jennings et al., 2002; Kennedy 2007; Antoine-Moussiaux et al., 2008]. Several pathogenesis aspects of trypanosomiasis including the roles of anti-parasite immunoglobulins, the roles of inflammatory and anti-inflammatory mediators, as well as genetic determinants of susceptibility for trypanosomes have been characterized in mice [Gray 1960; Bentivoglio et al., 1994; Antoine-Moussiaux et al., 2008; Masocha et al., 2008]Antoine-Moussiaux, 2008 #3;Inverso, 1988

#41;Morrison, 2011 #53].

Several strains of *T. brucei* are used to study hot-parasite interactions in trypanosomiasis. Pleomorphic strains are defined by their ability to differentiate, over time during infection, from replicating long-slender forms into non-replicating short-stumpy forms in the bloodstream of mammalian host, thus leading to chronic infections that last >30 days with waves of parasitemias [Breidbach et al., 2002; MacGregor et al., 2011]. Stumpy forms constitute the majority of the parasite population in the bloodstream [MacGregor et al., 2011] during chronic infection. Pleomorphics are therefore transmission competent since stumpies are the only transmission stages that are able to perpetuate the life cycle whithin the tse tse flies [MacGregor et al., 2011; MacGregor et al., 2012]. In contrast, monomorphic trypanosomes such as 427-derived "BSSM" parasites [Wirtz et al., 1999] are laboratory-adapted parasites unable to undergo differentiation from slenders into stumpies in the mammalian host. In addition to failing completion of development inside the tse tse fly, monomorphic parasites rapidly proliferate in the bloodstream leading to death of the mouse host within 7 days [Emmer et al., 2010].

In order to test the role of motility in infection and pathogenesis, a first goal was to set up mouse infection. Although this has been done in other laboratories, it was not previously done at UCLA. Furthermore, although mouse infection with monomorphic trypanosomes that give acute infection is being done by several laboratories, infection and pathogenesis models with pleomorphic forms that give a chronic infection are much less utilized and less established. A chronic infection model is particularly important for our studies, because this is ultimately required to fully assess the role of motility in the full spectrum of disease features. I therefore

collaborated with Professor John Mansfield at the University of Wisconsin, Madison to adapt mouse infection systems for the cell lines that we use for our studies. Here we establish how many parasites are needed to reproducibly establish infection and determine the course of infection for the *T. brucei* strains that will be subsequently used in construction of motility mutants. These include monomorphic strains that give acute infection as well as pleomorphic strains that give chronic infection. We find that all three pleomorphic parasite lines show multiple waves of parasitemia that mimic parasitemia waves seen in human African trypanosomiasis. We also show that chemotherapy using the drug berenil is effective at clearing bloodstream infection, providing a means to assess CNS invasion [Jennings et al., 1979; Poltera et al., 1980], which is a goal of future studies. These mouse infection models will make it possible to dissect pathogenesis mechanisms such as the requirement for parasite motility in infection and pathogenesis.

Results

Course of infection by BSSM parasites

By adapting published approaches [Inverso et al., 1988; Dubois et al., 2005], we have established a mouse infection model of *T. brucei* using the monomorphic, 427-derived "BSSM" parasites [Wirtz et al., 1999]. In contrast to the pleomorphic trypanosomes, which are fully able to differentiate, monomorphic trypanosomes are laboratory-adapted strains, which fail to differentiate to stumpy forms in the bloodstream and generally do not complete development within the tsetse fly [McCulloch et al., 2004]. BSSM parasites divide unchecked in the bloodstream and cause an acute infection in mice [Emmer et al., 2010]. To titrate the mouse system and determine how many parasites are needed to establish and maintain an infection, we tested different multiplicity of infections (MOI), from 1000 through 50 for the BSSM parasites. Following mouse infection by intraperitoneal route, which is classically used for trypanosome mouse infection [Herbert and Lumsden 1968; Greenblatt and Rosenstreich 1984; Jennings et al., 2002; Salmon et al., 2012]], each MOI tested resulted in infection (Figure 1A-D). We chose to use an MOI of 100 parasites for the BSSM-cell line because this MOI gave reproducible and predictable parasitemias in mice.

Next, using WT (control) parasites, we established the course of infection for BSSM parasites. We found that WT parasites show one to two waves of parasitemia within two weeks before the mice must be sacrificed. The first wave of parasitemia peaks at 3-5 days post infection (dpi), whereas the second wave, although rare (< 10%) for BSSM infections, appears 8-12 dpi

respectively (Figure 2A-B). Waves of parasitemia are also seen in human African trypanosomiasis, although the time frame differs.

Most of our trypanosome mutants generated so far have been generated using a tetracycline-inducible system (Appendix 2) [Ralston et al., 2011]. In order to induce the mutant protein during infection, doxycycline (tetracycline) is added to the mouse drinking water 5-7 days prior to and throughout infection. In order to assess the effect of doxycycline on both the mouse and parasite, we compared mice infected with WT parasites and treated or not with doxycycline. As expected WT BSSM parasites established infection even in doxycycline-treated mice (Figure 3). Differences in survival rates for plus or minus doxycycline infections were not significantly different ($p = 0.2116$). Therefore, doxycycline treatment did not cause any discernable effects on mice and WT parasites.

Course of infection by pleomorphic parasites TREU-667, TREU-927 and AnTat1.1

Trypanosomes invade host extravascular tissues including the central nervous system (CNS) and motility is suspected to be required for this. BSSM *T. brucei* continues to divide in the bloodstream and causes an acute infection in mice that progresses rapidly (7-14 days). This timeframe is too short and precludes assessment of the central nervous system (CNS) invasion, which generally takes 2 to 3 weeks [Jennings et al., 1979; Poltera et al., 1980; Gray et al., 1982]. BSSM is thus well-suited for testing bloodstream infection, owing to its superior genetic tractability, but constitutes a limitation for examining CNS invasion. In contrast, pleomorphic *T.*

brucei strains are distinguished by their capability to to cause chronic infections lasting several days to months [Breidbach et al., 2002; MacGregor et al., 2011]. In order to reliably investigate the role of trypanosome cell motility in CNS penetration, we therefore also established chronic infection models using three independent pleomorphic strains, TREU-667 [Jennings et al., 1979], TREU-927 [Goedbloed et al., 1973] and AnTat1.1 [MacGregor et al., 2011]. Importantly, TREU-667 and AnTat1.1 cause chronic (>30 days) infection and are established as CNS mouse infection models [Jennings et al., 1979; Poltera et al., 1980; MacGregor et al., 2011]. Upon injection, TREU667, TREU-927 and AnTat1.1 parasites established infections in mice that mirror the human infection, showing several waves of parasitemia and chronic infections lasting more than 50 days (Figure 4A-C).

Strategies for assessing CNS penetration by *T. brucei*

CNS invasion is of central importance to disease pathogenesis and consequences for therapeutic intervention but investigating CNS invasion by trypanosomes is challenging. We have established two independent yet complementary strategies to dependably assess CNS penetration by *T. brucei*. First, we used chemotherapy (Jennings, Whitelaw et al. 1979) to investigate invasion of the CNS. The trypanocidal drug diminazene aceturate (Berenil) clears bloodstream African trypanosome infection but does not cross the blood brain barrier (Jennings, Whitelaw et al. 1979). Therefore, if trypanosomes enter the CNS, they escape berenil chemotherapy and relapse after treatment (Jennings, Whitelaw et al. 1979). A relapse of bloodstream infection following clearance by berenil treatement therefore provides a bioassay

for CNS infection. To investigate the response of infections to chemotherapy and to assess whether CNS invasion occurred, we treated infected mice at 5-12 dpi (BSSM infections) or at 10 and 60 dpi (AnTat1.1 infections). Berenil-treatment resulted in clearance of parasites in the mouse bloodstream within twenty-four hours (BSSM) or forty-height hours (AnTAt1.1) after treatment. BSSM infections were kept for more than 120 days following treatment and no relapse was detected in two attempts, confirming that BSSM parasites do not penetrate the CNS (Figure 5A). However, AnTat1.1 infections that were treated with berenil at 60 dpi resulted in relapse infection following treatment (Figure 5B). Relapse after clearance of bloodstream infection indicates the parasites have indeed penetrated the CNS (Jennings, Whitelaw et al. 1979; Poltera, Hochmann et al. 1980). Therefore, berenil treatment is a suitable approach that will be used to examine CNS invasion by pleomorphic *T. brucei*.

In a second approach, after euthanasia and prior to tissue collection, mice receive an intracardiac perfusion of saline [Brooks et al., 2005] to remove the blood along with trypanosomes in blood. After perfusion mouse tissues are collected and histochemistry or imaging (Chapter 5) is performed on dissected tissues. Presence of parasites in tissues from which blood is removed indicates penetration from blood vessels into tissue spaces. Perfusions studies are underway. To test this approach, we used BSSM parasites expressing the mCherry fluorescent parasites (Chapters 4 and 5) to infect mice. Mouse tissues collected after perfusion 7 or 10 days following infection were subjected to imaging (Chapter 5). Preliminary data (not shown) were inconclusive as fluorescent signal was detected in tissues from control non-perfused as well as in perfused mice. This result indicates some parasites remain despite perfusion, or there may be some damage to blood vessel by perfusion, allowing escape from bloodstream.

Nonetheless, although challenging and our efforts to use it with BSSM parasites are so far inconclusive, this is an alternate approach for assessment of the CNS penetration. Perfusion experiments will be repeated using fluorescent pleomorphic parasites. The mouse infection models we have set up are relevant for discovering virulence factors that could be used as drug targets. For instance, we will use these systems to test if blocking parasite motility blocks infection or pathogenesis in mice (Chapters 3 and 4). Additionally, visualizing host-parasite interactions, which is the focus of Chapter 5, using imaging approaches will be achieved through these infection models. Therefore, our mouse infection models offer unique opportunities to investigate several aspects of trypanosome infection in the mammalian host.

Discussion

We have developed mouse infection models of African trypanosomiasis. This animal infection system provides us with an opportunity to address unresolved questions of pathogenesis in sleeping sickness. We used several ways to validate these murine infection systems. Firstly, we used BSSM parasites to calibrate the mouse infection system using monomorphic *T. brucei* parasites. Each multiplicity of infection (MOI) tested resulted in infection in BALB/c mice. Although all BSSM MOIs tested yielded acute infection as it was shown previously [Emmer et al., 2010], we found that 100 parasites is the lowest MOI that gave reproducible and predictable parasitemias. Second, we determined that the course of infection varies between one and two weeks for BSSM parasites, with a single [Emmer et al., 2010] or rarely two waves of parasitemias. Third, in the context of using tetracycline-inducible BSF motility mutants to test for pathogenesis mechanisms, we found that tetracycline has no discernable influence on both the mouse and WT BSSM control parasites as it was shown for another monomorphic *T. brucei* line [Griffiths et al., 2007]. This system can therefore be reliably used to study several features of trypanosomiasis infection including the importance of *T. brucei* cell motility in the bloodstream infection using conditional or non-conditional BSSM motility mutants (Appendix 2 and Chapters 3-4).

We have also established a *T. brucei* chronic infection model using pleomorphic cell lines. TREU-667, TREU-927 and AnTaT established infections in mice that mimic human infection with several waves of parasitemias and a chronic infection that lasted >50 days, corroborating previous investigations using pleomorphic lines [Jennings et al., 1979; Poltera et

al., 1980; Gray et al., 1982; MacGregor et al., 2011]. To provide a rigorous assessment for CNS penetration by *T. brucei* we validated a bioassay strategy to test for infection relapse after clearance of parasites from the blood with berenil treatment. While efforts to set up an independent, yet complimentary direct visualization approach are underway, we have already used berenil treatment to demonstrate CNS invasion by WT AnTat 1.1 parasites. Using related TREU-667 pleomorphic parasites, Jennings and colleagues have shown that berenil treatment by 14 dpi always results in no relapse, while treatment at 14-21 dpi does give relapse in some cases but not in others (Jennings, Whitelaw et al. 1979). In contrast, berenil treat ment after 21 dpi always results in relapse (Jennings, Whitelaw et al. 1979). We found that AnTat1.1 infections did relapse if treatment was given at 60 dpi, which is in line with observations by Jennings and colleagues (Jennings, Whitelaw et al. 1979), who used the TREU667 pleomorphic line. Treatment prior to 14 dpi for Antat1.1 and TREU667 infections does not give relapse constitutes are underway and will constitute a relevant control for this CNS invasion assay. Hence our system represents a powerful strategy for pathogenesis studies to investigate the role of *T. brucei* cell motility in the CNS invasion and this will be a focus of future work.

Although important advances have been recently made in addressing immunopathology questions, many unknowns remain in our understanding of pathogenesis mechanisms in African trypanosomiasis. For example, cellular and molecular mechanisms underlying CNS penetration by this parasite deserve a particular attention for investigation as CNS invasion is a defining step in pathogenesis of trypanosomiasis since it marks beginning of the lethal stage of the disease [Kennedy 2007]. Host factors such as lymphocytes and interferon-γ [Masocha et al., 2007; Masocha et al., 2008] as well as parasite factors such as the brucipain cysteine proteases

[Abdulla et al., 2008] have been shown to be important in regulating trypanosome penetration into the brain. Cell motility in *T. brucei* is believed to be essential for infection and pathogenesis. Unfortunately, it has not been possible to test this hypothesis because no one has been able to generate a viable bloodstream-form motility mutant. We recently generated bloodstream form *T. brucei* motility mutants that are viable and are mammalian infectious in an acute infection model (Appendix 2) [Ralston et al., 2011]. The availability of these motility mutants combined to the mouse infection system we have established will now allow studies investigating the impact of parasite motility in pathogenesis. Moreover, we will build on these advances to generate motility mutants for chronic infection models in order to test the requirement for parasite motility for CNS invasion.

Our mouse infection system is relevant for studying host-parasite interactions as well as for evaluating or devising new treatment strategies for African trypanosomiasis. As an example, we took advantage of the mouse infection system reported here to assess motility of *T. brucei* directly in blood from infected mice (Appendix 1) [Rodriguez et al., 2009] and those studies provided insights into mechanisms of trypanosome cell propulsion. Our systems represent a significant contribution in understanding pathogenesis mechanisms and should open ways to develop novel therapies for African sleeping sickness.

Experimental Procedures:

Ethics Statement.

All animal experiments scrupulously complied with the Institutional Animal Care and Use Committee of University of California, Los Angeles (Approved protocol permit: ARC # 2001-065).

Trypanosome culture.

Cultivation of BSSM trypanosomes [Wirtz et al., 1999] in culture was done as described previously [Ralston et al., 2006]. Briefly, cells were grown in HMI-9 medium supplemented with 15% heat-inactivated fetal calf serum (HIFCS) and maintained at 37 °C and 5% CO_2.

Mouse infections.

Mouse infections were done essentially as described [Dubois et al., 2005]]. BALB/c female mice (The Jackson Laboratory, Bar Harbor, ME), 6 to 10 weeks old, were injected intraperitoneally with 50, 100, 500, and 100 BSSM parasites or 10,000-50,000 TREU667, TREU927, or AnTat1.1 trypanosomes in 0.2 ml cold phosphate buffered saline (PBS) (pH 7.4) supplemented with 1% glucose or HMI-9 medium. To maintain cell viability in PBS, parasites were kept on ice prior to injection into mice. For BSSM + Tet infections, parasites were induced with 1 μg/ml tetracycline in culture 3 days prior to injection into mice and mice received 1 mg/ml doxycycline in their drinking water 5 to 7 days prior to infection and throughout the course of infection. Parasitemia was monitored daily beginning 2-3 days post infection using an improved Neubaeur hemocytometer [Herbert and Lumsden 1976].

Chemotherapy

For berenil treatment, mice received 40 mg/kg berenil [Jennings et al., 1979] intraperitoneally in a volume of 0.100 ml at day post infection 60 only when animals showed waves of parasitemia. Parasitemia post-berenil treatment was monitored as described above. After clearance of bloodstream infection following berenil treatment detection of parasitemia was considered as a relapse of infection.

Acknowledgements

We thank Professor John Mansfield and Mrs. Karen Demick (University of Wisconsin) for guidance with mouse infections. We are also grateful to Professor George Cross (Rockefeller University) for providing AnTat1.1 and TREU927 parasites. Professor Stephen Hajduk (University of Georgia) kindly provided us with TREU667 cells.

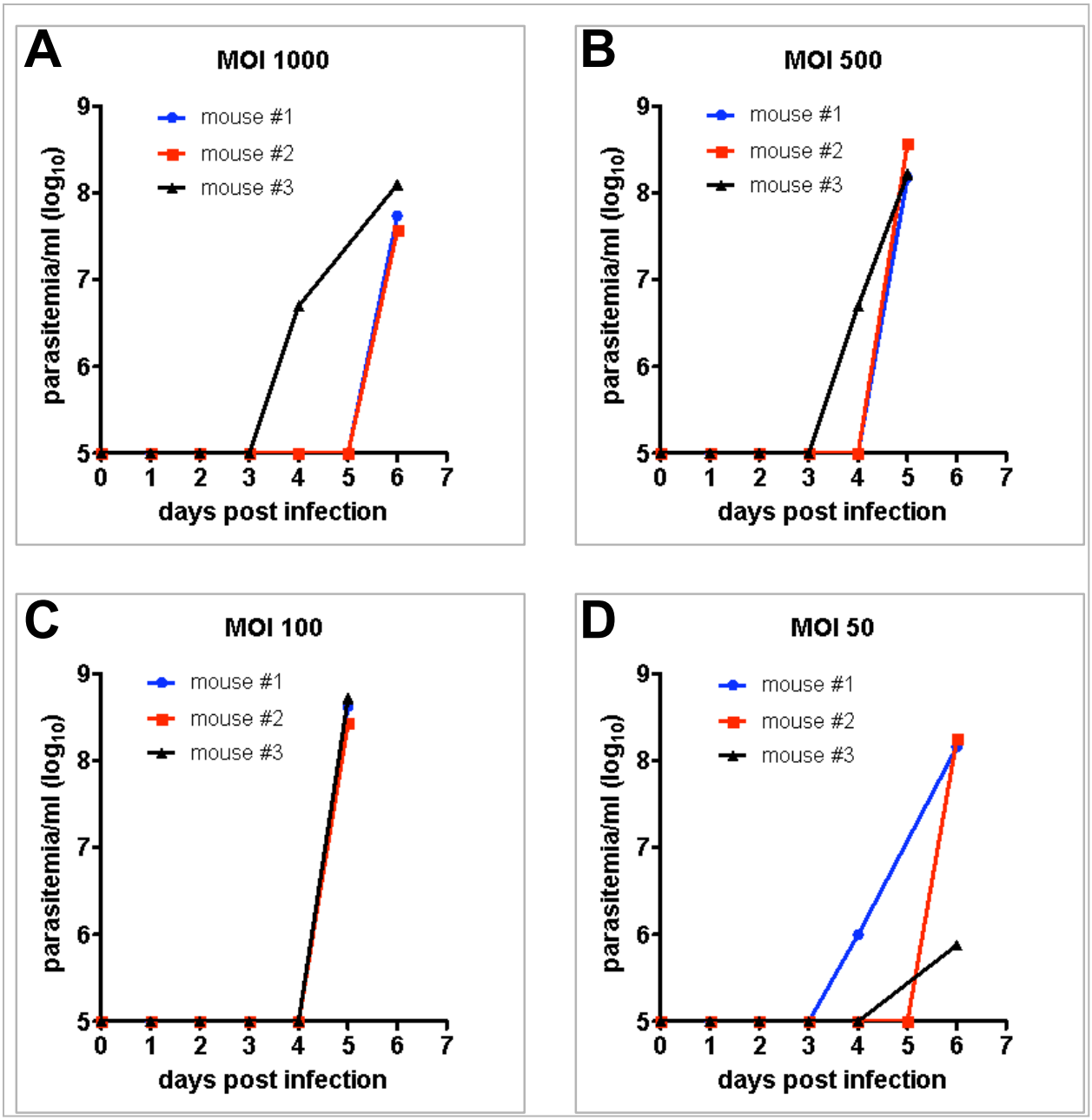

Figure 1. BSSM infections at different multiplicity of infection (MOI). Parasitemias of mice infected with 1000 (A), 500 (B), 100 (C), or 50 (D) BSSM parasites. Mice were infected at day 0 with the indicated MOI and parasitemia was determined beginning two days post infection (dpi). Representative data are shown for three mice for each MOI tested from a total of 8 (MOI 100-1000) and 5 (MOI 50) infections. Experiment was terminated when the first parasitemia

was detected. Two mice in the MOI 1000 group did not show detectable parasitemia. MOI is indicated on each panel.

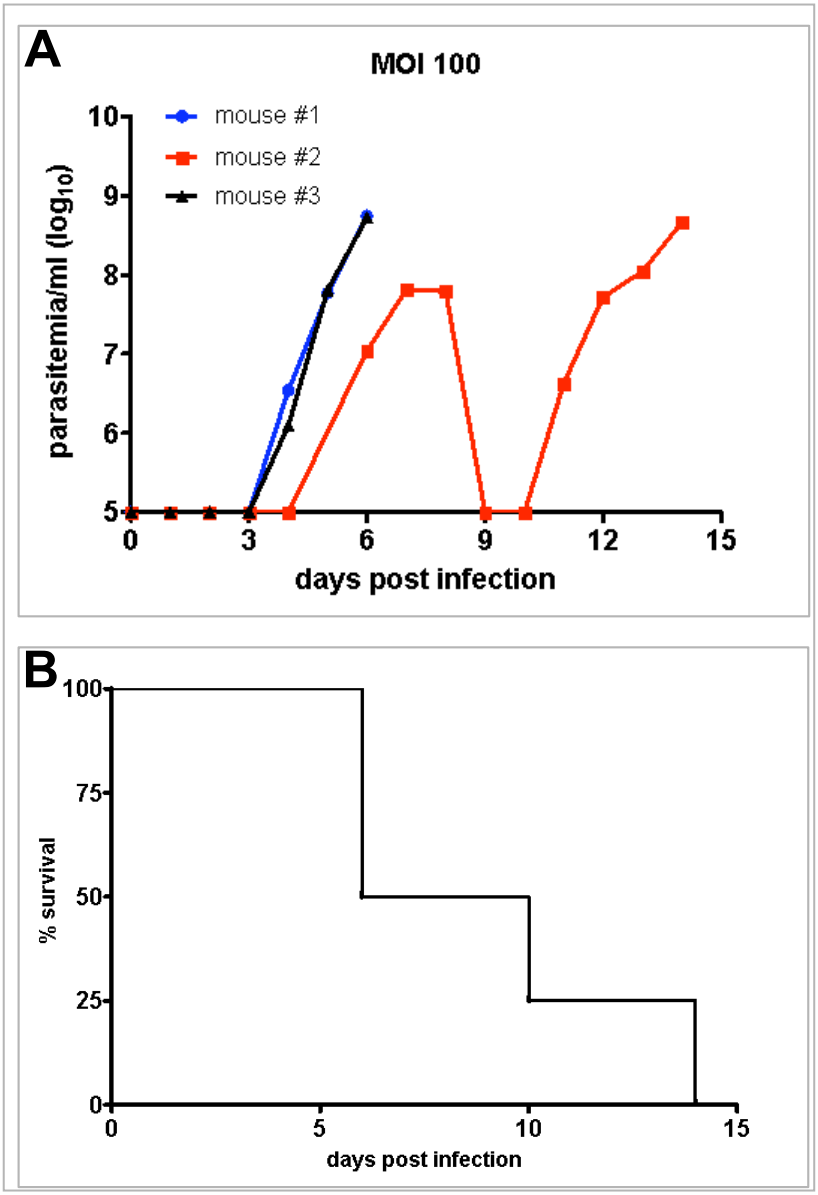

Figure 2. Course and dynamics of BSSM infections. (A) Parasitemias of BSSM parasites. Mice were infected at day 0 with 100 parasites and parasitemia was determined beginning three days post infection (dpi). Normally, mice showed a single wave of parasitemia (black and blue lines) but one mouse exhibited two waves (red line). (B) Survival curves for mice shown in panel A (n = 3).

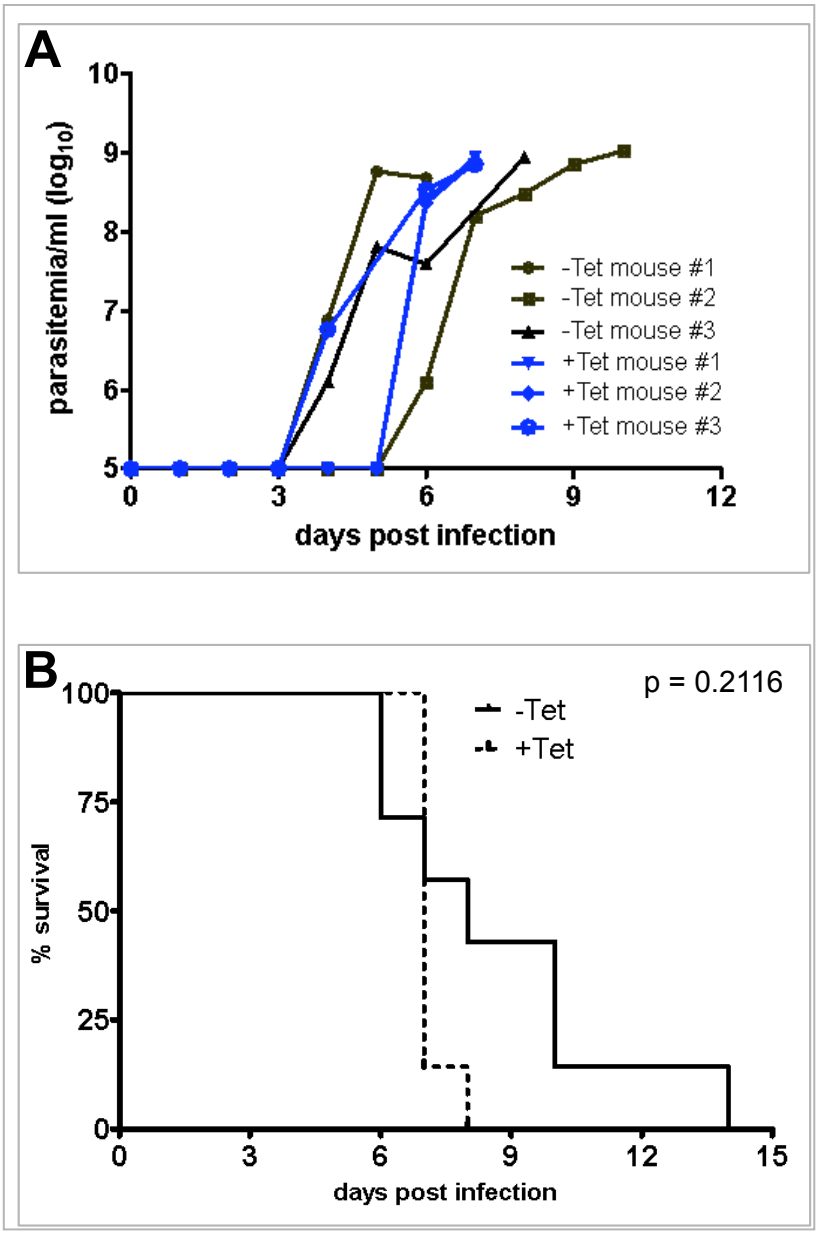

Figure 3. Tetracycline has no discernable effect on mice and wild type BSSM *T. brucei*. (A) Parasitemias of BSSM parasites. Mice were maintained without tetracycline (black lines, - Tet) or with tetracycline (blue lines, + Tet) in the drinking water. Mice were infected at day 0 with 100 parasites and parasitemia was determined beginning three days post infection. Representative data are shown for three infections. (B) Survival curves for BSSM-infected mice,

maintained without tetracycline (-Tet, solid lines, n = 7) or with tetracycline (+Tet, dashed line, n = 7) in the drinking water. Any differences were not significant (*p* is indicated).

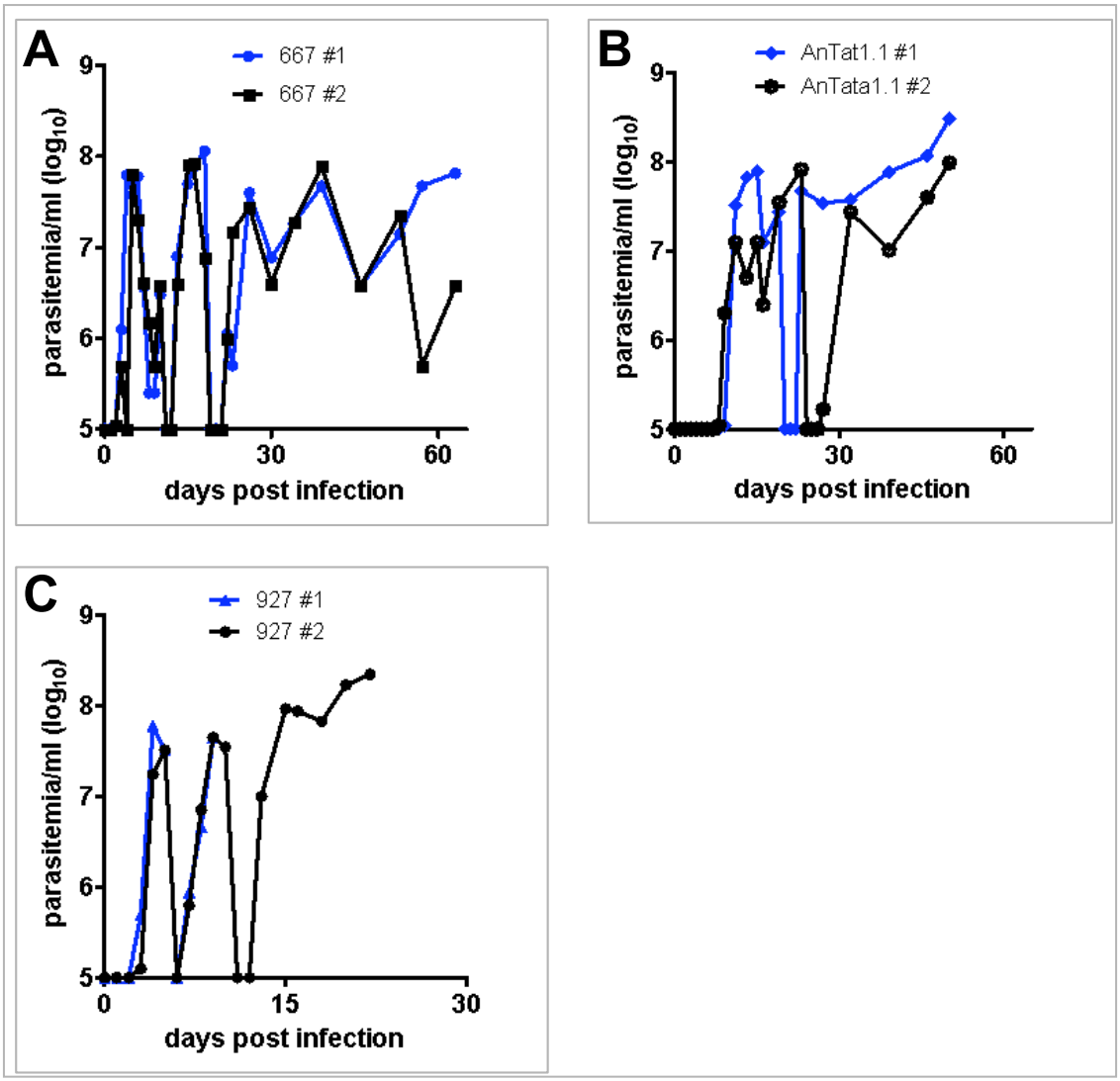

Figure 4. Infection of pleomorphic trypanosomes TREU667, TREU927, and AnTat1.1.

Parasitemias of mice infected with TREU667 (A), TREU927 (B), and AnTAt1.1 (C) parasites. Mice were infected at day 0 with the indicated parasite line and parasitemia was determined beginning two days post infection (dpi). Data are shown for two infections for each parasite line. Mice showed several waves of parasitemia and infection lasted more than fifty days for TREU667 and AnTat1.1 infections. For TREU927 infections, mouse #1 exhibited one wave of

parasitemia and died at dpi 10, whereas mouse #2 physically looked unhealthy and was sacrificed at dpi 22.

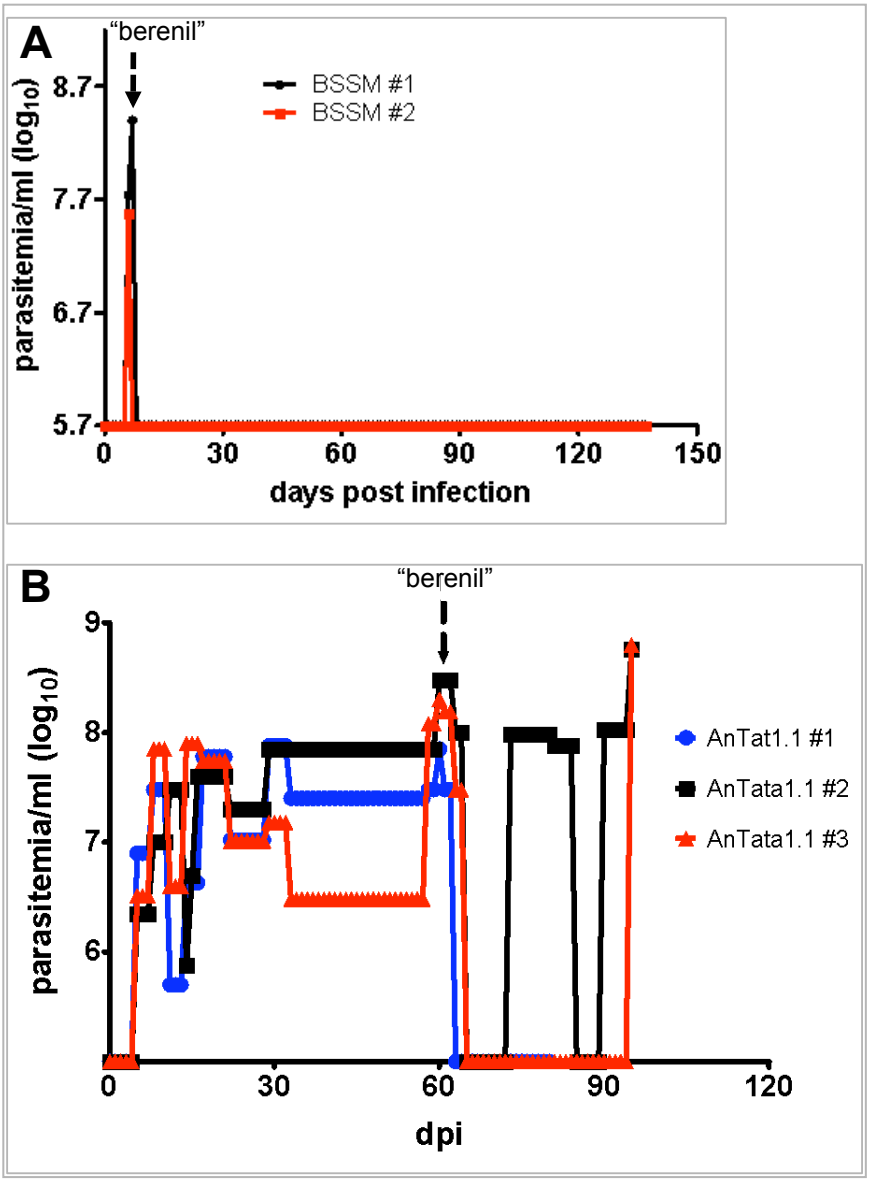

Figure 5. Berenil treatment of mice infected with BSSM or AnTat1.1 parasites.

Parasitemias of mice infected with BSSM (A) or AnTat1.1 (B) parasites. Mice were infected with BSSM or AnTat1.1 parasites at day 0 and then treated intraperitoneally with berenil (dotted arrow) after detection of parasitemia at day post infection (dpi) 6 or 7 (BSSM) or at dpi 60 (AnTat1.1). While BSSM-infected mice cleared bloodstream infection within 24h, bloodstream infection clearance was within 48h for AnTat1.1-infected mice. BSSM infections (A) never

relapsed although infections were kept for more than 120 days post berenil treatment. For AnTat1.1 infections (B), mouse #1 (blue line) was found dead with body lesions twenty days after berenil treatment (or dpi 81), probably resulting from fighting. Mouse #2 (black line) and #3 (red line) each showed relapse of infection, fourteen days after berenil treatment. The experiment was terminated thirty five days after berenil treatment, or at dpi 95.

CHAPTER 2 REFERENCES

Abdulla, M. H., O'Brien, T., Mackey, Z. B., Sajid, M., Grab, D. J. and McKerrow, J. H. (2008). "RNA interference of Trypanosoma brucei cathepsin B and L affects disease progression in a mouse model." PLoS Negl Trop Dis 2(9): e298.

Antoine-Moussiaux, N., Magez, S. and Desmecht, D. (2008). "Contributions of experimental mouse models to the understanding of African trypanosomiasis." Trends Parasitol 24(9): 411-418.

Bentivoglio, M., Grassi-Zucconi, G., Peng, Z. C., Bassetti, A., Edlund, C. and Kristensson, K. (1994). "Trypanosomes cause dysregulation of c-fos expression in the rat suprachiasmatic nucleus." Neuroreport 5(6): 712-714.

Blum, J., Schmid, C. and Burri, C. (2006). "Clinical aspects of 2541 patients with second stage human African trypanosomiasis." Acta Trop 97(1): 55-64.

Breidbach, T., Ngazoa, E. and Steverding, D. (2002). "Trypanosoma brucei: in vitro slender-to-stumpy differentiation of culture-adapted, monomorphic bloodstream forms." Exp Parasitol 101(4): 223-230.

Brooks, D. G., Teyton, L., Oldstone, M. B. and McGavern, D. B. (2005). "Intrinsic functional dysregulation of CD4 T cells occurs rapidly following persistent viral infection." J Virol 79(16): 10514-10527.

Dubois, M. E., Demick, K. P. and Mansfield, J. M. (2005). "Trypanosomes expressing a mosaic variant surface glycoprotein coat escape early detection by the immune system." Infect Immun 73(5): 2690-2697.

Emmer, B. T., Daniels, M. D., Taylor, J. M., Epting, C. L. and Engman, D. M. (2010). "Calflagin inhibition prolongs host survival and suppresses parasitemia in Trypanosoma brucei infection." Eukaryot Cell 9(6): 934-942.

Foote, S. J., Iraqi, F. and Kemp, S. J. (2005). "Controlling malaria and African trypanosomiasis: the role of the mouse." Brief Funct Genomic Proteomic 4(3): 214-224.

Goedbloed, E., Ligthart, G. S., Minter, D. M., Wilson, A. J., Dar, F. K. and Paris, J. (1973). "Serological studies of trypanosomiasis in East Africa. II. Comparisons of antigenic types of Trypanosoma brucei subgroup organisms isolated from wild tsetse flies." Ann Trop Med Parasitol 67(1): 31-43.

Gray, A. R. (1960). "Precipitating antibody in trypanosomiasis of cattle and other animals." Nature 186: 1058-1059.

Gray, G. D., Jennings, F. W. and Hajduk, S. L. (1982). "Relapse of monomorphic and pleomorphic Trypanosoma brucei infections in the mouse after chemotherapy." Z Parasitenkd 67(2): 137-145.

Greenblatt, H. C. and Rosenstreich, D. L. (1984). "Trypanosoma rhodesiense infection in mice: sex dependence of resistance." Infect Immun 43(1): 337-340.

Griffiths, S., Portman, N., Taylor, P. R., Gordon, S., Ginger, M. L. and Gull, K. (2007). "RNA interference mutant induction in vivo demonstrates the essential nature of trypanosome flagellar function during mammalian infection." Eukaryot Cell 6(7): 1248-1250.

Gruby, M. (1843). "Analysis and observation of a novel hematozoan species, *Trypanosoma sanguinis*." C R Hebd Seqnces Acad Sci 17:: 1134-1136.

Herbert, W. J. and Lumsden, W. H. (1968). "Infectivity and virulence of Trypanosoma (trypanozoon) brucei for mice. I. Comparison of two mouse strains." J Comp Pathol 78(3): 341-344.

Herbert, W. J. and Lumsden, W. H. (1976). "Trypanosoma brucei: a rapid "matching" method for estimating the host's parasitemia." Exp Parasitol 40(3): 427-431.

Inverso, J. A., De Gee, A. L. and Mansfield, J. M. (1988). "Genetics of resistance to the African trypanosomes. VII. Trypanosome virulence is not linked to variable surface glycoprotein expression." J Immunol 140(1): 289-293.

Jelinek, T., Bisoffi, Z., Bonazzi, L., van Thiel, P., Bronner, U., de Frey, A. et al. (2002). "Cluster of African trypanosomiasis in travelers to Tanzanian national parks." Emerg Infect Dis 8(6): 634-635.

Jennings, F. W., Rodgers, J., Bradley, B., Gettinby, G., Kennedy, P. G. and Murray, M. (2002). "Human African trypanosomiasis: potential therapeutic benefits of an alternative suramin and melarsoprol regimen." Parasitol Int 51(4): 381-388.

Jennings, F. W., Whitelaw, D. D., Holmes, P. H., Chizyuka, H. G. and Urquhart, G. M. (1979). "The brain as a source of relapsing Trypanosoma brucei infection in mice after chemotherapy." Int J Parasitol 9(4): 381-384.

Kennedy, P. G. (2007). "Animal models of human African trypanosomiasis--very useful or too far removed?" Trans R Soc Trop Med Hyg 101(11): 1061-1062.

MacGregor, P., Savill, N. J., Hall, D. and Matthews, K. R. (2011). "Transmission stages dominate trypanosome within-host dynamics during chronic infections." Cell Host Microbe 9(4): 310-318.

MacGregor, P., Szoor, B., Savill, N. J. and Matthews, K. R. (2012). "Trypanosomal immune evasion, chronicity and transmission: an elegant balancing act." Nat Rev Microbiol 10(6): 431-438.

Masocha, W., Amin, D. N., Kristensson, K. and Rottenberg, M. E. (2008). "Differential invasion of Trypanosoma brucei brucei and lymphocytes into the brain of C57BL/6 and 129Sv/Ev mice." Scand J Immunol 68(5): 484-491.

Masocha, W., Rottenberg, M. E. and Kristensson, K. (2007). "Migration of African trypanosomes across the blood-brain barrier." Physiol Behav 92(1-2): 110-114.

McCulloch, R., Vassella, E., Burton, P., Boshart, M. and Barry, J. D. (2004). "Transformation of monomorphic and pleomorphic Trypanosoma brucei." Methods Mol Biol 262: 53-86.

Morrison, L. J. and MacLeod, A. (2011). "African trypanosomiasis." Parasite Immunol 33(8): 421-422.

Poltera, A. A., Hochmann, A., Rudin, W. and Lambert, P. H. (1980). "Trypanosoma brucei brucei: a model for cerebral trypanosomiasis in mice--an immunological, histological and electronmicroscopic study." Clin Exp Immunol 40(3): 496-507.

Ralston, K. S., Kabututu, Z. P., Melehani, J. H., Oberholzer, M. and Hill, K. L. (2009). "The Trypanosoma brucei flagellum: moving parasites in new directions." Annu Rev Microbiol 63: 335-362.

Ralston, K. S., Kisalu, N. K. and Hill, K. L. (2011). "Structure-function analysis of dynein light chain 1 identifies viable motility mutants in bloodstream-form Trypanosoma brucei." Eukaryot Cell 10(7): 884-894.

Ralston, K. S., Lerner, A. G., Diener, D. R. and Hill, K. L. (2006). "Flagellar motility contributes to cytokinesis in Trypanosoma brucei and is modulated by an evolutionarily conserved dynein regulatory system." Eukaryot Cell 5(4): 696-711.

Rodgers, J. (2010). "Trypanosomiasis and the brain." Parasitology 137(14): 1995-2006.

Rodriguez, J. A., Lopez, M. A., Thayer, M. C., Zhao, Y., Oberholzer, M., Chang, D. D. et al. (2009). "Propulsion of African trypanosomes is driven by bihelical waves with alternating chirality separated by kinks." Proc Natl Acad Sci U S A 106(46): 19322-19327.

Salmon, D., Vanwalleghem, G., Morias, Y., Denoeud, J., Krumbholz, C., Lhomme, F. et al. (2012). "Adenylate cyclases of Trypanosoma brucei inhibit the innate immune response of the host." Science 337(6093): 463-466.

Schindler, R. and Sachs, R. (1970). "[Serologic studies in dogs after infection with Trypanosoma brucei]." Z Tropenmed Parasitol 21(4): 339-346.

Schindler, R., Schroder, G. and Stieger, R. (1970). "[Studies on immunity and serological reactions in monkeys after infection with Plasmodium cynomolgi bastianelli]." Z Tropenmed Parasitol 21(3): 239-245.

Stich, A., Abel, P. M. and Krishna, S. (2002). "Human African trypanosomiasis." BMJ 325(7357): 203-206.

WHO (2010). "Fact sheet no. 259 - African trypanosomiasis."

Wirtz, E., Leal, S., Ochatt, C. and Cross, G. A. (1999). "A tightly regulated inducible expression system for conditional gene knock-outs and dominant-negative genetics in Trypanosoma brucei." Mol Biochem Parasitol 99(1): 89-101.

Chapter 3

Mouse infection and pathogenesis by *Trypanosoma brucei* motility mutants

(Submitted for publication)

Abstract

The flagellum of *Trypanosoma brucei* is an essential and multifunctional organelle that drives parasite motility and is receiving increased attention as a potential drug target. In the mammalian host, parasite motility is suspected to contribute to infection and disease pathogenesis. However, it has not been possible to test this hypothesis owing to lack of motility mutants that are viable in the bloodstream life cycle stage that infects the mammalian host. We recently identified a bloodstream-form motility mutant in 427-derived *T. brucei* in which point mutations in the LC1 dynein subunit disrupt propulsive motility but do not affect viability. Here we demonstrate that the LC1 point mutant fails to show enhanced cell motility upon increasing viscosity of the surrounding medium, which is a hallmark of wild type *T. brucei*, thus indicating that motility of the mutant is fundamentally altered compared to wild type cells. We next used the LC1 point mutant to assess the influence of trypanosome motility on infection in mice. We surprisingly found that disrupting parasite motility has no discernible effect on *T. brucei* bloodstream infection. Infection time-course, maximum parasitemia, number of waves of parasitemia, clinical features and disease outcome are indistinguishable between motility mutant and control parasites. Our studies provide an important step toward understanding the contribution of parasite motility to infection and a foundation for future investigations of *T. brucei* interaction with the mammalian host.

Summary

Trypanosoma brucei is a deadly human pathogen that causes significant human mortality and limits economic development in some of the most impoverished regions of the world. Trypanosome motility is considered to be important for infection and pathogenesis. However, until the present work, it was not possible to test this hypothesis because all motility mutants generated previously were not viable. We recently overcame this barrier by identifying a viable motility mutant and in the present study, we have used this mutant to provide the first analysis of the impact of trypanosome motility on infection and pathogenesis. We found that normal motility is dispensable for trypanosome bloodstream infection and pathogenesis in mice. These studies represent an important contribution to understanding pathogenesis mechanisms and host-parasite interactions, and inform efforts to exploit the flagellum as a drug target.

Introduction

African trypanosomes, i.e. *Trypanosoma brucei* and related species, are protozoan parasites that cause sleeping sickness in humans and related diseases in wild and domestic animals. These parasites cause significant human mortality and limit economic development over vast regions of sub-Saharan Africa. Trypanosome infection of a mammalian host is a multistep process. Following transmission *via* the bite of an infected tsetse fly, the parasites must first establish and then maintain an infection in the bloodstream despite being extracellular and constantly exposed to the host immune system. Antigenic variation of the parasite surface coat and active clearance of host immunoglobulin bound to the parasite surface enable the trypanosome population to evade immune destruction and persist in the bloodstream indefinitely (Barry and McCulloch 2001; Borst 2002; Pays 2005). Bloodstream infection represents stage one of the disease and manifests clinically as flu-like symptoms with recurrent waves of fever and development of lymphadenopathy (Stich et al., 2002; Rodgers 2010). After a period of weeks to months, parasites penetrate the blood vessel endothelium and invade the central nervous system (CNS) (Stich et al., 2002; Rodgers 2010) bringing on stage two of the disease. During this stage, patients develop chronic meningoencephalitis with headaches and neurological changes that severely disturb sleep. Coma and death follow if the disease is left untreated (Stich et al., 2002; Rodgers 2010).

Trypanosomes are highly motile and the contribution of parasite motility to infection and pathogenesis is a long-standing question. Cell motility in *T. brucei* is driven by a single flagellum that runs alongside the cell and is laterally connected to the cell body (Ralston et al.,

2009). The *T. brucei* flagellum possesses a canonical "9 + 2" axoneme as the platform for assembly of dynein motors that drive flagellum beating (Supplemental Figure S1A-D) (Ralston et al., 2009). The prominent influence of the flagellum on trypanosome biology is apparent even in original descriptions of these organisms, which centered on their distinctive, helical cell locomotion as observed in blood samples from infected amphibians (Gruby 1843). In those studies the parasite's auger-like movement, twisting and rotating around its long axis as it moved forward, led to the genus name "*Trypanosoma*", which combines the Greek words *trypanon* (auger) and *soma* (body). Since then, parasite motility has captured the attention of many scientists and an "undulating membrane" (now known to correspond to the flagellum) is a prominent feature in most descriptions of these organisms. Early work by Walker (Walker 1961) demonstrated that motility is driven by a tractile flagellar beat that initiates at the tip of the flagellum and travels to the flagellum base, the opposite of what is seen in most other eukaryotic flagella. More recent analyses of *Trypanosoma brucei* motility using high-speed, high-resolution video microscopy provided adjustments to the original "auger-like" description and further emphasized that parasite motility is a prominent feature of these pathogens in the blood (Rodriguez et al., 2009; Uppaluri et al., 2011; Heddergott et al., 2012; Weisse et al., 2012).

Parasite motility is widely considered to be important for infection and pathogenesis in the mammalian host and motility functions of the trypanosome flagellum are receiving increasing attention as potential targets for therapeutic intervention (Broadhead et al., 2006; Ralston and Hill 2006; Ginger et al., 2008; Ralston et al., 2009). Specific requirements for motility in the mammalian host are not clear, but motility has been hypothesized to participate in parasite immune evasion and for penetration of the blood brain barrier and other extravascular

tissues. For example, parasite forward movement has been suggested to drive movement of surface-bound immunoglobulin to the posterior end of the cell, where it is internalized, thereby allowing the parasite to resist opsonization and immune destruction (Engstler et al., 2007). As an extracellular pathogen, *T. brucei* presumably depends on its own motility for penetration of the vascular endothelium and entry into the CNS. Recent studies have even suggested that *T. brucei* motility is adapted specifically to the bloodstream environment (Heddergott et al., 2012). Unfortunately, direct investigation of a requirement for parasite motility in any aspect of host infection or pathogenesis has not been possible, because of the lack of viable motility mutants in the bloodstream life cycle stage that infects the mammalian host (Ginger et al., 2008; Ralston and Hill 2008).

Parasite "motility" refers to propulsive translocation of the cell, rather than simple writhing of the cell body, which may be caused by uncontrolled flagellum beating. Indeed, all *T. brucei* motility mutants so far described retain a beating flagellum despite defects in sustained propulsive translocation of the cell (Hutchings et al., 2002; Branche et al., 2006; Broadhead et al., 2006; Ralston and Hill 2006; Ralston and Hill 2008). Most *T. brucei* motility mutants have been generated by RNAi knockdown of specific flagellar proteins and these knockdowns were lethal in bloodstream form cells, leading to the suggestion that disrupting motility is lethal (Branche et al., 2006; Broadhead et al., 2006; Ralston and Hill 2006; Ralston and Hill 2008). However, most if not all, *T. brucei* flagellar protein knockdowns have known or suspected structural defects, including some that are far more substantial than just loss of the targeted protein (Ralston and Hill 2008). Thus, it is not possible with RNAi alone to distinguish between phenotypes arising from defective motility versus pleotropic consequences of ablating target

gene expression.

We recently developed a system to study flagellum protein function that employs loss of function point mutants to replace an endogenous protein, rather than simply depleting proteins via RNAi (Ralston et al., 2011). As such, the system enables one to perturb protein function, while avoiding pleotropic structural defects that might arise when depleting building blocks of axonemal protein complexes. Using this system, we identified a point mutation, $K_{203}A/R_{210}A$, in the LC1 subunit of outer arm dynein (Supplemental Figure S1A-D) that disrupts cell motility, but does not disrupt the structure of outer arm dynein (Ralston et al., 2011). Bloodstream form LC1 $K_{203}A/R_{210}A$ mutants, henceforth referred to as "K/R" mutants, were generated by introducing a Tet-inducible copy of the mutant LC1 gene into a Tet-inducible LC1 knockdown line. Tet-induction in the parental LC1 knockdown is lethal, while tet-induction of the K/R mutant yields motility mutants that are viable, thereby offering a unique opportunity to examine the influence of motility on trypanosome infection (Ralston et al., 2011).

In the current work, we analyze parasite motility in multiple environments and demonstrate that motility in the K/R mutant is fundamentally altered compared to wild type cells. The motility defect of the LC1 K/R point mutant is at least as severe as that caused by LC1 knockdown, supporting the idea that lethality in the knockdown is not simply due to defective motility. We also exploit the availability of a viable *T. brucei* bloodstream-form motility mutant to directly test the requirement for parasite motility in mouse infection and pathogenesis. We find that, contrary to the prevailing notion, establishment and maintenance of infection in the bloodstream, as well as gross pathology and lethal outcome are indistinguishable between wild

type and motility mutant parasites.

Results

K/R mutant parasites exhibit similar extent of motility defect as knockdown parasites.

The contribution of parasite motility to *T. brucei* infection and pathogenesis in the mammalian host has not been studied. To address this question, we used the *T. brucei* K/R motility mutant, a conditional mutant that has normal motility in the absence of tetracycline, but defective motility in the presence of tetracycline (Ralston et al., 2011). As part of the current study, we performed an in-depth analysis of cell motility in the K/R mutant compared to parental LC1 knockdowns to assess the extent of the motility defect. We previously analyzed motility in K/R point mutants versus LC1 knockdowns at 24 hours post induction (hpi), but at this time point lethal cell division failure was already evident in the parental line and interfered with motility analysis (Ralston et al., 2011). We therefore examined motility at 12 hpi because at this time point a clear motility defect was evident in the parental line and cell division defects were not yet apparent (Figure 1). As shown in Figure 1 and Supplemental Videos 1, 2, and 4, motility K/R mutants and LC1 knockdown parasites at 12 hpi both have erratic flagellum beating that does not drive cell propulsion. Knockdown parasites are inviable owing to cell division failure that is evident within 26 hpi (Figure 1A, D and Supplemental Video 3), while K/R mutants remain viable. By 72 hpi, the motility defect is even more pronounced in K/R mutants (Figure 1J and supplemental video 5). In all cases, the flagellum beats rapidly, but the cells lack cell propulsion (Supplemental Video 5). We also examined flagellar beating using high speed, 1000 frames per second (fps), video microscopy (Supplemental Video 6). This analysis revealed slower flagellar beating and flagellum tip movements that did not propagate along the cell in

knockdown and K/R mutant cells compared to wild type. However, we could not discern a specific beat feature that distinguished LC1 knockdown versus point mutant cells.

The K/R mutant motility defect manifests in the bloodstream environment.

The environment encountered by parasites in an animal host differs from that of culture medium and these differences can influence parasite motility. For example, the viscosity of blood is significantly higher than that of culture medium and a hallmark of *T. brucei* motility is that cell velocity and propulsive motility increase with increasing viscosity of the medium (Heddergott et al., 2012). The ability of the parasite to increase motility when viscosity is raised is a consequence of the distinctive auger-like motility of the organism and is also observed for other microbes, such as spirochetes, that move via spiral cell motility (Berg and Turner 1979). As a context for mouse infection experiments, we therefore considered the possibility that increased viscosity might rescue the motility defect of K/R mutants. To test this, we examined parasite motility in normal medium versus medium in which viscosity was increased by adding 0.4 % methyl cellulose to approximate the viscosity of blood (Heddergott et al., 2012). In the presence of methyl cellulose, induced K/R cells exhibited a pronounced motility defect relative to uninduced controls (Figure 2 and Supplemental Figure S1E). This defect was evident when assessed by motility traces and total distance traveled (Figure 2A-B), but is most clearly evident when assessed by mean squared displacement, which measures propulsive motility (Figure 2C). Moreover, while addition of methylcellulose increased motility of uninduced cells, it did not significantly increase motility of induced cells. Therefore, rather than being rescued, the motility

defect of induced K/R mutants relative to control cells was more pronounced in the presence of methylcellulose.

Another difference in blood versus culture medium is that blood presents a heterogeneous environment, owing to the presence of red blood cells and other cell types. These external obstacles influence microbial cell motility (Berg and Turner 1979; Heddergott et al., 2012). We therefore examined motility of induced and uninduced K/R parasites in whole blood. The density of red blood cells made it impossible to reliably trace individual trypanosomes using dark field illumination as was done for parasites in culture medium. To overcome this, we generated a K/R mutant cell line that constitutively expresses mCherry fluorescent protein, thereby allowing us to track trypanosome cell movements using fluorescent microscopy. We then examined motility of parasites in whole blood. Both uninduced and induced cells showed increased motility in blood than was observed for parasites in culture medium. Nonetheless, induced K/R cells exhibited a clear motility defect relative to uninduced controls even in whole blood (Figure 3 and Supplemental Videos 7).

To compare the extent to which cell motility is disrupted in different environments, we determined the mean squared displacement slope for induced relative to uninduced cells in each condition, culture medium with or without methylcellulose, and whole blood (Figure 3D). The combined data show that the LC1 K/R mutant exhibits a motility defect that is at least as pronounced as that of the parental LC1 knockdown and further, that this defect is manifest in culture medium with or without methyl cellulose, as well as in whole blood (Figure 3D). Given that this motility defect is penetrant even in whole blood, the K/R mutant presents a unique

opportunity for assessing the impact of parasite motility on mouse infection.

Motility mutants establish bloodstream infection and cause trypanosomiasis pathology in mice.

K/R mutants that were uninduced or induced for 72 hours with tetracycline were used to infect mice as described in Methods. Following infection, mice were examined and parasitemia was determined daily. For - Tet controls, parasitemia was first detected by four days post infection and mice usually developed a single wave of unremitting parasitemia with terminal outcome by 7 – 8 days post-infection (Figure 4A-B). One mouse in each group exhibited two waves of parasitemia, but in no case did infected mice clear the second wave or survive longer than 14 days. These infection parameters mimic what we observed with the parental blood stream single marker (BSSM) trypanosome cell line (not shown) and are consistent with previous studies using BSSM *T. brucei* (Emmer et al., 2010). In + Tet mice the infection time-course, maximum parasitemia, number of waves of parasitemia and mouse survival times were indistinguishable from – Tet controls (Figure 4A-B). In the single case where two waves of parasitemia were observed, the VSG expressed by the infecting population was lost in the second wave (Figure 4C), indicating that VSG switching remains active in the K/R mutant.

Splenomegaly and anemia are hallmark clinical features of trypanosomiasis in many hosts including humans (Amole et al., 1982) and we therefore examined infected mice for these pathologies. Mice infected with K/R mutants and treated with tetracycline exhibited weight loss,

anemia and splenomegaly that were indistinguishable from that observed in control (- Tet) infections (Figure 4D-F). We did not observe any discernible difference in mouse behavior between - Tet and + Tet infections. Hepatomegaly was not observed in either group of mice (not shown). Therefore, + Tet mice infected with K/R mutants established bloodstream infection and showed clinical features of trypanosomiasis that parallel that observed with – Tet control infections.

Infection of mice by + Tet K/R motility mutants was a surprising result. We considered the possibility that the mouse environment might select for revertants with wild type motility and these wild type parasites are responsible for the infection. We also considered the possibility that Tet was somehow not effective under the conditions used. If either of these situations occurred, parasites from infected +Tet mice would no longer exhibit a motility defect. We therefore examined motility and protein expression in parasites taken directly from infected mice. As shown in figure 5, K/R mutants taken directly from + Tet mice retained the motility defect (Figure 5A-B and Supplemental Videos 8-9) and expression of mutant LC1 protein (Figure 5C) that were observed in culture. As an independent test, we asked whether Tet treatment was able to clear infection by the parental LC1 knockdown line as well as Tet-inducbile trypanin knockdown parasites, both of which are non-viable under +Tet conditions (Ralston et al., 2011). In both cases, Tet treatment cleared the infection within 24 hr of treatment and no revertant cells emerged (Figure 5D and Supplemental Figure S1F). Therefore, using multiple independent tests, Tet was effective under the conditions used and mouse infection did not simply select for revertants.

DISCUSSION

African trypanosomes are deadly pathogens and infection of the mammalian host proceeds via multiple steps. Following a tsetse bite, parasites must first establish infection in the bloodstream and then defend against a potent immune response in order to maintain the infection. Subsequently, parasites invade extravascular tissues, including the CNS, leading to host tissue damage, neurologic dysfunction and an ultimately lethal outcome (Stich et al., 2002; Rodgers 2010). Here we used trypanosome motility mutants in a mouse infection model to examine impact of parasite motility on the first of these steps, namely establishment and maintenance of a bloodstream infection. We also examined pathogenic features and progression to terminal outcome. Surprisingly, infection dynamics, including time-course, maximum parasitemia, and number of waves of parasitemia, as well as pathological features and mouse survival rates were indistinguishable between control and motility mutant parasites.

Parasite motility is generally considered to be important for infection and motility functions of the trypanosome flagellum are considered candidate targets for therapeutic intervention (Broadhead et al., 2006; Ralston and Hill 2006; Ginger et al., 2008). Our studies present the first direct tests of the role for parasite motility in mouse infection and were made possible by availability of viable bloodstream-form motility mutants (Ralston et al., 2011). Previously, *T. brucei* motility mutants were generated using RNAi to simply deplete endogenous flagellar proteins and this is lethal in cultured bloodstream form cells, thereby limiting their utility for mouse infection studies. The K/R mutant differs in that the endogenous LC1 protein is replaced with a non-functional mutant and this mutant is viable (Ralston et al., 2011).

The induced K/R mutant retains some residual motility and we cannot rule out the possibility that this is enough to support any motility needs for bloodstream infection. However, induced K/R mutant parasites exhibit a pronounced motility defect relative to control cells under all conditions examined, i.e. culture medium alone, culture medium containing methyl cellulose to increase viscosity, whole blood and in diluted blood taken directly from infected mice. The defect is at least as severe as that seen in the parental LC1 knockdown line, which is non-viable. Moreover, induced K/R mutants do not show significant increase in velocity or propulsive motility when the viscosity of culture medium is raised. In contrast, cell velocity and propulsive motility of control trypanosomes increase when viscosity of the culture medium is raised (Figure 2) owing to specific features of the parasite's cell propulsion mechanism (Berg and Turner 1979; Heddergott et al., 2012). Thus, in addition to the decrease in cell motility the mechanism of cell movement in induced K/R mutants is fundamentally altered compared to control cells.

We considered the possibility that infection is caused by revertants, which might arise for example if cells become insensitive to tetracycline, become resistant to RNAi, or develop mechanisms to overcome LC1 functional defects. This was not the case, because K/R mutants taken directly from infected mice retain their motility defect. Likewise, revertants did not develop during infection with two independent tet-inducible RNAi lines. Moreover, mice infected with K/R mutants do not show any delay in time course of infection that would be expected if revertants had to emerge. Our findings therefore demonstrate that *T. brucei* can accommodate severe disruptions in motility mechanism and overall capacity for cell movement without affecting bloodstream infection.

While not essential for survival in the bloodstream during acute infection, we favor the idea that parasite motility is required for subsequent steps of infection, such as persistence in the bloodstream during a chronic infection (MacGregor et al., 2011) or penetration of the CNS (Jennings et al., 1979). For example, trypanosome forward motility facilitates removal of host immunoglobulin from the cell surface in culture (Engstler et al., 2007) and this activity likely enables parasite persistence in the bloodstream over extended periods in the face of potent immune responses by the host. Persistent infection also enables CNS invasion (Jennings et al., 1982) . It is generally thought that *T. brucei* requires more than two weeks to gain access to brain tissue (Jennings et al., 1979; Poltera et al., 1980; Gray et al., 1982), although this has been debated recently (Frevert et al., 2012). Rapid progression of infection with 427-derived parasites used in our studies, with maximum mouse survival ≤14 days, precludes reliable assessment CNS penetration, and additional work with motility mutants in chronic infection models (Jennings et al., 1979; Gray et al., 1982; MacGregor et al., 2011) will be required. *T. brucei* isolates that give chronic infection have historically been recalcitrant to molecular genetic manipulation, although advances in this direction have been made recently (Macgregor et al., 2013). 427-derived parasites were selected for our studies because of their experimental tractability and because they allowed the first-ever direct analysis of motility in any aspect of *T. brucei* infection. The demonstration here that induced K/R mutants are viable and mammalian-infectious will now enable studies of parasite motility in chronic infection models.

The role of parasite motility in infection and pathogenesis of trypanosomiasis is a longstanding question that has not previously been amenable to experimental investigation. As

such, development of a motility mutant infection model describe here provides an important foundation for future studies of flagellum biology in the context of host infection.

Experimental procedures:

Ethics Statement. All animal experiments strictly complied with the Institutional Animal Care and Use Committee of University of California, Los Angeles (Approved protocol permit: ARC # 2001-065).

Trypanosome culture. Cultivation, transfection and RNAi induction of trypanosomes in culture were done as described previously (Ralston et al., 2006). The *T. brucei* bloodstream trypanin knockdown, LC1 knockdown, LC1-K203A/R210A (K/R) motility mutant and bloodstream single marker (BSSM), cells were described previously (Wirtz et al., 1999; Ralston et al., 2011). K/R-mCherry cells were generated by stable transfection of K/R cells with the pNKmCherry plasmid (described below). To generate pNKmCherry, the mCherry gene (accession number AY678264) was PCR amplified from pmCherry plasmid (Hajagos et al., 2012) and cloned into the expression vector pHD496-H (Hutchings et al., 2002) using the Hind*III* and Bam*HI* cloning sites. pHD496-H contains a ribosomal RNA promoter to drive constitutive expression of the mCherry gene and a hygromycin-resistance cassette to enable selection (Biebinger and Clayton 1996; Hutchings et al., 2002). Primers used to PCR amplify mCherry are as follow: 5' ATGGTGAGCAAGGGCGAGG 3' (forward primer), 5' TTACTTGTACAGCTCGTCCATGC 3' (reverse primer). All DNA sequences were verified by direct sequencing.

Mouse infections. Mouse infections were done essentially as described (Dubois et al., 2005). BALB/c female mice (The Jackson Laboratory, Bar Harbor, ME), 6 to 10 weeks old, were injected intraperitoneally with 100 parasites in 0.2 ml cold phosphate buffered saline (PBS) (pH 7.4) supplemented with 1% glucose. To maintain cell viability in PBS, parasites were kept on ice prior to injection into mice. For + Tet infections, parasites were induced with 1 μg/ml

tetracycline in culture three days prior to injection into mice and mice received 1 mg/ml doxycycline in their drinking water 5 to 7 days prior to infection and throughout the course of infection. Parasitemia was monitored daily beginning 3 days post infection using an improved Neubaeur hemocytometer (Herbert and Lumsden 1976). After euthanasia, mice were weighed and tissues were collected for weighing. For trypanin knockdown and LC1 knockdown infections, parasites were maintained in culture without tetracycline and mice received 1 mg/ml doxycycline in drinking water only when animals showed the first wave of parasitemia.

Parasite motility assays. Knockdown, K/R and K/R-mCherry parasites were grown without or with tetracycline to a density of 1.5-2.0 x 10^6 cells/ml and cell motility analysis was done at the hours post induction (hpi) described in each figure. For methyl cellulose experiments, cells were maintained with or without addition of 0.4% (v/v) to approximate the viscosity of blood (Heddergott et al., 2012). For mCherry K/R parasites, cells (50 microliters) were added to freshly drawn, undiluted mouse blood (500 microliters). All samples were analyzed in a pre-warmed motility chambers within 5 minutes after collection. Motility traces were done as described (Ralston et al., 2011). Briefly, parasites were examined in motility chambers using dark field optics on a Zeiss Axioskop II compound microscope with a 10x objective (Figures 1 and 2) or using fluorescence optics on a Zeiss Axiovert 200 M inverted microscope with a 20x objective (Figure 3). Videos were captured using a COHU analog video camera. Analog format movies were converted to digital format with an ADVC-300 digital video converter (Canopus, Co., Ltd.). Movies were recorded at 30 frames per second (fps) and converted to AVI format and then to stacks of TIFF images using Adobe Premiere Elements software (Adobe Systems). TIFF image stacks were analyzed using Metamorph software (Molecular Devices) to trace parasite

movement over the indicated time period. Trace data were used to calculate the total distance travelled, as well as the mean squared displacement (MSD) of individual cells in the x and y dimensions. MSD was calculated according to the formula $MSD = \langle r_i(t)^2 \rangle = \langle (p_i(t) - p_i(0))^2 \rangle$, where r_i is the distance travelled by the parasite over time interval t and p_i is the position of the parasite at any given time. For figures 1 and 2, the timescale of t ranged from 1 to 25 seconds in increments of 1 second. For figures 3 and 5, the timescale of t ranged from 1 to 8 seconds in increments of 0.3 second. MSD is calculated for each instance i of a given time interval. Several cell MSDs were then averaged to obtain an ensemble average.

For motility experiments on parasites from mouse infections (Figure 5), blood samples were collected from infected mice 7-13 days post infection (dpi). Samples were kept at 37°C and analyzed in a pre-warmed motility chamber within 5 to 10 minutes after collection. To record motility traces, blood samples were diluted 1:100 in warm HMI-9 culture medium to enable tracing of individual parasites among red blood cells and videos were recorded and processed as described above, using differential interference contrast (DIC) optics on a Zeiss Axiovert 200 M inverted microscope with a 100x oil-immersion objective. For high-resolution videos of individual cells (Supplemental Videos 1-9), videos were captured in motility chambers using DIC optics (Supplemental Videos 1-6, 8-9) or using fluorescence optics (Supplemental Videos 7) on a Zeiss Axiovert 200 M inverted microscope with a 100x oil-immersion (Supplemental Videos 1-6, 8-9) or 20x (Supplemental Videos 7) objective.

Hi-speed videos: The experimental setup used to record high-speed trypanosome motility consists of an inverted DMI6000 B microscope (Leica Microsystems, Wetzlar, Germany) equipped with a 100X objective (Leica HCX PL APO 100x/1.40-0.70 oil) and Differential interference Contrast (DiC) optics, a halogen-based white trans-illumination system

and a PC-controlled Photron FocusScope SV200-i high-speed CMOS camera (Photron USA Inc.) mounted in the trinocular port. The images provided by the high-speed camera are directly observed in the PC monitor. System control is achieved through the Photron FASTCAM Viewer software (PFV Version 3). Images were captured at 1,000 frames per sec (fps) with 512 x 512 pixel image resolution.

Western blot analysis of parasites from mice. Western blots were done as described previously (Ralston et al., 2011). To obtain parasites from mice, mice were euthanized and blood was collected in heparinized tubes 7-13 days post infection. Parasites were separated from whole blood using DE 52 anion exchange columns, as described (Lanham and Godfrey 1970). Purified parasites were examined with a microscope to assess purity and parasite yield was determined by counting in a hemocytometer. Purified parasites were washed three times in PBS and then boiled in Laemmli sample buffer for Western blot analysis. Blots were probed with anti-HA monoclonal antibody (Covance) at 1:5000 diliution, anti- β-tubulin monoclonal antibody (Developmental Studies Hybridoma Bank, University of Iowa) at 1:5000 diliution, or anti-variable surface glycoprotein VSG 221 (McDowell et al., 1998) at 1:100,000 dilution

Statistical analysis. Statistical analysis and graphical output was done with GraphPad Prism 5. The significance of survival was determined by Log-rank (Mantel-Cox) Test. We used the Student unpaired two-tailed t test to determine significant differences in motility. The significance of total body weight, spleen weight, liver weight, and number of red blood cells was calculated by one-way ANOVA with Bonferroni's post-test for multiple comparisons. Significance (p value) is reported in each figure.

ACKNOWLEDGMENTS

Funding for this work was supplied by grants to K.L.H. from the Burroughs Wellcome Fund and NIH-NIAID (AI052348). Neville K. Kisalu is a recipient of the Shapiro Fellowship and the UCLA Dissertation Year Fellowship. Gerasimos Langousis is recipient of the Warsaw fellowship. We are grateful to John Mansfield and Karen Demick (University of Wisconsin) for guidance with mouse infections. We thank Jose Rodriguez (UCLA) for technical support with motility trace analysis. We thank Josh Beck (UCLA) for kindly providing us with the mCherry DNA. We are also appreciative of Shimon Weiss (UCLA) and members of our laboratory for pertinent comments on the work and critical reading of the manuscript. High-speed video microscopy was performed at the California NanoSystems Institute Advanced Light Microscopy/Spectroscopy and the Macro-Scale Imaging Shared Facilities at UCLA. Auhors have no conflict of interest.

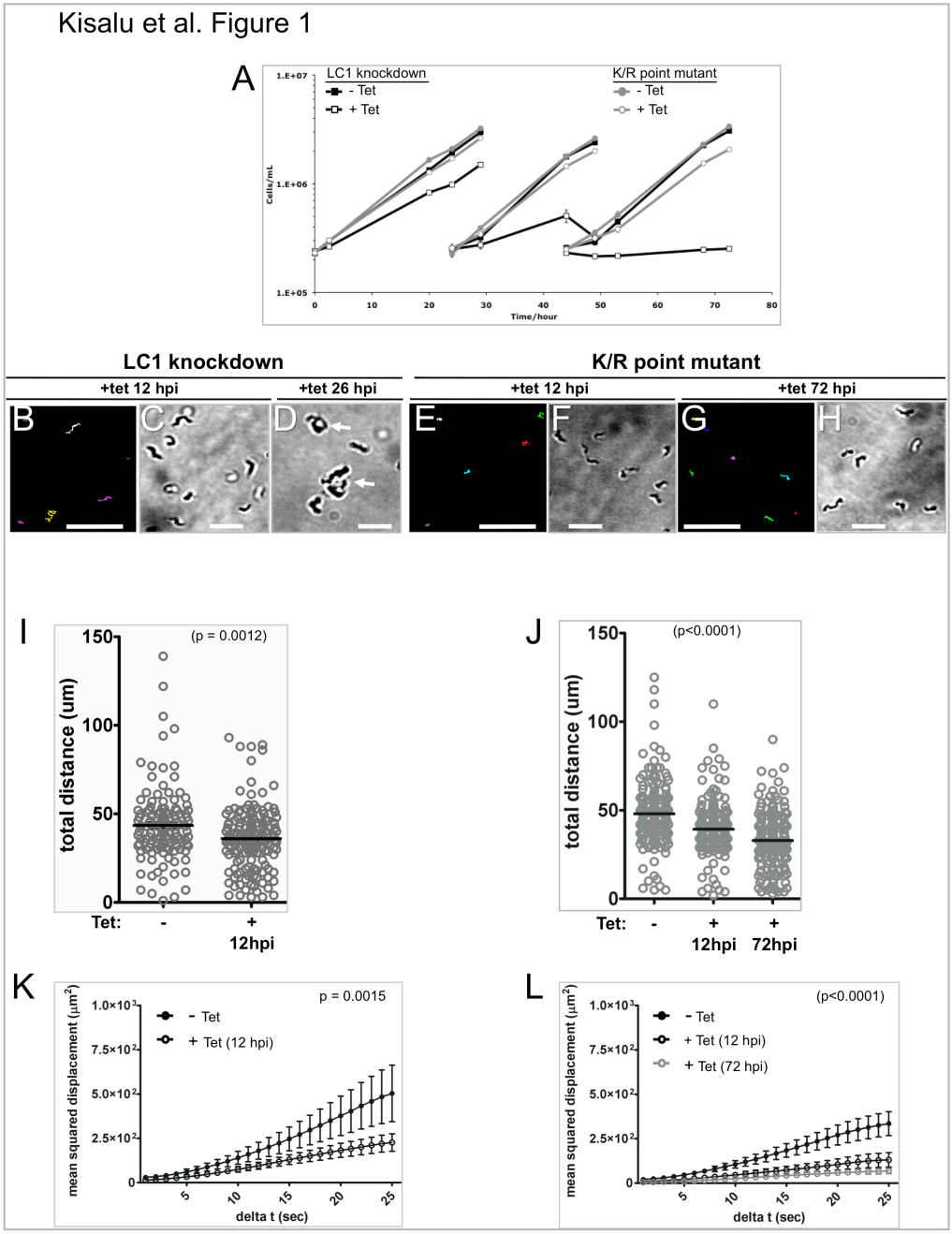

Figure 1. LC1 knockdown and LC1 K/R point mutant parasites show similar motility defects but the knockdown is lethal, while the point mutant is viable. (A) Growth rates of LC1-knockdown cells (black lines) and K/R point mutants (gray lines). At time zero cultures were incubated with (open symbols) or without (closed symbols) tetracycline and diluted back to the starting density at 24 h and 48 h. (B, E and G) Motility traces of LC1 knockdown and LC1

K/R point mutant parasites grown with Tet for the indicated hours post-induction (hpi). Each line traces the path of a single cell for 30 seconds. (C, D, F, and H) DIC images of cultures grown with tetracycline for the indicated hpi. Arrows in panel D show cells accumulating as amorphous masses, indicating cell division failure by 26hpi for the LC1 knockdown. Scale bar is 95 um (panels B, E and G) or 25 μm (panels C, D, F and H). (I and J) Quantification of distance traveled in 30 seconds by individual LC1 knockdown (I) and K/R point mutant (J) cells grown in the absence (-) or presence (+) of Tet for the indicated times. For the LC1 knockdown, n=126 for –Tet and 159 for +Tet. For the K/R point mutant, n=180 for –Tet, 167 for +Tet(12hpi) and 190 for +Tet(72hpi). Horizontal lines indicate the mean of each data set, with bars showing the 95% confidence interval. (K and L) Mean squared displacement plotted as a function of time interval for LC1 knockdown (K) and K/R point mutant (L) trypanosomes grown without (closed circles) or with (open circles) Tet for the indicated time. n=52 for all samples and error bars show standard error of the mean.

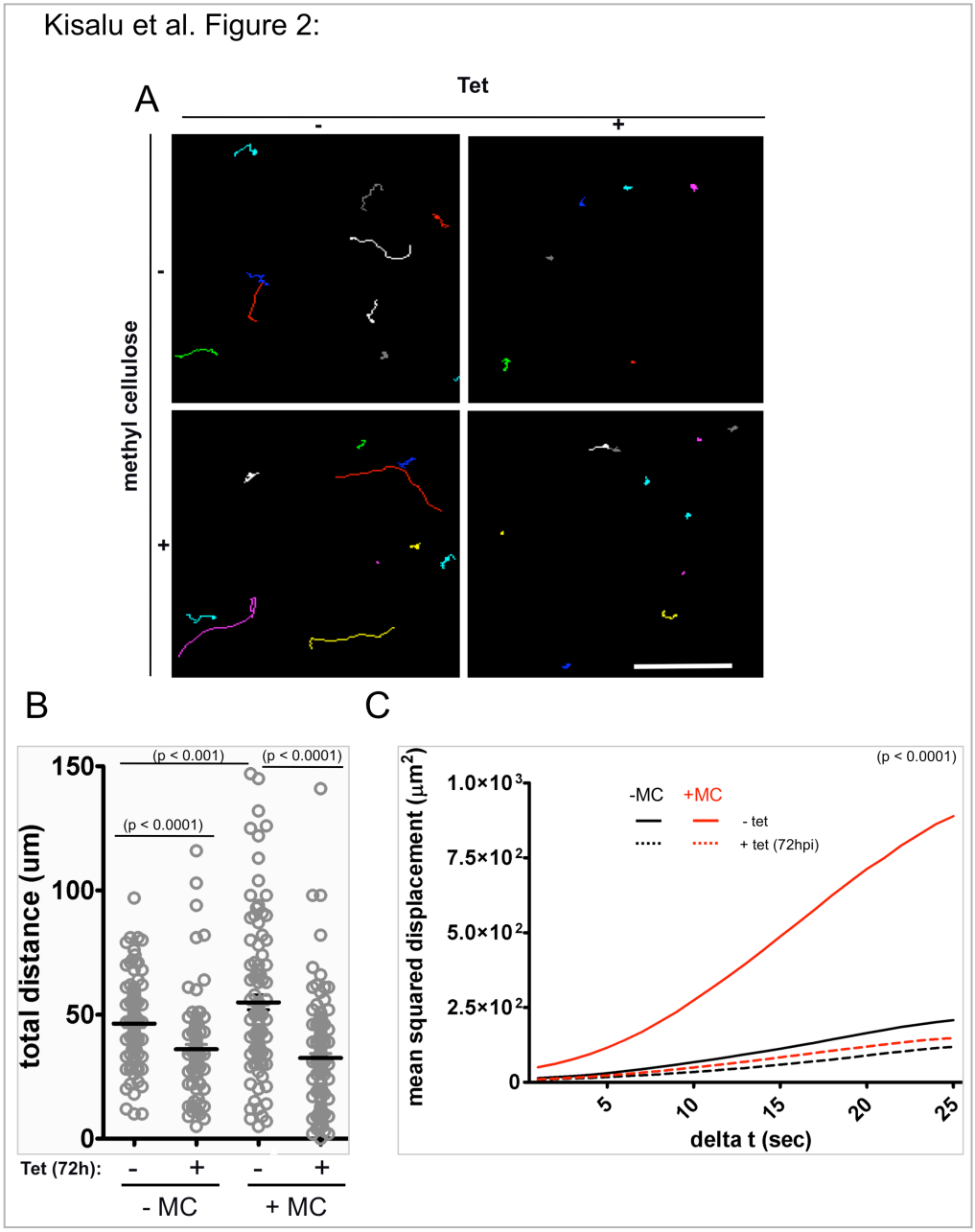

Figure 2. Increasing viscosity improves motility of control (-Tet) but not of K/R mutant parasites in culture. (A) Motility traces of K/R parasites grown with or without tetracycline for 72 hours as indicated and with or without methyl cellulose (0.4%, w/v) as indicated. Each line traces the path of a single cell for 30 seconds. Scale bar is 100um. (B) Quantification of distance traveled in 30 seconds by uninduced (-) and Tet-induced (+) K/R mutants measured in

the absence (-MC) or presence (+MC) of methyl cellulose. For samples in the absence of MC, n=112 for –Tet and 96 for +Tet. For samples with MC, n=102 for –Tet and 126 for +Tet). (C) Mean squared displacement plotted as a function of time interval for K/R point mutants maintained in the absence (solid lines) or presence (dashed lines) of Tet and measured without (black lines) or with (red lines) methyl cellulose (MC). n = 52 cells for each culture. For clarity, error bars are not shown, but are provided in supplemental figure S1E.

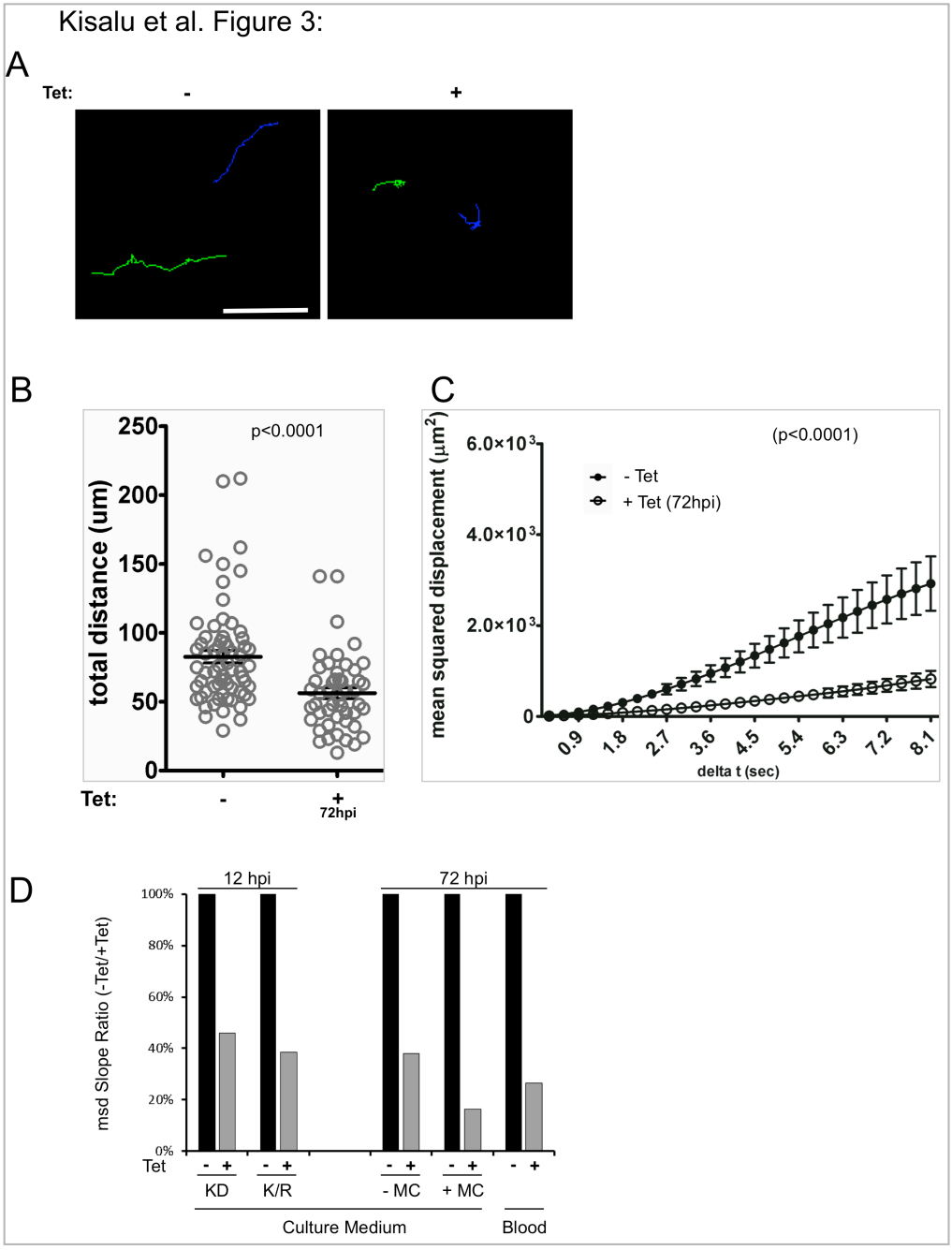

Figure 3. K/R mutant parasites exhibit defective motility in whole blood. (A) Motility traces of K/R point mutants expressing mCherry and maintained in the absence (-Tet) or presence (+Tet) of tetracycline for 72 hours. Motility traces were done in undiluted whole blood. Each line traces the path of single cell for 11 seconds. Scale bar, 50 μm. (B) Quantification of

distance traveled in 11 seconds by uninduced (-) and or Tet-induced (+, 72hpi) mCherry K/R mutants measured in whole blood. n = 66 for –Tet and n=50 for +Tet. (C) Mean squared displacement is plotted as a function of time interval for uninduced (-Tet, closed symbols) and Tet-induced (+Tet 72hpi, open symbols) mCherry K/R point mutants measured in blood. n = 52 cells for each culture. n=52 for –Tet and 50 for +Tet and error bars show standard error of the mean, $p < 0.0001$. (D) Comparison of the mean squared displacement analyses for LC1 knockdown (KD) and K/R point mutants (K/R) grown in the absence (-) or presence (+) of tet for the indicated hours post induction (hpi). MSD analyses are from figures 1K-L, 2C and 3C, done in culture medium with (+MC) or without (-MC) methyl cellulose, or in whole blood (blood) as indicated. The culture medium –MC slope data are the average from figure 1L and 2C msd analyses. For each condition, the slope of the best fit line through the msd data is plotted as a percentage of the slope of the –Tet sample for that condition. A decrease in slope indicates decreased propulsive motility.

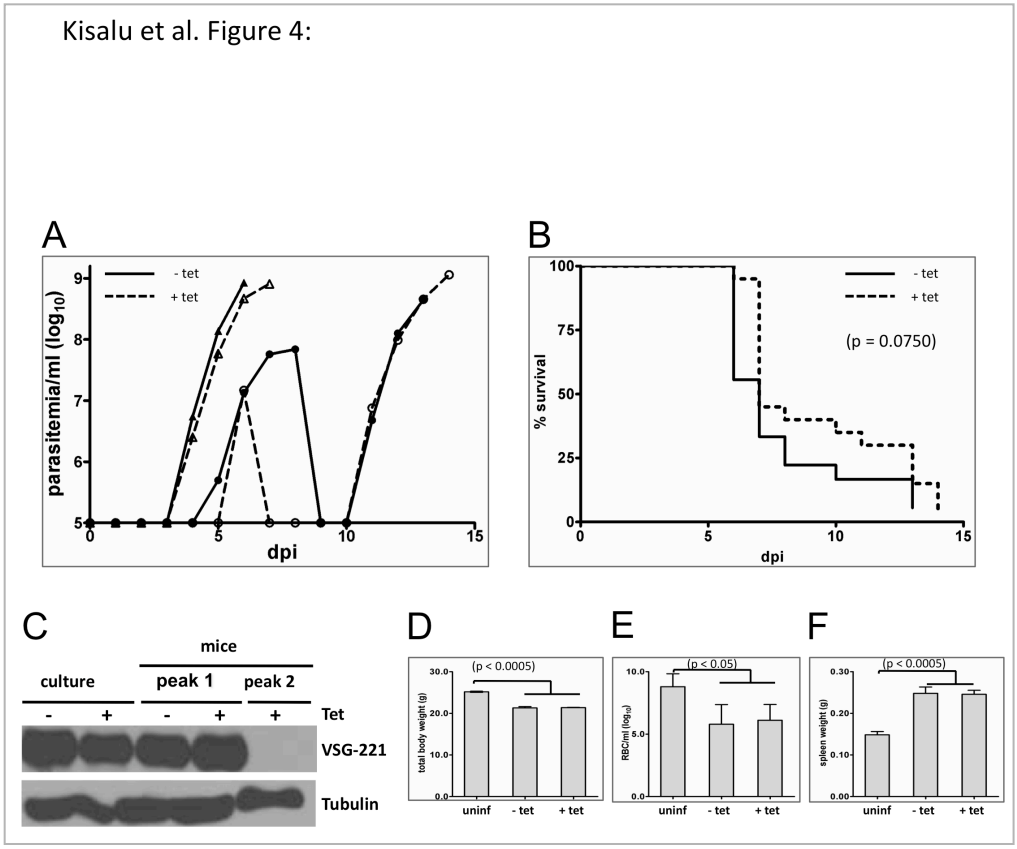

Figure 4. Motility is dispensable for infection and pathogenesis. (A) Parasitemias of mice infected with K/R point mutants. Mice were maintained without tetracycline (solid lines, - Tet) or with tetracycline (dashed lines, + Tet) in the drinking water. Mice were infected at day 0 and parasitemia was determined beginning three days post infection (dpi). Representative data are shown for two – Tet and + Tet mice from a total of 18 –Tet and 20 +Tet infections. Typically, mice exhibited a single wave of parasitemia (triangles) but one mouse in each group showed two waves (circles). (B) Survival curves for all K/R-infected mice, maintained without tetracycline (-Tet, solid lines, n = 18) or with tetracycline (+Tet, dashed line, n = 20) in the drinking water. Any differences were not significant ($p = 0.0750$). One mouse in each group did not show detectable parasitemia. (C) Western blot of total protein prepared from K/R point mutants grown in culture (culture) or purified from infected mice (mice) maintained with (+) or without (-) Tet.

Parasites from mice were taken at parasitemia peak 1 or peak 2 as indicated. Blots were probed with antibody against VSG221 or β-tubulin as a loading control. (D-F) Uninfected mice (uninf) or mice infected with K/R point mutants maintained without (- Tet) or with (+ Tet) tetracycline, were examined for total body weight (D) anemia (E) and spleen weight (F). Body weight and spleen weight were determined seven dpi. (Uninfected mice n = 3; mice infected with K/R mutants - Tet n = 4; + Tet n = 6.). Anemia was assessed seven dpi. (Uninfected mice n = 4; - Tet infections n = 5; + Tet infections n = 7.) Error bars show standard deviation.

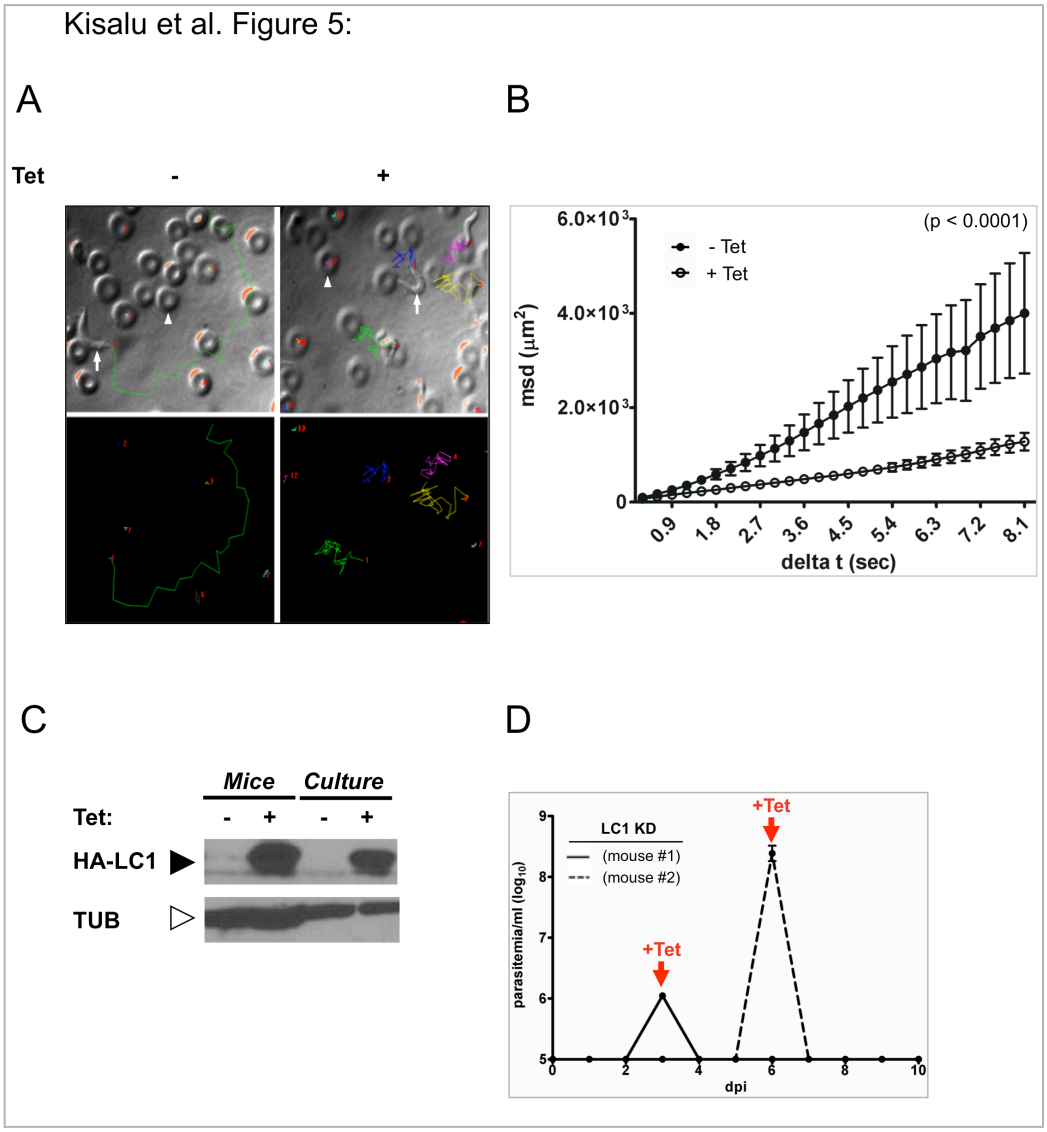

Figure 5. Defective motility in K/R point mutants from infected mice. (A) Motility traces of K/R parasites taken from infected mice that were maintained without (- Tet) or with (+Tet) tetracycline in the drinking water. Each line traces the path of single cell over 8.1 seconds. Upper panels show traces overlaid on phase contrast images. Representative trypanosomes (arrows) and red blood cells (arrowheads) are indicated. Lower panels show traces. Each line color represents a different cell. (B) Mean squared displacement is plotted as a function of time

interval for K/R parasites from infected mice, maintained with (+Tet, open circles, n = 39 parasites) or without (-Tet, closed symbols, n = 17) tetracycline in the drinking water. Error bars show standard error of the mean, $p < 0.0001$. (C) Western blot of total protein from K/R parasites purified from infected mice or maintained in culture. Tetracycline was provided in the mouse drinking water or culture medium as indicated. Blots were probed with antibody against the HA epitope to detect HA-LC1, or β-tubulin as a loading control. (D) Parasitemias of two mice infected with LC1 knockdown parasites (LC1-KD). Mice were infected with LC1-KD parasites at day 0 and then treated with tetracycline in drinking water upon detection of parasites in blood (+Tet arrows). Mice cleared infection within 24 h of tetracycline treatment, demonstrating the efficacy of tetracycline treatment.

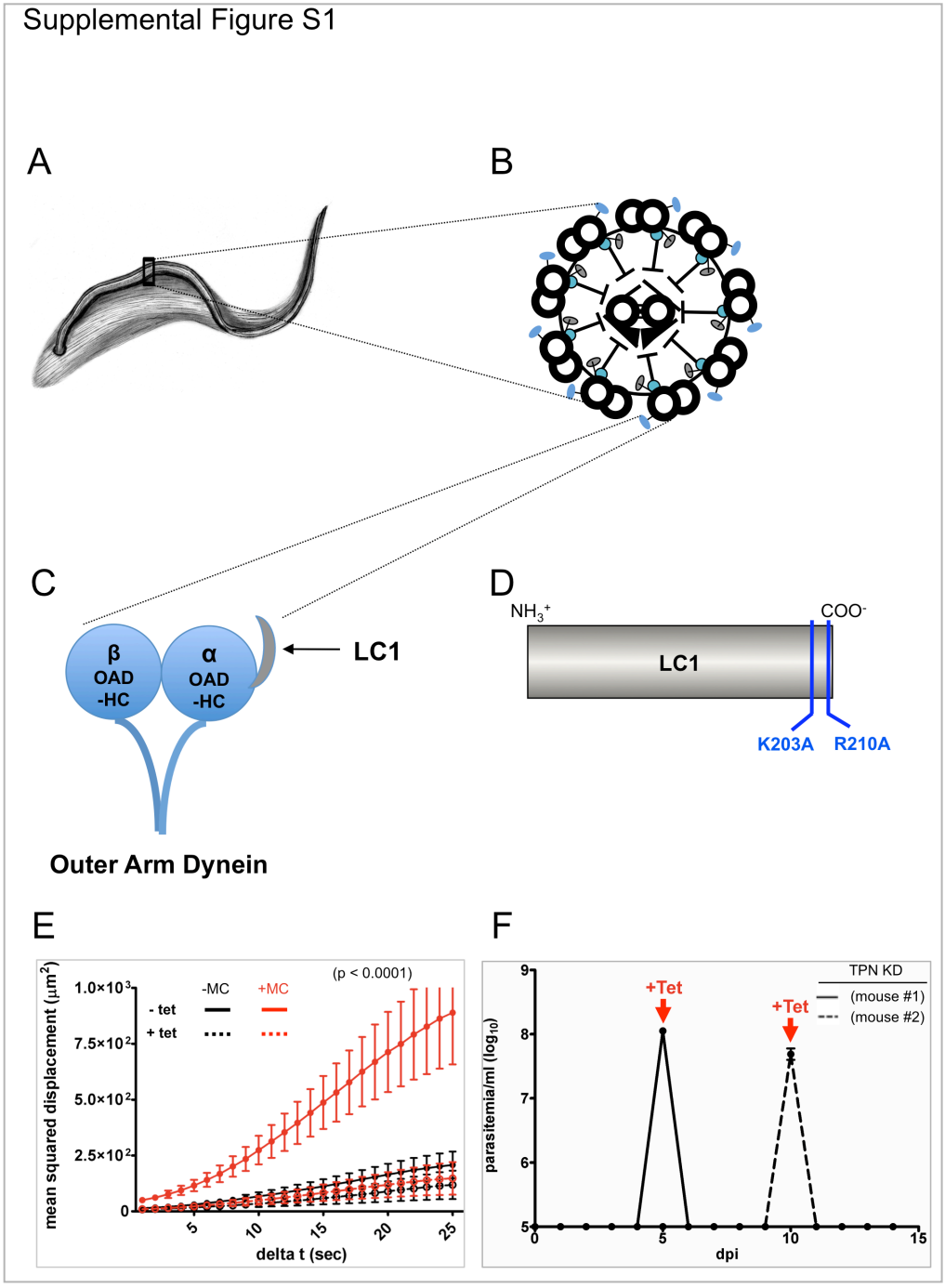

Supplemental Figure S1.

(A) Cartoon of a *T. brucei* cell. (B) A schematic diagram of an axoneme cross section as would be observed looking posterior to anterior near the boxed region in (A). (C) Simplified diagram of outer arm dynein, showing the two heavy chains (α and β) and the location of LC1. (D) LC1

schematic showing residues mutated in the K/R mutant used in this study. Panel A adapted from (Hill et al., 2000) with permission. (E) Mean squared displacement of K/R parasites in media without or with methyl cellulose. Same graph as shown in Figure 2C, but including error bars that show standard error of the mean (SEM). See figure 2C legend for details. (F) Tetracycline treatment clears infection by trypanin knockdown parasites. Parasitemias of two mice infected with trypanin knockdown parasites (TPN-KD). Mice were infected with TPN-KD parasites at day 0 and then treated with tetracycline in drinking water upon detection of parasites in blood (+Tet arrows). Mice cleared infection within 24 h of tetracycline treatment, demonstrating the efficacy of tetracycline treatment.

Supplemental Videos

Video 1. Wild type motility of LC1 knockdown trypanosomes in –Tet cultures.

Representative live video shows propulsive motility of LC1 knockdown parasites taken from –Tet cultures. Parasites move rapidly and translocate with tip of flagellum leading. Frame rate for capture and playback is 30 frames/sec.

Video 2. Defective motility of LC1 knockdown trypanosomes from +Tet cultures (12 hpi)

Representative live video shows defective motility of LC1 knockdown parasites grown in +Tet cultures for 12 hours. Flagellum beating is evident, but parasite propulsive motility is disrupted. Frame rate for capture and playback is 30 frames/sec.

Video 3. Defective motility by LC1 knockdown trypanosomes from +Tet cultures (26 hpi)

Representative live video shows cell division failure of LC1 knockdown parasites grown in +Tet cultures for 26 hours. Cells accumulate as an amorphous mass, but the flagella continue to beat vigorously. Frame rate for capture and playback is 30 frames/sec.

Video 4. Defective motility by by K/R trypanosomes from +Tet cultures (12 hpi).

Representative live video shows defective motility of K/R parasites grown in +Tet cultures for 12 hours. Flagellum beating is evident, but parasite propulsive motility is disrupted. Frame rate for capture and playback is 30 frames/sec.

Video 5. Defective motility by K/R trypanosomes from +Tet cultures (72 hpi).

Representative live video shows defective motility of K/R parasites grown in +Tet cultures for

72 hours. Flagellum beating is evident, but parasite propulsive motility is disrupted. Frame rate for capture and playback is 30 frames/sec.

Video 6. Combined high-speed videos of flagellar beating in minus Tet (control) trypanosomes, LC1 Knockdown and K/R trypanosomes from +Tet cultures. The first clip (from 0 to 8 seconds) shows representative flagellar beating in control cells (LC1 grown in the absence of Tet). Tip-to-base flagellar beats are evident. The second clip (from 10 to 18 seconds) shows representative flagellar beating in LC1 knockdown parasites grown in +Tet cultures for 12 hours. The third clip (from 20 to 28 seconds) shows representative flagellar beating in K/R parasites grown in +Tet cultures for 12 hours. The fouth clip (from 31 to 39 seconds) shows representative flagellar beating in K/R parasites grown in +Tet cultures for 72 hours. For all videos, frame rate for capture is 1000 frames/sec and playback is 60 frames/sec.

Video 7. Combined videos show wild type motility of mCherry K/R trypanosomes from -Tet cultures and defective motility of mCherry K/R trypanosomes from +Tet cultures (72 hpi) in whole blood. The first clip (from 0 to 5 seconds) shows representative motility of mCherry K/R trypanosomes from -Tet cultures, added to mouse blood. Parasites move rapidly and translocate with tip of flagellum leading. Frame rate for capture and playback is 30 frames/sec. The second clip (from 7 to 12 seconds) shows representative motility of mCherry K/R trypanosomes from +Tet cultures, added to mouse blood. Flagellum beating is evident, but parasite propulsive motility is disrupted. Frame rate for capture and playback is 30 frames/sec. For both videos, cultured trypanosomes were added directly to whole blood.

Video 8. Wild type motility of K/R trypanosomes from –Tet mouse infections.

Representative live video shows propulsive motility of parasites taken from mice infected with K/R trypanosomes and maintained without tetracycline. Parasites move rapidly and translocate with tip of flagellum leading. Samples were taken seven days post-infection. Red blood cells are readily distinguishable from parasites as biconcave disks. Frame rate for capture and playback is 30 frames/sec.

Video 9. Defective motility of K/R trypanosomes from +Tet mouse infections.

Representative live video shows defective motility of parasites taken from mice infected with K/R trypanosomes and maintained with tetracycline in the drinking water. Flagellum beating is evident, but parasite propulsive motility is blocked. Samples were taken seven days post-infection. Red blood cells are readily distinguishable from parasites as biconcave disks. Frame rate for capture and playback is 30 frames/sec.

CHAPTER 3 References

Amole, B. O., Clarkson, A. B., Jr. and Shear, H. L. (1982). "Pathogenesis of anemia in Trypanosoma brucei-infected mice." Infect Immun 36(3): 1060-1068.

Barry, J. D. and McCulloch, R. (2001). "Antigenic variation in trypanosomes: enhanced phenotypic variation in a eukaryotic parasite." Adv Parasitol 49: 1-70.

Berg, H. C. and Turner, L. (1979). "Movement of microorganisms in viscous environments." Nature 278(5702): 349-351.

Biebinger, S. and Clayton, C. (1996). "A plasmid shuttle vector bearing an rRNA promoter is extrachromosomally maintained in Crithidia fasciculata." Exp Parasitol 83(2): 252-258.

Borst, P. (2002). "Antigenic variation and allelic exclusion." Cell 109(1): 5-8.

Branche, C., Kohl, L., Toutirais, G., Buisson, J., Cosson, J. and Bastin, P. (2006). "Conserved and specific functions of axoneme components in trypanosome motility." J Cell Sci 119(Pt 16): 3443-3455.

Broadhead, R., Dawe, H. R., Farr, H., Griffiths, S., Hart, S. R., Portman, N. et al. (2006). "Flagellar motility is required for the viability of the bloodstream trypanosome." Nature 440(7081): 224-227.

Dubois, M. E., Demick, K. P. and Mansfield, J. M. (2005). "Trypanosomes expressing a mosaic variant surface glycoprotein coat escape early detection by the immune system." Infect Immun 73(5): 2690-2697.

Emmer, B. T., Daniels, M. D., Taylor, J. M., Epting, C. L. and Engman, D. M. (2010). "Calflagin inhibition prolongs host survival and suppresses parasitemia in Trypanosoma brucei infection." Eukaryot Cell 9(6): 934-942.

Engstler, M., Pfohl, T., Herminghaus, S., Boshart, M., Wiegertjes, G., Heddergott, N. and Overath, P. (2007). "Hydrodynamic flow-mediated protein sorting on the cell surface of trypanosomes." Cell 131(3): 505-515.

Frevert, U., Movila, A., Nikolskaia, O. V., Raper, J., Mackey, Z. B., Abdulla, M. et al. (2012). "Early invasion of brain parenchyma by african trypanosomes." PLoS One 7(8): e43913.

Ginger, M. L., Portman, N. and McKean, P. G. (2008). "Swimming with protists: perception, motility and flagellum assembly." Nat Rev Microbiol 6(11): 838-850.

Gray, G. D., Jennings, F. W. and Hajduk, S. L. (1982). "Relapse of monomorphic and pleomorphic Trypanosoma brucei infections in the mouse after chemotherapy." Z Parasitenkd 67(2): 137-145.

Gruby, M. (1843). "Analysis and observation of a novel hematozoan species, *Trypanosoma sanguinis*." C R Hebd Seqnces Acad Sci 17:: 1134-1136.

Hajagos, B. E., Turetzky, J. M., Peng, E. D., Cheng, S. J., Ryan, C. M., Souda, P. et al. (2012). "Molecular dissection of novel trafficking and processing of the Toxoplasma gondii rhoptry metalloprotease toxolysin-1." Traffic 13(2): 292-304.

Heddergott, N., Kruger, T., Babu, S. B., Wei, A., Stellamanns, E., Uppaluri, S. et al. (2012). "Trypanosome motion represents an adaptation to the crowded environment of the vertebrate bloodstream." PLoS Pathog 8(11): e1003023.

Herbert, W. J. and Lumsden, W. H. (1976). "Trypanosoma brucei: a rapid "matching" method for estimating the host's parasitemia." Exp Parasitol 40(3): 427-431.

Hill, K. L., Hutchings, N. R., Grandgenett, P. M. and Donelson, J. E. (2000). "T lymphocyte-triggering factor of african trypanosomes is associated with the flagellar fraction of the cytoskeleton and represents a new family of proteins that are present in several divergent eukaryotes." J Biol Chem 275(50): 39369-39378.

Hutchings, N. R., Donelson, J. E. and Hill, K. L. (2002). "Trypanin is a cytoskeletal linker protein and is required for cell motility in African trypanosomes." J Cell Biol 156(5): 867-877.

Jennings, F. W., Gray, G. D. and Whitelaw, D. D. (1982). "Chemotherapy of Trypanosoma brucei in mice with diminazene aceturate. Variation in the aparasitaemic period over 5 years." Z Parasitenkd 67(3): 337-340.

Jennings, F. W., Whitelaw, D. D., Holmes, P. H., Chizyuka, H. G. and Urquhart, G. M. (1979). "The brain as a source of relapsing Trypanosoma brucei infection in mice after chemotherapy." Int J Parasitol 9(4): 381-384.

Lanham, S. M. and Godfrey, D. G. (1970). "Isolation of salivarian trypanosomes from man and other mammals using DEAE-cellulose." Exp Parasitol 28(3): 521-534.

Macgregor, P., Rojas, F., Dean, S. and Matthews, K. R. (2013). "Stable transformation of pleomorphic bloodstream form Trypanosoma brucei." Mol Biochem Parasitol 190(2): 60-62.

MacGregor, P., Savill, N. J., Hall, D. and Matthews, K. R. (2011). "Transmission stages dominate trypanosome within-host dynamics during chronic infections." Cell Host Microbe 9(4): 310-318.

McDowell, M. A., Ransom, D. M. and Bangs, J. D. (1998). "Glycosylphosphatidylinositol-dependent secretory transport in Trypanosoma brucei." Biochem J 335 (Pt 3): 681-689.

Pays, E. (2005). "Regulation of antigen gene expression in Trypanosoma brucei." Trends Parasitol 21(11): 517-520.

Poltera, A. A., Hochmann, A., Rudin, W. and Lambert, P. H. (1980). "Trypanosoma brucei brucei: a model for cerebral trypanosomiasis in mice--an immunological, histological and electronmicroscopic study." Clin Exp Immunol 40(3): 496-507.

Ralston, K. S. and Hill, K. L. (2006). "Trypanin, a component of the flagellar Dynein regulatory complex, is essential in bloodstream form African trypanosomes." PLoS Pathog 2(9): e101.

Ralston, K. S. and Hill, K. L. (2008). "The flagellum of Trypanosoma brucei: new tricks from an old dog." Int J Parasitol 38(8-9): 869-884.

Ralston, K. S., Kabututu, Z. P., Melehani, J. H., Oberholzer, M. and Hill, K. L. (2009). "The Trypanosoma brucei flagellum: moving parasites in new directions." Annu Rev Microbiol 63: 335-362.

Ralston, K. S., Kisalu, N. K. and Hill, K. L. (2011). "Structure-function analysis of dynein light chain 1 identifies viable motility mutants in bloodstream-form Trypanosoma brucei." Eukaryot Cell 10(7): 884-894.

Ralston, K. S., Lerner, A. G., Diener, D. R. and Hill, K. L. (2006). "Flagellar motility contributes to cytokinesis in Trypanosoma brucei and is modulated by an evolutionarily conserved dynein regulatory system." Eukaryot Cell 5(4): 696-711.

Rodgers, J. (2010). "Trypanosomiasis and the brain." Parasitology 137(14): 1995-2006.

Rodriguez, J. A., Lopez, M. A., Thayer, M. C., Zhao, Y., Oberholzer, M., Chang, D. D. et al. (2009). "Propulsion of African trypanosomes is driven by bihelical waves with alternating chirality separated by kinks." Proc Natl Acad Sci U S A 106(46): 19322-19327.

Stich, A., Abel, P. M. and Krishna, S. (2002). "Human African trypanosomiasis." BMJ 325(7357): 203-206.

Uppaluri, S., Nagler, J., Stellamanns, E., Heddergott, N., Herminghaus, S., Engstler, M. and Pfohl, T. (2011). "Impact of microscopic motility on the swimming behavior of parasites: straighter trypanosomes are more directional." PLoS Comput Biol 7(6): e1002058.

Walker, P. J. (1961). "Organization of function in trypanosome flagella." Nature 189: 1017-1018.

Weisse, S., Heddergott, N., Heydt, M., Pflasterer, D., Maier, T., Haraszti, T. et al. (2012). "A quantitative 3D motility analysis of Trypanosoma brucei by use of digital in-line holographic microscopy." PLoS One 7(5): e37296.

Wirtz, E., Leal, S., Ochatt, C. and Cross, G. A. (1999). "A tightly regulated inducible expression system for conditional gene knock-outs and dominant-negative genetics in Trypanosoma brucei." Mol Biochem Parasitol 99(1): 89-101.

Chapter 4

Generating viable bloodstream form motility mutants in pleomorphic *Trypanosoma brucei*

Abstract

Entry of *Trypanosoma brucei* in the host system nervous central (CNS) is a defining step in pathogenesis of trypanosomiasis as it indicates establishment of the final and fatal stage of the disease. Parasite flagellar motility is suspected to play a role in CNS invasion by *T. brucei* but this hypothesis remains untested. We previously identified the first-ever viable bloodstream motility mutant or K/R (Appendix 2) that allowed to directly examine the requirement of parasite motility in pathogenesis in the mammalian host. Using the K/R we have demonstrated that disrupting parasite motility is dispensable for establishment of infection in the mouse bloodstream (Chapter 3). K/R mutant cells derived from the laboratory-adapted strain 427-BSSM that causes an acute infection that progress rapidly in mice. This accelerated disease progression precludes any reliable assessment of the CNS penetration, which generally takes more than 14 days. Additionally the K/R mutant is an RNAi-based cell line. The RNAi approach requires several genetic manipulations in *T. brucei*. In order to determine a requirement of flagellar motility in the CNS invasion, we elected to employ a gene "knock-in" strategy to generate motility mutants in chronic infection or pleomorphic *T. brucei* strains that can invade the brain. This approach bypasses the need for RNAi. Application of the "gene knock-in" strategy allowed replacement of endogenous WT LC1 allele with an HA epitope-tagged copy harboring the K/R mutation in both BSSM and AnTat1.1 pleomorphic. Importantly, upon integration of the mutant at a single allele in BSSM and AnTat1.1 yielded mutants with defective motility. The *T. brucei* flagellum has emerged as an attractive drug target candidate. Construction of motility mutants in pleomorphic *T. brucei* parasites that cause chronic infection will now enable, for the first time, to test if blocking parasite motility blocks invasion of the CNS.

Introduction

African trypanosomes, *Trypanosoma brucei*, are protozoan parasites that cause African sleeping sickness, a disease with devastating health and economic consequences. The disease is always fatal unless treated and existing drugs are toxic and associated with drug resistance [Ralston and Hill 2008]. Trypanosomes are transmitted between human hosts by a tsetse fly insect vector and entry into specific tissues mediates parasite development in the insect and pathogenesis in the mammalian hosts [Hill]. Trypanosomes are extracellular during all stages of infection and rely on their own flagellum-dependent motility to penetrate host tissues. Recent investigations of the flagellum identified conserved and novel proteins [Broadhead et al., 2006; Ralston and Hill 2006; Baron et al., 2007; Oberholzer et al., 2011]. They also discovered novel functions for the flagellum in cell morphogenesis, cell division, immune evasion, and sensing [Kohl et al., 2003; Broadhead et al., 2006; Ralston and Hill 2006; Ralston and Hill 2008; Oberholzer et al., 2011]. Thus, the flagellum and flagellar motility are extremely important for parasite biology and disease pathogenesis. These findings also showed the flagellum is essential and led to the idea that the flagellum and its many proteins represent novel drug targets [Kohl et al., 2003; Broadhead et al., 2006; Ralston and Hill 2006; Griffiths et al., 2007]. Unfortunately, capitalizing on these discoveries has been hampered because no-one has been able to generate motility mutants that are viable in the BSF life cycle stage, i.e. the stage that infects mammals. More broadly, it has been very challenging to determine specific mechanisms of flagellum protein function, because systems for routine structure-function analysis of flagellar proteins are lacking.

RNAi knockdown of flagellar proteins is usually lethal in bloodstream form (BSF) *T. brucei* cells in culture [Branche et al., 2006; Broadhead et al., 2006; Ralston and Hill 2006], causing speculation that normal motility is essential [Broadhead et al., 2006; Ralston and Hill 2006]. However, loss of flagellar proteins also causes structural defects [Bastin et al., 1996; Ralston and Hill 2006; Baron et al., 2007; Ralston and Hill 2008] and it is not clear if lethality is caused by defects in motility, or is a pleotropic effect of flagellum protein knockdown, for example occurring as a result of structural defects. Distinguishing between these explanations is important for investigating a fundamental aspect of trypanosome biology and exploiting the flagellum as a drug target. To address this question, we established in *T. brucei* a system that allows replacement of an endogenous protein with a mutated version [Ralston et al., 2011] (Appendix 1). The mutant protein lacks function, but still assembles in the flagellum, allowing us to separate phenotypes caused by loss of function versus structural defects. With this strategy we identified amino acids in the axonemal dynein light chain 1, "LC1", that are required for motility (Appendix 2) [Ralston et al., 2011]. Notably, while LC1 knockdown causes loss of the entire outer arm dynein motor, expression of the LC1-K203A/R210A point mutant (aka K/R) supports dynein assembly, but does not support normal motility. In BSF cells LC1 knockdown is lethal, while the LC1 K/R mutant disrupted motility defects but did not affect viability (Appendix 2) [Ralston et al., 2011]. These results demonstrate that disrupting motility in BSF cells is not lethal, and indicate that pleotropic effects of knockdown, such as structural defects, are the cause of lethality in flagellum protein knockdowns.

The K/R BSF motility mutant provided the first-ever opportunity to directly study the role of motility in pathogenesis in the mammalian host, which is a topic of Chapter 3. Using the

K/R mutant for mouse infections, we showed that parasite motility is dispensable for *T. brucei* infection in the bloodstream (Chapter 3). We were next interested in whether parasite motility is required for invasion of the CNS. However, The K/R motility mutant was generated using 427-derived BSSM *T. brucei* [Wirtz et al., 1999], which causes an acute infection in mice, with lethal outcome generally seen in seven days. This poses a problem for CNS invasion studies, because penetration of the blood brain barrier takes >14 days [Jennings et al., 1979; Poltera et al., 1980]. Therefore, although the K/R mutant is good for analysis of bloodstream infection, rapid progression of infection (Chapter 3) unfortunately prevented assessment of the CNS invasion. To allow assessment of the requirement of parasite motility in the CNS invasion we therefore developed an alternate approach for generating motility mutants that does not require RNAi and can be readily applied to pleomorphic trypanosome strains capable of infecting the host CNS.

Here we apply a targeted gene "knock-in" approach to generate motility mutants without needing to employ RNAi and the genetic manipulations that Tet-inducible RNAi entails in *T. brucei*. We replaced one endogenous WT LC1 allele with an HA epitope-tagged copy harboring the K/R mutation. We did this both in BSSM trypanosomes and in AnTat1.1 pleomorphic trypanosomes. HA-LC1-K/R is expressed from the endogenous promoter and correctly localizes to the flagellum. Interestingly, both the BSSM and AnTat1.1 LC1 mutants are defective in motility upon integration of the mutant at a single allele, demonstrating that the K/R mutation is dominant negative, as observed for the analogous mutation in *Chlamydomonas* [Patel-King and King 2009]. Availability of motility mutants in a pleomorphic *T. brucei* line that causes chronic infection, will enable direct investigation of the role motility plays in blood-brain barrier traversal by African trypanosomes.

Results

Construction of targeting plasmids for gene replacement in *T. brucei*

Mammalian-infectious form trypanosomes are profoundly sensitive to disruption of flagellar proteins [Broadhead et al., 2006; Ralston and Hill 2006; Ralston and Hill 2008], as knockdown almost invariably is lethal. On the other hand expression of point mutants that block function is tolerated when structural integrity is maintained (Appendix 2) [Ralston et al., 2011]. In prior studies we used tet-inducible RNAi together with tet-inducible protein expression to express an outer dynein LC1 point mutant in a background where endogenous LC1 expression was ablated in BSF *T. brucei* (Appendix 2) [Ralston et al., 2011]. The approach was successful at generating viable motility mutants in BSF *T. brucei*. However, the approach required a specialized BSF cell line genetically engineered to enable tet-inducible RNAi and tet-inducible gene expression [Wirtz et al., 1999] and was thus not generally applicable to pleomorphic cell lines. Since the time we initiated our original studies, it has been demonstrated that the the analogous LC1 K/R point mutation in *C. reinhardtii* is dominant negative [Patel-King and King 2009]. We therefore reasoned that if the K/R mutation was likewise dominant in *T. brucei*, motility mutants could be constructed simply by replacing one wild type LC1 allele with the K/R mutant, thereby simplifying genetic manipulation to a single stable transfection, which is readily achieved in pleomorphic *T. brucei*.

We generated constructs for knockin of LC1 K/R mutants (Figure 1A). The constructs contain a full LC1 open reading frame, with an N-terminal HA tag and harbouring the K/R mutation, followed by intergenic region and a selectable drug resistance marker. The entire

cassette is flanked by LC1 5'UTR and 3'UTR sequences from upstream and downstream of the LC1 gene to allow replacement of the endogenous gene by homologous recombination. Homologous recombination for gene deletion is a well-established approach in T brucei [Oberholzer et al., 2009]..

Generating K/R knock-in mutants in monomorphic (BSSM) trypanosomes

The K/R knockin was first introduced into BSSM parasites because of its experimental tractability and because we knew that the mutant could be supported in this line even without the endogenous protein, thereby providing a suitable line for testing the knockin strategy. Motility of the BSSM line is also extremely well-characterized, facilitating analysis of any motility defects in culture [Hill 2003; Kohl et al., 2003; Branche et al., 2006; Ralston and Hill 2006; Griffiths et al., 2007; Rodriguez et al., 2009; Emmer et al., 2010; Ralston et al., 2011; Heddergott et al., 2012; Hughes et al., 2012]. BSSM cells were initially transfected with the K/R cassette, which includes the K/R mutant LC1 gene (Methods) and phleomycin resistant clones were selected. PCR analysis demonstrated successful insertion of the knock-in construct at the LC1 locus, resulting in replacement of one WT LC1 allele (Figure 1B). Next we assessed whether the K/R mutant gene is expressed in the transfected cells. Western blot experiments using anti-HA antibodies established that K/R mutant protein is produced in these cells (Figure 2A). The growth rates of K/R knock in parasites were indistinguishable from those of the parental BSSM cells (Figure 2B).

In the flagellated protist *Chlamydomonas reinhardtii,* mutations analogous LC1-K/R

have been shown to be dominant negative, with mutants showing motility defects [Patel-King and King 2009]. To determine if the K/R mutation exerts a dominant negative effect on motility in *T. brucei*, we conducted a functional analysis for motility in K/R knock-in BSSM trypanosomes. Motility analysis demonstrated these cells are defective in propulsive motility (Figure 3A-B), as observed previously for the mutant expressed in absence of wild type protein (Appendix 2) [Ralston et al., 2011]. .

Generating K/R knockin motility mutants in pleomorphic trypanosomes

We next introduced LC1-K/R motility mutants into Antat1.1 (Figure 1A-B) parasites to allow direct investigation of the requirement of parasite motility in CNS penetration. As for the BSSM cells, preliminary data show that AnTat1.1 parasites exhibit defective motility upon integration of the mutant at a single allele.

Discussion

To allow determination of the role of parasite motility in the blood-brain barrier traversal, we have applied a targeted gene replacement strategy to generate motility mutants in pleomorphic AnTAt 1.1 parasites that are established as a mouse CNS infection model. Our targeted gene knock out strategy provides a more suitable alternative to knockdowns that require more elaborate genetic manipulation [Ralston et al., 2011]. We have demonstrated by PCR analysis that the K/R mutant integrated correctly into the LC1 locus in both the BSSM and AnTat1.1 cells. Additionally, western blot analysis revealed that the HA-tagged LC1-K/R protein is expressed well in BSSM cells. Although assessment and quantification of the motility defect in AnTat1.1 is currently underway, we have already shown in bloodstream form BSSM that K/R is a dominant-negative mutation, since expression of this mutation at a single allele disrupts motility, but these mutant parasites are viable in culture. Initial examination of the Antat1.1 K/R mutant indicates it too has defective motility. Construction in motility mutants in TREU667 [Jennings et al., 1979], another pleomorphic cell line suitable for chronic infection model is underway.

CNS invasion is a critical step in the pathogenesis of trypanosomiasis as it signals establishment of the lethal phase of the disease. CNS penetration also limits the number of drugs available for treatment because after *T. brucei* invades the CNS, drugs that do not cross the blood brain barrier are ineffective against this pathogen. Furthermore, parasites within the CNS may persist after drug treatment and CNS infection is known to be a source of infection relapse [Jennings et al., 1979; Gray et al., 1982; Rodgers 2010]. Unfortunately, despite the crucial role of

CNS invasion to disease pathogenesis and potential for therapeutic intervention, the mechanisms and route by which trypanosomes traverse the blood brain barrier are unclear.

Much of our knowledge on how trypanosomes gain access to the CNS comes from animal infection models because of the inability to directly visualize parasites in the brain tissues of human patients. A few routes for CNS penetration have been suggested [Mulenga et al., 2001; Frevert et al., 2005; Wolburg et al., 2012]. In the first model [Mulenga et al., 2001; Frevert et al., 2005] trypanosomes enter endothelial tight junctions of the blood-brain barrier within brain microvessels to directly penetrate the brain parenchyma. Another model proposes that trypanosomes first penetrate epithelial tight junctions of blood-CSF-barrier in the choroid plexus to invade the CSF from where parasites enter the brain parenchyma [Wolburg et al., 2012]. Parasite motility is believed to be essential for CNS invasion in both models. With the identification here of motility mutants in pleomorphic BSF *T. brucei* that causes chronic infection, it will now make it possible for the first time to test this hypothesis and that is the focus of ongoing work.

Experimental Procedures:

Trypanosome culture and transfection.

Cultivation and transfection of trypanosomes in culture were done as described previously [LaCount et al., 2002; MacGregor et al., 2011; Ralston et al., 2011]. The *T. brucei* bloodstream single marker (BSSM) [Wirtz et al., 1999] or pleomorphic AnTat1.1 [Macgregor et al., 2013] cells were described previously. BSSM-K/R and AnTat1.1-K/R cells were generated by stable transfection with the K/R cassette excised from pMOTAg53M-K/R. The K/R cassette contains the 3xHA-LC1-K/R mutant gene flanked at the 5' end by 900 bp of the 5' intergenic region to LC1 and at the 3' end by the α or β intergenic region of tubulin, the phleomycin resistance marker, and by 887 bp of the 3' intergenic region to LC1. To generate pMOTAg53M-K/R, the HA-LC1-K/R mutant gene was PCR-amplified from the pKR10-LC1-K/R plasmid [Ralston et al., 2011], whereas the 5' and 3' intergenic regions to LC1 were PCR-amplified from BSSM genomic DNA prior to serial cloning into pMOTag53M [Oberholzer et al., 2006]. The 5' and 3' intergenic regions to LC1 are used to allow homologous recombination for gene replacement. Primers used to PCR amplify the constructs are as follows: 5' ATGGGCCCACC A TGCCGTACCCGTACGA 3' (forward primer) and 5' ATGTCGACTTAGGCGCCGCGCTCCGC 3' (reverse primer), HA-LC1-K/R; 5' ATGGTACCGAGCCCAACTCTTGAAGAAGGGT 3' (forward primer) and 5' ATGGGCCCTACTATAAACCTCTATAGTCGTG 3' (reverse primer), 5'intergenic region to LC1; 5' AT GGATCCGAGTGCATGAACGAACACATTC 3' (forward primer) and 5' ATG CGGCCGCTGGTGCGCACTCACTTTCTTG 3' (reverse primer), 3' intergenic region to LC1.

All DNA sequences were verified by direct sequencing. Clones were obtained by limiting dilution after drug selection. To check the genomic integration of the K/R cassette the following primers were used: 5' CTGCCGTCAGCAACGAGTG 3' (forward primer) and 5' CGTCTAAAATCTTACCAGCAATC 3' (reverse primer). The forward and reverse primers sit within the open reading frame of the upstream and downstream genes to LC1.

Protein preparation and western blot analysis

Western blots were done as described previously [Ralston et al., 2011]. Parasites grown in culture were washed three times in PBS and then boiled in Laemmli sample buffer for Western blot analysis. Blots were probed with anti-HA monoclonal antibody (Covance) at 1:5000 dilution, anti- β-tubulin monoclonal antibody (Developmental Studies Hybridoma Bank, University of Iowa) at 1:5000 dilution.

Parasite motility assays

All samples were analyzed in a pre-warmed motility chamber within 5 minutes after collection. Motility traces were done as described [Ralston et al., 2011]. Briefly, parasites were examined in motility chambers using dark field optics on a Zeiss Axiovert 200 M inverted microscope with a 100x objective. Videos were captured using a COHU analog video camera. Analog format movies were converted to digital format with an ADVC-300 digital video converter (Canopus, Co., Ltd.). Movies were recorded at 30 frames per second (fps) and converted to AVI format and then to stacks of TIFF images using Adobe Premiere Elements

software (Adobe Systems). TIFF image stacks were analyzed using Metamorph software (Molecular Devices) to trace parasite movement over the indicated time period. Trace data were used to calculate the total distance travelled, as well as the mean squared displacement (MSD) of individual cells in the x and y dimensions. MSD was calculated according to the formula $MSD = \langle r_i(t)^2 \rangle = \langle (p_i(t) - p_i(0))^2 \rangle$, where r_i is the distance travelled by the parasite over time interval t and p_i is the position of the parasite at any given time. The timescale of t ranged from 1 to 25 seconds in increments of 1 second. MSD is calculated for each instance i of a given time interval. Several cell MSDs were then averaged to obtain an ensemble average.

Statistical analysis

Statistical analysis and graphical output was done with GraphPad Prism 5. We used the Student unpaired two-tailed t test to determine significant differences in motility. Significance (p value) is reported on figure 3B.

Acknowledgements

We thank Professor Keith Matthews and Dr. Paula Macgregor (University of Edinburgh) for their assistance with transfection of pleomorphic trypanosomes. We are also grateful to Dr. Katherine Ralston (University of Virginia) for technical support for the generation of the K/R construct. I am appreciative to Edna Miao for her technical support.

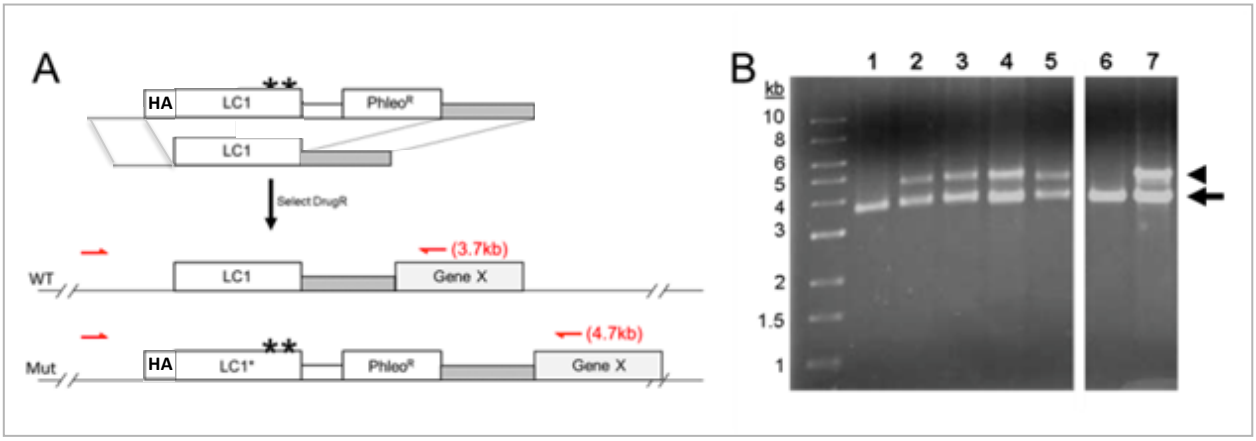

Figure 1. Figure 1. LC1-K/R motility mutants in BSSM and pleomorphic (AnTat1.1) trypanosomes. (A) Introducing the N-terminal HA tagged LC1-K/R mutant into BSSM and AnTat1.1. Red arrows indicate position of primers used for B, and size of expected product indicated. (B) PCR yields the expected products from the endogenous (arrow) and mutant (arrowhead) genes. AnTat1.1 parent (1); four PhleoR clones (2-5). BSSM cells as control (6) and BSSM harboring the mutant (7).

A

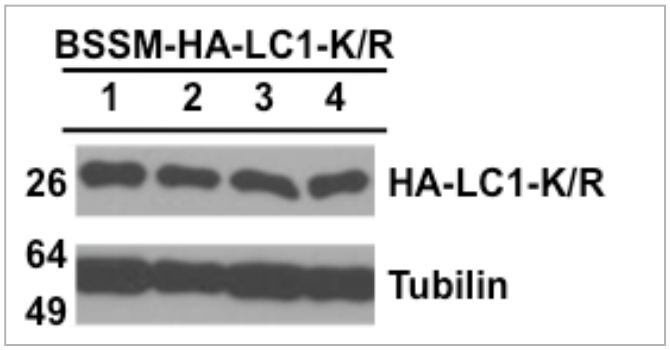

B

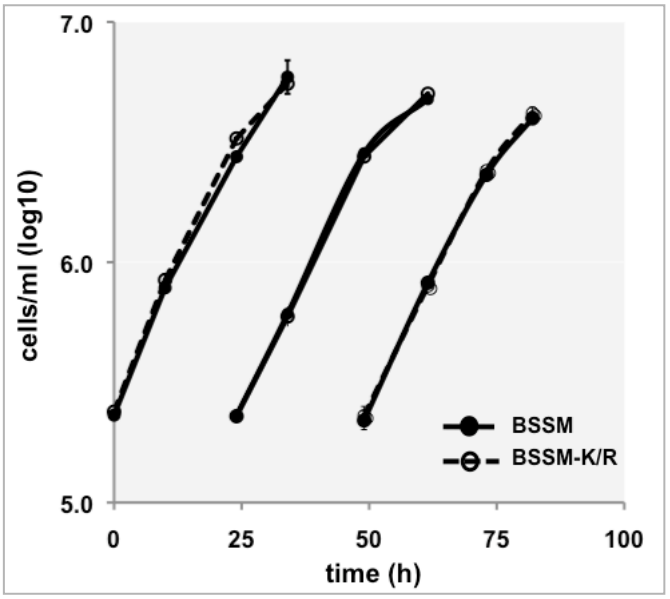

Figure 2. (A) Western blot of total protein from BSSM-K/R parasites maintained in culture. Blots of four clones are shown. Blots were probed with an antibody against the HA epitope to detect HA-LC1-K/R, or β-tubulin as a loading control. (B) Growth rates of BSSM cells (solid lines, filled circles) and BSSM-K/R point mutants (dotted lines, open circles). Cultures were diluted back to the starting density at 24 h and 48 h.

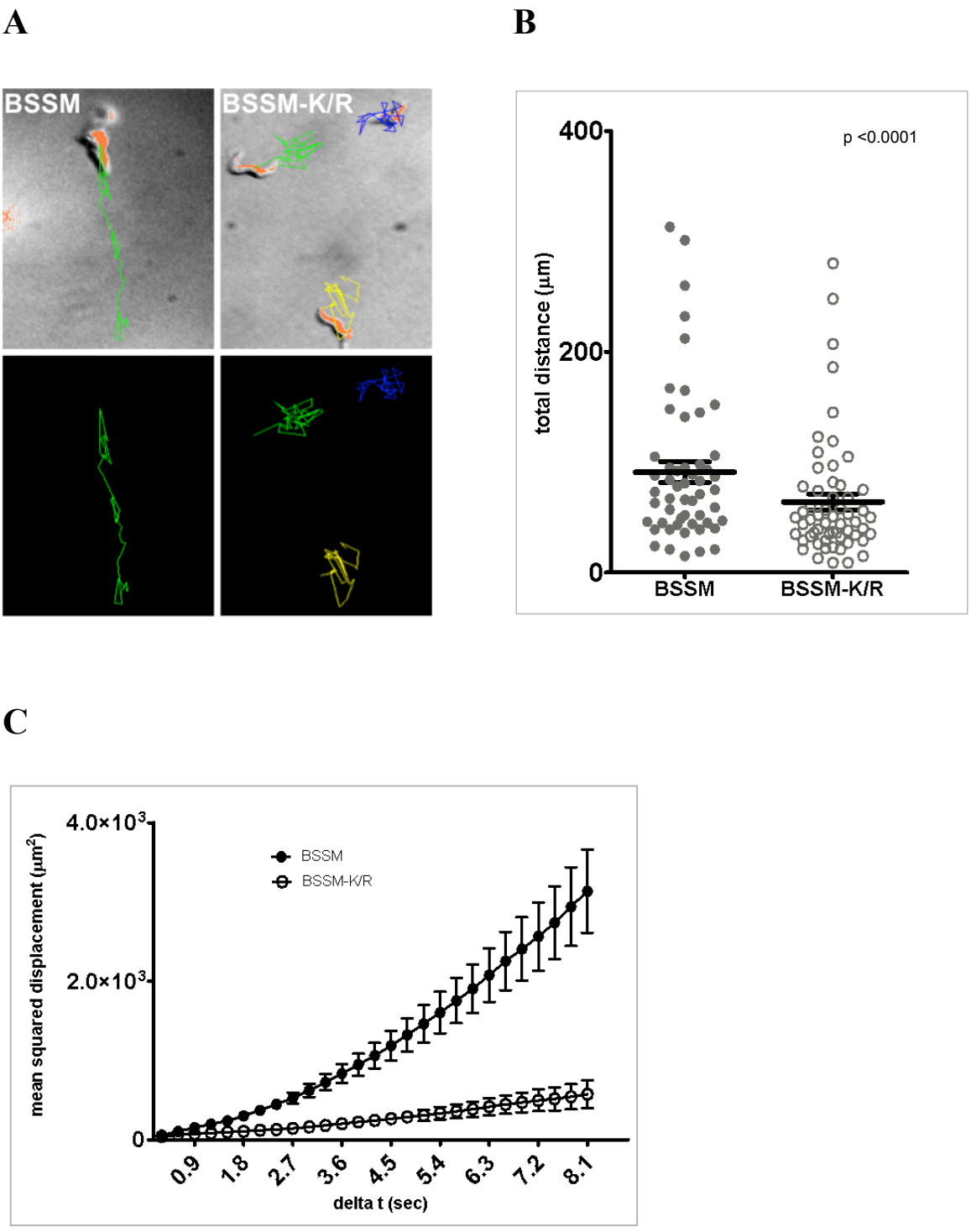

Figure 3. Motility phenotypes of control BSSM and BSSM-K/R mutant parasites. (A) Motility traces of control BSSM and K/R mutant parasites grown in culture. Each line traces the

path of a single cell for 8.1 seconds. Upper panels show traces overlaid on phase contrast images. Lower panels show traces. (B) Quantification of distance traveled in 8.1 seconds by BSSM and K/R mutants. Horizontal lines indicate the mean of each data set, with bars showing the 95% confidence interval, $p < 0.0234$. For BSSM, n= 54; for K/R, n= 58. (C) Mean squared displacement (msd) plotted as a function of time interval for BSSM (closed circles) and K/R point mutants (open circles); n = 24 (BSSM) and n = 35 (K/R) cells. Error bars show standard error of the mean, .

CHAPTER 4 REFERENCES

Baron, D. M., Ralston, K. S., Kabututu, Z. P. and Hill, K. L. (2007). "Functional genomics in Trypanosoma brucei identifies evolutionarily conserved components of motile flagella." J Cell Sci 120(Pt 3): 478-491.

Bastin, P., Matthews, K. R. and Gull, K. (1996). "The paraflagellar rod of kinetoplastida: solved and unsolved questions." Parasitol Today 12(8): 302-307.

Branche, C., Kohl, L., Toutirais, G., Buisson, J., Cosson, J. and Bastin, P. (2006). "Conserved and specific functions of axoneme components in trypanosome motility." J Cell Sci 119(Pt 16): 3443-3455.

Broadhead, R., Dawe, H. R., Farr, H., Griffiths, S., Hart, S. R., Portman, N. et al. (2006). "Flagellar motility is required for the viability of the bloodstream trypanosome." Nature 440(7081): 224-227.

Emmer, B. T., Daniels, M. D., Taylor, J. M., Epting, C. L. and Engman, D. M. (2010). "Calflagin inhibition prolongs host survival and suppresses parasitemia in Trypanosoma brucei infection." Eukaryot Cell 9(6): 934-942.

Frevert, U., Engelmann, S., Zougbede, S., Stange, J., Ng, B., Matuschewski, K. et al. (2005). "Intravital observation of Plasmodium berghei sporozoite infection of the liver." PLoS Biol 3(6): e192.

Gray, G. D., Jennings, F. W. and Hajduk, S. L. (1982). "Relapse of monomorphic and pleomorphic Trypanosoma brucei infections in the mouse after chemotherapy." Z Parasitenkd 67(2): 137-145.

Griffiths, S., Portman, N., Taylor, P. R., Gordon, S., Ginger, M. L. and Gull, K. (2007). "RNA interference mutant induction in vivo demonstrates the essential nature of trypanosome flagellar function during mammalian infection." Eukaryot Cell 6(7): 1248-1250.

Heddergott, N., Kruger, T., Babu, S. B., Wei, A., Stellamanns, E., Uppaluri, S. et al. (2012). "Trypanosome motion represents an adaptation to the crowded environment of the vertebrate bloodstream." PLoS Pathog 8(11): e1003023.

Hill, K. L. (2003). "Biology and mechanism of trypanosome cell motility." Eukaryot Cell 2(2): 200-208.

Hughes, L. C., Ralston, K. S., Hill, K. L. and Zhou, Z. H. (2012). "Three-dimensional structure of the Trypanosome flagellum suggests that the paraflagellar rod functions as a biomechanical spring." PLoS One 7(1): e25700.

Jennings, F. W., Whitelaw, D. D., Holmes, P. H., Chizyuka, H. G. and Urquhart, G. M. (1979). "The brain as a source of relapsing Trypanosoma brucei infection in mice after chemotherapy." Int J Parasitol 9(4): 381-384.

Kohl, L., Robinson, D. and Bastin, P. (2003). "Novel roles for the flagellum in cell morphogenesis and cytokinesis of trypanosomes." EMBO J 22(20): 5336-5346.

LaCount, D. J., Barrett, B. and Donelson, J. E. (2002). "Trypanosoma brucei FLA1 is required for flagellum attachment and cytokinesis." J Biol Chem 277(20): 17580-17588.

Macgregor, P., Rojas, F., Dean, S. and Matthews, K. R. (2013). "Stable transformation of pleomorphic bloodstream form Trypanosoma brucei." Mol Biochem Parasitol 190(2): 60-62.

MacGregor, P., Savill, N. J., Hall, D. and Matthews, K. R. (2011). "Transmission stages dominate trypanosome within-host dynamics during chronic infections." Cell Host Microbe 9(4): 310-318.

Mulenga, C., Mhlanga, J. D., Kristensson, K. and Robertson, B. (2001). "Trypanosoma brucei brucei crosses the blood-brain barrier while tight junction proteins are preserved in a rat chronic disease model." Neuropathol Appl Neurobiol 27(1): 77-85.

Oberholzer, M., Langousis, G., Nguyen, H. T., Saada, E. A., Shimogawa, M. M., Jonsson, Z. O. et al. (2011). "Independent analysis of the flagellum surface and matrix proteomes provides insight into flagellum signaling in mammalian-infectious Trypanosoma brucei." Mol Cell Proteomics 10(10): M111 010538.

Oberholzer, M., Lopez, M. A., Ralston, K. S. and Hill, K. L. (2009). "Approaches for functional analysis of flagellar proteins in African trypanosomes." Methods Cell Biol 93: 21-57.

Oberholzer, M., Morand, S., Kunz, S. and Seebeck, T. (2006). "A vector series for rapid PCR-mediated C-terminal in situ tagging of Trypanosoma brucei genes." Mol Biochem Parasitol 145(1): 117-120.

Patel-King, R. S. and King, S. M. (2009). "An outer arm dynein light chain acts in a conformational switch for flagellar motility." J Cell Biol 186(2): 283-295.

Poltera, A. A., Hochmann, A., Rudin, W. and Lambert, P. H. (1980). "Trypanosoma brucei brucei: a model for cerebral trypanosomiasis in mice--an immunological, histological and electronmicroscopic study." Clin Exp Immunol 40(3): 496-507.

Ralston, K. S. and Hill, K. L. (2006). "Trypanin, a component of the flagellar Dynein regulatory complex, is essential in bloodstream form African trypanosomes." PLoS Pathog 2(9): e101.

Ralston, K. S. and Hill, K. L. (2008). "The flagellum of Trypanosoma brucei: new tricks from an old dog." Int J Parasitol 38(8-9): 869-884.

Ralston, K. S., Kisalu, N. K. and Hill, K. L. (2011). "Structure-function analysis of dynein light chain 1 identifies viable motility mutants in bloodstream-form Trypanosoma brucei." Eukaryot Cell 10(7): 884-894.

Rodgers, J. (2010). "Trypanosomiasis and the brain." Parasitology 137(14): 1995-2006.

Rodriguez, J. A., Lopez, M. A., Thayer, M. C., Zhao, Y., Oberholzer, M., Chang, D. D. et al. (2009). "Propulsion of African trypanosomes is driven by bihelical waves with alternating chirality separated by kinks." Proc Natl Acad Sci U S A 106(46): 19322-19327.

Wirtz, E., Leal, S., Ochatt, C. and Cross, G. A. (1999). "A tightly regulated inducible expression system for conditional gene knock-outs and dominant-negative genetics in Trypanosoma brucei." Mol Biochem Parasitol 99(1): 89-101.

Wolburg, H., Mogk, S., Acker, S., Frey, C., Meinert, M., Schonfeld, C. et al. (2012). "Late stage infection in sleeping sickness." PLoS One 7(3): e34304.

Chapter 5

Live-cell imaging of *Trypanosoma brucei* in ex vivo mouse tissues and in live zebrafish

(Manuscript in preparation for submission)

Abstract

The protozoan parasite *Trypanosoma brucei* causes lethal African sleeping sickness in humans. There is no vaccine and existing drugs are toxic and increasingly ineffective. Entry of trypanosomes into tissue mediates pathogenesis of this parasite. Historically, assessment of *T. brucei* infection has relied upon determining parasitemia in blood, as well as limited use of histochemistry to assess parasite presence in chemically fixed tissues. Here, we report the development of an advanced live-cell imaging approach using *T. brucei* expressing the fluorescent protein mCherry. This system enabled visualization of *T. brucei* at macroscale level *ex vivo* in mouse tissues as well as *in vivo* in intact zebrafish embryos. We further validated the use of mCherry parasites at a microscale level by visualizing trypanosomes at single-cell resolution in *ex vivo* mouse tissues and in blood vessels of live fish. Parasites in mouse brain tissue and in fish were largely confined within blood vessels. These systems have the potential for enabling detailed dynamic studies of infection, uncovering novel features of host-parasite interactions, and facilitating diagnostics, vaccine and drug development, all of which should improve patient management in sleeping sickness.

Introduction

African trypanosomes, *Trypanosoma brucei*, are protozoan parasites that cause sleeping sickness, a fatal disease with devastating health and economic consequences in Sub-Saharan Africa. The disease is inevitably fatal unless treated. There is no vaccine and existing drugs are toxic and associated with drug resistance [Barry and McCulloch 2001]. Trypanosomes are transmitted between human hosts by a tsetse fly insect vector and entry into specific host tissues is a critical step in the pathogenesis of sleeping sickness [Borst 2002]. Following infection through the bite of a tsetse fly trypanosomes actively divide in the mammalian host but finally leave the bloodstream and penetrate the central nervous system (CNS) [Stich et al., 2002; Rodgers 2010]. CNS invasion marks the lethal stage of sleeping sickness. Very little is known about the fundamentals of *T. brucei* motility in the bloodstream, the interaction of this parasite with host cells, and the mechanisms used by trypanosomes to invade extravascular tissues.

Traditionally, monitoring of *T. brucei* infection has relied upon microscopic examination to determine parasitemia in blood, as well as limited use of histochemistry to assess parasite presence in chemically fixed tissues [Poltera et al., 1980]. Although such approaches immensely contributed to our understanding on host–parasite interactions, these techniques have substantial disadvantages. For instance, microscopic examination is laborious, time-consuming and microscopy counts can be subjective. Histochemistry does not mirror the dynamics of the infection process.

Advanced biological imaging approaches, e.g. bioluminescence and live-cell fluorescence, have been recently utilized to study host-pathogen interactions in protozoan parasites [Frevert et al., 2005; Hitziger et al., 2005; Lang et al., 2005; Heussler and Doerig 2006; Coombes and Robey 2010; Bustamante and Tarleton 2011; Frevert et al., 2012]. Such approaches have provided a number of powerful utilities that enable detailed dynamic studies of parasite dissemination in host tissues, facilitate vaccine development and drug discovery, and uncover novel features of parasite interaction with host cells. Surprisingly, advanced live-cell fluorescence and bioluminescence imaging has been relatively underutilized in studies of *T. brucei*, although a few recent studies demonstrate the potential for these approaches to provide insight into infection and host-parasite interaction [Claes et al., 2009; Giroud et al., 2009; Frevert et al., 2012; Salmon et al., 2012; Maclean et al., 2013].

Luciferase bioluminescence systems have been used for *in vivo* analysis of *T. brucei* infection [Claes et al., 2009] and to monitor parasite dissemination in live mice and *ex-vivo* tissues using different field isolates of *T. brucei* [Giroud et al., 2009]. As illustrated in these works, bioluminescence has advantages for non-invasive imaging at multiple time points in live animals, but is limited by restricted distribution of substrate within host tissues and relatively low spatial and temporal resolution. As such, route of substrate administration impacts detection in specific tissues and single cells are not resolved [Claes et al., 2009; Giroud et al., 2009]. Thus, while useful for some host-pathogen interaction studies, bioluminescence has limitations and fluorescence imaging can fill some of these gaps.

Live-cell fluorescence imaging generally offers complementary strengths and

weaknesses relative to bioluminescence [Heussler and Doerig 2006]. For example, fluorescence-based methods offer the ability to image single cells in a short time scale and do not require provision of substrate [Heussler and Doerig 2006]. To complement the above studies we report development of a live-cell imaging approach using fluorescent mCherry *T. brucei*. This system allowed us visualization of individual live parasites in real time within the context of the mouse tissue environment. The system also allowed imaging of trypanosomes at single-cell resolution *in vivo* in whole live fish. To our knowledge this is the first report of imaging *T. brucei* in fish.

Results

Visualization of trypanosomes at macroscale level in mouse tissues and in whole zebrafish.

Measuring parasitemia in peripheral blood samples taken from infected mice provides a reasonable proxy for trypanosome infection. However, we wanted to examine the presence of trypanosomes in visceral organs as a more rigorous assessment of infection. Our ultimate goal was to directly visualize live, individual parasites and we therefore elected to use fluorescent trypanosomes. The mCherry red fluorescent protein was chosen because its spectral properties offer better penetrating power in deep tissues compared to other fluorescent markers such as green fluorescent protein [Shaner et al., 2004].

We first set out to establish whether BSSM trypanosomes expressing mCherry were viable and suitable for use in mouse infections. We engineered trypanosomes to constitutively express mCherry by stably transfecting BSSM cells with the plasmid pNKmC, which encodes mCherry driven by a constitutive promoter (Methods). Fluorescent imaging showed that the mCherry protein is distributed throughout the cell (Figure 1A). When cultivated *in vitro*, mCherry parasites did not show any significant difference in growth rate compared to parental BSSM parasites (Figure 1B) and mCherry expression was stable through at least five weeks of continuous culture (Figure 1C). Mice infected with mCherry parasites showed the same infection dynamics as BSSM parasites, giving typically one and at most two waves of parasitemia leading to a terminal outcome in one to two weeks (Figure 1E-D).

Analysis of whole blood taken from infected mice allowed direct visualization of individual parasites (Figure 1F). To assess parasitemia in visceral organs, we used the Maestro® 2 *in vivo* spectral imaging system. The Maestro system enables *in vivo* fluorescence imaging of small animals and tissues in the visible-infrared spectral range with exquisite sensitivity. This system uses a liquid crystal tunable filter that allows precise spectral unmixing of the emission spectra to remove auto-fluorescence. We assessed the sensitivity of the system using *in vitro* cultivated mCherry parasites and found a detection limit of 10,000 - 25,000 parasites (Figure 1G). While these *in vitro* numbers do not necessarily extrapolate directly to detection limits *in vivo*, they provide a reasonable estimate of the minimum number of parasite necessary for visualization with the Maestro system and demonstrate linearity of the response (Figure 1H).

We next examined tissues taken from infected mice. Parasite-dependent fluorescence was readily detected in spleens and livers (Figure 2A-B) of mice infected with mCherry parasites, while tissues from uninfected mice, or mice infected with unlabeled parasites showed only background fluorescence. Whole brains from uninfected mice gave high background fluorescence and this limited reliable fluorescence imaging of parasites in this organ using the Maestro system (not shown). To determine if fluorescence in tissues was stable for extended periods, we cryopreserved tissue samples for examination at a later date. Parasite fluorescence was readily detected in tissue samples eight months after sample preparation with two freeze-thaw cycles (Figure 2C).

Mouse thickness and opaque skin limit fluorescent imaging below 100 μm. Additionally

high-resolution, non-invasive imaging of microbes or immune cells is hard to accomplish in mice. Our ultimate goal was to do high-resolution, deep tissue imaging in whole live animals and in particular to examine at a timescale that would allow analysis of parasite motility. Having established mCherry parasites as suitable for observing *T. brucei* with fluorescent imaging in mouse tissues we asked whether we could image trypanosomes in zebrafish embryos after infection with *T. brucei*. The advantages of using a larval zebrafish model include transparency and the possibility to microscopically image the whole live fish with minimal manipulation, offering opportunities to non-invasively visualize the dynamics of infection using fluorescent imaging at high-resolution at several different time points during infection [Tobin et al., 2012]. Wild type fish embryos were infected with mCherry *T. brucei* as described in Methods. Direct examination of whole fish showed clear imaging of parasites as well as of blood cells in live fish (Figure 2D-F and Video 1). All parasites observed move in the direction of the blood flow (Video 1). Visualization of the whole live fish, demonstrates this system's potential for investigating tissue-to-tissue dissemination of trypanosomes *in vivo* at high resolution.

Direct visualization of trypanosomes at single-cell resolution in mouse tissues and in zebrafish blood vessels.

An advantage of fluorescence as an imaging modality for infection studies is that it offers the potential for directly imaging individual cells within the complex milieu of the host environment. We therefore asked whether we could resolve individual parasites in brain, spleen, or liver tissue from mice infected with mCherry trypanosomes using epifluorescence

microscopy. Individual red fluorescent parasites were readily detected in thick sections of all these organs from BSSM- mCherry infected mice (Figure 3A-). Within brain tissue, parasites were primarily found to align single file along structures that appear to blood vessels (Figure 4A-C), indicating that these trypanosomes are confined within blood vessels. Spleen and liver tissue samples were less organized, no clear vessels were apparent and parasites were randomly distributed through the sample (Figure 3D-E).

Imaging of mCherry *T. brucei* in zebrafish indicated that the parasites were withing blood vessels (Figure 3 amd Video 1). To test this directly, we next utilized transgenic zebrafish that express green fluorescent protein in vascular endothelia cells (Methods), so that we could directly visualize blood vessels. This showed that individual trypanosomes are within blood vessels (Figure 4 and Video 2). Therefore, mCherry trypanosomes allow for direct imaging of parasites at the single-cell level in whole blood, *ex vivo* in tissues from infected mice, as well as within blood vessels in live fish.

Discussion

In the present analysis, we developed systems to directly image live *T. brucei* in mouse tissues and in intact fish, which should aid in filling an important gap in our understanding of trypanosome infection and host-parasite interaction. We engineered bloodstream trypanosomes that constitutively express mCherry fluorescent protein, enabling fluorescence imaging of parasites within mouse tissues and whole fish via multiple modalities, e.g. fluorescence imaging of whole tissues and epifluorescence microscopy for live- cell imaging of parasites at the single-cell level. Expression of mCherry was found to be extremely stable with no significant impact on parasite viability in culture or infection dynamics in a mouse model. Fluorescence intensity and percent of mCherry-positive parasites in the population (>99%) remained unchanged through five weeks of analysis in culture, suggesting that the strategy will be suitable for chronic infection models [Matthews 2005], where infection lasts several weeks. Likewise, stability of parasite detection in cryopreserved tissues for more than eight months should facilitate clinical analyses in cases where clinical examination is removed from the site of experimental analysis. Also noteworthy, is the fact that direct, single-cell imaging is readily obtained using standard epifluorescence microscopy and is thus achievable in most research laboratories, without the need for sophisticated equipment or procedures.

Successful visualization of trypanosomes within the entire live fish offers unique opportunities to non-invasively image trypanosome infection dynamics at multiple time points in live animals at high spatial and temporal resolution. Notably, some species of trypanosomes infect fish as a natural host [Haag et al., 1998; Overath et al., 1998; Lischke

et al., 2000; Burreson 2007] and there is some work done on fish immune response to infection [Katzenback et al., 2013]. Hence, the system reported here should be broadly applicable for direct analysis of host-parasite interactions during *T. brucei* infection in many contexts, as well as analysis of fish-trypanosome interactions in natural infections.

The mCherry system reported here will complement recently developed bioluminescence and fluorescence systems for imaging *T. brucei* during infection. Claes and co-workers developed luciferase bioluminescence systems for *in vivo* analysis of *T. brucei* infection [Claes et al., 2009]. Giroud and colleagues utilized this bioluminescence system to demonstrate differences in parasite dissemination in live animals and *ex-vivo* tissues in a murine model of infection using different *T. brucei* clinical isolates [Giroud et al., 2009]. As discussed above, despite its benefit for allowing repeated imaging of host-parasite interactions on the same live animal over time, bioluminescence cannot resolve cells at single resolution level and depends on substrate repartition within the animal [Claes et al., 2009; Giroud et al., 2009]. To compensate some of these limitations, fluorescence imaging modalities used alone or in combination with bioluminescence can be used.

A few studies have used fluorescent *T. brucei* in mouse infection models. Balmer and colleagues reported use of FACS analysis to distinguish between green and red fluorescent parasites in blood samples from mice harboring mixed parasite infections [Balmer and Tostado 2006]. Frevert and colleagues [Frevert et al., 2012] recently reported using intravital microscopy to observe 427- derived *T. brucei* in mouse CNS tissue within 2 days of infection, which is earlier than indicated by previous studies [Gray et al., 1982]. Differences might stem

from different infective doses used (10^2 [Gray et al., 1982] versus 10^5-10^6 [Frevert et al., 2012]) or means of parasite detection (bioassay [Gray et al., 1982] versus direct visualization [Frevert et al., 2012]). Salmon and colleagues recently used fluorescent *T. brucei* and Imagestream® analysis of blood samples to reveal changes in host cell gene expression depending upon whether or not the host cells are in direct contact with parasites [Salmon et al., 2012]. Our studies complement those important studies by combining analysis of infection by genetically modified parasite lines with direct imaging of parasites in mouse tissues. The availability of multiple imaging modalities for studying *T. brucei* infection should advance efforts to understand how these parasites interact directly with host tissues and cells.

We used zebrafish for non-invasive imaging of trypanosomes at single cell resolution *in vivo* in live fish. Application of the zebrafish model to infectious diseases has led to milestone discoveries for understanding infection dynamics [Meijer and Spaink 2011]. For example, the role of macrophages in promoting pathogen dissemination [Davis and Ramakrishnan 2009] was described by using fish infection systems. In the case of mycobacteria, disease mechanisms such as virulence and host susceptibility observed during zebrafish infection are conserved in human infection with *M. tuberculosis*. Even though Zebrafish have proved to be valuable model infection systems for viruses, bacteria and fungi [Phennicie et al., 2010; Brothers et al., 2011; Ludwig et al., 2011], the application of this system to parasitic infections is very limited although a few investigations have used the zebrafish model to study establishment of infection with *Giardia* [Yang et al., 2010];[Tysnes et al., 2012]. Interestingly fish are natural hosts for certain trypanosome species, such as *T. carassii* [Haag et al., 1998; Overath et al., 1998; Lischke et al., 2000]. Ongoing studies in our lab are focused on establishing genetically modified *T. carassii* to

enable host-parasite interactions in a natural host. Transparent mutant adult zebrafish exist [White et al., 2008]. The demonstration that we can successfully image trypanosomes in the entire fish offers the potential for visualization of infection dynamics in the entire host including tissue-to-tissue dissemination of trypanosomes at high-resolution in real time.

In summary, the availability of multiple imaging modalities for studying trypanosome infection should advance efforts to evaluate trypanosome immunology, pathology, physiology and other features of pathogenesis and host-parasite interaction. Patient management is challenging in sleeping sickness. Our systems have therefore potential broad application for studying host-pathogen interaction. Such understanding constitutes a benchmark for therapeutics and diagnostics development, which should improve patient management in African sleeping sickness.

Materials and Methods

Ethics Statement. All animal experiments complied with the Institutional Animal Care and Use Committee of University of California, Los Angeles (Approved protocol permit: ARC #2001-065).

Trypanosome culture. Cultivation, transfection and RNAi induction of trypanosomes in culture were done as described previously [Ralston et al., 2006]. The *T. brucei* bloodstream LC1-K203A/R210A (K/R) motility mutant and bloodstream single marker (BSSM), cells were described previously [Wirtz et al., 1999; Ralston et al., 2011]. BSSM-mCherry cells and K/R-mCherry cells were generated by stable transfection of BSSM and K/R cells, respectively with the pNKmCherry plasmid (described below). To generate pNKmCherry, the mCherry gene (accession number AY678264) was PCR amplified from pmCherry plasmid (kindly provided by Josh Beck) and cloned into the expression vector pHD496-H [Hutchings et al., 2002] using the Hind*III* and Bam*HI* cloning sites. pHD496-H contains a ribosomal RNA promoter to drive constitutive expression of the mCherry gene and a hygromycin-resistance cassette to enable selection [Biebinger and Clayton 1996]. Primers used to PCR amplify mCherry are as follow: 5' ATGGTGAGCAAGGGCGAGG 3' (forward primer), 5' TTACTTGTACAGCTCGTCCATGC 3' (reverse primer). All DNA sequences were verified by direct sequencing.

Mouse infections. BALB/c female mice (The Jackson Laboratory, Bar Harbor, ME), 6 to 10 weeks old, were injected intraperitoneally with 100 parasites diluted in 0.2 ml of HMI-9

medium. Parasites were kept on ice prior to injection into mice. For + Tet infections, parasites were induced with 1 mg/ml tetracycline in culture three days prior to injection into mice and mice received 1 mg/ml doxycycline in their drinking water 5 to 7 days prior to infection and throughout the course of infection. Parasitemia was monitored daily beginning 3 days post infection using an improved Neubaeur hemocytometer [Herbert and Lumsden 1976]. After euthanasia, mice were weighed and tissues were collected for weighing and imaging.

Flow cytometry analysis. For flow cytometry analysis, 1.5 – 2.0 x 10^6 cells were washed twice in PBS-1% glucose (PBS-G), and resuspended in 0.5mL of PBS-G prior to data acquisition on a BD LSRII analyzer (BD Biosciences). The photomultiplier tube voltages for the forward scatter, side scatter, and the detector for mCherry were set based on the control, BSSM sample. For consistency, and because laser power can drift with time, the fluorescence intensity measurement was standardized as follows. After the initial flow acquisition experiments, a sample of chicken red blood cells (CRBC) was run and their fluorescence intensity in the mCherry channel was recorded. A sample of CRBC with the same lot number as the one used for the first experiment was run at each of the subsequent flow acquisitions and compared to the intensity value from the original run. If needed, minor voltage adjustments were made to match the mean CRBC fluorescence intensity from the initial experiment. Control non-fluorescent and mCherry samples were then acquired with identical instrument settings. FACSDIVA software was used for data acquisition and data analysis was performed using Cellquest.

Ex vivo fluorescence imaging and epifluorescence microscopy of mouse tissues. For fluorescence imaging of whole organs, tissues were collected 6-8 days post infection, kept on ice

in PBS-1% glucose and imaged within one hour using Maestro® 2 *in vivo* spectral imaging system (CRi/Caliper Life Sciences, Woburn, MA). Fluorescence from mCherry trypanosomes was imaged using a band pass filter of 503 to 548 nm for excitation coupled with a 560 nm long pass filter for emission. Fluorescence images were captured automatically by 10 nm increments from 560 to 750 nm under constant light illumination. The resulting spectral imaging TIFF data set was analyzed with the vendor's software. The fluorescence of uninfected control tissue was acquired simultaneously and used to sample out background auto-fluorescence. For epifluorescence imaging of individual parasites within tissues, the tissue samples were sectioned and directly visualized using a Zeiss Axioskop II or Axio Imager 2 compound fluorescence microscope, using 40x oil objective.

High-Speed Confocal Imaging: Anesthetized wild-type or flk:GFP* transgenic zebrafish with fluorescent vascular endothelia were side- or back-mounted and injected in the heart as previously described [Hove and Craig 2012] with red mCherry expressing trypanosomes (a few nanoliters of a pellet containing about 20 x 10^6 parasites) and imaged on a Leica TCS SP5 inverted confocal system (Leica Microsystems, Wetzlar, Germany). Images were acquired with a water immersion objective (HCX PL APO CS 20x/0.70NA) and analyzed with the Leica software. GFP was excited with a 488 nm argon laser line and a 561 HeNe laser was used for the excitation of mCherry expressing trypanosomes. Spectral windows for detection of GFP and mCherry fluorescence were 495-540 nm and 590-650 nm respectively. Multicolor images were acquired in a simultaneous scan. High-speed imaging was performed at a line frequency of 8000 Hz using the broadband resonant scanner of the Leica TCS SP5 which allows the recording of 27 full frames per second with an image format of 512 x 256 pixels. Pixel size was kept around 348

nm x 348 nm by applying a 4X digital zoom.

ACKNOWLEDGMENTS

We are grateful to John Mansfield (University of Wisconsin) and Karen Demick for guidance with mouse infections. We thank Josh Beck (UCLA) for kindly providing us with the mCherry DNA. We thank the Marine Biological Laboratory Biology of Parasitism summer research course students for assistance with experiments for Figure 3A-C. We are also appreciative of members of our laboratory for pertinent comments on the work and critical reading of the manuscript. Confocal imaging and *in vivo* fluorescence imaging were performed at the California NanoSystems Institute Advanced Light Microscopy/Spectroscopy and the Macro-Scale Imaging Shared Facilities at UCLA. Flow cytometry was performed in the UCLA Jonsson Comprehensive Cancer Center and Center for AIDS Research Flow Cytometry Core Facility. Gerasimos Langousis is the recipient of the Warsaw fellowship. Neville K. Kisalu is a recipient of the Shapiro Fellowship and Dissertation Year Fellowship from the UCLA Graduate Division.

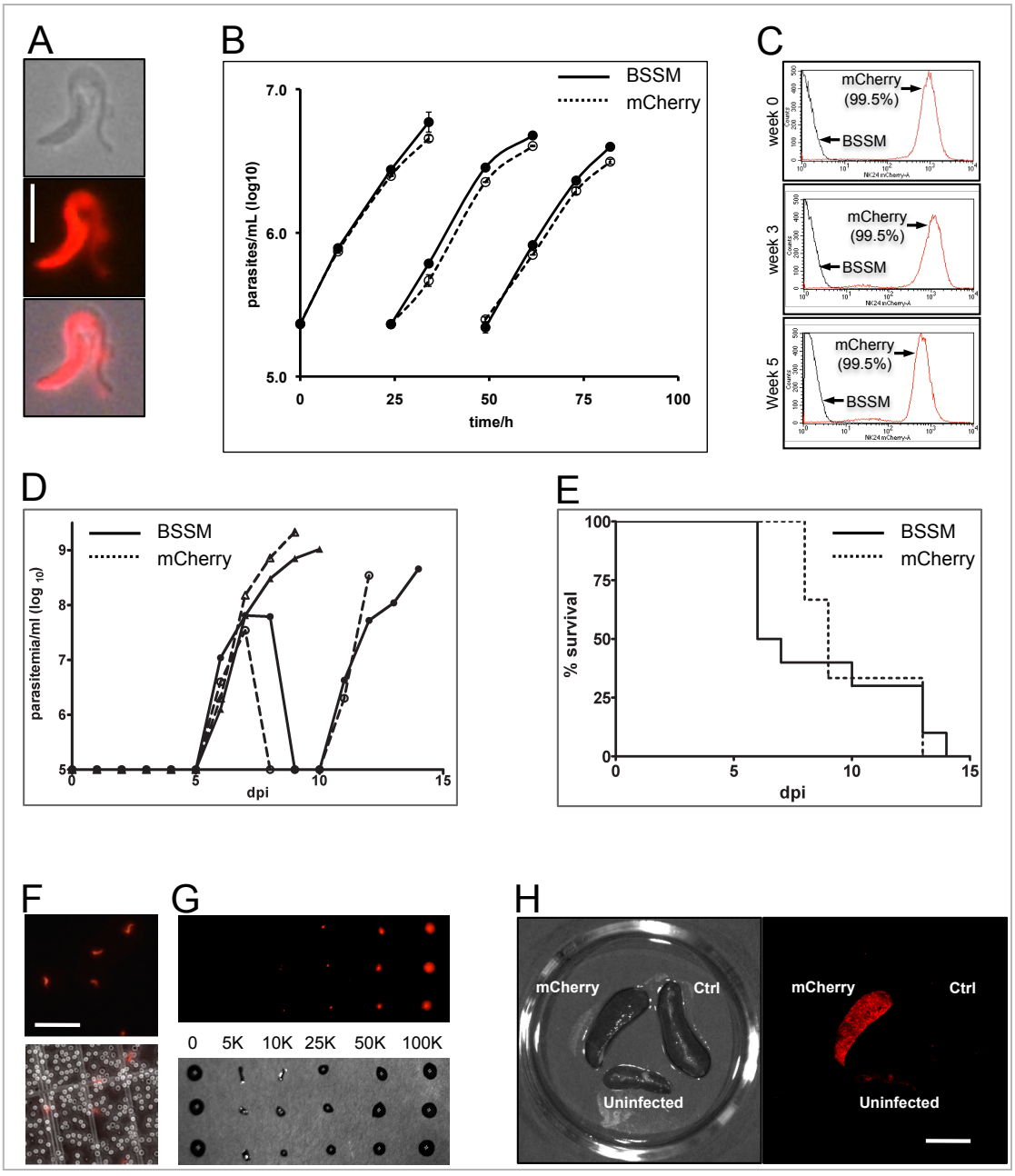

Figure 1 Bloodstream trypanosomes expressing mCherry fluorescent protein are suitable for mouse infection. (A) Live BSSM-mCherry *T. brucei* cells were imaged by fluorescence microscopy. Phase contrast, fluorescence and merged images are shown. Scale bar is 7 um. (B)

Growth curves for BSSM parental cells (solid lines) or BSSM-mCherry cells (dashed lines) in culture. Cultures were diluted to 2 x 10^5 cells/ml when the cell density reached 10^6 cells/ml and then counts continued. (C) Flow cytometry analysis of BSSM (black curves) and BSSM-mCherry (red curves) parasites maintained for five weeks in culture. Percent of the population scored as mCherry positive at each time point is shown in parentheses. (D) Parasitemias of mice infected with BSSM (solid lines) or BSSM-mCherry (dashed lines) parasites. Mice were infected at day 0 and parasitemia was determined daily beginning 3 days post infection. Representative data are shown for two BSSM and two BSSM-mCherry infections to illustrate the two basic outcomes of infection. Mice usually exhibited a single wave of parasitemia (triangles) but occasionally showed two waves (circles). (E) Survival curves for mice infected with BSSM (solid line, n = 4) or BSSM-mCherry (dashed line, n = 3 mice) parasites. No difference was observed (p = 0.8509). (F) Blood from a mouse infected with BSSM-mCherry parasites was examined by live cell fluorescence microscopy. Fluorescence (top) and merged (bottom) images are shown. Trypanosomes (red) are readily detected among host red blood cells. Scale bar is 50μm. (G) The indicated number of BSSM-mCherry cells in triplicate were imaged using the Maestro system. Fluorescent (top) and grayscale (bottom) images are shown. (H) Dose-response curve of parasite fluorescence detection using the Maestro system. Fluorescence intensities of serial dilutions of BSSM-mCherry parasites shown in Figure 1G were quantified using the Maestro imaging system software. Data are averages from three replicates for each cell number. Error bars show standard error of the mean.

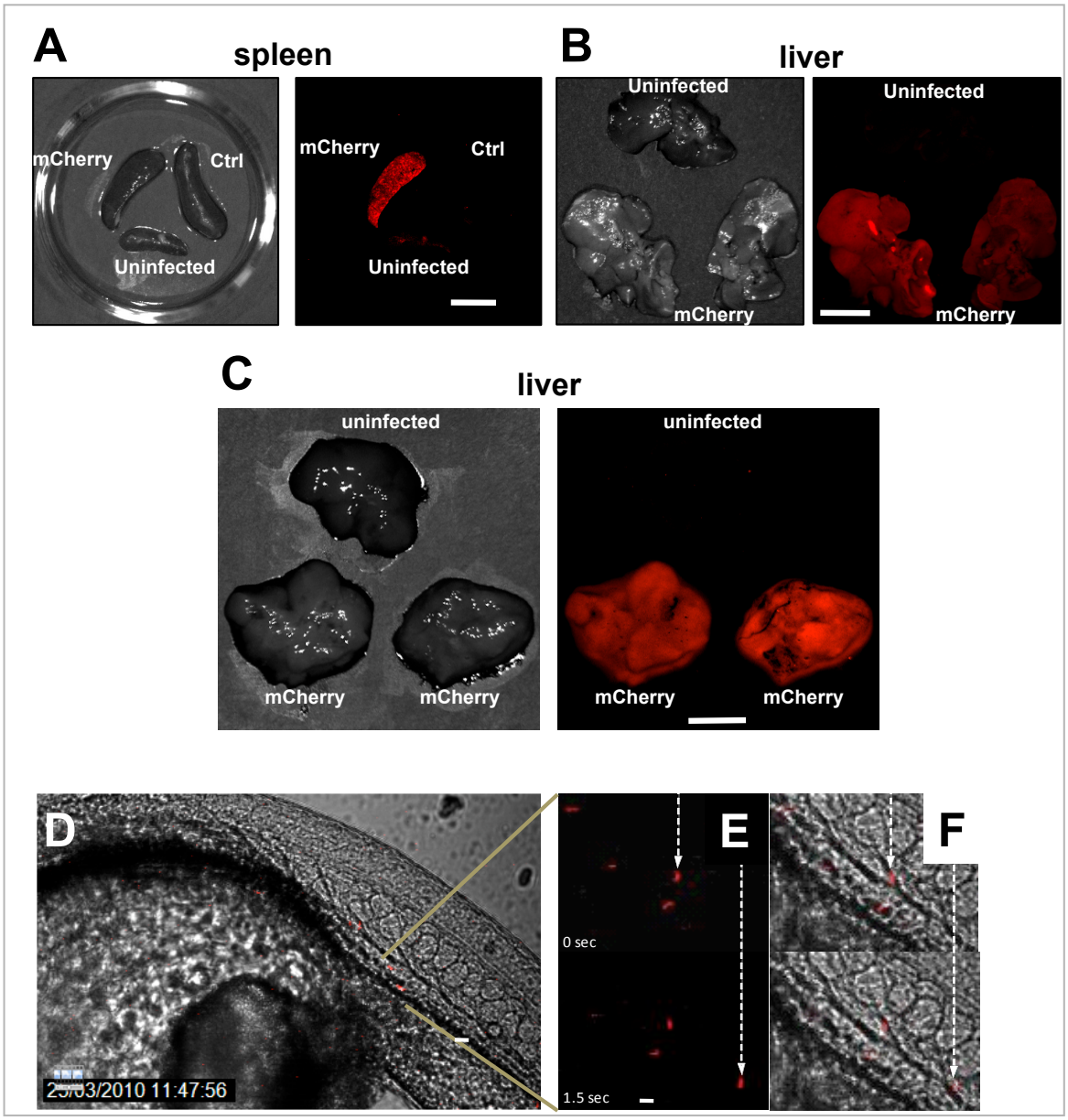

Figure 2. Bloodstream trypanosomes expressing mCherry fluorescent protein are visualized in mouse tissues and in blood vessels of live fish. (A) Spleens from uninfected mice (uninfected) and from mice infected with non-fluorescent control parasites (Ctrl) or BSSM-mCherry parasites (mCherry) were imaged using the Maestro imaging system. (B) Livers from

uninfected mice (uninfected) and from mice infected with mCherry parasites were imaged using the Maestro imaging system. Grayscale (left) and fluorescent (right) images are shown. Scale bar is 1cm. (C) Livers from uninfected mice (uninfected) or from mice infected with mCherry parasites (mCherry) were imaged after eight months of storage at -80 degrees, with two freeze/thaw cycles. These same livers were originally imaged on the day of preparation, shown in figure 2B. Thus, parasite fluorescence in tissues is stable for at least eight months. Grayscale (left) and fluorescence (right) images are shown. Scale bar is 1cm. (D-F) Red mCherry *T. brucei* were injected into the zebrafish blood circulation by cardiac injection. Live zebrafish were immobilized and imaged by video fluorescence microscopy. One frame of the video is shown (D), as well as close up time-lapsed images (E, F). Top and bottom images in panels E and F are taken 1.5 seconds apart. Single parasites can be seen moving in the blood vessels of live fish. For reference, a single trypanosome is indicated with a dashed arrow at t = 0 seconds (top panels) and the same trypanosome is indicated 1.5 seconds later (bottom panels). Fluorescent (E) and combined fluorescent/phase contrast (D & F) channels are shown. Scale bar 50 μm, panel A; scale bar 25 μm, panels B and C.

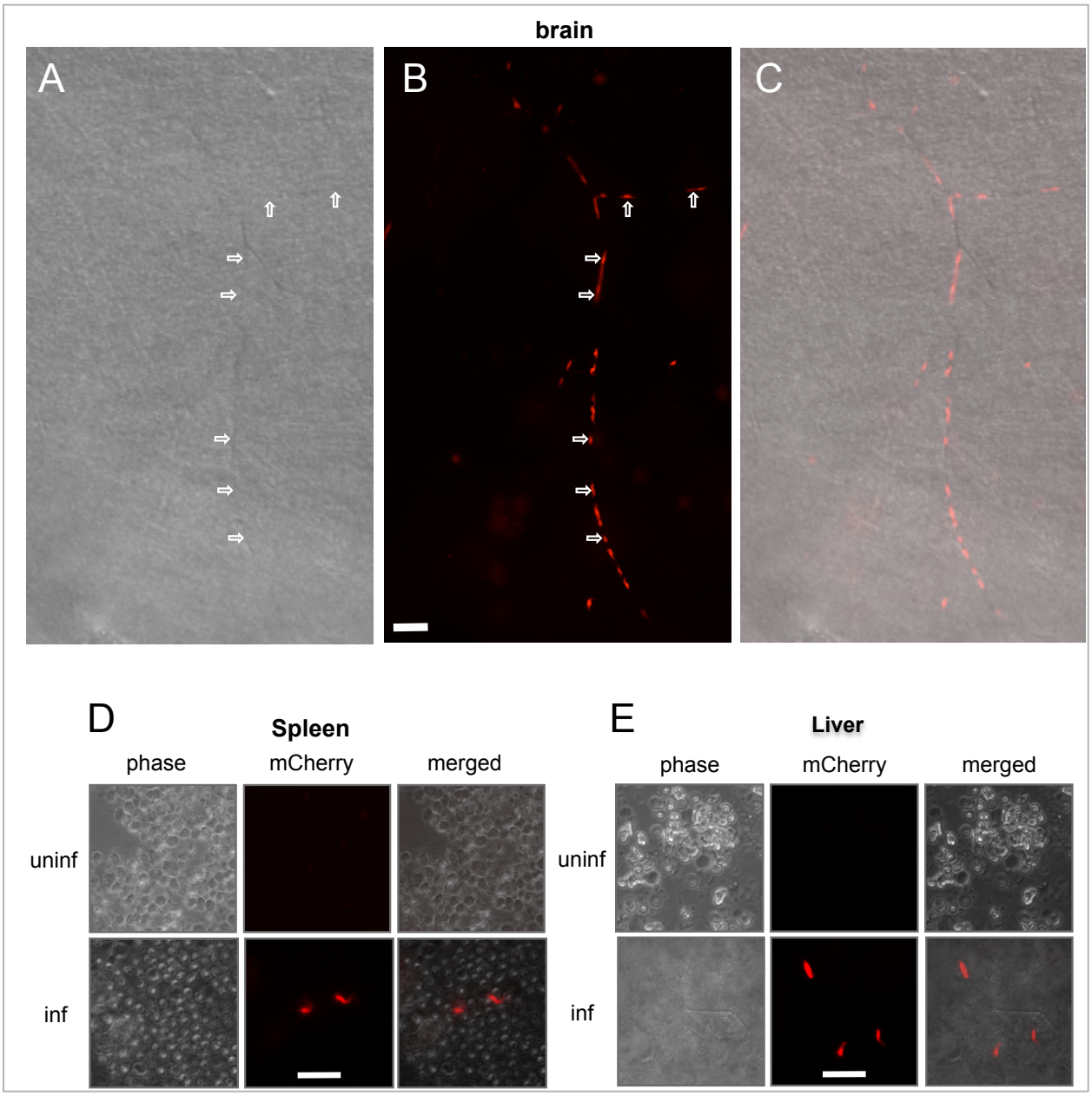

Figure 3. Direct fluorescence imaging of individual parasites in brain, spleen and liver tissues from infected mice. (A – C) Wet preparations of brain tissue from a mouse infected with BSSM-mCherry parasites were thick-sectioned and imaged by fluorescence microscopy at seven days post infection. Parasites (red) are readily seen aligned along blood vessels (arrows).

DIC (A), fluorescence (B) and merged (C) images are shown. Each panel is a composite image generated from two overlapping fields of view. Scale bar is 40 μm. (D – E) Fluorescence microscopy of spleen (D) or liver (E) tissues from uninfected mice (uninf) or mice infected with mCherry parasistes (mCherry). Wet preparations of tissues were thick-sectioned and examined by fluorescence microscopy. Individual parasites (red) are readily distinguished from host cells in each tissue type. Phase contrast (left), fluorescence (center) and merged (right) images are shown for all samples. Scale bar is 25 μm.

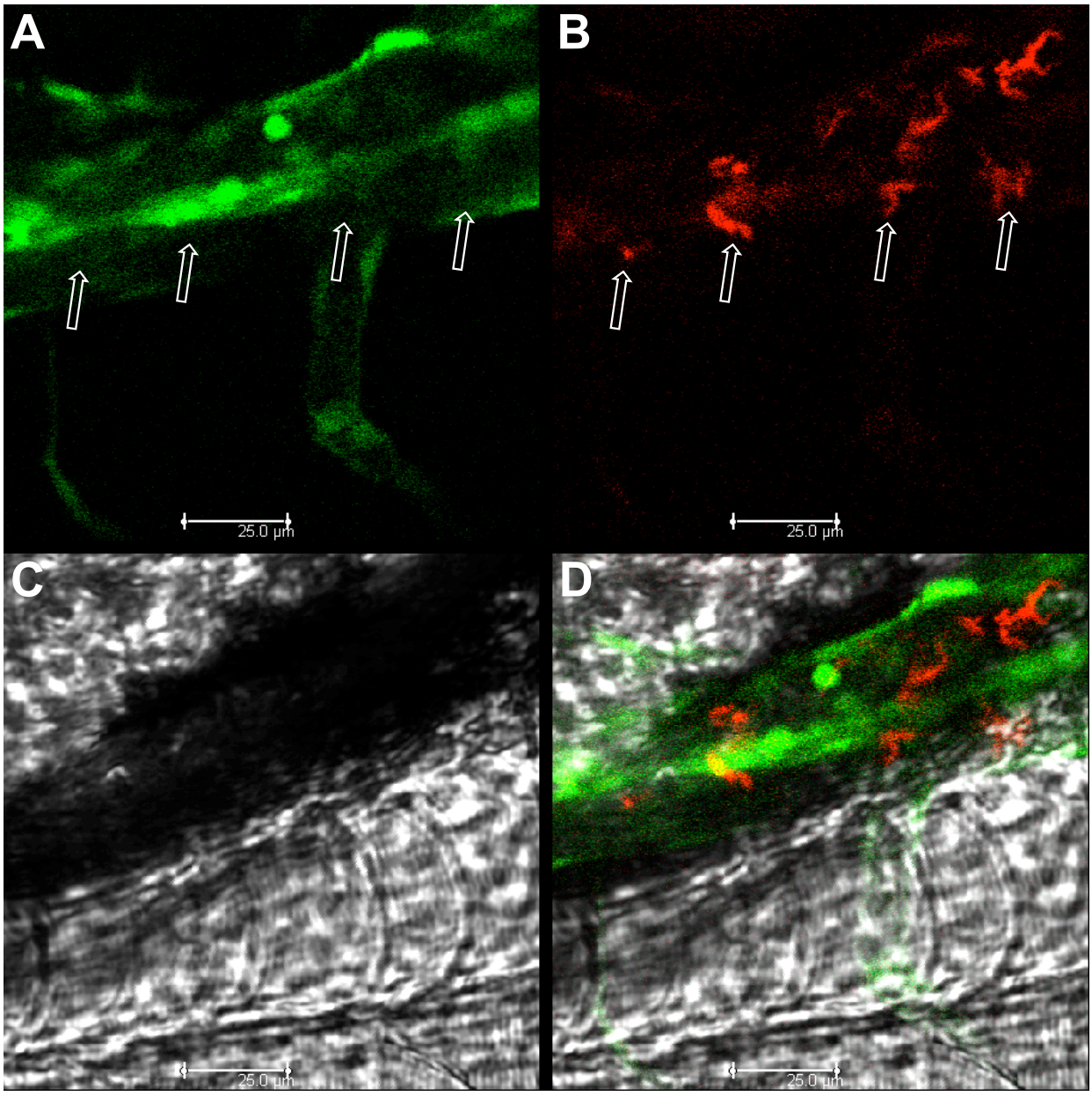

Figure 4. Individual red fluorescent trypanosomes are readily imaged within blood vessels of live fish. Red mCherry *T. brucei* were injected by cardiovascular injection in a transgenic zebrafish having green fluorescent vascular endothelia. Live zebrafish were immobilized and imaged by video microscopy in fluorescent (A) and (B), phase contrast (C), or combined fluorescent/phase contrast (D) channels. Single red fluorescent parasites (B) can be seen in the

lumen of a green blood vessel (A). Arrows represent blood vessels (A) or individual parasites (B), Scale bar is 25 μm.

Supporting Information

Supporting Videos

Video 1. *T. brucei* mCherry parasites are resolved at single-cell resolution in zebrafish. Representative live video shows individual parasites in blood vessels of a live wild type fish. Videos were taken immediately after cardiac injection of parasites. Frame rate is 15 frames/sec for capture and playback. Fish tissues and blood cells (gray) are readily distinguishable from parasites (red).

Video 2. Individual *T. brucei* mCherry parasites are visualized in fluorescently labeled blood vessels of zebrafish. Representative live video shows a single parasite in a blood vessel of a live transgenic fish with fluorescent green blood vessels. The fish blood vessel (green) and is readily distinguishable from the parasite (red). Frame rate is 15 frames/sec for capture and playback. .

CHAPTER 5 REFERENCES

Balmer, O. and Tostado, C. (2006). "New fluorescence markers to distinguish co-infecting Trypanosoma brucei strains in experimental multiple infections." Acta Trop 97(1): 94-101.

Barry, J. D. and McCulloch, R. (2001). "Antigenic variation in trypanosomes: enhanced phenotypic variation in a eukaryotic parasite." Adv Parasitol 49: 1-70.

Biebinger, S. and Clayton, C. (1996). "A plasmid shuttle vector bearing an rRNA promoter is extrachromosomally maintained in Crithidia fasciculata." Exp Parasitol 83(2): 252-258.

Borst, P. (2002). "Antigenic variation and allelic exclusion." Cell 109(1): 5-8.

Brothers, K. M., Newman, Z. R. and Wheeler, R. T. (2011). "Live imaging of disseminated candidiasis in zebrafish reveals role of phagocyte oxidase in limiting filamentous growth." Eukaryot Cell 10(7): 932-944.

Burreson, E. M. (2007). "Hemoflagellates of Oregon marine fishes with the description of new species of Trypanosoma and Trypanoplasma." J Parasitol 93(6): 1442-1451.

Bustamante, J. M. and Tarleton, R. L. (2011). "Methodological advances in drug discovery for Chagas disease." Expert Opin Drug Discov 6(6): 653-661.

Claes, F., Vodnala, S. K., van Reet, N., Boucher, N., Lunden-Miguel, H., Baltz, T. et al. (2009). "Bioluminescent imaging of Trypanosoma brucei shows preferential testis dissemination which may hamper drug efficacy in sleeping sickness." PLoS Negl Trop Dis 3(7): e486.

Coombes, J. L. and Robey, E. A. (2010). "Dynamic imaging of host-pathogen interactions in vivo." Nat Rev Immunol 10(5): 353-364.

Davis, J. M. and Ramakrishnan, L. (2009). "The role of the granuloma in expansion and dissemination of early tuberculous infection." Cell 136(1): 37-49.

Frevert, U., Engelmann, S., Zougbede, S., Stange, J., Ng, B., Matuschewski, K. et al. (2005). "Intravital observation of Plasmodium berghei sporozoite infection of the liver." PLoS Biol 3(6): e192.

Frevert, U., Movila, A., Nikolskaia, O. V., Raper, J., Mackey, Z. B., Abdulla, M. et al. (2012). "Early invasion of brain parenchyma by african trypanosomes." PLoS One 7(8): e43913.

Giroud, C., Ottones, F., Coustou, V., Dacheux, D., Biteau, N., Miezan, B. et al. (2009). "Murine Models for Trypanosoma brucei gambiense disease progression--from silent to chronic infections and early brain tropism." PLoS Negl Trop Dis 3(9): e509.

Gray, G. D., Jennings, F. W. and Hajduk, S. L. (1982). "Relapse of monomorphic and pleomorphic Trypanosoma brucei infections in the mouse after chemotherapy." Z Parasitenkd 67(2): 137-145.

Haag, J., O'HUigin, C. and Overath, P. (1998). "The molecular phylogeny of trypanosomes: evidence for an early divergence of the Salivaria." Mol Biochem Parasitol 91(1): 37-49.

Herbert, W. J. and Lumsden, W. H. (1976). "Trypanosoma brucei: a rapid "matching" method for estimating the host's parasitemia." Exp Parasitol 40(3): 427-431.

Heussler, V. and Doerig, C. (2006). "In vivo imaging enters parasitology." Trends Parasitol 22(5): 192-195; discussion 195-196.

Hitziger, N., Dellacasa, I., Albiger, B. and Barragan, A. (2005). "Dissemination of Toxoplasma gondii to immunoprivileged organs and role of Toll/interleukin-1 receptor signalling for host resistance assessed by in vivo bioluminescence imaging." Cell Microbiol 7(6): 837-848.

Hove, J. R. and Craig, M. P. (2012). "High-speed confocal imaging of zebrafish heart development." Methods Mol Biol 843: 309-328.

Hutchings, N. R., Donelson, J. E. and Hill, K. L. (2002). "Trypanin is a cytoskeletal linker protein and is required for cell motility in African trypanosomes." J Cell Biol 156(5): 867-877.

Katzenback, B. A., Plouffe, D. A. and Belosevic, M. (2013). "Goldfish (Carassius auratus L.) possess natural antibodies with trypanocidal activity towards Trypanosoma carassii in vitro." Fish Shellfish Immunol 34(5): 1025-1032.

Lang, T., Goyard, S., Lebastard, M. and Milon, G. (2005). "Bioluminescent Leishmania expressing luciferase for rapid and high throughput screening of drugs acting on amastigote-harbouring macrophages and for quantitative real-time monitoring of parasitism features in living mice." Cell Microbiol 7(3): 383-392.

Lischke, A., Klein, C., Stierhof, Y. D., Hempel, M., Mehlert, A., Almeida, I. C. et al. (2000). "Isolation and characterization of glycosylphosphatidylinositol-anchored, mucin-like surface glycoproteins from bloodstream forms of the freshwater-fish parasite Trypanosoma carassii." Biochem J 345 Pt 3: 693-700.

Ludwig, M., Palha, N., Torhy, C., Briolat, V., Colucci-Guyon, E., Bremont, M. et al. (2011). "Whole-body analysis of a viral infection: vascular endothelium is a primary target of infectious hematopoietic necrosis virus in zebrafish larvae." PLoS Pathog 7(2): e1001269.

Maclean, L., Myburgh, E., Rodgers, J. and Price, H. P. (2013). "Imaging African Trypanosomes." Parasite Immunol.

Matthews, K. R. (2005). "The developmental cell biology of Trypanosoma brucei." J Cell Sci 118(Pt 2): 283-290.

Meijer, A. H. and Spaink, H. P. (2011). "Host-pathogen interactions made transparent with the zebrafish model." Curr Drug Targets 12(7): 1000-1017.

Overath, P., Ruoff, J., Stierhof, Y. D., Haag, J., Tichy, H., Dykova, I. and Lom, J. (1998). "Cultivation of bloodstream forms of Trypanosoma carassii, a common parasite of freshwater fish." Parasitol Res 84(5): 343-347.

Phennicie, R. T., Sullivan, M. J., Singer, J. T., Yoder, J. A. and Kim, C. H. (2010). "Specific resistance to Pseudomonas aeruginosa infection in zebrafish is mediated by the cystic fibrosis transmembrane conductance regulator." Infect Immun 78(11): 4542-4550.

Poltera, A. A., Hochmann, A., Rudin, W. and Lambert, P. H. (1980). "Trypanosoma brucei brucei: a model for cerebral trypanosomiasis in mice--an immunological, histological and electronmicroscopic study." Clin Exp Immunol 40(3): 496-507.

Ralston, K. S., Kisalu, N. K. and Hill, K. L. (2011). "Structure-function analysis of dynein light chain 1 identifies viable motility mutants in bloodstream-form Trypanosoma brucei." Eukaryot Cell 10(7): 884-894.

Ralston, K. S., Lerner, A. G., Diener, D. R. and Hill, K. L. (2006). "Flagellar motility contributes to cytokinesis in Trypanosoma brucei and is modulated by an evolutionarily conserved dynein regulatory system." Eukaryot Cell 5(4): 696-711.

Rodgers, J. (2010). "Trypanosomiasis and the brain." Parasitology 137(14): 1995-2006.

Salmon, D., Vanwalleghem, G., Morias, Y., Denoeud, J., Krumbholz, C., Lhomme, F. et al. (2012). "Adenylate cyclases of Trypanosoma brucei inhibit the innate immune response of the host." Science 337(6093): 463-466.

Shaner, N. C., Campbell, R. E., Steinbach, P. A., Giepmans, B. N., Palmer, A. E. and Tsien, R. Y. (2004). "Improved monomeric red, orange and yellow fluorescent proteins derived from Discosoma sp. red fluorescent protein." Nat Biotechnol 22(12): 1567-1572.

Stich, A., Abel, P. M. and Krishna, S. (2002). "Human African trypanosomiasis." BMJ 325(7357): 203-206.

Tobin, D. M., May, R. C. and Wheeler, R. T. (2012). "Zebrafish: a see-through host and a fluorescent toolbox to probe host-pathogen interaction." PLoS Pathog 8(1): e1002349.

Tysnes, K. R., Jorgensen, A., Poppe, T., Midtlyng, P. J. and Robertson, L. J. (2012). "Preliminary experiments on use of zebrafish as a laboratory model for Giardia duodenalis infection." Acta Parasitol 57(1): 1-6.

White, R. M., Sessa, A., Burke, C., Bowman, T., LeBlanc, J., Ceol, C. et al. (2008). "Transparent adult zebrafish as a tool for in vivo transplantation analysis." Cell Stem Cell 2(2): 183-189.

Wirtz, E., Leal, S., Ochatt, C. and Cross, G. A. (1999). "A tightly regulated inducible expression system for conditional gene knock-outs and dominant-negative genetics in Trypanosoma brucei." Mol Biochem Parasitol 99(1): 89-101.

Yang, R., Reid, A., Lymbery, A. and Ryan, U. (2010). "Identification of zoonotic Giardia genotypes in fish." Int J Parasitol 40(7): 779-785.

Chapter 6

Identification of a residue critical for IFT88 function in *Trypanosoma brucei*

Abstract

Cilia and flagella[1] have emerged to occupy a central position in human physiology. Ciliary dysfunction results in several disorders and diseases termed ciliopathies. Many ciliopathy genes and disease gene candidates have been identified [Fliegauf et al., 2007], but there is limited information about specific functions and molecular mechanisms of flagellum proteins underlying most ciliopathies. *Situ inversus* is a genetic disorder in which major visceral organs are reversed from their normal body position. IFT88 is required for assembly of the flagellum and mutations in the IFT88 gene have been linked to *situs inversus* and respiratory malfunction in humans. Genetic studies in humans done by our collaborators identified several changes in the IFT88 gene between normal and diseased individuals. However, it was not possible to distinguish between disease causing mutations and benign polymorphisms in part because of the lack of facile methods for systematic mutational analysis of ciliary genes. IFT88 is conserved between humans and trypanosomes. We recently established systems for structure-function analysis of proteins in the protozoan parasite *Trypanosoma brucei*, which has emerged as an excellent model to study eukaryotic flagella. In these systems a mutant protein is expressed in a background where the endogenous, wild type protein is depleted or absent, allowing discovery of protein domains or amino acids required for function. In the present study we have exploited this system to test the function of IFT88 mutations synonymous with those observed in humans with *situs inversus*. Expression in *T. brucei* of the above mutations allowed identification of a single amino acid essential for IFT88 function. IFT88R597H mutation disrupted flagellum function while IFT88R260Q did not, thus distinguishing between loss of function mutations and benign polymorphisms. To our knowledge this is the first time a single residue has ever been identified to be essential for the function of IFT88. The IFT88R597H

1. Cilia and flagella can be used interchangeably.

mutation described here provides a unique opportunity to decipher cilia functions in adult mammals by introducing the corresponding mutation in a vertebrate system.

Introduction

Cilia are microtubule-based organelles projecting from the surface of virtually every cell type in mammals. Cilia are evolutionary conserved and are required for many cellular functions including motility, signaling, sensory reception, and sexual reproduction [Badano et al., 2006]. These organelles are essential for human physiology. For example, cilia-driven motility is essential to clear mucus out of respiratory tracts, move eggs in oviducts, and generate the flow essential for determining left–right asymmetry of the viscera in the embryo [Badano et al., 2006; Bisgrove and Yost 2006; Willaredt et al., 2008]. As such, cilia defects cause many diseases generally known as ciliopathies, including polycystic kidney disease.

Intraflagellar transport (IFT) is implicated in eukaryotic cilia assembly but also participates in non-ciliary functions such as membrane trafficking in non-ciliated cells [Finetti et al., 2009]. IFT is the bidirectional movement of multimeric complexes along cilia. Microtubule-based motor proteins Kinesin-2 and cytoplasmic dynein 2 move IFT proteins and their cargos along the axoneme of cilia [Rosenbaum and Witman 2002; Pedersen and Rosenbaum 2008]. Most IFT proteins contain domains known to mediate protein–protein interaction. The IFT system in *Chlamydomonas reinhardtii* has 20 proteins organized in two biochemically different complexes. Complex A returns IFT trains from the flagellum tip to the cell body for turnover, whereas complex B is important for the anterograde movement required for cilia formation and maintenance [Piperno and Mead 1997; Cole et al., 1998; Cole 2003]. Many subunits of the IFT machinery have been discovered, however very little is known about how the IFT proteins carry out their function individually or together. For example, it is unclear how IFT proteins interact with the cargoes they transport [Bhogaraju et al., 2013; Bhogaraju et al., 2013].

The IFT Complex B protein IFT88 is homologous to the polycystic kidney disease gene Tg737 in mice. The *Chlamydomonas reinhardtii* IFT88 has 9-10 tetratricopeptide repeats (TPR) (Fig. 2A), which are degenerate 34–amino acid repeats [Lamb et al., 1995] predicted to form amphipathic helices and to mediate protein-protein interactions [Pazour et al., 2000]. This protein is highly conserved among ciliated organisms including trypanosomes, fish, and humans. IFT88 localizes to cilia [Taulman et al., 2001; Kohl et al., 2003] and is required for cilium assembly in many ciliated organisms [Perkins et al., 1986; Pazour et al., 2000; Haycraft et al., 2001; Kohl et al., 2003; Tsujikawa and Malicki 2004].

Disruption of IFT88 has been shown to cause defects in a variety of organisms. Disruption of IFT88 in *Chlamydomonas* abrogates flagella formation and affects signaling [Pazour et al., 2000; Satir 2007]. Mice with hypomorphic mutations in the IFT88 homolog Tg737 assemble shorter cilia in their kidneys and have severe polycystic kidney disease with phenotypes similar to human autosomal recessive polycystic kidney disease (ARPKD) [Moyer et al., 1994; Yoder et al., 1996; Pazour et al., 2000; Haycraft et al., 2001; Huangfu et al., 2003]. Null alleles of Tg737 have a more severe phenotype because these mutant mice lack cilia on the embryonic node, have defects in Hedgehog signaling, manifest left–right asymmetry impairment, and die *in utero* [Murcia et al., 2000]. IFT88 disruption in zebrafish causes defects in sensory neurons [Tsujikawa and Malicki 2004; Sukumaran and Perkins 2009]. Roles for IFT88 in cell division [Robert et al., 2007; Delaval et al., 2011] as well as bone and cartilage formation have also been demonstrated [Ochiai et al., 2009], exemplifying critical functions of this protein. Our collaborator Dr. Heymut Omran in Germany had identified mutations in IFT88 that are associated with *situs inversus*, a congenital condition in which left to right asymmetry is

disrupted and the major abdominal organs are reversed from their normal positions. However, it isn't known if these substitutions are disease-causing mutations or simply polymorphisms that don't affect function.

African trypanosomes *Trypanosoma brucei* and related subspecies are protozoan parasites that cause African sleeping sickness, a fatal disease with devastating health and economic consequences in sub-Saharan Africa. These parasites are highly motile and rely on their own flagellum-dependent motility to move into different tissues to cause disease. Other roles of the flagellum in *T. brucei* include cell division and morphogenesis, sensing, and pathogenesis [Ralston and Hill 2008]. *T. brucei* has emerged as an execellent model system to study the eukaryotic cilium or flagellum [Ralston and Hill 2008; Vincensini et al., 2011]. Conserved and specific flagellar proteins have been identified in *T. brucei* [Li et al., 2004; Branche et al., 2006; Broadhead et al., 2006; Baron et al., 2007]. However, there is scant information on how flagellar proteins actually work, because all studies to date have used RNAi, which can determine if a protein is required for flagellum function, but does not give information about mechanisms. We established a facile system for structure function studies in *T. brucei* (Appendix 2) [Ralston et al., 2011]. This strategy is based on the expression of a mutant protein in a background where the endogenous, wild type copy is depleted. This system allows identification of key protein domains and residues that are essential for flagellum function. In the present study we applied this system to discover residues required for IFT88 function. Expression in *T. brucei* of the corresponding IFT88 mutations found in patients with *situs inversus* led to identification of the IFT88R597H point mutation that disrupted flagellum function, indicating this residue is essential for IFT88 function in this parasite. Given the

conserved nature of this residue in IFT88 in both trypanosomes and humans, our data suggest a similar effect of the corresponding mutation *in situs inversus* in humans.

Results

Generation of 3' UTR RNAi (knockdown) IFT88 cell line.

A major obstacle to investigations of flagellum protein structure-function is an absence of systems for detailed mutational assessment of a given gene. To bridge this gap we recently developed a two-plasmid system for RNAi-based structure-function studies in *T. brucei* (Appendix 2) [Ralston et al., 2011]. The two-plasmid system relies on robust systems for inducible RNAi and protein expression in *T. brucei* to guide tetracycline-inducible RNAi against a target mRNA 3'UTR, with simultaneous inducible expression of an epitope-tagged version of the targeted gene that is immune to RNAi. In this system the p2T7TiB RNAi [LaCount et al., 2002] plasmid is used to drive tetracycline-inducible expression of target dsRNA, whereas the pKR10 [Ralston et al., 2011] vector drives tetracycline-inducible expression of an RNAi-resistant wild-type or mutant version of the target gene's open reading frame (ORF) bearing an epitope tag. This system allows replacement in *T. brucei* of an endogenous protein with a mutated copy in a background where the endogenous protein is absent or has been depleted. The mutated protein still assembles, but may not function, enabling identification of recessive as well as dominant mutations. With this strategy we previously identified amino acids in the dynein light chain 1, "LC1", that are required for motility (Appendix 2) [Ralston et al., 2011].

To generate the IFT88 3' UTR RNAi cell line, 29-13 cells harboring the machinery for tetracycline-inducible gene expression (Wirtz et al., 1999) were stably transfected with p2T7-Ti-B constructs to guide RNAi against the first 502 bp of the 3′ UTR of IFT88. Upon tetracycline-

induction, quantitative real time PCR (qRT PCR) analysis demonstrated that IFT88 was successfully knocked down (Figure 1A). Transcription in *T. brucei* is polycistronic [Vanhamme and Pays 1995]. Thus, qRT PCR analysis was done to show that IFT88 was depleted without affecting the mRNA of the downstream gene (Figure 1A). IFT88 ablation caused lethality (Figure 3E) characterized by accumulation of large amorphous masses that failed to divide (Figure 1D). Defective motility was also observed upon IFT88 knockdown as demonstrated by the sedimentation assay (Figure 1B), as well as motility traces (Figure 4B-C) and high resolution video microscopy (Videos 1-2) of individual parasites. Some induced cells have very short flagella while others lack flagella completely (Figure 1D and Video 2). These results mirror the phenotypes of the IFT88 ORF RNAi mutants described previously [Kohl et al., 2003]

To see whether wild type (WT) IFT88 rescues the phenotype of IFT88 knockdowns in our system, we cloned the IFT88 ORF in-frame with an HA epitope tag into the expression vector pKR10 [Ralston et al., 2011]. The resulting plasmid was subsequently introduced into the IFT88 3' UTR knockdown cell line. Following tetracycline-induction, wild type (WT) HA-IFT88 protein was produced in induced cells as demonstrated by western blot analysis (Figure 1C). In addition, HA-IFT88 correctly localized to the flagellum (Figure 4A) as was previously shown for the endogeous IFT88 [Kohl et al., 2003]. Importantly, WT HA-IFT88 rescued the IFT88 RNAi knockdown lethality phenotype, restored flagella assembly and motility in induced cells as demonstrated by the sedimentation assay (Figure 1B), DIC images (Figure 1D), growth rates (Figure 3E), motility traces (Figure 4B-C), and high-resolution video microscopy (Video 3). These data therefore demonstrate that we specifically targeted IFT88 in *T. brucei.*

IFT 88 amino acids to target for mutagenesis in *T. brucei*

Dr. Heymut Omran, our collaborator at the University Hospital Muenster at Munich, Germany, identified genetic changes in the IFT88 coding sequence from patients with *situs inversus* (Figure 2A). These mutations include R266Q, E331X, S356N, R607H and are summarized in Table 1. To determine if the above mutations are conserved in *T. brucei,* we performed sequence alignment. Alignment of human and trypanosome IFT88 sequences demonstrates strong sequence conservation between the proteins (Figure 2B). Overall, TbIFT88 is 40% identical to HsIFT88. Sequence alignment revealed that amino acids R266, E331 and R607 are conserved in *T. brucei*, whereas S356 is not conserved (Figure 2B). Their corresponding residues in *T. brucei* are R260, E325, R597, and S350 respectively (Figure 2B). E331X introduces a premature stop codon in the IFT88 polypeptide. Introduction of a premature stop codon in IFT88 has been shown to disrupt IFT88 function in mice and zebra fish [Moyer et al., 1994; Pazour et al., 2000; Huangfu et al., 2003; Tsujikawa and Malicki 2004; Willaredt et al., 2008]. Serine 356 is not conserved in *T. brucei*. For these reasons, we decided to focus on the R266Q and R607H mutations. Notably both R266Q and R607H mutations appear to locate within regions of high conservation (Figure 2C) and within the IFT88 TPR motifs. To test whether these mutations disrupt IFT88 function, we mutagenized and introduced the corresponding R260Q and R597H mutations in *T. brucei* (Fig. 3A-B). IFT88 point mutant genes were cloned in-frame with an HA epitope tag into the expression vector pKR10 [Ralston et al., 2011]. The resulting plasmids were subsequently used to transfect the IFT88 3' UTR knockdown *T. brucei*.

Phenotypes of IFT88 point mutants

Upon tetracycline induction, both mutant proteins HA-IFT88R260Q and HA-IFT88R597H, hereafter referred to as R260Q and R597H, were well expressed in induced cells (Figure 3C). Both mutant proteins correctly localize to the flagellum (Fig. 4A) as reported previously for the endogenous IFT88 [Kohl et al., 2003]. Expression of the point mutants rescued the lethality phenotype of IFT88 knockdown. Moreover, the point mutants assemble flagella with normal length and have normal growth rates, although R597H cells grow slowly compared to uninduced cells (Figure 3D-E). R260Q mutant cells (not shown) exhibited no discernable defects, indicating this amino acid is not required for IFT88 function in *T. brucei*. By contrast, R597H mutants have defective motility, as demonstrated by motility traces (Figure 4B-C), and video microscopy (Videos 4-6). A proportion of R597H mutants spin (Video 5) like the previously described dynein regulatory trypanin mutants [Hill et al., 2000], whereas some cells move backward (Video 6) as seen in the LC1 knockdown mutants [Baron et al., 2007]. Taken together these data indicate that R597H is a hypomorphic mutation that causes a partial loss of IFT88 function in *T. brucei* and strongly suggest the implication of the corresponding mutation in *situs inversus* observed in humans harboring this mutation.

Discussion

We have successfully knocked down the IFT88 transcript by directing RNAi against its 3' UTR . IFT88 3' UTR RNAi reproduced the IFT88 ORF RNAi phenotype [Kohl et al., 2003] and caused lethality in *T. brucei*. Expression of a HA-tagged WT-IFT88 rescues the lethality phenotype associated with depletion of the endogenous IFT88. Sequence alignment showed three out of four IFT88 residues mutated in humans with *situs inversus* are conserved in *T. brucei*. These amino acids are located within regions of high conservation and within the TPR motifs of the IFT88 polypeptide. We have reconstructed the corresponding R260Q and R597H mutations in *T. brucei* using our recently established RNAi system for structure function analysis of flagellar proteins (Appendix 2) [Ralston et al., 2011]. Expression in *T. brucei* of R260Q and R597H mutations rescued the lethality phenotype of IFT88 knockdown as well as restored normal flagella length. Although expression of R260Q did not cause any discernable defects in the induced cells, R597H in contrast is a partial loss of function mutation that disrupted motility in this parasite. Hence the amino acid R597 is required for IFT88 function in *T. brucei*.

Previous investigations have shown that IFT88 knockdown in *T. brucei* blocks flagellum assembly, impairs cell size, shape, polarity, cell division, as well as causes lethality [Kohl et al., 2003; Absalon et al., 2008]. However, the phenotypes of IFT88 point mutants differ significantly from the phenotypes resulting from complete ablation of IFT88 in this parasite. R260Q mutant trypanosomes do not exhibit any discernable abnormal phenotype. This might signify either the synonymous mutation is a benign polymorphism that does not affect function or species-specific differences for the requirement of this amino acid. It is also possible that R260Q causes subtle changes in the flagellum function that we were unable to track. It has previously been shown

that replacement of glutamine by arginine in IFT172, another intraflagellar transport protein necessary for the retrograde movement in flagella, is predicted to be a structurally conservative amino acid substitution in the *C. elegans* and *C. reinhardtii* orthologs of IFT172 [Karlin and Ghandour 1985; Tran et al., 2008]. It is therefore possible that IFT88-R260Q is a structurally conservative residue substitution in *T. brucei*. R266Q, the corresponding IFT88R260Q mutation in humans, is heterozygous. However, using our structure-function analysis system we expressed this mutation as a homozygous mutation in *T. brucei*. Previous investigations have shown that some heterozygous mutations, when expressed as homozygous mutations, restore function [Liu et al., ; Crosby et al., 1992; Liu et al., 2011], which could explain why we did not discern any abnormal phenotypes in the R260Q mutants in trypanosomes.

R597H parasites assemble flagella but are defective in motility. It is unclear how R597H disrupts flagellum function in *T. brucei*. Structurally, R597 is located within one of the seven TPR motifs that are found without spacing between residues 441–676 of IFT88 in *C. reinhardtii* [Pazour et al., 2000]. Several investigations evoke interactions between the TPR-polypeptide IFT88 and ciliary cargos [Bhowmick et al., 2009; Trivedi et al., 2012; Bhogaraju et al., 2013]. Since TPR motifs mediate protein-protein interactions [Lamb et al., 1995; Cole 2003; Jekely and Arendt 2006; Taschner et al., 2012; van Dam et al., 2013] it is therefore possible that R597H disrupts the interaction between IFT88 and its cargoes or interacting partners, thereby compromising flagellum function in *T. brucei*. Furthermore, IFT associations with its cargos are believed to be transient since such interactions, with fast off-rates, may be useful as they would facilitate cargo unloading when the IFT trains reach the flagellum tip [Lechtreck et al., 2009]. It is possible that the R597H substitution disrupts this mechanism.

The eukaryotic flagellum or cilium has emerged as a major signaling center for virtually all organisms where it has been examined. Indeed, flagella are essential for sensing and mating in *Chlamydomonas* [Badano et al., 2006] and many proteins that are important for signal transduction have been localized to the flagellum of several organisms [Perkins et al., 1986; Huangfu et al., 2003; Haycraft et al., 2005; Huangfu and Anderson 2005; Badano et al., 2006; Caspary et al., 2007; Fliegauf et al., 2007] including *T. brucei* [Perkins et al., 1986; Huangfu et al., 2003; Haycraft et al., 2005; Huangfu and Anderson 2005; Badano et al., 2006; Caspary et al., 2007; Fliegauf et al., 2007; Oberholzer et al., 2011]. Hence it is possible that R597H disrupts the sensing mechanism of the flagellum in *T. brucei*. Testing such a hypothesis is beyond the scope of the present study and further investigations are needed to address this idea. Nevertheless, our data clearly indicate that R597H is a hypomorphic mutation that partially disrupts flagellum function in *T. brucei*.

IFT88 is essential for ciliary and non-ciliary functions such as trafficking and cell division [Robert et al., 2007; Delaval et al., 2011], exemplifying the role of this protein in many biological processes. Consequently, loss of IFT88 homologs in vertebrates including humans is associated with a broad range of pathologies. Indeed, ablation of *polaris,* the IFT88 homolog in mice, causes motile and sensory cilia impairment with randomized left-right asymmetry, absence of cilia in the node, abnormal brain morphology, severe polycystic kidney disease accompanied by retinal defects, and early embryonic lethality [Murcia et al., 2000; Pazour et al., 2000; Huangfu et al., 2003; Tsujikawa and Malicki 2004; Badano et al., 2006]. Total disruption of the IFT mechanism is incompatible with life [Badano et al., 2006] because it blocks cilia and flagella biogenesis as was demonstrated for null IFT88 mutants in small animals. Ciliary motility is

required for left-right flow in the node, which is essential for the establishment of left-right asymmetry of the body during the development. This could explain why, up to date, no null IFT88 human patients have been found.

A number of hypomorphic IFT88 mutations have been generated [Moyer et al., 1994; Pazour et al., 2000; Huangfu et al., 2003; Tsujikawa and Malicki 2004]; despite their hypomorphic nature, all the above mutants are nonetheless lethal in small animals early after birth, precluding any ciliary function studies in adult tissues. The fact that the R597H mutation does not cause any observable lethality in trypanosomes may be consistent with the observation that patients harboring the corresponding R607H mutation can attain adulthood. It also suggests that this mutation only impedes discrete cilia and flagella functions in humans. Data obtained in *T. brucei* therefore strongly suggest that the R607H mutation is involved in *situs inversus* humans. Additional studies in small animals are needed to confirm whether this mutation causes *situs inversus*.

How might R607H cause *situs inversus*? Firstly, it is possible that R607H disrupts motility functions of cilia or flagella, which leads to decreased generation of the left-right flow in the node during early embryonic development in vertebrates. Decreased or absent motility of nodal cilia has been shown to disrupt the left-right body symmetry in mice [Huangfu et al., 2003]. Second, the mouse IFT88 homolog *polaris* has been shown to be required for the Sonic Hedgehog signaling pathway in animals [Murcia et al., 2000; Haycraft et al., 2005; Caspary et al., 2007; Veland et al., 2009]. It is tempting to speculate that R607H disrupts cilia sensory function in mammals as has been reported for several IFT mutants including IFT88 mutants [Pazour et al., 2002; Yoder et al., 2002; Huangfu et al., 2003; Haycraft et al., 2005; Huangfu and

Anderson 2005; Liu et al., 2005; May et al., 2005; Nauli et al., 2008; Tran et al., 2008]. Finally, R607H could also impede both motility and sensory functions of cilia in humans.

Our understanding of morphological defects and the role of cilia and flagella over time is hindered by the lethality of IFT mutants and severe systemic pathology leading to early mortality in hypomorphic and null mutants [Takeda et al., 1999; Murcia et al., 2000; Davenport et al., 2007]. Conditional null alleles of *Tg737*, the mouse IFT88 homolog, have been utilized to overcome such barriers [Davenport and Yoder 2005]. Identification of another IFT88 hypomorphic mutation described here should complement the above studies and provides a unique opportunity to study the role of cilia and flagella in adult animals.

Experimental procedures

Sequence Alignment

Human IFT88 protein sequence was downloaded from the GeneDB website. *Homo sapiens* and *T. brucei* IFT88 sequence alignments were performed with the Clustal W algorithm [Thompson et al., 1994] using Vector NTI software (Vector NTI Advance Suite 8, InforMax Inc., Bethesda, MD)

DNA plasmids and sequencing

The RNAi plasmid was constructed in p2T7^{Ti}B, which comprises two opposing tetracycline-inducible T7 promoters aimed to generate an intermolecular double stranded RNA upon tetracycline-induced transcription [LaCount et al., 2002]. In order to generate p2T7^{Ti}B/IFT88-UTR, a 502-bp fragment that corresponds to nucleotides 1 – 502 of the IFT88 (Tb11.55.0006) 3′ UTR was amplified by PCR from 29-13 genomic DNA and cloned into p2T7^{Ti}B at the TOPO recognition sites flanked by the opposed T7 promoters. Full-length IFT88 (Tb11.55.0006) was PCR-amplified from 29-13 genomic DNA. Mutant IFT88 genes were generated by site-directed mutagenesis with the QuickChange II kit (Stratagene). The pKR10 expression vector described in [Ralston et al., ; Ralston et al., 2011] was used to express the full-length open reading frames of the IFT88 wild type (WT) or mutant genes in parasites. Briefly,

full-length IFT88 WT and point mutant genes were first separately subcloned into pCR-Blunt-II-TOPO (Invitrogen) before cloning them downstream of the HA tag into the *Xho* I and *Mfe* I sites in pKR10. All DNA constructs were verified by direct sequencing and linearized at the unique pKR10 *Not*I site prior to parasite transfection. Sequencing was performed at UCLA Genotyping and Sequencing Core Facility or at Genewiz. Primers used to PCR-amplify WT IFT88 gene are as follow: 5' ATG GAC TTA CAA CAG GGT GAC 3' and 5' TAT TCC CGG GAG GTC AAT TTC 3'. Primers used to generate points mutants are as follow: IFT88R260Q 5' GCC ATT AAA ATG TAC CAA ATG ACG TTG GAC GAG 3' and 5' CTC GTC CAA CGT CAT TTG GTA CAT TTT AAT GGC 3'; IFT88R598H 5' CCC TCT ACG CTC ACG AAG GGG ACG AC 3' and 5' GTC GTC CCC TTC GTG AGC GTA GAG GG 3'. Nucleotide substitutions are underlined on the primer sequences. Primers used to sequence the full-length IFT88 WT and point mutant genes are as follows: 5' ATG GAC TTA CAA CAG GGT GAC 3'; 5' CTC TGC AAG CAG CGT GAG A 3'; 5' GGT GCG GAA GGG GAA GAC G 3'; 5' TAT GAA AAG GCA CGA ACT TAC TAC 3'; 5' CGT AAG TAC CCG GAG AAC CT 3'.

Cell culture and transfection

For all experiments we used procyclic form 29-13 cells [Wirtz et al., 1999] engineered to express T7 polymerase and tet repressor. Cells were grown at 28 ºC in Cunningham's SM supplemented with 10% heat-inactivated fetal calf serum (HIFCS) as described in [Ralston et al., 2006]. Transfections were carried out as described [Ralston et al., 2011]. Briefly, cells were washed and resuspended to $5x10^7$ cells/ml in electroporation medium (EM) simultaneously with

linearized plasmid DNA (10 μg). Electroporation was carried out using a Bio-Rad Gene Pulser. After transfection, cells were shifted to fresh medium and incubated overnight in order to recover before initiation of drug selection within 24 hours post-transfection. Cells were cloned by limiting dilution following transfection. To assess cell growth, parasites were split into two flasks and cultured with or without tetracycline (1 μg/ml) before parasites were counted in a Coulter counter and the means of two independent counts are reported for growth curves.

RNA preparation and quantitative real-time (RT)-PCR

RNA preparation and quantitative RT-PCR were performed as in [Ralston et al., ; Ralston et al., 2011]. Briefly, cells were split with or without tetracycline (1 μg/ml) and grown for 72 hours. Total RNAs were extracted using an RNeasy kit (Qiagen). Real-time PCR was performed using SYBR master mix (Bio-Rad) and gene-specific primers after reverse transcription using oligo dT primers (Invitrogen) and the SS RT II kit (Invitrogen) on DNase I (Invitrogen)-treated RNA samples (2 μg). Housekeeping genes RPS23 (Tb10.70.7020/Tb10.70.7030) and GAPDH (Tb927.6.4280/Tb927.6.4300) were used as normalization controls and the relative gene expression was done by the $2^{-\Delta\Delta CT}$ method as described previously [Livak and Schmittgen 2001]. Data presented are averages from two independent runs of -Tet and +Tet cultures. Error bars indicate the standard deviations. Quantitative RT-PCR primers used were as follows: RPS23 5′ AGA TTG GCG TTG GAG CGA AA 3′ and 5′ GAC CGA AAC CAG AGA CCA GCA 3′; GAPDH, 5′ GGC TGA TGT CTC TGT GGT GGA 3′ and 5′ GGC TGT CGC TGA TGA AGT CG 3′; IFT88 5’ ACA GTT GGG

CTG GGC GAT AA 3' and 5' CTG CTT TGC ACC GCC TTT TT 3'; Tb11.55.0007 (gene downstream of IFT88) 5′ AAG AGC GAG CCA GCC CAA AT 3′ and 5′ GCC ACG CGA CGA AGT ATT CC.

Western blot

Total cell lysate preparations were made from parasites cultured for 72 hours with or without tetracycline (1 μg/ml). These total lysates were used for western blot experiments performed as previously described [Hill et al., 2000]. An anti-HA monoclonal antibody (Covance) was use to probe the HA-IFT88 proteins, while an anti-β-tubulin monoclonal antibody (Developmental Studies Hybridoma Bank, University of Iowa) was used as a control for protein loading.

Immunofluorescence assays

Immunofluorescence analysis was performed as previously described [Oberholzer et al., 2011]. Cells were washed three times in PBS and air-dried onto coverslips. Cells were incubated for 10 min in methanol and 10 min in acetone at -20°C. Following a rehydration step in PBS, the slides were blocked in blocking solution (PBS + 5% BSA + 5% Normal donkey serum (Gibco)) for 1.5 h. Cells were subsequently incubated for 1.5 h with the primary anti-HA antibody (Covance) diluted 1:1,000 in blocking solution. After 5 washes of 10 min each in PBS

+ 0.05% Tween-20, samples were stained for 1.5 h with the secondary antibody (donkey anti-mouse Alexa Fluor 488) diluted in blocking solution. After washing five times in PBS + 0.05% Tween-20 and once in PBS, cells were mounted with Vectashield containing DAPI (Vector Laboratories). Images were acquired with a 63x objective on a Zeiss Axioskop II compound microscope and processed using Axiovision (Zeiss, Inc.) and Adobe Photoshop (Adobe Systems, Inc.).

Motility assays

All motility assays including sedimentation assays, motility traces, and high-resolution video microscopy were carried out as previously described [Ralston et al., ; Ralston et al., 2011]. Briefly, cells were grown for 72 hours with or without tetracycline. For sedimentation assays [Bastin et al., 1999], parasites were reconstituted to $5x10^6$ cells/ml and incubated in fresh culture medium under normal growth conditions. Measurements of the optical density at 600 nm (OD600) for resuspended and undisturbed samples were taken every two hours for a period of ten hours. The ΔOD600 expresses the difference obtained by subtracting the OD600 of the resuspended from the undisturbed sample. Data presented are averages from two independent experiments of -Tet and +Tet cultures. Error bars indicate the standard deviations.

To record motility traces, cells were grown with or without tetracycline and cell motility analysis was done at 72 hours post induction (hpi). Motility traces were done as described [Ralston et al., 2011]. Briefly, parasites were examined in polyglutamate-coated slide chambers [Gadelha et al., 2005] using dark field optics on a Zeiss Axioskop II compound microscope with a 10x objective. Videos were captured using a COHU analog video camera. Analog format

movies were converted to digital format with an ADVC-300 digital video converter (Canopus, Co., Ltd.). Movies were recorded at 30 frames per second (fps) and converted to AVI format and then to stacks of TIFF images using Adobe Premiere Elements software (Adobe Systems). TIFF image stacks were analyzed using Metamorph software (Molecular Devices) to trace parasite movement over the indicated time period. Trace data were used to calculate the total distance travelled. The statistical analysis for significance was calculated by comparing datasets to RNAi –Tet using the student's unpaired two-tailed T test.

For high-resolution videos of individual cells, videos were captured in motility chambers using DIC optics on a Zeiss Axiovert 200 M inverted microscope with a 100x oil-immersion objective.

Acknowledgments

Funding for the work was provided by grants to my advisor Professor Kent L. Hill from NIH-NIAID (AI052348) and Burroughs Wellcome Fund. I am a recipient of the UCLA Shapiro Fellowship and of the UCLA Dissertation Year Fellowship (2012-2013). I am grateful to Madeleine Cross for excellent technical assistance.

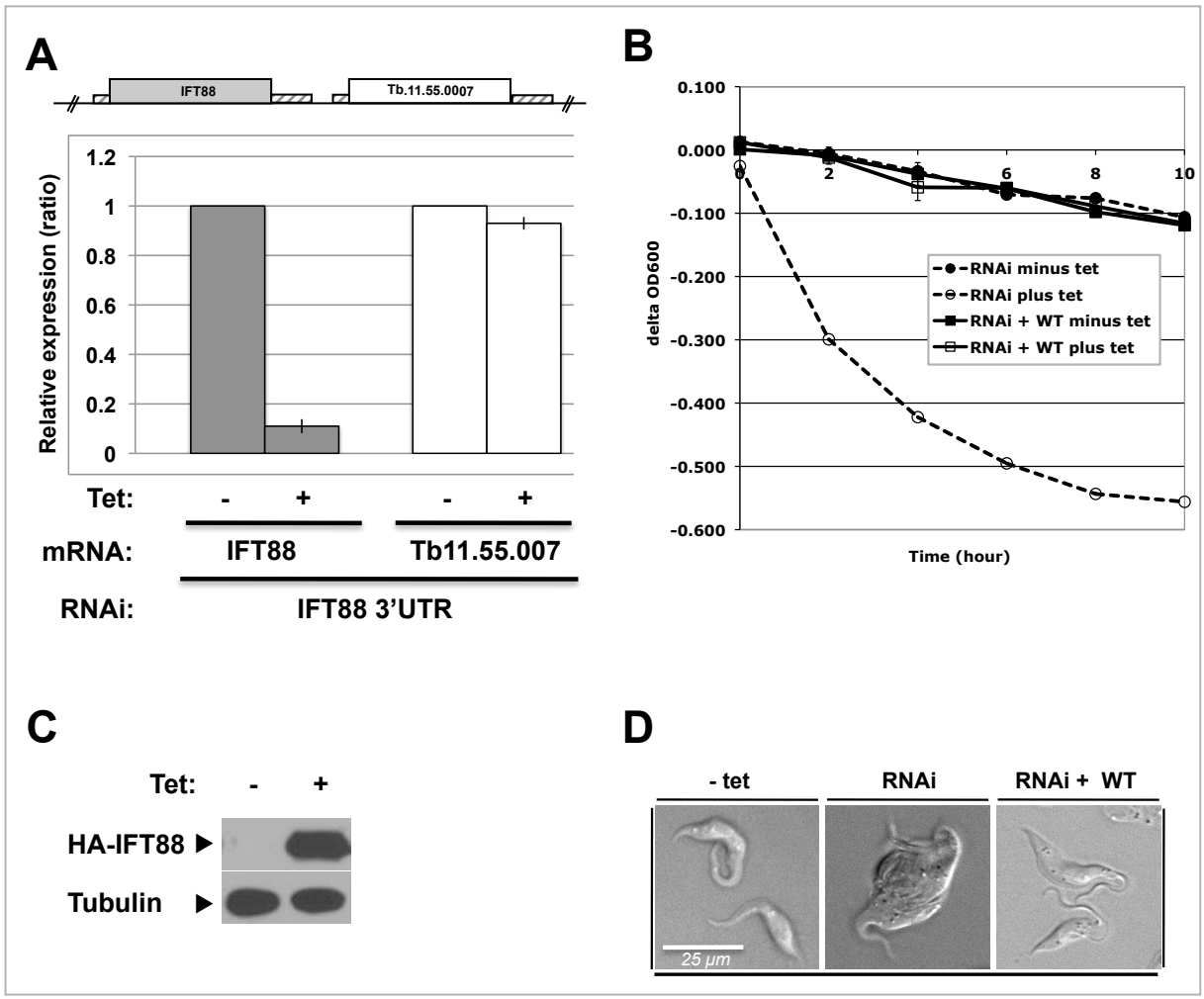

Figure 1. WT IFT88 rescues the lethality phenotype of IFT88 3' UTR knockdown. (A) Quantitative RT-PCR assay of IFT88 expression in IFT88 3'UTR RNAi cells (RNAi). Data are averages from two independent sets of minus and plus tetracycline cultures. Error bars indicate the standard deviations. Both the targeted gene (IFT88) and the gene immediately downstream (Tb11.02.0007) were analyzed. (B) Sedimentation assay of IFT88 RNAi (RNAi) or IFT88 3' UTR RNAi rescued with HA-IFT88 (RNAi + WT) parasites from –Tet and +Tet cultures. Sedimentation curves are the averages of two independent experiments, while error bars

represent standard deviations. (C) Western blot of total protein from IFT88 3' UTR knockdown parasites rescued with wild type HA-IFT88 grown in the presence or absence of tetracycline for 72 h. Blots were probed with antibody against the HA epitope to detect HA-IFT88, or β-tubulin as a loading control. (D) DIC images of live RNAi and RNAi + WT-IFT88 parasites from -Tet or +Tet cultures. Representative RNAi parasites from +Tet culture are inviable and accumulate as amorphous masses with short or no flagella, whereas RNAi + WT-IFT88 are viable and have normal morphology and flagella length. For all panels cells were induced for 72 h.

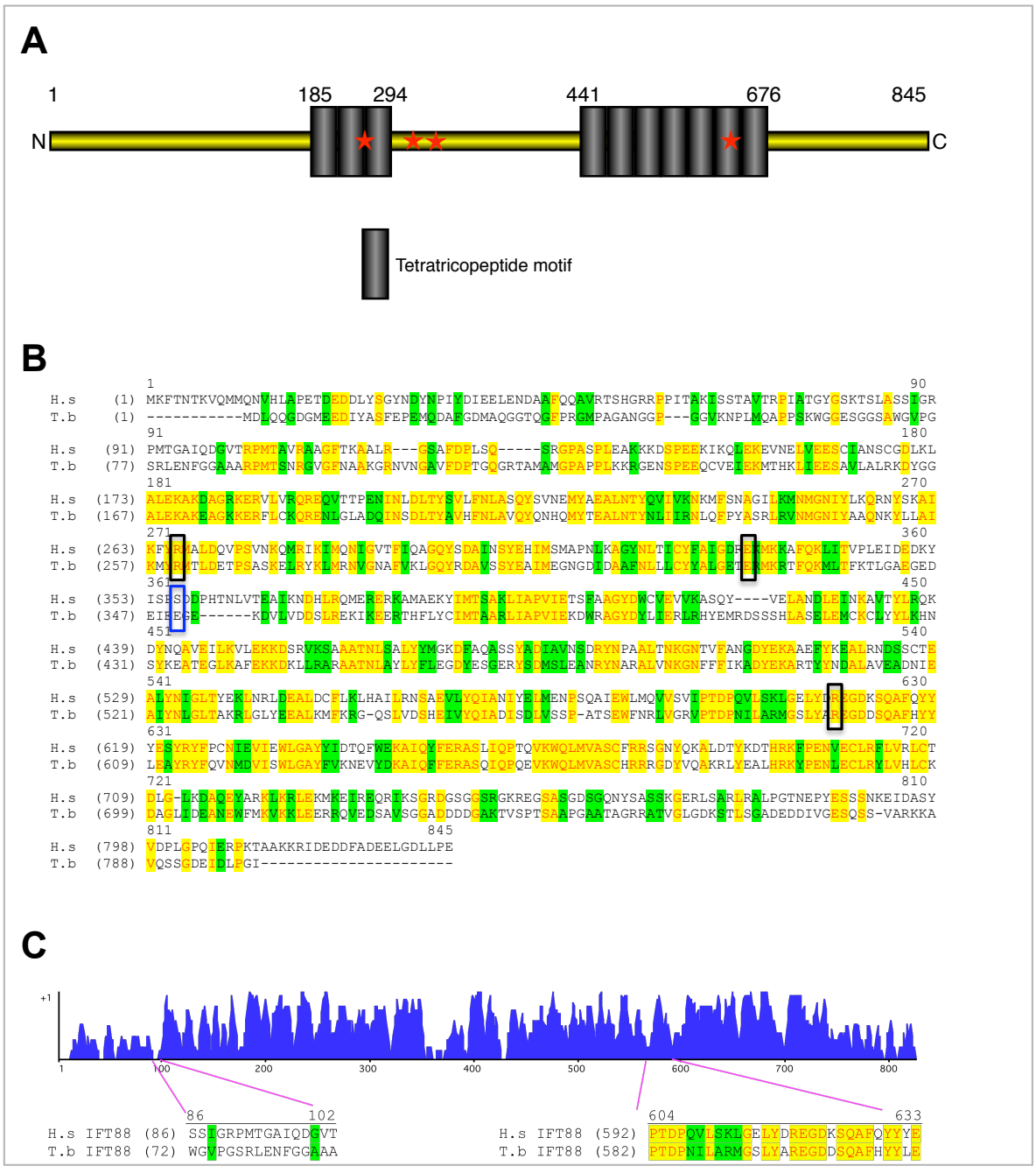
A
1
185
294
441
676
845
N
C
Tetratricopeptide motif
B
H.s (1) MKFTNTKVQMMQNVHLAPETDEDDLYSGYNDYNPIYDIEELENDAAFQQAVRTSHGRRPPITAKISSTAVTRPIATGYGSKTSLASSIGR
T.b (1) ----------MDLQQGDGMEEDIYASFEPEMQDAFGDMAQGGTQGFPRGMPAGANGGP---GGVKNPLMQAPPSKWGGESGGSAWGVPG
H.s (91) PMTGAIQDGVTRPMTAVRAAGFTKAALR---GSAFDPLSQ-----SRGPASPLEAKKKDSPEEKIKQLEKEVNELVEESCIANSCGDLKL
T.b (77) SRLENFGGAAARPMTSNRGVGFNAAKGRNVNGAVFDPTGQGRTAMAMGPAPPLKKRGENSPEEQCVELEKMTHKLIEESAVLALRKDYGG
H.s (173) ALEKAKDAGRKERVLVRQREQVTTPENINLDLTYSVLFNLASQYSVNEMYAEALNTYQVIVKNKMFSNAGILKMNMGNIYLKQRNYSKAI
T.b (167) ALEKAKEAGKKERFLCKQRENLGLADQINSDLTYAVHFNLAVQYQNHQMYTEALNTYNLIIRNLQFPYASRLRVNMGNIYAAQNKYLLAI
H.s (263) KFYRIALDQVPSVNKQMRIKIMQNIGVTFIQAGQYSDAINSYEHIMSMAPNLKAGYNLTICYFAIGDLENMKKAFQKLITVPLEIDEDKY
T.b (257) KMYRITLDETPSASKELRYKLMRNVGNAFVKLGQYRDAVSSYEAIMEGNGDIDAAFNLLLCYYALGETEKMKRTFQKMLTFKTLGAEGED
H.s (353) ISPSDDPHTNLVTEAIKNDHLRQMEKERKAMAEKYIMTSAKLIAPVIETSFAAGYDWCVEVVKASQY----VELANDLEINKAVTYLRQK
T.b (347) EIPEEG------KDVLVDDSLREKIKEERTHFLYCIMTAARLIAPVIEKDMRAGYDYLIERLRHYEMRDSSSHLASELEMCKCLYYLKHN
H.s (439) DYNQAVEILKVLEKKDSRVKSAAATNLSALYYMGKDFAQASSYADIAVNSDRYNPAALTNKGNTVFANGDYEKAAEFYKEALRNDSSCTE
T.b (431) SYKEATEGLKAFEKKDKLLRARAATNLAYLYFLEGDYESGERYSDMSLEANRYNARALVNKGNFFFIKADYEKARTYYNDALAVEADNIE
H.s (529) ALYNIGLTYEKLNRLDEALDCFLKLHAILRNSAEVLYQIANIYYLMENFSQAIEWLMQVVSVIPTDPQVLSKLGELYLDRGDKSQAFQYY
T.b (521) AIYNLGLTAKRLGLYEEALKMFKRG-QSLVDSHFIVYQIADISDLWSSP-ATSEWFNRLVGRVPTDPNILARMGSLYAREGDDSQAFHYY
H.s (619) YFSYRYFPCNIEVIEWLGAYYIDTQFWEKAIQYFERASLIQPTQVKWQLMVASCFRRSGNYQKALDTYKDTHRKFPENVECLRFLVRLCT
T.b (609) LEAYRYFQVNMDVISWLGAYFVKNEVVDKAIQFFERASQIQPQEVKWQLMVASCHRRRGDIVQAKRLYEALHRKYPENLECLRYLVHLCK
H.s (709) DLG-LKDAQEYARKLKRLEKMKEIRFQRIKSGRDGSGGSFGKREGSASGDSGQNYSASSKGERLSARLRALPGTNEPYESSSNKEIDASY
T.b (699) DAGLIDEANFWFMKVKKLEERRQVEDSAVSGGADDDDGAKTVSPTSAAPGAATAGRRATVGLGDKSTLSGADEDDIVGESQGS-VARKKA
H.s (798) VDPLGPQIERPKTAAKKRIDEDDFADEELGDLLPE
T.b (788) VQSSGDEIDLPGI----------
C
+1
1
100
200
300
400
500
600
700
800
86
102
H.s IFT88 (86) SSTGRPMTGAIQDGVT
T.b IFT88 (72) WGVPGSRLENFGGAAA
604
633
H.s IFT88 (592) PTDPQVLSKLGELYDREGDKSQAFQYYYE
T.b IFT88 (582) PTDPNILARMGSLYAREGDDSQAFHYYLE

Figure 2. *H. sapiens* IFT88 homolog is highly similar to *T. brucei* IFT88. (A) Schematic representation of IFT88 protein with domain structure. Gray boxes indicate tetratricopeptide (TPR) motifs. Numbers show sequence positions, whereas stars represent positions of amino acids mutated in humans with *situs inversus*. (B) IFT88 Sequence Alignment between *H. sapiens* and *T. brucei* (accession numbers are listed in Experimental Procedures). Both proteins are 45% identical. Yellow represents strictly conserved amino acids, whereas conservative substitutions are highlighted in green. Amino acids targeted for mutational analysis are boxed. Black boxes, conserved; blue box, not conserved. (C) Amino acid sequence similarity plot (Vector NTI, Invitrogen) of IFT88 homologues from *T. brucei* (Tb) and *H. sapiens* (Hs). A value of +1 corresponds to a stretch of identical amino acids. Representative regions of low similarity (residues 72–101) and high similarity (residues 592–610) are shown below the chart. Strictly conserved positions are highlighted in yellow and conservative substitutions are green.

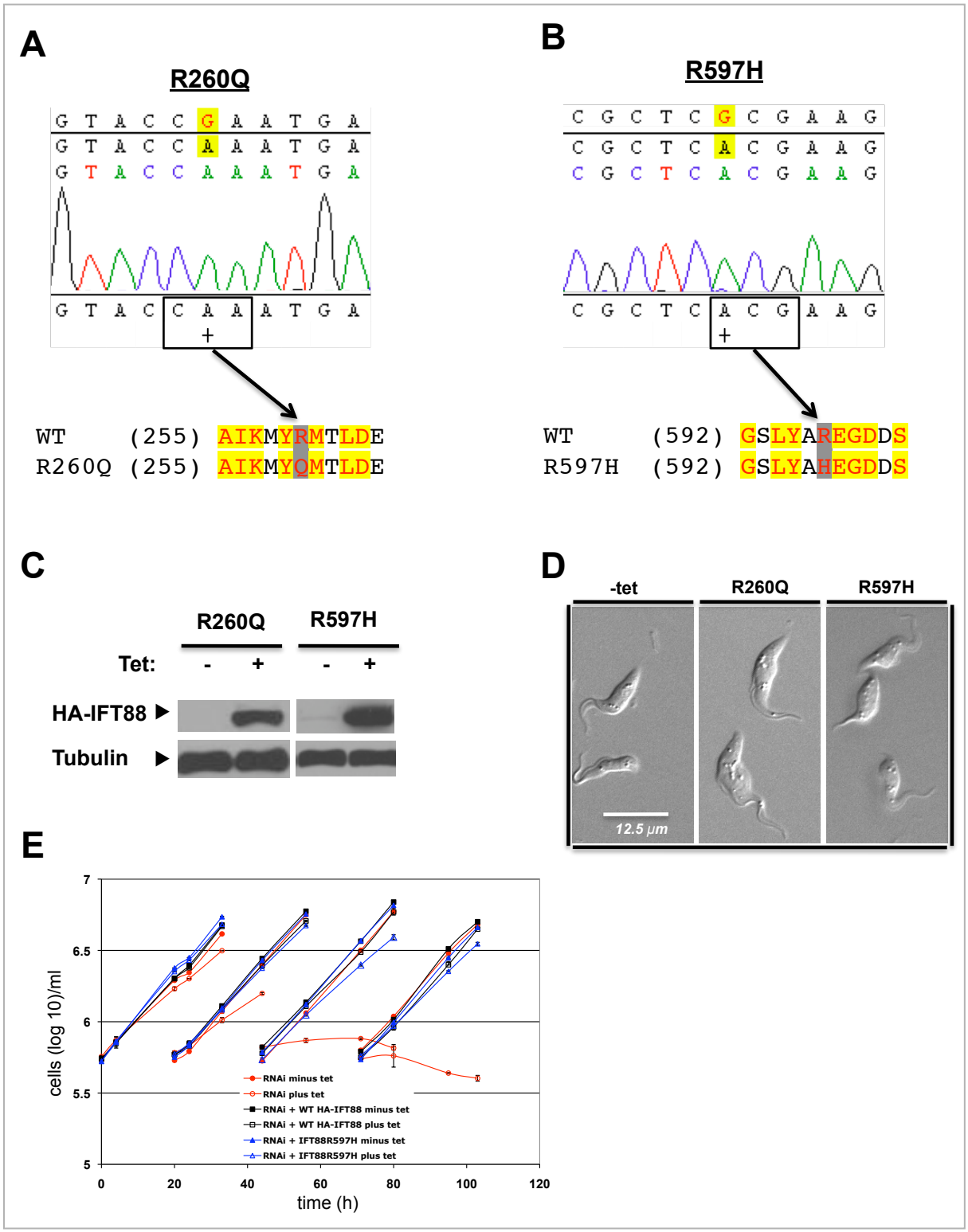
A
R260Q
WT (255) AIKMYRMTLDE
R260Q (255) AIKMYQMTLDE
B
R597H
WT (592) GSLYAREGDDS
R597H (592) GSLYAHEGDDS
C
R260Q
R597H
Tet: - + - +
HA-IFT88
Tubulin
D
-tet
R260Q
R597H
12.5 µm
E
cells (log 10)/ml
time (h)
RNAi minus tet
RNAi plus tet
RNAi + WT HA-IFT88 minus tet
RNAi + WT HA-IFT88 plus tet
RNAi + IFT88R597H minus tet
RNAi + IFT88R597H plus tet

Figure 3. IFT88 point mutants rescue lethality of IFT88 RNAi. (A and B) Panel A, R260Q (IFT88R260Q); Panel B, R597H (IFT88R597H). Nucleotide sequence alignment of WT IFT88 and contig assemblies of R260Q (A) and R597H (B) mutants. Only short regions of the alignment with mutations are shown. The guanine nucleotide targeted for mutational analysis is shown in red on the top (WT) line of the sequence alignments for both R260Q and R597H. The adenine nucleotide introduced to replace guanine is shown with a + sign in the boxed codon on the bottom line under the chromatograms. Boxed nucleotides indicate the changed coding sequences that resulted from the mutations. The arrow points to the change in amino acid highlighted in gray on the polypeptide sequence alignments. (C) Western blot of total protein from R260Q and R597H cells from –Tet and +Tet cultures. Blots were probed with antibody against the HA epitope to detect HA-IFT88, or β-tubulin as a loading control. (D) DIC images of live R260Q and R597H cells from -Tet or +Tet cultures. Representative cells from +Tet culture show that point mutants rescue the lethality phenotype of IFT88 knockdown. For panels A through D cells were induced for 72 h. (E) Growth rates of IFT88 RNAi (red lines), RNAi + WT, or R597H cells. Cultures were grown with (open symbols) or without (closed symbols) tetracycline added at time zero. Cells were diluted back to the starting density each day.

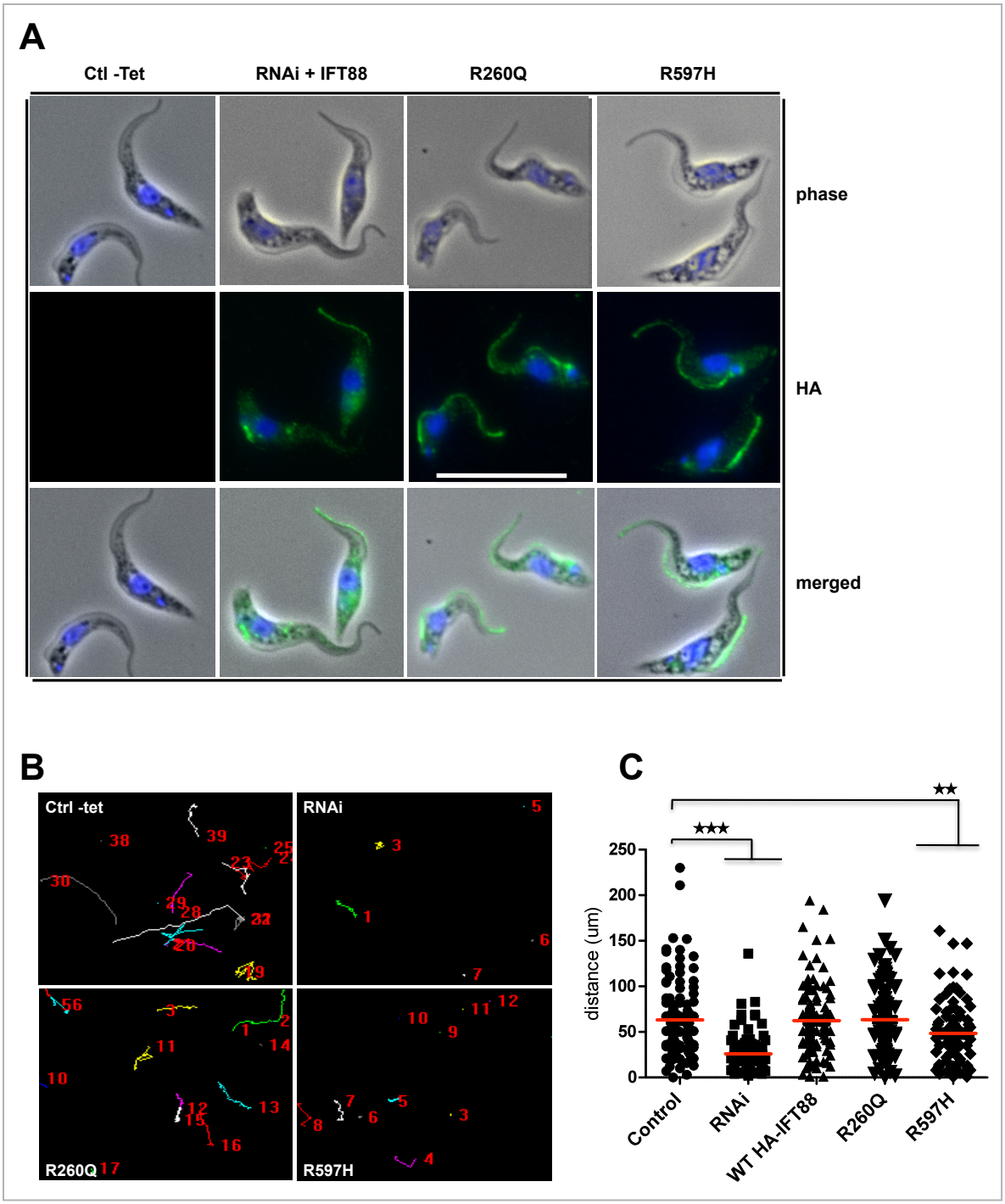
A
Ctl -Tet
RNAi + IFT88
R260Q
R597H
phase
HA
merged
B
Ctrl -tet
RNAi
R260Q
R597H
C
distance (um)
250
200
150
100
50
0
Control
RNAi
WT HA-IFT88
R260Q
R597H

Figure 4. IFT88R597H disrupts motility in *T. brucei*. (A) Immunofluorescence analysis of IFT88 cells from –Tet and +Tet cultures. Cells were stained for the HA epitope (shown in green). DAPI staining shows the DNA in blue. WT-IFT88, R260Q, and R597H mutant proteins localize along the flagellum. (B) Motility traces of RNAi, RNAi + WT-IFT88, R260Q or R597H cells from –Tet and +Tet cultures. Lines trace the movement of individual cells, and numbers in each panel represent individual cells and are randomly generated by the software. (C) Quantification of total distance traveled by individual cells in motility traces (n = 100 cells for each culture). Horizontal lines are the mean of each data set. Bars indicate the 95% confidence interval. Results for the data sets were compared to those for RNAi minus Tet. ***, significant difference ($P < 0.005$). For all panels cells were induced for 72h.

Nucleotide position	Nucleotide change	Exon	Residue change	Mutation type
797	G>A	11	R266Q	Heterozygous
991	G>T	12	E331X	Heterozygous
1067	G>A	12	S356N	Homozygous
1820	G>A	19	R607H	Homozygous

Table 1. Features of IFT88 mutations from humans with *situs inversus*. Nucleotide position on IFT88, nucleotide substitution, exon number where each mutation is located, the resulting amino acid change, and the nature of mutation are indicated.

Supplemental Videos

Video 1. Wild type motility of IFT88 knockdown trypanosomes in –Tet cultures.

Representative live video shows propulsive motility of IFT88 knockdown parasites taken from –Tet cultures. Parasites move rapidly and translocate with tip of flagellum leading. Frame rate for capture and playback is 30 frames/sec.

Video 2. Defective motility by LC1 knockdown trypanosomes from +Tet cultures.

Representative live video shows cell division failure of IFT88 knockdown parasites grown in +Tet cultures for 72 hours. Cells accumulate as an amorphous mass having shortened or no flagella. Frame rate for capture and playback is 30 frames/sec.

Video 3. Expression of wild type, HA-IFT88 rescues the phenotype of IFT88 knockdown. Representative live video, taken from +Tet cultures (72hpi), shows restoration of viability and propulsive motility in IFT88 knockdown parasites complemented with WT-IFT88. Parasites assemble normal flagella, complete cell division, move and translocate with tip of flagellum leading. Frame rate for capture and playback is 30 frames/sec.

Video 4. Defective motility by R597H trypanosomes.

Representative live video shows defective motility of R597H parasites grown in +Tet cultures for 72 hours. Flagellum beating is evident, but parasite propulsive motility is disrupted. Frame rate for capture and playback is 30 frames/sec.

Video 5. Defective motility by R597H trypanosomes.

Representative live video shows defective motility of R597H parasites grown in +Tet cultures for 72 hours. Flagellum beating is evident, but cell translocation is blocked and parasite spins. Frame rate for capture and playback is 30 frames/sec.

Video 6. Defective motility by R597H trypanosomes.

Representative live video shows defective motility of R597H parasites grown in +Tet cultures for 72 hours. Flagellum beating is evident, but parasite moves backward. Frame rate for capture and playback is 30 frames/sec.

CHAPTER 6 REFERENCES

Absalon, S., Blisnick, T., Kohl, L., Toutirais, G., Dore, G., Julkowska, D. et al. (2008). "Intraflagellar transport and functional analysis of genes required for flagellum formation in trypanosomes." Mol Biol Cell 19(3): 929-944.

Badano, J. L., Mitsuma, N., Beales, P. L. and Katsanis, N. (2006). "The ciliopathies: an emerging class of human genetic disorders." Annu Rev Genomics Hum Genet 7: 125-148.

Baron, D. M., Kabututu, Z. P. and Hill, K. L. (2007). "Stuck in reverse: loss of LC1 in Trypanosoma brucei disrupts outer dynein arms and leads to reverse flagellar beat and backward movement." J Cell Sci 120(Pt 9): 1513-1520.

Baron, D. M., Ralston, K. S., Kabututu, Z. P. and Hill, K. L. (2007). "Functional genomics in Trypanosoma brucei identifies evolutionarily conserved components of motile flagella." J Cell Sci 120(Pt 3): 478-491.

Bastin, P., Pullen, T. J., Sherwin, T. and Gull, K. (1999). "Protein transport and flagellum assembly dynamics revealed by analysis of the paralysed trypanosome mutant *snl-1*." J. Cell Sci. 112(Pt 21): 3769-3777.

Bhogaraju, S., Cajanek, L., Fort, C., Blisnick, T., Weber, K., Taschner, M. et al. (2013). "Molecular Basis of Tubulin Transport Within the Cilium by IFT74 and IFT81." Science 341(6149): 1009-1012.

Bhogaraju, S., Engel, B. D. and Lorentzen, E. (2013). "Intraflagellar transport complex structure and cargo interactions." Cilia 2(1): 10.

Bhowmick, R., Li, M., Sun, J., Baker, S. A., Insinna, C. and Besharse, J. C. (2009). "Photoreceptor IFT complexes containing chaperones, guanylyl cyclase 1 and rhodopsin." Traffic 10(6): 648-663.

Bisgrove, B. W. and Yost, H. J. (2006). "The roles of cilia in developmental disorders and disease." Development 133(21): 4131-4143.

Branche, C., Kohl, L., Toutirais, G., Buisson, J., Cosson, J. and Bastin, P. (2006). "Conserved and specific functions of axoneme components in trypanosome motility." J Cell Sci 119(Pt 16): 3443-3455.

Broadhead, R., Dawe, H. R., Farr, H., Griffiths, S., Hart, S. R., Portman, N. et al. (2006). "Flagellar motility is required for the viability of the bloodstream trypanosome." Nature 440(7081): 224-227.

Caspary, T., Larkins, C. E. and Anderson, K. V. (2007). "The graded response to Sonic Hedgehog depends on cilia architecture." Dev Cell 12(5): 767-778.

Cole, D. G. (2003). "The intraflagellar transport machinery of Chlamydomonas reinhardtii." Traffic 4(7): 435-442.

Cole, D. G., Diener, D. R., Himelblau, A. L., Beech, P. L., Fuster, J. C. and Rosenbaum, J. L. (1998). "Chlamydomonas kinesin-II-dependent intraflagellar transport (IFT): IFT particles contain proteins required for ciliary assembly in Caenorhabditis elegans sensory neurons." J Cell Biol 141(4): 993-1008.

Crosby, J. L., Varnum, D. S., Washburn, L. L. and Nadeau, J. H. (1992). "Disorganization is a completely dominant gain-of-function mouse mutation causing sporadic developmental defects." Mech Dev 37(3): 121-126.

Davenport, J. R., Watts, A. J., Roper, V. C., Croyle, M. J., van Groen, T., Wyss, J. M. et al. (2007). "Disruption of intraflagellar transport in adult mice leads to obesity and slow-onset cystic kidney disease." Curr Biol 17(18): 1586-1594.

Davenport, J. R. and Yoder, B. K. (2005). "An incredible decade for the primary cilium: a look at a once-forgotten organelle." Am J Physiol Renal Physiol 289(6): F1159-1169.

Delaval, B., Bright, A., Lawson, N. D. and Doxsey, S. (2011). "The cilia protein IFT88 is required for spindle orientation in mitosis." Nat Cell Biol 13(4): 461-468.

Finetti, F., Paccani, S. R., Riparbelli, M. G., Giacomello, E., Perinetti, G., Pazour, G. J. et al. (2009). "Intraflagellar transport is required for polarized recycling of the TCR/CD3 complex to the immune synapse." Nat Cell Biol 11(11): 1332-1339.

Fliegauf, M., Benzing, T. and Omran, H. (2007). "When cilia go bad: cilia defects and ciliopathies." Nat Rev Mol Cell Biol 8(11): 880-893.

Gadelha, C., Wickstead, B., de Souza, W., Gull, K. and Cunha-e-Silva, N. (2005). "Cryptic paraflagellar rod in endosymbiont-containing kinetoplastid protozoa." Eukaryot Cell 4(3): 516-525.

Haycraft, C. J., Banizs, B., Aydin-Son, Y., Zhang, Q., Michaud, E. J. and Yoder, B. K. (2005). "Gli2 and Gli3 localize to cilia and require the intraflagellar transport protein polaris for processing and function." PLoS Genet 1(4): e53.

Haycraft, C. J., Swoboda, P., Taulman, P. D., Thomas, J. H. and Yoder, B. K. (2001). "The C. elegans homolog of the murine cystic kidney disease gene Tg737 functions in a ciliogenic pathway and is disrupted in osm-5 mutant worms." Development 128(9): 1493-1505.

Hill, K. L., Hutchings, N. R., Grandgenett, P. M. and Donelson, J. E. (2000). "T lymphocyte-triggering factor of african trypanosomes is associated with the flagellar fraction of the cytoskeleton and represents a new family of proteins that are present in several divergent eukaryotes." J Biol Chem 275(50): 39369-39378.

Huangfu, D. and Anderson, K. V. (2005). "Cilia and Hedgehog responsiveness in the mouse." Proc Natl Acad Sci U S A 102(32): 11325-11330.

Huangfu, D., Liu, A., Rakeman, A. S., Murcia, N. S., Niswander, L. and Anderson, K. V. (2003). "Hedgehog signalling in the mouse requires intraflagellar transport proteins." Nature 426(6962): 83-87.

Jekely, G. and Arendt, D. (2006). "Evolution of intraflagellar transport from coated vesicles and autogenous origin of the eukaryotic cilium." Bioessays 28(2): 191-198.

Karlin, S. and Ghandour, G. (1985). "Multiple-alphabet amino acid sequence comparisons of the immunoglobulin kappa-chain constant domain." Proc Natl Acad Sci U S A 82(24): 8597-8601.

Kohl, L., Robinson, D. and Bastin, P. (2003). "Novel roles for the flagellum in cell morphogenesis and cytokinesis of trypanosomes." EMBO J 22(20): 5336-5346.

LaCount, D. J., Barrett, B. and Donelson, J. E. (2002). "Trypanosoma brucei FLA1 is required for flagellum attachment and cytokinesis." J Biol Chem 277(20): 17580-17588.

Lamb, J. R., Tugendreich, S. and Hieter, P. (1995). "Tetratrico peptide repeat interactions: to TPR or not to TPR?" Trends Biochem Sci 20(7): 257-259.

Lechtreck, K. F., Luro, S., Awata, J. and Witman, G. B. (2009). "HA-tagging of putative flagellar proteins in Chlamydomonas reinhardtii identifies a novel protein of intraflagellar transport complex B." Cell Motil Cytoskeleton 66(8): 469-482.

Li, J. B., Gerdes, J. M., Haycraft, C. J., Fan, Y., Teslovich, T. M., May-Simera, H. et al. (2004). "Comparative genomics identifies a flagellar and basal body proteome that includes the BBS5 human disease gene." Cell 117(4): 541-552.

Liu, A., Wang, B. and Niswander, L. A. (2005). "Mouse intraflagellar transport proteins regulate both the activator and repressor functions of Gli transcription factors." Development 132(13): 3103-3111.

Liu, L., Okada, S., Kong, X. F., Kreins, A. Y., Cypowyj, S., Abhyankar, A. et al. (2011). "Gain-of-function human STAT1 mutations impair IL-17 immunity and underlie chronic mucocutaneous candidiasis." J Exp Med 208(8): 1635-1648.

Liu, L., Okada, S., Kong, X. F., Kreins, A. Y., Cypowyj, S., Abhyankar, A. et al. "Gain-of-function human STAT1 mutations impair IL-17 immunity and underlie chronic mucocutaneous candidiasis." J Exp Med.

Livak, K. J. and Schmittgen, T. D. (2001). "Analysis of relative gene expression data using real-time quantitative PCR and the 2(-Delta Delta C(T)) Method." Methods 25(4): 402-408.

May, S. R., Ashique, A. M., Karlen, M., Wang, B., Shen, Y., Zarbalis, K. et al. (2005). "Loss of the retrograde motor for IFT disrupts localization of Smo to cilia and prevents the expression of both activator and repressor functions of Gli." Dev Biol 287(2): 378-389.

Moyer, J. H., Lee-Tischler, M. J., Kwon, H. Y., Schrick, J. J., Avner, E. D., Sweeney, W. E. et al. (1994). "Candidate gene associated with a mutation causing recessive polycystic kidney disease in mice." Science 264(5163): 1329-1333.

Murcia, N. S., Richards, W. G., Yoder, B. K., Mucenski, M. L., Dunlap, J. R. and Woychik, R. P. (2000). "The Oak Ridge Polycystic Kidney (orpk) disease gene is required for left-right axis determination." Development 127(11): 2347-2355.

Nauli, S. M., Kawanabe, Y., Kaminski, J. J., Pearce, W. J., Ingber, D. E. and Zhou, J. (2008). "Endothelial cilia are fluid shear sensors that regulate calcium signaling and nitric oxide production through polycystin-1." Circulation 117(9): 1161-1171.

Oberholzer, M., Langousis, G., Nguyen, H. T., Saada, E. A., Shimogawa, M. M., Jonsson, Z. O. et al. (2011). "Independent analysis of the flagellum surface and matrix proteomes provides insight into flagellum signaling in mammalian-infectious Trypanosoma brucei." Mol Cell Proteomics 10(10): M111 010538.

Ochiai, T., Nagayama, M., Nakamura, T., Morrison, T., Pilchak, D., Kondo, N. et al. (2009). "Roles of the primary cilium component Polaris in synchondrosis development." J Dent Res 88(6): 545-550.

Pazour, G. J., Baker, S. A., Deane, J. A., Cole, D. G., Dickert, B. L., Rosenbaum, J. L. et al. (2002). "The intraflagellar transport protein, IFT88, is essential for vertebrate photoreceptor assembly and maintenance." J Cell Biol 157(1): 103-113.

Pazour, G. J., Dickert, B. L., Vucica, Y., Seeley, E. S., Rosenbaum, J. L., Witman, G. B. and Cole, D. G. (2000). "Chlamydomonas IFT88 and its mouse homologue, polycystic kidney disease gene tg737, are required for assembly of cilia and flagella." J Cell Biol 151(3): 709-718.

Pedersen, L. B. and Rosenbaum, J. L. (2008). "Intraflagellar transport (IFT) role in ciliary assembly, resorption and signalling." Curr Top Dev Biol 85: 23-61.

Perkins, L. A., Hedgecock, E. M., Thomson, J. N. and Culotti, J. G. (1986). "Mutant sensory cilia in the nematode Caenorhabditis elegans." Dev Biol 117(2): 456-487.

Piperno, G. and Mead, K. (1997). "Transport of a novel complex in the cytoplasmic matrix of Chlamydomonas flagella." Proc Natl Acad Sci U S A 94(9): 4457-4462.

Ralston, K. S. and Hill, K. L. (2008). "The flagellum of Trypanosoma brucei: new tricks from an old dog." Int J Parasitol 38(8-9): 869-884.

Ralston, K. S., Kisalu, N. K. and Hill, K. L. "Structure-Function Analysis of Dynein Light Chain 1 Identifies Viable Motility Mutants in Bloodstream-Form Trypanosoma brucei." Eukaryot Cell 10(7): 884-894.

Ralston, K. S., Kisalu, N. K. and Hill, K. L. (2011). "Structure-function analysis of dynein light chain 1 identifies viable motility mutants in bloodstream-form Trypanosoma brucei." Eukaryot Cell 10(7): 884-894.

Ralston, K. S., Lerner, A. G., Diener, D. R. and Hill, K. L. (2006). "Flagellar motility contributes to cytokinesis in Trypanosoma brucei and is modulated by an evolutionarily conserved dynein regulatory system." Eukaryot Cell 5(4): 696-711.

Robert, A., Margall-Ducos, G., Guidotti, J. E., Bregerie, O., Celati, C., Brechot, C. and Desdouets, C. (2007). "The intraflagellar transport component IFT88/polaris is a centrosomal protein regulating G1-S transition in non-ciliated cells." J Cell Sci 120(Pt 4): 628-637.

Rosenbaum, J. L. and Witman, G. B. (2002). "Intraflagellar transport." Nat Rev Mol Cell Biol 3(11): 813-825.

Satir, P. (2007). "Cilia biology: stop overeating now!" Curr Biol 17(22): R963-965.

Sukumaran, S. and Perkins, B. D. (2009). "Early defects in photoreceptor outer segment morphogenesis in zebrafish ift57, ift88 and ift172 Intraflagellar Transport mutants." Vision Res 49(4): 479-489.

Takeda, S., Yonekawa, Y., Tanaka, Y., Okada, Y., Nonaka, S. and Hirokawa, N. (1999). "Left-right asymmetry and kinesin superfamily protein KIF3A: new insights in determination of laterality and mesoderm induction by kif3A-/- mice analysis." J Cell Biol 145(4): 825-836.

Taschner, M., Bhogaraju, S. and Lorentzen, E. (2012). "Architecture and function of IFT complex proteins in ciliogenesis." Differentiation 83(2): S12-22.

Taulman, P. D., Haycraft, C. J., Balkovetz, D. F. and Yoder, B. K. (2001). "Polaris, a protein involved in left-right axis patterning, localizes to basal bodies and cilia." Mol Biol Cell 12(3): 589-599.

Thompson, J. D., Higgins, D. G. and Gibson, T. J. (1994). "Improved sensitivity of profile searches through the use of sequence weights and gap excision." Comput Appl Biosci 10(1): 19-29.

Tran, P. V., Haycraft, C. J., Besschetnova, T. Y., Turbe-Doan, A., Stottmann, R. W., Herron, B. J. et al. (2008). "THM1 negatively modulates mouse sonic hedgehog signal transduction and affects retrograde intraflagellar transport in cilia." Nat Genet 40(4): 403-410.

Trivedi, D., Colin, E., Louie, C. M. and Williams, D. S. (2012). "Live-cell imaging evidence for the ciliary transport of rod photoreceptor opsin by heterotrimeric kinesin-2." J Neurosci 32(31): 10587-10593.

Tsujikawa, M. and Malicki, J. (2004). "Genetics of photoreceptor development and function in zebrafish." Int J Dev Biol 48(8-9): 925-934.

van Dam, T. J., Townsend, M. J., Turk, M., Schlessinger, A., Sali, A., Field, M. C. and Huynen, M. A. (2013). "Evolution of modular intraflagellar transport from a coatomer-like progenitor." Proc Natl Acad Sci U S A 110(17): 6943-6948.

Vanhamme, L. and Pays, E. (1995). "Control of gene expression in trypanosomes." Microbiol Rev 59(2): 223-240.

Veland, I. R., Awan, A., Pedersen, L. B., Yoder, B. K. and Christensen, S. T. (2009). "Primary cilia and signaling pathways in mammalian development, health and disease." Nephron Physiol 111(3): p39-53.

Vincensini, L., Blisnick, T. and Bastin, P. (2011). "[The importance of model organisms to study cilia and flagella biology]." Biol Aujourdhui 205(1): 5-28.

Willaredt, M. A., Hasenpusch-Theil, K., Gardner, H. A., Kitanovic, I., Hirschfeld-Warneken, V. C., Gojak, C. P. et al. (2008). "A crucial role for primary cilia in cortical morphogenesis." J Neurosci 28(48): 12887-12900.

Wirtz, E., Leal, S., Ochatt, C. and Cross, G. A. (1999). "A tightly regulated inducible expression system for conditional gene knock-outs and dominant-negative genetics in *Trypanosoma brucei*." Mol. Biochem. Parasitol. 99(1): 89-101.

Yoder, B. K., Richards, W. G., Sommardahl, C., Sweeney, W. E., Michaud, E. J., Wilkinson, J. E. et al. (1996). "Functional correction of renal defects in a mouse model for ARPKD through expression of the cloned wild-type Tg737 cDNA." Kidney Int 50(4): 1240-1248.

Yoder, B. K., Tousson, A., Millican, L., Wu, J. H., Bugg, C. E., Jr., Schafer, J. A. and Balkovetz, D. F. (2002). "Polaris, a protein disrupted in orpk mutant mice, is required for assembly of renal cilium." Am J Physiol Renal Physiol 282(3): F541-552.

Chapter 7

Identification of Trypanin domains required for function and targeting to the flagellum

Abstract

The nexin-dynein regulatory complex (NDRC) has emerged as a critical regulator of axonemal dynein. Flagellar beating results from the precise coordinated action of dynein motors arranged in the flagellar axoneme. Both chemical and mechanical signals are involved in regulating cilia motility. While some NDRC components have been identified, our understanding of the composition, assembly and mechanism of this complex remain limited. Trypanin, a subunit of the NDRC, is a reversible inhibitor of dynein and is essential for normal motility in *Trypanosoma brucei.* Recent investigations showed that the requirement of trypanin for cilium motility extends to vertebrates, where it is required for inner ear development and human cilium function. However, domains and residues necessary for trypanin assembly and function remain to be determined. We recently developed structure-function approaches for systematic mutational analysis of flagellar proteins in *T. brucei* that permit quick identification of important protein domains and residues. We have generated a systematic deletion series of trypanin and have expressed the mutants in *T. brucei* using the above structure-function system. These studies allowed identification of domains that are essential for microtubule binding and flagellum targeting. The flagellum is essential in *T. brucei* and flagellar defects cause a wide variety of human inherited diseases. Improving our knowledge of the molecular mechanism underlying assembly of the NDRC will thus increase our understanding of human genetic diseases and advance efforts to develop new therapies for trypanosomiasis.

Introduction

Motile cilia (flagella) are highly conserved organelles that are required for human development and physiology. Flagellar defects have been implicated in a wide variety of human genetic diseases [Fliegauf et al., 2007]. Functional flagella also drive locomotion of several human pathogens that affect many people worldwide [Ginger et al., 2008; Ralston and Hill 2008]Increasing our understanding of the molecular mechanism of flagellar motility will be crucial in developing a deeper knowledge of human inherited diseases caused by defects in motile cilia and devising new treatments for infectious diseases.

The flagellum of the protozoan parasite *Trypanosoma brucei*, the causal agent of sleeping sickness, displays a unique waveform that is characteristic of the genus and drives cell motility in the mammalian host and tsetse fly vector [Gruby 1843; Walker 1961; Rodriguez et al., 2009; Heddergott et al., 2012]. The *T. brucei* flagellum possesses the canonical "9 + 2" configuration of motile axonemes, which is the platform for assembly of dynein motors [Ralston et al., 2009]. Dyneins are ATP-driven, microtubule-based molecular motors that drive the flagellar movement. Nexin links connect contiguous microtubule doublets and restrict microtubule sliding in order to promote bending of the axoneme [Summers and Gibbons 1971; Satir 2007]. For proper flagellum beating, thousands of dyneins must be coordinately regulated spatially and temporally [Baron et al., 2007]. Molecular mechanisms underlying the dynein regulation are poorly understood although it has been proposed that dynein regulation involves mechanical and chemical signals [Lindemann and Kanous 1997; Porter and Sale 2000; Smith and Yang 2004; Lindemann and Lesich 2010].

The dynein regulatory complex (DRC) is a key regulator of axonemal dyneins [Howard et al., 1994; Ralston et al., 2006; Colantonio et al., 2009; Heuser et al., 2009]. This complex was originally identified through suppressor mutant screens for extragenic suppressors of flagellar paralysis in radial spoke and central pair mutants in the flagellated green algae *Chlamydomonas reinhardtii* [Huang et al., 1982]. These genetic investigations identified five genetic loci (*PF2, PF3, SUP-PF-3, SUP-PF-4* and *SUP-PF-5*) that are required for assembly of the DRC [Huang et al., 1982; Mastronarde et al., 1992; Piperno et al., 1992; Gardner et al., 1994; Porter et al., 1994; Porter and Sale 2000]. The current model is that the DRC constitutively inhibits the dyneins in the absence of central pair and radial spoke signals, leading to paralysis of central pair and radial spoke mutants. The central pair apparatus disseminates signals through the radial spokes to the DRC in order to release dynein inhibition [Omoto et al., 1999; Porter and Sale 2000]. For dynein regulation within the axoneme, the DRC therefore acts as a reversible inhibitor of dyneins in response to signals from the central pair apparatus and radial spokes [Huang et al., 1982; Piperno et al., 1992; Gardner et al., 1994; Hutchings et al., 2002; Rupp and Porter 2003; Ralston et al., 2006].

The DRC is a megadalton complex of several polypeptides that are firmly associated with axonemal microtubules and are resistant to treatments that detach other axonemal proteins such as the outer and inner dynein arms [Piperno et al., 1994]. The identities of some DRC components are known. These include trypanin, trypanin related protein (TRP) and component of motile flagella (CMF) 70 in *T. brucei* [Ralston et al., 2006; Kabututu et al., 2010]; K. L. (in preparation)], as well as the DRC candidate CMF22 [Bower et al., 2013; Nguyen 2013].

Additional studies in *Chlamydomonas* have expanded the inventory of DRC subunits [Lin et al., 2011; Bower et al., 2013]. Despite these advances, additional DRC members, member interactions and molecular mechanisms remain to be determined.

Trypanin is the homolog of Paralyzed Flagella 2 (*PF2*) in *Chlamydomonas* [Rupp and Porter 2003]. Trypanin and its orthologs are members of the ‘‘Trypanin family’’. These proteins are essential for microtubule-based flagellar motility [Hill et al., 2000; Hutchings et al., 2002; Ralston et al., 2006; Ralston et al., 2011]. Trypanin localizes along the flagellar axoneme and is intimately connected to the detergent- and salt- insoluble flagellar cytoskeleton [Hill et al., 2000; Hutchings et al., 2002; Ralston et al., 2011], and remains associated with the axoneme after treatment with 1M NaCl [Ralston et al., 2011]. Unfortunately, how the DRC attaches to microtubules is not well understood. Trypanin has been suggested to be a molecular linker of the DRC to microtubules [Bekker et al., 2007] and association with the axoneme is believed to be crucial for DRC function. Genetic studies have demonstrated a requirement for trypanin in regulating the flagellum beat in *T. brucei* [Ralston et al., 2006] similar to the DRC role in *Chlamydomonas* [Huang et al., 1982; Piperno et al., 1992; Piperno et al., 1994; Hutchings et al., 2002; Rupp and Porter 2003]. Although it causes defective flagellum beating, depletion of trypanin in *T. brucei* suppresses flagellar paralysis in central-pair mutants [Ralston et al., 2006] as shown previously in *C. reinhardtii* [Huang et al., 1982; Brokaw and Kamiya 1987; Hutchings et al., 2002; Rupp and Porter 2003]. Trypanin RNAi knockdown in procyclic *T. brucei* reproduces the phenotype of *Chlamydomonas pf2* mutants, which fail to coordinate flagellar beat, lack propulsive cell motility, and exclusively spin and tumble in place [Hutchings et al., 2002; Ralston et al., 2006]. In contrast, trypanin is essential in the bloodstream stage of *T. brucei*

[Ralston et al., 2006]. The DRC is therefore a good starting point for exploring the flagellum as a drug target for sleeping sickness.

The requirement for the DRC in cilium motility and development in vertebrates [Colantonio et al., 2009], including a connection to human genetic disease [Merveille et al., 2011] has been demonstrated. Indeed, the trypanin homolog GAS8 (also known as GAS11) in vertebrates has been shown to be essential for inner ear development in zebrafish [Colantonio et al., 2009]. However, despite its critical role in human biology and in disease, the molecular mechanisms by which trypanin or the DRC accomplishes its function are completely unknown. Although microtubule association domains in the mammalian trypanin homolog GAS11 were recently identified [Bekker et al., 2007], critical functional domains of trypanin are unknown. We recently developed structure-function methods for systematic mutational analysis of flagellar proteins in *T. brucei* (Appendix 2) [Ralston et al., 2011]. We previously conducted mutational analysis of conserved amino acids and residues predicted to be phophorylated within the trypanin protein, which did not reveal any discernable impact on motility [Ralston et al., 2011]. In the current study we have generated a systematic deletion series of trypanin and have expressed the mutants in *T. brucei* using the aforementioned structure-function system. These studies allowed identification of domains for microtubule binding and flagellum targeting.

Results

Deletion analysis

Phosphorylation is known to influence flagellar beating in several organisms [Porter and Sale 2000], and it has been proposed that several conserved residues of trypanin are phosphorylated *in vivo* (D. Baron and K. Hill, unpublished). Mutational analysis of conserved trypanin residues and amino acids believed to be phosphorylated did not reveal any discernable impact on motility. In order to identify domains required for trypanin function we conducted a domain deletion analysis. A schematic representation of the experimental design is shown in Figure 1. In order to investigate the domains within trypanin that are essential for targeting and function, we have generated a systematic deletion series (Figure 2) of trypanin mutants for expression in *T. brucei* using our structure-function system [Ralston et al., 2011]. The deletion series includes the inhibitory microtubule association domain or IMAD (AA 1-113) alone, the GAS11 microtubule association domain or GMAD (AA 114-257) alone, a combination of IMAD and GMAD (AA 1-257), ΔIMAD (AA 114-453), ΔGMAD (AA 1-113, 258-453), and ΔIMAD-ΔGMAD (AA 258-453) (Figure 2).

We recently generated a Trypanin 3' UTR RNAI [Ralston et al., 2011] cell line that allows simultaneous downregulation of the endogenous trypanin and expression of a mutant version of this gene upon tetracycline induction [Ralston et al., 2011]. All the above trypanin deletion fragments are therefore expressed within the Trypanin 3' UTR RNAI background where the endogenous trypanin has been ablated . As a control, we used a Trypanin 3' UTR RNAI cell line rescued with full-length, wild type HA epitope-tagged trypanin [Ralston et al., 2011]. Full-

length (FL) trypanin is tightly associated with the detergent- and salt- insoluble cytoskeleton (P1) [Hill et al., 2000; Hutchings et al., 2002; Bekker et al., 2007; Ralston et al.,] [Ralston et al., 2011] as well as to the axoneme (P2) after salt treatment and localizes along the flagellar axoneme. As expected, following tetracycline induction of the aforementioned control cells, FL trypanin partitions in P1 and P2 as demonstrated by the fractionation assay (Figure 3A) and localizes along the axoneme (Figure 3B-C).

The N-terminus or inhibitory microtubule association domain (IMAD) (AA 1-113) (Figure 2) has been shown to attenuate microtubule binding of the trypanin homolog Gas11 in mammalians [Bekker et al., 2007]. This domain was also suggested to allow correct localization of Gas11 where this protein is needed within the cell, for instance the Golgi or at the basal body of the primary cilium, or sites of dynein regulation [Colantonio et al., 2006]. Upon tetracycline induction, western blot analysis showed that IMAD was produced in induced cells at levels similar to full-length trypanin (Figure 3B). Two attempts to fractionate this mutant protein failed.

GAS11 microtubule association domain or GMAD (AA 114-257) is adjacent to IMAD. GMAD, a conserved and predicted coiled-coil region [Hill et al., 1999; Hill et al., 2000], is a microtubule-binding domain that was, like IMAD, recently identified in the trypanin mammalian homolog Gas11 [Bekker et al., 2007]. A GFP fusion protein encompassing GMAD has been shown to co-localize with microtubules when exogenously expressed in COS7 cells [Hill et al., 1999; Hill et al., 2000]. Conservation of GMAD in trypanin strongly suggests that this fragment binds microtubule and therefore could decorate microtubules throughout induced cells. Upon tetracycline induction GMAD was expressed at comparable levels to the full-length (FL)

trypanin but GMAD unexpectedly partitioned to the detergent-soluble protein fraction (S1) as well as to P1 and P2 fractions (Figure 4A). We performed an indirect fluorescence assay to determine the localization of GMAD on fraction P1. As shown in Figure 4B, GMAD is localized throughout the cell including in the flagellum, possibly binding microtubules everywhere. We reasoned that GMAD could localize to the flagellum in lysed cells but fail to reach the flagellum in intact, whole cells. To test this possibility we performed the IFA on whole cells. IFA performed on induced whole cells strikingly revealed that GMAD is localized to the cytoplasm but not to the flagellum (Figure 4C). Additionally, induced GMAD mutants are defective in motility as demonstrated by sedimentation assay (Figure 4D) and video microscopy (Videos 1 and 2). Hence, GMAD is mislocalized and causes a motility defect in *T. brucei*.

To determine the functional requirement of the GMAD domain, we deleted this domain (ΔGMAD) as shown in Figure 1B. Western blot analysis and preliminary fractionation show that ΔGMAD is expressed and partitions similar to FL trypanin (Figure 5A). ΔGMAD localization and phenotype determination of ΔGMAD cells is underway. Expression of IMAD along with GMAD (Figure 1B) restores the flagellum localization similar to FL trypanin as demonstrated by western blot analysis and fractionation (Figure 5B) and whole cell IFA (Figure 5C). These data suggest IMAD mediates trypanin targeting to the flagellum. Additionally IMAD-GMAD cells have normal motility. The C-terminus domain or ΔIMAD-ΔGMAD is a domain of unknown function. Although ΔIMAD-ΔGMAD localization by IFA and phenotype characterization are underway, this mutant is produced in induced cells and partitions like FL trypanin as demonstrated by western blot analysis and fractionation (Figure 4E).

Discussion

Domains mediating trypanin's function or targeting have not been studied. In the current study we have targeted all sections of trypanin including unique and conserved regions that define proteins of the Trypanin family. We employed our recently established structure-function system as well as IFA analysis and fractionation to identify domains required for trypanin function and targeting. The structure-function system allows expression of mutants in *T. brucei* depleted of the endogenous protein, while whole-cell IFA is a powerful approach to localize proteins within cells. Using a series of trypanin fragment deletions, we have identified the IMAD region as required for trypanin targeting to the flagellum. The GMAD fragment expressed alone is mislocalized and causes a motility defect in *T. brucei*. We surprisingly found that expressing GMAD along with IMAD correctly localizes GMAD to the flagellum.

The observation that GMAD decorates trypanosome cytoskeletons suggests this domain stably and indiscriminately binds microtubules, and is consistent with previous studies demonstrating that this domain in the mammalian homolog Gas11 binds microtubules [Bekker et al., 2007]. Partitioning of GMAD in S1 could signify saturation of microtubule binding sites. It has been suggested that Gas11 is the DRC member that mediates DRC attachment to microtubules through the GMAD domain [Bekker et al., 2007]. However, we surprisingly found that ΔGMAD or the C-terminus (ΔIMAD-ΔGMAD) domain that lacks IMAD and the GMAD domain partition in P1 (cytoskeletons) and P2 (flagellar skeletons), indicating interaction with microtubules. This result suggests trypanin has an additional microtubule-binding domain within the C-terminus fragment. It also suggests that the C-terminus microtubule interaction is indirect

through another DRC partner. Further studies are needed to address such hypotheses. GMAD expression causes a motility defect *in T. brucei*. The precise reason for the defective motility phenotype is unknown. We speculate that GMAD competes with other proteins for microtubule binding. It is also possible that GMAD mislocalization interferes with other protein functions. Studies to characterize GMAD function in ΔGMAD mutants are underway.

Previous investigations suggested IMAD allows correct localization of Gas11, the trypanin homolog in mammalians [Bekker et al., 2007], where this protein is needed within the cell at the sites of dynein regulation such as the basal body or Golgi [Bekker et al., 2007]. Indeed, expression of IMAD along with GMAD alone redirects GMAD alone to the flagellum in *T. brucei*, corroborating Bekker and colleagues' findings. Further studies are needed to define how IMAD mediates correct localization of trypanin to the flagellum. IMAD localization and phenotypic assessment of IMAD mutant cells is underway. The C-terminus (ΔIMAD-ΔGMAD) domain, which lacks IMAD and GMAD, correctly partitions to P1 and P2 as mentioned above. The C-terminus domain of trypanin could therefore be another microtubule binding domain in *T. brucei*. This domain could also be a platform assembly for other DRC partners that may have the potential to regulate trypanin binding to microtubule or dock the dynein regulatory complex to microtubules.

In summary, many DRC subunits have been identified but molecular mechanisms fundamental to the function of the DRC remain to be determined. Identification of key trypanin domains required for motility and targeting described herein represents a unique opportunity for more detailed description of molecular mechanisms underlying trypanin's function in regulating

flagellum motility in *T. brucei*. Flagellum motility has a major role in human biology and disease. Our studies should therefore provide a structural foundation that will ultimately enable description of flagellum motility mechanisms at the molecular level. Furthermore, identification of domains that are unique to *T. brucei* may represent candidate drug targets for sleeping sickness. Future studies will assess function to define dynein regulation domains as well as discovering key residues that are essential for function within the identified domains of trypanin. These studies therefore will generate insight into mechanisms of flagellum dynein regulation and potentially aid efforts to use the flagellum as a drug target.

Experimental Procedures

DNA Constructs, cell cultures and transfection

Wild type (WT), Full-length trypanin ORF was generated previously [Ralston et al., 2011]. Trypanin deletion mutants were PCR-amplified and cloned downstream of the HA tag into the *Xho* I and *Mfe* I (IMAD and IMAD-GMAD) or *Mfe* I and *Mfe* I (GMAD and ΔIMAD) sites in pKR10 [Ralston et al., ; Ralston et al., 2011]. All DNA constructs were verified by direct sequencing and linearized at the unique pKR10 *Not*I site prior to cell transfection. Sequencing was performed at UCLA Genotyping and Sequencing Core Facility or at Genewiz. Primers used to PCR-amplify trypanin domain deletions are as follows: IMAD 5' ATGCCACCACGGACCGCTG 3' and 5' CTTGCACGCCTGCGCCTTC 3'; GMAD 5' GATGAAAGTGACCGTCTGCTTC 3' and 5' CTGCTTCATCTGCGCTATTTC 3'; IMAD-GMAD 5' ATGCCACCACGGACCGCTG 3' and 5' CTGCTTCATCTGCGCTATTTC 3'; ΔIMAD 5' GATGAAAGTGACCGTCTGCTTC 3' and 5' CTCAAAGTTGCTACGTGGCAG 3'.

For all experiments we used procyclic form Trypanin 3' UTR RNAI [Ralston et al., 2011] engineered to allow simultaneous depletion of the endogenous trypanin and expression of a mutant copy of this protein upon tetracycline induction. As a control for the fractionation assay and indirect immunofluorescence analysis, we used a Trypanin 3' UTR RNAI cell line that expresses a full-length, wild type HA epitope-tagged trypanin upon tetracycline induction [Ralston et al., 2011]. Cells were grown at 28 ºC in Cunningham's SM supplemented with 10%

heat-inactivated fetal calf serum (HIFCS) as described in [Ralston et al., 2006]. Transfections were carried out as described [Ralston et al., 2011]. Briefly, Trypanin 3' UTR RNAI cells were washed and resuspended to $5x10^7$ cells/ml in electroporation medium (EM) simultaneously with linearized plasmid DNA (10 μg). Electroporation was carried out using a Bio-Rad Gene Pulser. After transfection, cells were shifted to fresh medium and incubated overnight in order to recover before initiation of drug selection within 24 hours post-transfection. Cells were cloned by limiting dilution following transfection. To assess cell growth, parasites were split into two flasks and cultured with or without tetracycline (1 μg/ml) before parasites were counted in a Coulter counter and the means of two independent counts are reported for growth curves.

Western blot

Total cell lysate preparations were made from parasites cultured for 72 hours with or without tetracycline (1 μg/ml). Flagellum skeleton protein extracts were prepared exactly as described by Ralston and colleagues [Ralston et al., 2011]. Total cell lysates and flagellum skeleton protein extracts were used for western blot experiments performed as previously described [Hill et al., 2000]. An anti-HA monoclonal antibody (Covance) was use to probe the HA-trypanin proteins, while an anti-β-tubulin monoclonal antibody (Developmental Studies Hybridoma Bank, University of Iowa) was used as a control for protein loading.

Immunofluorescence assay

Immunofluorescence analysis was performed as previously described [Oberholzer et al., 2011]. Cells or cytoskeletons (P1 fraction) were washed three times in PBS and air-dried onto coverslips. Cells were incubated for 10 min in methanol and 10 min in acetone at -20°C. Following a rehydration step in PBS, the slides were blocked in blocking solution (PBS + 5% BSA + 5% Normal donkey serum (Gibco)) for 1.5 h. Cells were subsequently incubated for 1.5 h with the primary anti-HA antibody (Covance) diluted 1:1,000 in blocking solution. After 5 washes of 10 min each in PBS + 0.05% Tween-20, samples were stained for 1.5 h with the secondary antibody (donkey anti-mouse Alexa Fluor 488) diluted in blocking solution. After washing five times in PBS + 0.05% Tween-20 and once in PBS, cells were mounted with Vectashield containing DAPI (Vector Laboratories). Images were acquired with a 63x objective on a Zeiss Axioskop II compound microscope and processed using Axiovision (Zeiss, Inc.) and Adobe Photoshop (Adobe Systems, Inc.).

Motility assays

All motility assays including sedimentation assays, motility traces, and high-resolution video microscopy were carried out as previously described [Ralston et al., 2011]. Briefly, cells were grown for 72 hours with or without tetracycline. For sedimentation assays [Bastin et al., 1999], parasites were reconstituted to $5x10^6$ cells/ml and incubated in fresh culture medium at growth conditions. Measurements of the optical density at 600 nm (OD600) for resuspended and undisturbed samples were taken every two hours for a period of ten hours. The sample ΔOD600 expresses the difference in OD600 obtained by subtracting the OD600 of the resuspended from

the undisturbed sample. Data presented are averages from two independent experiments of -Tet and +Tet cultures. Error bars indicate the standard deviations.

To record motility traces, cells were grown with or without tetracycline and cell motility analysis was done at 72 hours post induction as described [Ralston et al., 2011]. Briefly, parasites were examined in polyglutamate-coated slide motility,chambers [Gadelha et al., 2005] using dark field optics on a Zeiss Axioskop II compound microscope with a 10x objective. Videos were captured using a COHU analog video camera. Analog format movies were converted to digital format with an ADVC-300 digital video converter (Canopus, Co., Ltd.). Movies were recorded at 30 frames per second (fps) and converted to AVI format and then to stacks of TIFF images using Adobe Premiere Elements software (Adobe Systems). TIFF image stacks were analyzed using Metamorph software (Molecular Devices) to trace parasite movement over the indicated time period. Trace data were used to calculate the total distance travelled. The statistical analysis for significance was calculated by comparing datasets to RNAi –Tet using the student's unpaired two-tailed T test.

For high-resolution videos of individual cells, videos were captured in motility chambers using DIC optics on a Zeiss Axiovert 200 M inverted microscope with a 100x oil-immersion objective.

Acknowledgments

Funding for the work was provided by grants to my advisor Professor Kent L. Hill from NIH-NIAID (AI052348) and Burroughs Wellcome Fund. I am a recipient of the UCLA Shapiro Fellowship and of the UCLA Dissertation Year Fellowship (2012-2013). I am grateful to Dr. Katherine Ralston for drawing the plasmid maps shown in Figure 1 and to Denis Sambolin for technical assistance.

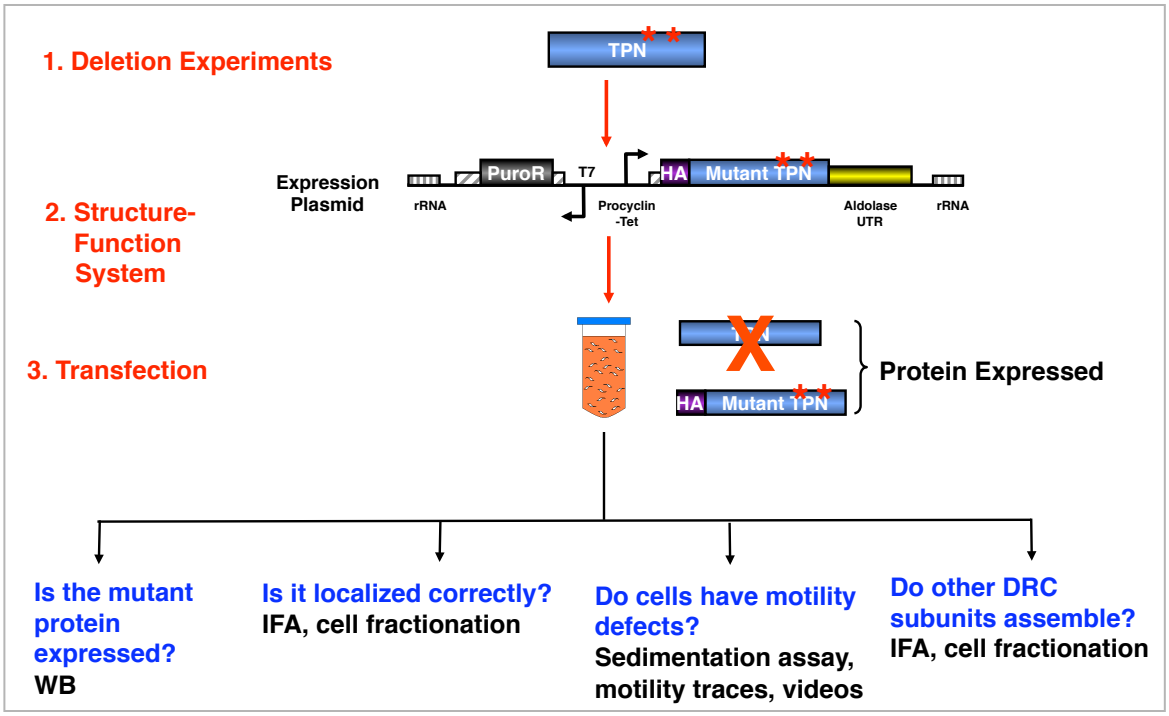

Figure 1. Study experimental procedure. A schematic representation of the study experimental procedure. Following generation of trypanin domain deletion mutants by PCR (1), the mutant contructcs are cloned into the expression vector pKR10 (2) prior to transfection into procyclic trypanin-3'UTR RNAi trypanosomes (3). Expression and localization of mutant proteins as well as phenotype assessment of mutant cells are determined using various modalities.

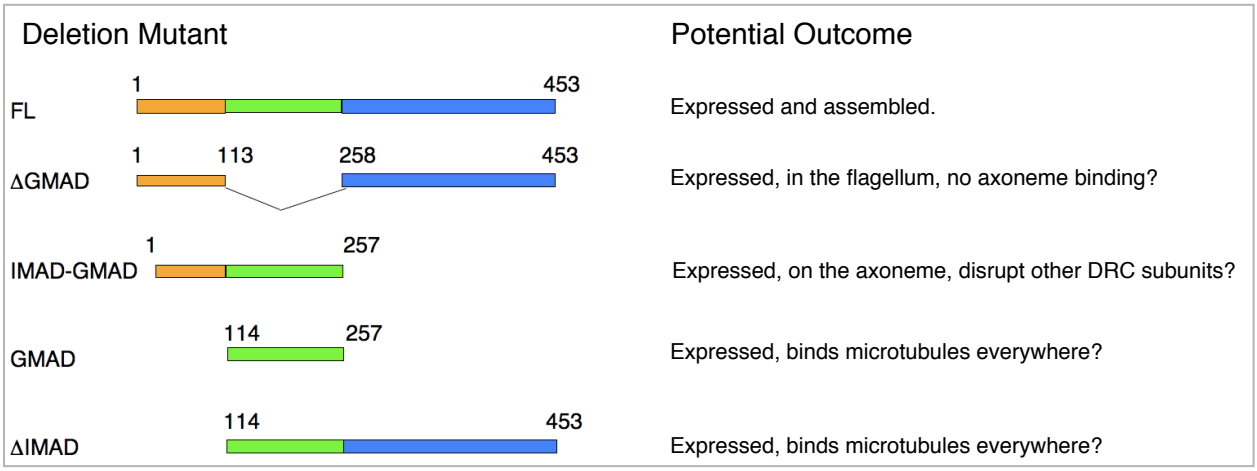

Figure 2. Schematic representation of Trypanin deletion mutants employed in this study and potential outcome for mutant proteins. Full-length (FL) trypanin, ΔGMAD, IMAD-GMAD, GMAD, and ΔIMAD fragments are shown. Corresponding amino acids are indicated: ΔGMAD (residues 1-113 and 258-453), IMAD-GMAD (residues 1-257), GMAD (residues 114-257), and ΔIMAD (residues 114-453).

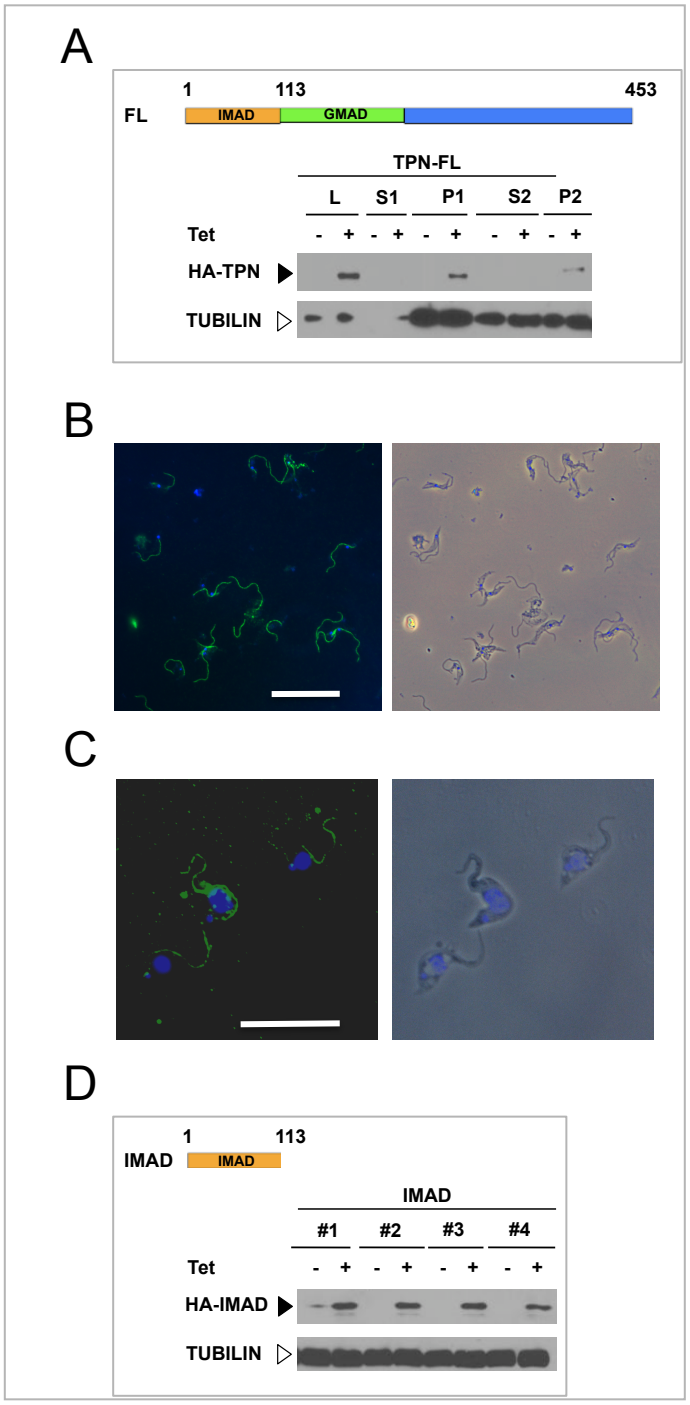

Figure 3. Both FL and IMAD trypanin are expressed at similar levels in *T. brucei*. (A) Western blot analysis and flagellum fractionation of cell extracts from wild type cells from –Tet

and +Tet cultures. Blots were probed with an antibody against the HA epitope to detect HA-tagged full-length (FL) trypanin, or β-tubulin as a loading control. L, total cell lysate; S1, detergent soluble fraction; P1, detergent-insoluble flagellar cytoskeleton; S2, NaCl-soluble fraction; P2, NaCl-insoluble flagellar skeleton (axoneme). Immunofluorescence analysis of cytoskeletons from fraction P1 (B) or whole cells (C) from +Tet cultures. Cytoskeletons or cells were stained for the HA epitope (shown in green). DAPI staining shows the DNA in blue. FL-trypanin localizes along the flagellum. (D) Western blot analysis of cell extracts from IMAD cells grown in the absence or presence of tetracycline. Blots were probed with an antibody against the HA epitope to detect HA-IMAD, or β-tubulin as a loading control. Four different clones of the IMAD cell line are shown. Scale bar 25μm.

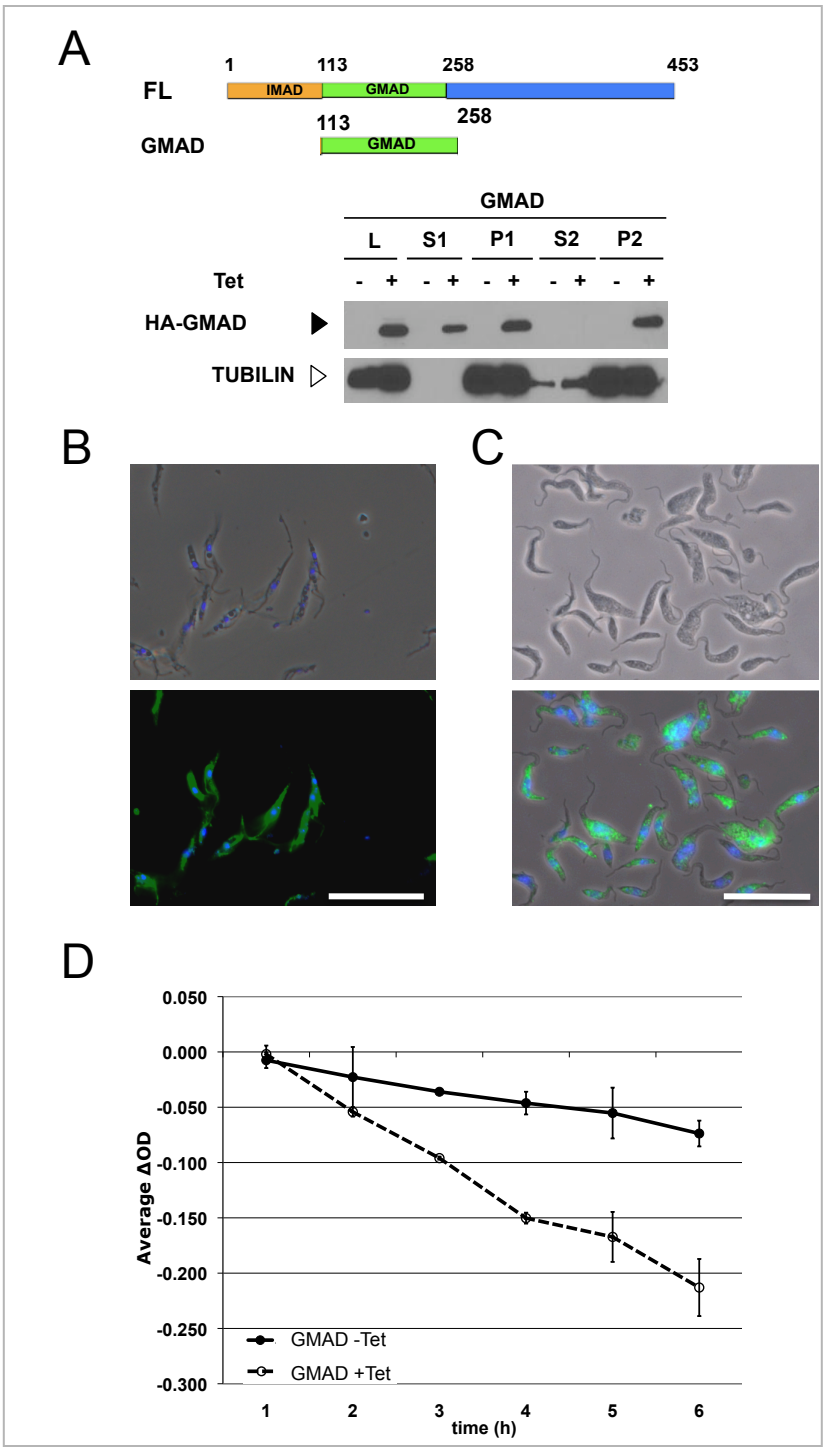

Figure 4. GMAD is misslocalized and causes a motility defect in *T. brucei*. (A) Western blot analysis and flagellum fractionation of cell extracts from GMAD cells grown with or without tetracycline. Blots were probed with an antibody against the HA epitope to detect HA-GMAD,

or β-tubulin as a loading control. Immunofluorescence analysis of cytoskeletons (B) from P1 fraction or whole cells (C) from +Tet cultures. Cytoskeletons or cells were stained for the HA epitope (shown in green). DAPI staining shows the DNA in blue. GMAD decorates entire cytoskeletons but fails to localize to the flagellum in whole cells. (D) Sedimentation assay of GMAD cells from –Tet and +Tet cultures. Sedimentation curves are the averages of two independent experiments, while error bars represent standard deviations. Scale bar 25μm.

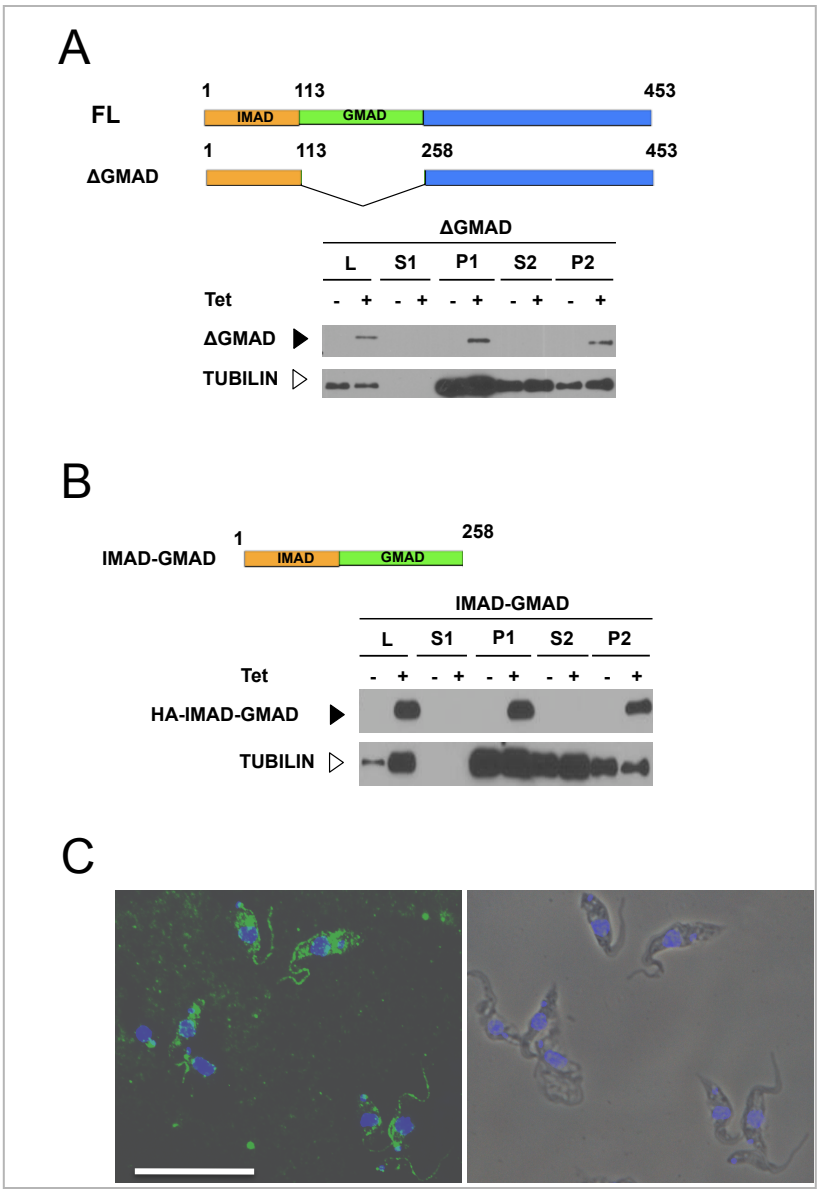

Figure 5. IMAD restores correct localization of GMAD in *T. brucei*. Western blot analysis and Flagellum fractionation of cell extracts of ΔGMAD (A) or IMAD-GMAD (B) from –Tet and +Tet cultures. Blots were probed with an antibody against the HA epitope to detect HA-GMAD, or β-tubulin as a loading control. (C) Immunofluorescence analysis of IMAD-GMAD cells from +Tet cultures. Cells were stained for the HA epitope (shown in green). DAPI staining shows the

DNA in blue. GMAD decorates cytoskeletons but fails to localize to the flagellum in whole cells. (D) Sedimentation assay of GMAD mutant cells from –Tet and +Tet cultures. Scale bar 25μm.

Supplemental Videos

Video 6-1. Wild type motility of GMAD trypanosomes in –Tet cultures.

Representative live video shows propulsive motility of GMAD parasites taken from –Tet cultures. Parasites move rapidly and translocate with tip of flagellum leading. Frame rate for capture and playback is 30 frames/sec.

Video 6-2. Defective motility by GMAD trypanosomes in +Tet cultures.

Representative live video shows defective motility of GMAD parasites grown in +Tet cultures for 72 hours. Flagellum beating is evident, but parasite propulsive motility is disrupted. Frame rate for capture and playback is 30 frames/sec.

CHAPTER 7 REFERENCES

Baron, D. M., Kabututu, Z. P. and Hill, K. L. (2007). "Stuck in reverse: loss of LC1 in Trypanosoma brucei disrupts outer dynein arms and leads to reverse flagellar beat and backward movement." J Cell Sci 120(Pt 9): 1513-1520.

Bastin, P., Pullen, T. J., Sherwin, T. and Gull, K. (1999). "Protein transport and flagellum assembly dynamics revealed by analysis of the paralysed trypanosome mutant *snl-1*." J. Cell Sci. 112(Pt 21): 3769-3777.

Bekker, J. M., Colantonio, J. R., Stephens, A. D., Clarke, W. T., King, S. J., Hill, K. L. and Crosbie, R. H. (2007). "Direct interaction of Gas11 with microtubules: implications for the dynein regulatory complex." Cell Motil Cytoskeleton 64(6): 461-473.

Bower, R., Tritschler, D., Vanderwaal, K., Perrone, C. A., Mueller, J., Fox, L. et al. (2013). "The N-DRC forms a conserved biochemical complex that maintains outer doublet alignment and limits microtubule sliding in motile axonemes." Mol Biol Cell 24(8): 1134-1152.

Brokaw, C. J. and Kamiya, R. (1987). "Bending patterns of Chlamydomonas flagella: IV. Mutants with defects in inner and outer dynein arms indicate differences in dynein arm function." Cell Motil Cytoskeleton 8(1): 68-75.

Colantonio, J. R., Bekker, J. M., Kim, S. J., Morrissey, K. M., Crosbie, R. H. and Hill, K. L. (2006). "Expanding the role of the dynein regulatory complex to non-axonemal functions: association of GAS11 with the Golgi apparatus." Traffic 7(5): 538-548.

Colantonio, J. R., Vermot, J., Wu, D., Langenbacher, A. D., Fraser, S., Chen, J. N. and Hill, K. L. (2009). "The dynein regulatory complex is required for ciliary motility and otolith biogenesis in the inner ear." Nature 457(7226): 205-209.

Fliegauf, M., Benzing, T. and Omran, H. (2007). "When cilia go bad: cilia defects and ciliopathies." Nat Rev Mol Cell Biol 8(11): 880-893.

Gadelha, C., Wickstead, B., de Souza, W., Gull, K. and Cunha-e-Silva, N. (2005). "Cryptic paraflagellar rod in endosymbiont-containing kinetoplastid protozoa." Eukaryot Cell 4(3): 516-525.

Gardner, L. C., O'Toole, E., Perrone, C. A., Giddings, T. and Porter, M. E. (1994). "Components of a "dynein regulatory complex" are located at the junction between the radial spokes and the dynein arms in Chlamydomonas flagella." J Cell Biol 127(5): 1311-1325.

Ginger, M. L., Portman, N. and McKean, P. G. (2008). "Swimming with protists: perception, motility and flagellum assembly." Nat Rev Microbiol 6(11): 838-850.

Gruby, M. (1843). "Analysis and observation of a novel hematozoan species, *Trypanosoma sanguinis*." C R Hebd Seqnces Acad Sci 17:: 1134-1136.

Heddergott, N., Kruger, T., Babu, S. B., Wei, A., Stellamanns, E., Uppaluri, S. et al. (2012). "Trypanosome motion represents an adaptation to the crowded environment of the vertebrate bloodstream." PLoS Pathog 8(11): e1003023.

Heuser, T., Raytchev, M., Krell, J., Porter, M. E. and Nicastro, D. (2009). "The dynein regulatory complex is the nexin link and a major regulatory node in cilia and flagella." J Cell Biol 187(6): 921-933.

Hill, K. L., Hutchings, N. R., Grandgenett, P. M. and Donelson, J. E. (2000). "T lymphocyte-triggering factor of african trypanosomes is associated with the flagellar fraction of the cytoskeleton and represents a new family of proteins that are present in several divergent eukaryotes." J Biol Chem 275(50): 39369-39378.

Hill, K. L., Hutchings, N. R., Russell, D. G. and Donelson, J. E. (1999). "A novel protein targeting domain directs proteins to the anterior cytoplasmic face of the flagellar pocket in African trypanosomes." J Cell Sci 112 Pt 18: 3091-3101.

Howard, D. R., Habermacher, G., Glass, D. B., Smith, E. F. and Sale, W. S. (1994). "Regulation of Chlamydomonas flagellar dynein by an axonemal protein kinase." J Cell Biol 127(6 Pt 1): 1683-1692.

Huang, B., Ramanis, Z. and Luck, D. J. (1982). "Suppressor mutations in Chlamydomonas reveal a regulatory mechanism for Flagellar function." Cell 28(1): 115-124.

Hutchings, N. R., Donelson, J. E. and Hill, K. L. (2002). "Trypanin is a cytoskeletal linker protein and is required for cell motility in African trypanosomes." J Cell Biol 156(5): 867-877.

Kabututu, Z. P., Thayer, M., Melehani, J. H. and Hill, K. L. (2010). "CMF70 is a subunit of the dynein regulatory complex." J Cell Sci 123(Pt 20): 3587-3595.

Lin, J., Tritschler, D., Song, K., Barber, C. F., Cobb, J. S., Porter, M. E. and Nicastro, D. (2011). "Building blocks of the nexin-dynein regulatory complex in Chlamydomonas flagella." J Biol Chem 286(33): 29175-29191.

Lindemann, C. B. and Kanous, K. S. (1997). "A model for flagellar motility." Int Rev Cytol 173: 1-72.

Lindemann, C. B. and Lesich, K. A. (2010). "Flagellar and ciliary beating: the proven and the possible." J Cell Sci 123(Pt 4): 519-528.

Mastronarde, D. N., O'Toole, E. T., McDonald, K. L., McIntosh, J. R. and Porter, M. E. (1992). "Arrangement of inner dynein arms in wild-type and mutant flagella of Chlamydomonas." J Cell Biol 118(5): 1145-1162.

Merveille, A. C., Davis, E. E., Becker-Heck, A., Legendre, M., Amirav, I., Bataille, G. et al. (2011). "CCDC39 is required for assembly of inner dynein arms and the dynein regulatory complex and for normal ciliary motility in humans and dogs." Nat Genet 43(1): 72-78.

Nguyen, H. K., Sandhu, J. S., Langousis, G. & Hill, K. (2013). "CMF22 is a broadly conserved axonemal protein and is required for propulsive motility in Trypanosoma brucei." Euk Cell In Press.

Oberholzer, M., Langousis, G., Nguyen, H. T., Saada, E. A., Shimogawa, M. M., Jonsson, Z. O. et al. (2011). "Independent analysis of the flagellum surface and matrix proteomes provides insight into flagellum signaling in mammalian-infectious Trypanosoma brucei." Mol Cell Proteomics 10(10): M111 010538.

Omoto, C. K., Gibbons, I. R., Kamiya, R., Shingyoji, C., Takahashi, K. and Witman, G. B. (1999). "Rotation of the central pair microtubules in eukaryotic flagella." Mol Biol Cell 10(1): 1-4.

Piperno, G., Mead, K., LeDizet, M. and Moscatelli, A. (1994). "Mutations in the "dynein regulatory complex" alter the ATP-insensitive binding sites for inner arm dyneins in Chlamydomonas axonemes." J Cell Biol 125(5): 1109-1117.

Piperno, G., Mead, K. and Shestak, W. (1992). "The inner dynein arms I2 interact with a "dynein regulatory complex" in Chlamydomonas flagella." J Cell Biol 118(6): 1455-1463.

Porter, M. E., Knott, J. A., Gardner, L. C., Mitchell, D. R. and Dutcher, S. K. (1994). "Mutations in the SUP-PF-1 locus of Chlamydomonas reinhardtii identify a regulatory domain in the beta-dynein heavy chain." J Cell Biol 126(6): 1495-1507.

Porter, M. E. and Sale, W. S. (2000). "The 9 + 2 axoneme anchors multiple inner arm dyneins and a network of kinases and phosphatases that control motility." J Cell Biol 151(5): F37-42.

Ralston, K. S. and Hill, K. L. (2008). "The flagellum of Trypanosoma brucei: new tricks from an old dog." Int J Parasitol 38(8-9): 869-884.

Ralston, K. S., Kabututu, Z. P., Melehani, J. H., Oberholzer, M. and Hill, K. L. (2009). "The Trypanosoma brucei flagellum: moving parasites in new directions." Annu Rev Microbiol 63: 335-362.

Ralston, K. S., Kisalu, N. K. and Hill, K. L. "Structure-Function Analysis of Dynein Light Chain 1 Identifies Viable Motility Mutants in Bloodstream-Form Trypanosoma brucei." Eukaryot Cell 10(7): 884-894.

Ralston, K. S., Kisalu, N. K. and Hill, K. L. (2011). "Structure-function analysis of dynein light chain 1 identifies viable motility mutants in bloodstream-form Trypanosoma brucei." Eukaryot Cell 10(7): 884-894.

Ralston, K. S., Lerner, A. G., Diener, D. R. and Hill, K. L. (2006). "Flagellar motility contributes to cytokinesis in Trypanosoma brucei and is modulated by an evolutionarily conserved dynein regulatory system." Eukaryot Cell 5(4): 696-711.

Rodriguez, J. A., Lopez, M. A., Thayer, M. C., Zhao, Y., Oberholzer, M., Chang, D. D. et al. (2009). "Propulsion of African trypanosomes is driven by bihelical waves with alternating chirality separated by kinks." Proc Natl Acad Sci U S A 106(46): 19322-19327.

Rupp, G. and Porter, M. E. (2003). "A subunit of the dynein regulatory complex in Chlamydomonas is a homologue of a growth arrest-specific gene product." J Cell Biol 162(1): 47-57.

Satir, P. (2007). "Cilia biology: stop overeating now!" Curr Biol 17(22): R963-965.

Smith, E. F. and Yang, P. (2004). "The radial spokes and central apparatus: mechano-chemical transducers that regulate flagellar motility." Cell Motil Cytoskeleton 57(1): 8-17.

Summers, K. E. and Gibbons, I. R. (1971). "Adenosine triphosphate-induced sliding of tubules in trypsin-treated flagella of sea-urchin sperm." Proc Natl Acad Sci U S A 68(12): 3092-3096.

Walker, P. J. (1961). "Organization of function in trypanosome flagella." Nature 189: 1017-1018.

Chapter 8

Conclusion

The *T. brucei* flagellum is an essential and multifunctional organelle that drives parasite motility. Motility functions of the trypanosome flagellum are receiving growing attention as potential targets for therapeutic intervention. Examining a requirement for parasite motility for infection and pathogenesis in African trypanosomiasis has been the focus of this dissertation. The role of trypanosome motility in infection and pathogenesis of trypanosomiasis is a longstanding question that has not previously been investigated, because of the lack of viable motility mutants in the mammalian infectious life cycle stage. The trypanosome flagellum has emerged as a potential drug target in sleeping sickness and a widely accepted system to study the eukaryotic flagellum. However, without knowledge of molecular mechanisms or motility mutant models to test *in vivo*, there is an important gap in our understanding of this major component of trypanosome biology and pathogenesis.

To bridge this gap, we developed facile systems for detailed mutation analysis of flagellar proteins in *T. brucei*. Application of these strategies led to identification of residues required for LC1 function and more importantly allowed generation of the first-ever viable motility mutants in mammalian infectious, bloodstream form *T. brucei*. Using an acute infection model, we have demonstrated that, contrary to the predominant notion, parasite propulsive motility is dispensable for bloodstream infection. These studies represent the foremost direct analysis of parasite motility in any aspect of *T. brucei* infection. While not essential for survival in the bloodstream during an acute infection, it is possible that parasite motility is required for subsequent steps of infection, such as penetration of the central nervous system. Further work with motility mutants in chronic infection models to test this hypothesis will be required and is the focus of ongoing investigations. As such, development of a motility mutant infection model described here

provides an important foundation for future investigations of flagellum biology in the context of mammalian host infection and development in the tsetse fly.

Conventionally, assessment of *T. brucei* infection has been dependent on determining parasitemia in blood, as well as restricted use of histochemistry to examine parasite presence in fixed tissues. To better characterize infection dynamics and host-parasite interactions during infection, we developed an advanced live-cell imaging approach using *T. brucei* expressing the fluorescent protein mCherry. This system enabled observation of *T. brucei ex vivo* in mouse tissues as well as *in vivo* in blood vessels of whole zebrafish at single-cell resolution. Important areas of focus include examining parasite interaction with cells of the host immune system, investigating parasite penetration of the vascular endothelium and entry into the CNS, as well as determining infection progression in African trypanosomiasis. Zebrafish could be exploited as an appropriate alternative animal infection model of trypanosomiasis to address such questions. The availability of *Trypanosoma carassii* that naturally infects fish coupled to the advantages that the fish model offers such as transparency, which allows non-invasive imaging of infection dynamics in whole live fish, should facilitate these investigations. Application of the zebrafish model to infectious diseases has led to landmark discoveries for understanding infection dynamics.

T. brucei has emerged as an excellent system to study the eukaryotic flagellum. Cilia play a critical role in human development and physiology. Defects in cilia or flagella cause a wide range of diseases and developmental defects. The identities and functions of several flagellar proteins have been determined but there is sparse information on molecular mechanisms that

underlie these proteins functions. In addition to investigating the contribution of flagellar motility to infection and pathogenesis, we exploited our structure-function strategies to define residues required for the function of IFT88, a protein required for flagellum assembly. We tested residues that correspond to IFT88 mutations observed in human patients with defective cilia and demonstrated which of these mutations are loss-of-function mutations versus polymorphisms. We have also identified domains required for trafficking of trypanin, a protein required for normal motility. While identification of essential proteins or domains that are specific to *T. brucei* may constitute potential drug targets, conserved components should have broad application to the biology of the eukaryotic flagellum. Flagellum motility drives propulsion of many pathogenic parasites, altogether responsible for mortality and morbidity in approximately 0.5 billion people worldwide. As such, in addition to being a good model system, the flagellum of *T. brucei* and its many proteins are potential drug targets not only in African trypanosomiasis, but also in other parasitic diseases such as Chagas disease or Leishmaniasis.

Collectively these studies contribute to understanding *T. brucei* pathogenesis mechanisms and should advance efforts for therapeutics and diagnostics development, all of which is expected to alleviate case management in sleeping sickness. The flagellum is essential to many human pathogens and plays a critical role in human development. Studies of molecular mechanisms of flagellar proteins have general application for understanding biology of the eukaryotic flagellum. Hence our studies expand our understanding of flagellum motility functions in *T. brucei*, with direct application to other flagellated protozoan pathogens. These investigations also contribute to uncover basic facets of eukaryotic cell biology as it applies to human health and disease.

Appendix 1

Propulsion of African trypanosomes is driven by bihelical waves with alternating chirality separated by kinks

Propulsion of African trypanosomes is driven by bihelical waves with alternating chirality separated by kinks

Jose A. Rodriguez[a,b], Miguel A. Lopez[c], Michelle C. Thayer[c], Yunzhe Zhao[d], Michael Oberholzer[c], Donald D. Chang[d], Neville K. Kisalu[c], Manuel L. Penichet[a,b,c], Gustavo Helguera[b], Robijn Bruinsma[d], Kent L. Hill[a,c], and Jianwei Miao[d,1]

[a]Molecular Biology Institute, [b]Department of Surgery, Division of Surgical Oncology, and [c]Department of Microbiology Immunology and Molecular Genetics, The David Geffen School of Medicine, and [d]Department of Physics and Astronomy, University of California, Los Angeles, CA 90095

Edited by Howard C. Berg, Harvard University, Cambridge, MA, and approved September 16, 2009 (received for review June 23, 2009)

Trypanosoma brucei, a parasitic protist with a single flagellum, is the causative agent of African sleeping sickness. Propulsion of *T. brucei* was long believed to be by a drill-like, helical motion. Using millisecond differential interference-contrast microscopy and analyzing image sequences of cultured procyclic-form and bloodstream-form parasites, as well as bloodstream-form cells in infected mouse blood, we find that, instead, motility of *T. brucei* is by the propagation of kinks, separating left-handed and right-handed helical waves. Kink-driven motility, previously encountered in prokaryotes, permits *T. brucei* a helical propagation mechanism while avoiding the large viscous drag associated with a net rotation of the broad end of its tapering body. Our study demonstrates that millisecond differential interference-contrast microscopy can be a useful tool for uncovering important short-time features of microorganism locomotion.

millisecond differential interference-contrast microscopy | *Trypanosoma brucei* | cilium | flagellum

The protozoan parasite *Trypanosoma brucei* is the causative pathogen of African sleeping sickness, a fatal disease indigenous to subSaharan Africa where 60 million people are at risk of infection (1, 2). *T. brucei* is transmitted between human hosts by a tsetse fly vector, and parasite motility is important in both hosts. In the tsetse fly, procyclic-form (PCF) parasites colonize the midgut and then migrate through the alimentary canal to the salivary glands, where maturation into human infectious forms occurs (3, 4). From the salivary gland, mature parasites can be injected into the blood of a mammalian host that has been bitten by the fly. In the mammalian host, migration of bloodstream-form (BSF) parasites through the blood-brain barrier initiates onset of the fatal course of the disease (5, 6). *T. brucei* is extracellular at all stages of infection and depends on its own flagellum-mediated motility for dissemination. Flagellar motility of *T. brucei* in various environments is believed to be central not only to host-parasite interaction, but also to cell division, morphogenesis, and development (3, 6–15).

The *T. brucei* cell body is roughly 20-μm long, with a relatively large posterior section tapering off into a long, narrow anterior section. It has a single flagellum, with the classic "9 + 2" microtubule axoneme architecture that is attached to the cell body along its length. Based on microscopy studies, it is believed that propulsion of *T. brucei* proceeds by left-hand (LH) helical waves propagating along the flagellum, from tip to base, driving the cell forward in a drill-like motion (see Fig. 1*A*) (15–17). The genus name of the parasite actually derives from this distinctive motility (from the Greek *trypanon* or auger, and *soma* or body), first described in 1843 (18). Here, we use millisecond resolution differential interference-contrast (DIC) microscopy, combined with other microscopy methods, to provide a quantitative analysis of *T. brucei* cell propulsion. Our results reveal that *T. brucei* forward motility is characterized by the propagation of kinks separating helical waves of alternate chirality.

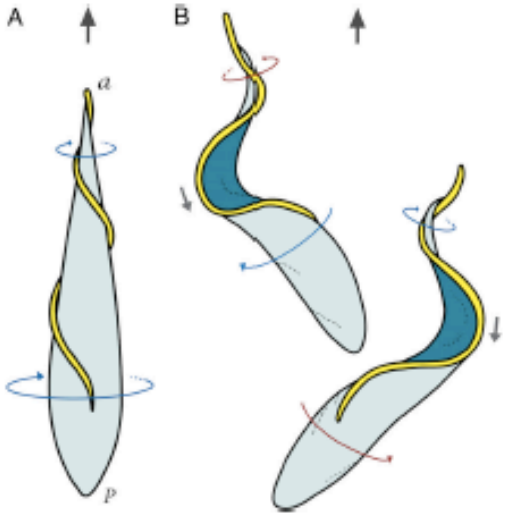

Fig. 1. Models of forward motility for *T. brucei* in aqueous media. (*A*) The traditional model: propulsion is caused by helical waves propagating from the tip to the base of the flagellum with LH chirality, resulting in a drill-like motion of the cell body ("*a*" and "*p*" represent the anterior and posterior end of the cell). (*B*) The bihelical model in which alternating LH and right hand (RH) helical waves propagate down the flagellum separated by a kink. The flagellum of the bottom cell exhibits a LH helical wave (*blue arrow*) at the tip and a RH helical wave (*red arrow*) near the base, separated by a "minus" kink (*gray arrow*). The flagellum of the top cell shows a RH helical wave at the tip and a LH helical wave near the base, separated by a "plus" kink. Kinks propagate in a direction opposite to that of cell propulsion. Two dominant cell-body configurations are associated with the propagation of kinks, with the cell body rocking back and forth between the two alternating configurations.

Results

Helical Waves with Alternating Chirality. To investigate *T. brucei* propulsion in standard culture conditions, we used high-speed

Author contributions: J.A.R., R.B., K.L.H., and J.M. designed research; J.A.R., M.A.L., M.C.T., Y.Z., M.O., D.D.C., N.K.K., and J.M. performed research; J.A.R., M.A.L., M.C.T., Y.Z., M.O., D.D.C., M.L.P., G.H., R.B., K.L.H., and J.M. analyzed data; and J.A.R., R.B., K.L.H., and J.M. wrote the paper.

The authors declare no conflict of interest.

This article is a PNAS Direct Submission.

[1]To whom correspondence should be addressed. E-mail: miao@physics.ucla.edu.

This article contains supporting information online at www.pnas.org/cgi/content/full/0907001106/DCSupplemental.

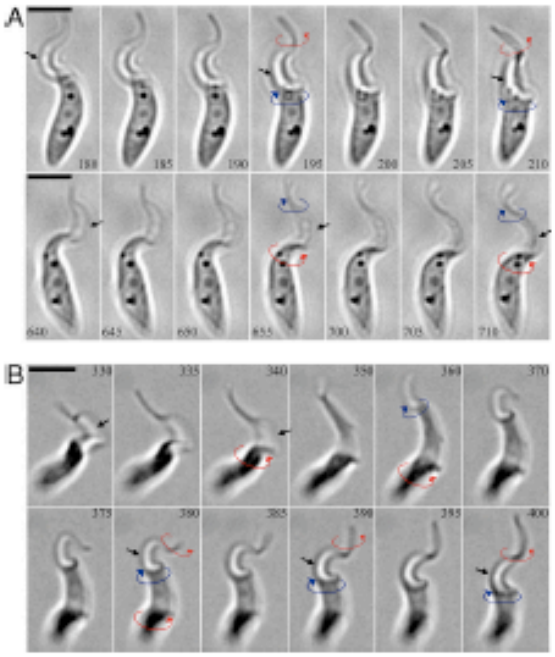

Fig. 2. Millisecond DIC microscopy imaging of PCF and BSF cell motility. (*A*) (*Top*) Image sequence of a PCF cell showing a RH (*red arrow*) helical wave at the tip and a LH (*blue arrow*) helical wave near the base of the flagellum, separated by a plus kink (*black arrow*). (*Bottom*) Image sequence of the same cell showing a LH helical wave at the tip and a RH helical wave near the base separated by a minus kink. The numerical values are in milliseconds. (Scale bars, 5 μm.) (*B*) Image sequence of a BSF cell showing bihelical waves that are separated by a minus kink (*Top*) immediately followed by a plus kink (*Bottom*).

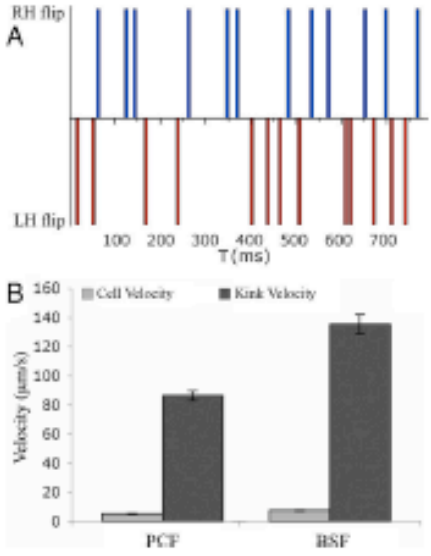

Fig. 3. Analysis of cell propulsion in PCF and BSF *T. brucei*. (*A*) Representative plot showing the distribution of the LH and RH helical waves at the anterior end of a PCF cell within a time interval of about 800 ms. The number of waves was determined by monitoring how many times the flagellum flipped to initiate a RH or LH wave, as indicated with blue and red vertical bars, respectively. Each flip represents a rotation of ≈ 180°. No more than three successive flips in the same direction are generated at the anterior end. Note that the rotation frequency in this example is somewhat higher than the average frequency of 19 ± 3 flips per second. (*B*) Cell velocities were calculated from 50 PCF (5 ± 2 μm/s) and 50 BSF (8 ± 2 μm/s) cells undergoing directional motion. The kink velocities were obtained from 27 kinks in five PCF cells (86 ± 3 μm/s) and 24 kinks in eight BSF cells (136 ± 7 μm/s), respectively. The ratio of the kink velocity to the cell velocity is about 16 for PCF and 18 for BSF cells.

DIC microscopy with a millisecond timescale [supporting information (SI) Fig. S1] (see *SI Text* for details]. The millisecond frame-by-frame analysis revealed that cell propulsion of *T. brucei* is characterized by repeated reversals in the rotation direction of the flagellum tip, which produced helical waves of alternating chirality propagating tip to base (Figs. 1*B* and Fig. S2, Movies S1 and S2). The image sequence in Fig. 2*A* (*Top*) shows such a bihelical wave in a PCF cell having RH chirality at the tip and LH chirality near the base of the flagellum (see Movie S1). At a later time, this same cell initiated a beat with opposite chirality (see Fig. 2*A Bottom*): that is, exhibiting LH chirality at the tip and RH chirality near the base of the flagellum. We quantified the frequency of LH and RH helical waves by tabulating how many times the flagellum tip flipped to initiate a wave in either direction. The average frequency, calculated from five cells, was 19 ± 3 flips per second, with each flip representing a rotation of ≈180°. This was split approximately equally between LH (9.7 ± 1.3 flips/s) and RH waves (9.0 ± 2.0 flips/s), as illustrated by the representative example shown in Fig. 3*A*. Typically, no more than three successive waves with the same chirality are generated at the flagellar tip. Thus, there appears to be no systematic bias for LH or RH chirality in the motility dynamics.

Next, we examined BSF *T. brucei* cells to determine whether helical waves with alternating chirality are a shared feature of both life-cycle stages. The millisecond DIC images clearly demonstrate bihelical waves in the flagellum of BSF cells (Movies S3 and S4). The image sequence in Fig. 2*B* shows a BSF cell monitored over a 70-ms time period. The top panels show a bihelical wave with LH chirality at the tip and RH chirality near the base of the flagellum. As this wave propagates toward the flagellum base, a new RH helical turn is initiated at the flagellum tip, producing a wave with RH, LH, RH chirality from tip to base (*Bottom*).

Kinks. A segment of a filament connecting two helical segments of opposite chirality is known as a "kink." We define a "plus" kink as one separating an anterior RH helical wave from a posterior LH helical wave, while a "minus" kink separates an anterior LH helical wave from a posterior RH helical wave. A kink separating two traveling helical waves, as in Fig. 2*A*, will itself travel along the filament. Traveling kinks have been encountered earlier in motility studies of prokaryotes, such as *Escherichia coli* (19, 20), where they appear to be associated with changes in course. In *Spiroplasma*, which do not have flagella (21), pairs of kinks traveling along the helical cell body cause the cell to swim in a zig-zag path. A theoretical study of *Spiroplasma* motility (22) proposed that recoil against the motion of fluid carried backwards by traveling kinks actually is the propulsive mechanism of *Spiroplasma*.

Well-defined kinks could be observed in the millisecond DIC images of both PCF and BSF *T. brucei* cells (see the *gray arrow* in Fig. 1*B*, Fig. 2, and Movies S1–S4). The kinks propagated down the flagellum along the cell body from tip to base (see Fig. 2, and Movies S1–S4), opposite to the direction of cell propulsion. Typical kink propagation velocities in *T. brucei* were 85 ± 18 μm/s in PCF cells and 136 ± 7 μm/s in BSF cells, more than an order of magnitude higher than the center-of-mass velocity of the cells (Fig. 3*B* and details in the *SI Text*). The observation that a 1.6-fold increase of kink velocity in BSF cells versus PCF cells correlates with a 1.6-fold increase in the center-of-mass velocity of BSF versus

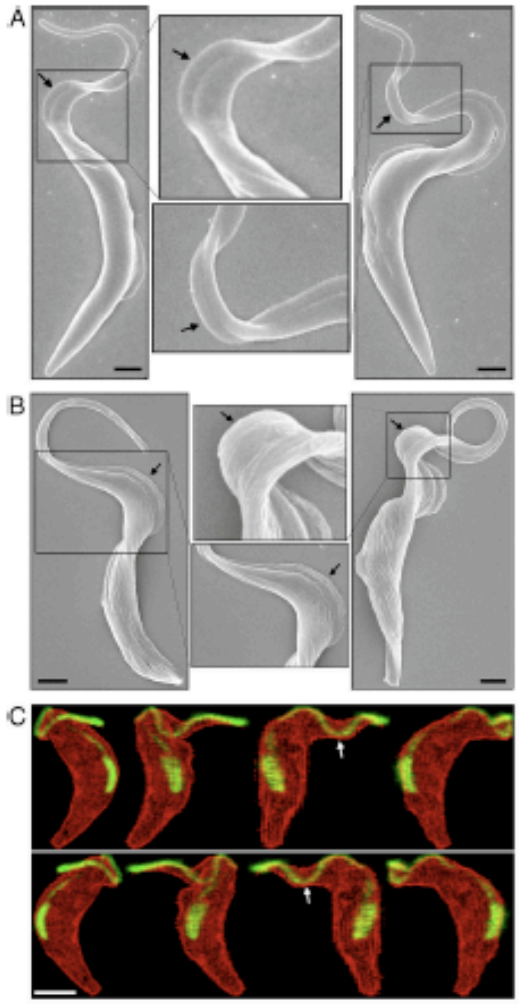

Fig. 4. SEM and confocal microscopy imaging of rapid-fixed PCF and BSF cells. (*A*) SEM images of PCF cells with bihelical waves separated by a plus (*Left*) or a minus (*Right*) kink. (*B*) SEM images of BSF cells with bihelical waves separated by a plus (*Left*) or a minus (*Right*) kink. The zoom-in views illustrate torsion of the cell body induced by the bihelical waves and kinks. (Scale bars, 1 μm.) (*C*) Confocal microscopy images of a GFP-labeled flagellum in a single PCF cell (see Movie S5). The cell is rotated along the vertical axis with ≈45° per image. The flagellum (*green*) wrapping around the surface of the cell body (*red*) exhibits RH chirality near the base and LH chirality near the tip, forming a minus kink (*white arrows*). (Scale bar, 3 μm.)

PCF cells (see Fig. 3*B*) suggests that kink motion is intrinsic to the propagation mechanism.

To further confirm the existence of helical waves and kinks in *T. brucei*, we used scanning electron microscopy (SEM) combined with a rapid-fixation technique that was optimized to preserve flagellar waveforms (23). SEM images of rapid-fixed cells indeed revealed bihelical waves and kinks in both PCF and BSF cells (Fig. 4 *A* and *B*). Interestingly, SEM images indicate that the cell body is subject to torsional strain, possibly generated by the flagellum. At the flagellar pocket where the flagellum emerges from the cytoplasm, there is a preferred LH chirality for the flagellum, consistent with earlier studies (24). As an independent test, we labeled the flagellum of PCF cells with a PFR2-GFP fusion protein and imaged these cells by three-dimensional (3D) confocal microscopy. In a representative 3D image (Fig. 4*C* and Movie S5), the flagellum (*green*) wraps around the surface of the cell body (*red*) and exhibits RH chirality near the base and LH chirality near the tip, forming a minus kink (*white arrows*).

Cell Body: Configurational Changes, Viscous Drag, and Torsional Stress. Arrival of kinks at the posterior end of the cell appears to correlate with transitions of the main body of the cell between two dominant configurations (see Figs. 1*B* and 2, Movies S1–S4). The configurational changes take place through alternating clockwise and counterclockwise rotations of the posterior end. In other words, the posterior end rocks back and forth about its own axis rather than completing full 360° rotations. The average frequency of the rocking motion of the posterior end was 5 ± 3 flips per second (calculated from five cells and 34 individual flips), compared to 19 ± 3 flips per second at the anterior end. The fact that the rotation frequency decreases significantly along the body of *T. brucei* is interesting. Different sections of a filament that supported a helical wave with a frequency gradient would, over time, be rotated with respect to each other over arbitrarily large angles, which for *T. brucei* would not be consistent with the mechanical integrity of the cell body. The reversals in rotation observed in *T. brucei* are thus necessary to maintain the frequency gradient.

The observation that the smaller anterior end of the body performs high-frequency complete rotations, while the larger posterior end only performs a low-frequency rocking motion, suggests a rationale why this may be an efficient mode of propagation for a microorganism with the asymmetric cell structure of *T. brucei*, given that at low Reynolds number viscous forces dominate (25). Note that a purely reciprocal motion (i.e., one that is symmetric under time reversal) cannot provide a net propulsive force to a microorganism, so the reciprocal rocking motion of the posterior end of *T. brucei* could not contribute a net propulsive force. On the other hand, the sequence of kinks traveling from the anterior to the posterior end separating helical sections with opposite chirality and opposite rotation direction obviously is nonreciprocal, and could therefore contribute a net propulsive force. Next, it follows from elementary hydrodynamics that a tapering cylindrical body rotating around its axis in a fluid is subject to a retarding viscous torque-per-unit length (τ_R) exerted by the surrounding medium that resists the rotation. This torque-per-unit length at a given point along the body is proportional to the local cross-section:

$$\tau_R = -4\pi\eta R_B^2\omega_B \qquad [1]$$

where η is the viscosity of the surrounding medium, R_B the radius of the cross section of the cell body at that point, and ω_B the rotation rate of the body. If, for example, we model the main body of *T. brucei* as a cylinder with a length L of ≈20 μm and a (constant) radius of ≈1 μm, then the power dissipated by viscous loss in water at the 20-Hz rotation rate of the tip would be substantial: about 10^6 times the ATP hydrolysis energy per second. Reducing this rotation frequency by a factor of four—the typical frequency reduction factor between posterior and anterior ends of *T. brucei*—reduces the power dissipation by more than an order of magnitude because power is proportional to the square of the rotation frequency. For a case in which the radius of the cell body near the anterior end is about five times less than that near the posterior end, a reasonable estimate for *T. brucei*, the viscous torque-per-unit length near the anterior end is about 25 times less than that near the posterior end, thus roughly compensating for the frequency increase of the anterior end. If the flagellum produced helical waves of uniform

chirality, then the posterior and anterior ends of the cell would necessarily rotate at the same "global" rate, which would be slowed greatly by the viscous torque on the cell body near its larger posterior end. The frequency gradient thus allows for high rotation rates at the smaller anterior end, which provides the traction force that pulls the cell body along, combined with reduced rotation rates toward the larger posterior end, which reduces viscous drag. Additionally, because the flagellum is attached laterally along the length of the cell body, a helical wave of the flagellum necessarily applies a torsional stress to the cell body, as also suggested by SEM images (see Fig. 4 *A* and *B*). Depending on the degree of viscoelasticity of the cell body, the cell body may well be able to store a significant amount of torsional elastic energy in reversible deformation of the microtubule cytoskeleton. This elastic energy could then be released when the flagellum started to rotate in the opposite direction, much like the rubber motor of a toy plane.

Rapid Swings of the Flagellar Tip of BSF Cells. Despite overall similarity, there is an interesting difference between the motilities of BSF and PCF cells. The anterior end of BSF cells exhibits more frequent and more pronounced movements than that of PCF cells under similar conditions (Fig. 5 *A* and *B*). Rapid swings of BSF flagellar tips were observed following large angle bends of this portion of the flagellum (Fig. 5*C*), a feature absent from PCF cells. To quantitatively analyze the rapid swings of the flagellar tip, we extracted 12 image sequences from two BSF cells undergoing fast forward locomotion. Each of the 12 trajectories (Fig. 5*D*) represents the distance traveled by the flagellar tip in each image sequence plotted as a function of the time elapsed (a linear fit of the average trajectories is shown as a *dashed line*). The slope of each trajectory corresponds to the velocity. The highest recorded velocity of the flagellar tip is 673 μm/s, while the average velocity (i.e., the slope of the dashed line) is 510 μm/s (see the *SI Text* for details). Note that these observations could not have been made with conventional video frame rates, suggesting that millisecond DIC microscopy could be a useful tool for exploring flagellar and ciliary motility in other organisms (26–29).

BSF Motility in Infected Mouse Blood. Our studies of *T. brucei* motility so far were carried out in standard culture medium used for most studies of trypanosome motility, which has a measured viscosity close to that of water (0.95cSt). In contrast, the macroscopic viscosity of human blood is about 35 times higher than that of water. What is perhaps most relevant is that in blood, the dense distribution of erythrocytes presents to *T. brucei* a highly inhomogeneous, although deformable, labyrinth that it must negotiate. Typical sizes of the free spaces of this labyrinth can be small compared to the length of a single BSF cell. To examine *T. brucei* motility in a more native medium, we investigated BSF cells in whole blood obtained from infected mice, 3 to 5 days after infection. Millisecond DIC images of actively swimming BSF *T. brucei* in infected mouse blood revealed the same motility motifs observed with cultured parasites (Fig. 6 *A* and *B*, Movie S6). Rapid swings of the flagellar tip were particularly striking, as they can be observed initiating contact with host blood cells and deforming them significantly (Fig. 6*C*). Comparison with the measured force-deformation curves of erythrocytes (30) indicates that the flagellum is capable of exerting forces in the 300 pN range (see the *SI Text* and Table S1).

Discussion

Using millisecond DIC microscopy, supplemented by SEM and 3D confocal microscopy, we have found that forward *T. brucei* motility is characterized by (*i*) tip-to-base propagation of kinks separating LH and RH helical waves, (*ii*) very high motility of the flagellum tip in BSF cells, and (*iii*) a pronounced rotation-frequency gradient along the cell body, with the anterior end performing rapid full rotations while the posterior end rocks back and forth more slowly. This specialized form of motility appears to reduce viscous dissipation by minimizing rotary motion of the large posterior end of the cell, while allowing *T. brucei* to negotiate complex viscous environments, such as mammalian blood.

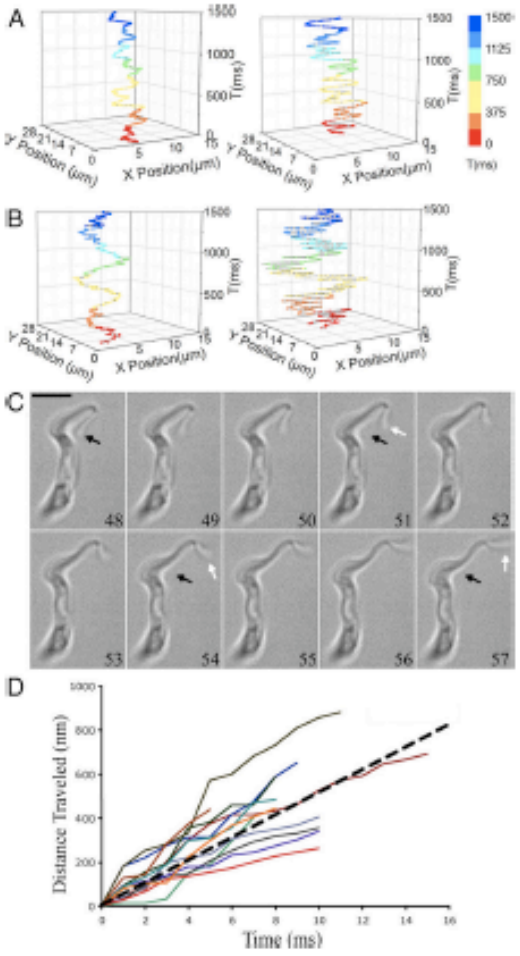

Fig. 5. Quantification of the motility of *T. brucei* cells. (*A*) Trajectory of the anterior (*Right*) and posterior (*Left*) end of a PCF cell as a function of time, where each color represents a different time period. (*B*) Trajectory of the motion of the anterior (*Right*) and posterior (*Left*) end of a BSF cell as a function of time. (*C*) Rapid motion of the BSF flagellar tip with a speed of 673 μm/s. White arrows show motion of the flagellar tip and the black arrows point to the initial tip position. The numerical numbers are in millisecond. (Scale bar, 5 μm.) (*D*) Twelve trajectories of rapid swings of the flagellar tip from two BSF cells of which the slopes represent the velocities of the flagellar tip swings. The average velocity (i.e., the slope of the dashed line) is 510 μm/s.

As noted earlier, the closest resemblance between the motility of *T. brucei* and that of other microorganisms is the prokaryote *Spiroplasma* (21, 31, 32). A comparison between these two widely divergent organisms is instructive. Both move in a zig-zag pattern, as kinks between waves of opposite chirality travel from the anterior to the posterior end. One can apply the theoretical analysis of kink motion in *Spiroplasma* (22) to *T. brucei* to argue that, also for *T.*

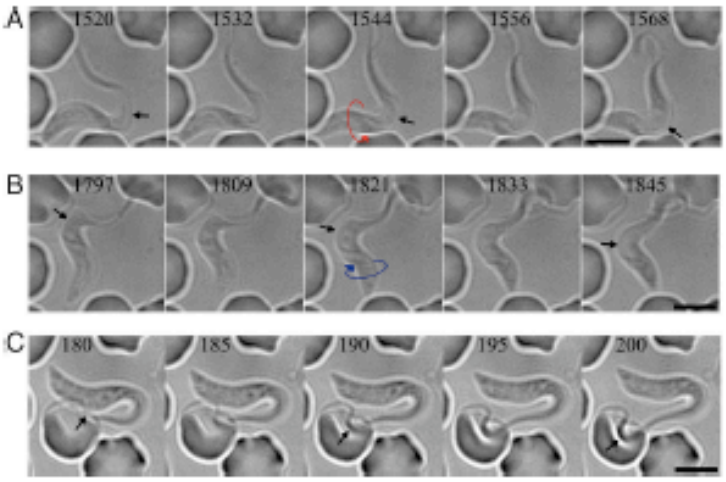

Fig. 6. Millisecond DIC microscopy imaging and analysis of BSF cell motility in infected mouse blood. (*A*) Image sequence of a BSF cell exhibiting bihelical waves separated by a plus kink, where the posterior end rotates clockwise, as indicated by the visible flagellum. The arrows pointing to the center of the kink show the kink propagation from the flagellar tip to base. The numerical values are in milliseconds. (Scale bars, 5 μm.) (*B*) Image sequence of the same BSF cell showing a minus kink where the posterior end rotates counterclockwise. (*C*) Rapid swing of the flagellum tip of the BSF cell was observed initiating contact with a host red blood cell over a time period of 20 ms.

brucei, the propulsive mechanism should be recoil against the motion of fluid carried backwards by the traveling kinks. However, whereas in *Spiroplasma* there is a preferred timing difference between kinks, which is consistent with the theoretical analysis, we encountered a broad distribution of timing differences, ranging between 150 and 300 ms. In addition, typical kink velocities of *T. brucei* (see Fig. 3*B*) are about an order of magnitude larger than that of *Spiroplasma* (about 10 μm/s), which may be because of the fact that *T. brucei* can recruit the efforts of large numbers of dynein molecular motors distributed along the axoneme (see below), whereas *Spiroplasma* presumably can rely on only a few motors. Interestingly, despite the higher kink velocity in *T. brucei*, the center of mass velocities of the two organisms is similar (in the range of 10 μm/s). This presumably reflects the larger viscous dissipative losses and also the larger mass of *T. brucei*, which by momentum conservation reduces the forward recoil velocity against the backward movement of fluid carried by the kinks. A key difference between *T. brucei* and *Spiroplasma* morphology is that *T. brucei* has a pronounced gradient in its body plan, while the body plan of *Spiroplasma* is so well described by a uniform helix (in the absence of kinks) that it is difficult to distinguish the anterior and posterior ends. In terms of motility, this translates into a uniform rotation frequency for *Spiroplasma* but a pronounced frequency gradient for *T. brucei*.

The eukaryotic axoneme is one of the most conserved structures in biology and was likely present in the last common ancestor of all extant eukaryotes (33). Axoneme motility is mediated by thousands of dynein motors that drive sliding and, ultimately, bending of microtubule doublets in the axoneme (34, 35). The switch point hypothesis is a generally accepted paradigm for wave propagation along the axoneme (36, 37). At its most basic, this hypothesis posits that axonemal dyneins are divided into two opposing groups, on either side of the axoneme, and that these groups are alternately activated or inactivated to cause axoneme bending in one direction or the other, thereby producing a plane wave. It has been demonstrated theoretically that arrays of coupled motor proteins subject to an external load can indeed switch collectively between two alternate directions of motion (38). Similarly, helical waves could be generated by assuming that the dynein motors also apply a rotary twist on each pair of microtubules of either chirality, thereby imposing a net twist on the cylindrical array of all nine outer doublet microtubules that would turn the plane wave into a helical wave, as has been proposed for waves in cilia (39). In such a model, the frequency of rotation would not be fixed but determined by the local, external load on the flagellum, determined in turn by the local radius of the flagellum. Because either helicity would be possible, there would now be dynamic instead of structural stability. Collective switching between these two helicity states, similar to the switch-point hypothesis, could then produce an array of moving kinks.

In summary, through quantitative and theoretical analysis of *T. brucei* motility, our results offer insights for considering propulsive mechanisms of microorganisms and provide new detail on an important, yet poorly understood, feature of trypanosome biology.

Materials and Methods

Millisecond DIC microscopy. A light microscope with DIC optics was assembled as follows. A Nikon Eclipse TE 2000-U inverted microscope was equipped with a Nikon Plan Apochromat 100× infinity-corrected oil DIC objective, which has a numerical aperture of 1.40 and a working distance of 0.13 mm. An open air motility chamber was placed on the microscope consisting of a glass slide, separated from a cover glass by an ≈200-μm spacer (40), placed onto the objective immersion oil. Cells were placed into the chamber in a volume of ≈100 μl in log phase. Illumination of the cells was achieved by using a Nikon 100W mercury lamp powered by an 18V to 40V source (Chiu Technical Instruments). Images were acquired using a latest generation CMOS-based Photron SA1.1 camera (Photron USA, Inc.) with 8-Gb onboard memory and a millisecond timescale.

Trypanosome Cell Maintenance and Motility Assays. PCF 29–13 and BSF-SM cells (41) were used throughout these experiments and maintained as previously described (9, 42). a Z1 Coulter Particle Counter (Beckman Coulter) to monitor cell doubling. For motility assays, cells were taken from mid-logarithmic phase cultures and placed in poly(L-glutamate)-treated glass motility chambers, described above, then imaged by using the millisecond DIC microscope. PCF cells were assayed at 25 °C, while BSF cells were assayed at 37 °C. Cells were not assayed for more than 15 min, and analyses were restricted to forward migrating cells. Image sequence acquisition, analysis, and quantification were performed as described in the *SI Text*.

Generation of GFP-PFR2 Cell Lines. The ORF of PFR2 (GenDB ID Tb927.8.4970) was PCR amplified from genomic DNA using Platinum Pfx polymerase (Invitrogen) according to the manufacturer's instructions. The forward and reverse primers used were as follows: PFR2-f 5′-TCTAGAATGAGCGGAAAGGAAGTTGAA-3′, forward. PFR2-r 5′-GGATCCCTACTGAGTGATCTGCGGC-3′, reverse (underlined are the 5′ XbaI and BamHI sites). The PCR product was ligated into a Zero Blunt TOPO PCR Cloning Kit vector (Invitrogen). The internal NotI site of the *PFR2* gene was destroyed by site-directed mutagenesis (changing C1773 into G) using a QuikChange Site-directed Mutagenesis Kit (Stratagene). The sequence was verified by sequencing at the University of California at Los Angeles genomics center. The gene encoding the PFR2 protein was subcloned using XbaI and BamHI sites into pKH10 (40, 41, 43). The construct was linearized using NotI, ethanol precipitated and transfected into PCF 29–13 cell line, as previously described (10, 42).

Transfectants were selected with 2.5 μg/ml Phleomycine (Cayla) and clonal lines were obtained by limited dilution. Individual clones were analyzed for the expression of the GFP-PFR2 fusion protein 48 h after induction with 1 μg/ml tetracycline.

Fluorescent Labeling and Confocal Microscopy Imaging of GFP-PFR2 Cells. For 3D confocal microscopy, cells expressing GFP-PFR2 (described above) were induced for 48 h with 1 μg/ml tetracycline, then washed once in prewarmed PBS and labeled with 0.5 μM CellTracker red, CMTPX (Molecular Probes, Invitrogen), in PBS for 15 min at 27 °C. Labeled cells were washed three times in prewarmed culture media. Cells were recovered for 5 min in culture media and fixed by adding paraformaldehyde (in PBS) to final concentration of 4% for 15 min directly in the labeled culture (23). Fixed cells were adhered to poly-L-Lysine coated slides for 20 min. Slides were washed once with PBS, blocked in PBS containing 0.1-mM glycine for 10 min, and mounted with Vectashield mounting medium (Vector Laboratories). Slides were then imaged using a Leica TCS-SP2-AOBS Multiphoton-FLIM confocal microscope using a 63× oil immersion objective. Images were acquired using the Leica confocal software supplied with the microscope. For 3D reconstruction of fixed cells, a series of images was acquired for the red (605 nm) and green (535 nm) emission channels in 0.35-μm increments for a distance of 12.2 μm. Processing and 3D rendering of images were carried out using the National Institutes of Health ImageJ software.

Millisecond DIC Imaging of BSF *T. brucei* in Infected Mouse Blood. Bloodstream form single marker cells were maintained in vitro as previously described (9). BALB/c mice (Jackson Laboratories) were inoculated with 100 mid-log phase cells intraperitoneally in warm sterile PBS pH 7.35 (Gibco) containing 1% glucose (44). Blood samples, 3 to 5 days after infection, were collected in heparinized capillary tubes (Fisher Scientific), monitored for parasitemia by counting in a hemocytometer, and imaged by the millisecond DIC microscope.

SEM Imaging of Rapid-Fixed PCF and BSF Cells. We adopted a rapid-fixation technique optimized to preserve flagellar waveforms (23). Cells were harvested by centrifugation, resuspended in fresh medium, recovered for 30 min, and then fixed by adding paraformaldehyde/glutaraldehyde to final concentration of 3% directly in the culture medium, fixed for 5 min, diluted to 1% fixative with 0.2M sodium cacodylate buffer (pH 7.4), and allowed to settle onto cover slips for 1 h. Fixative was removed and samples were dehydrated in ethanol. Samples were then dried overnight, sputter-coated with gold and imaged using a JEOL JSM-6700F FESEM.

Further details about image acquisition and analysis, measurements of cell and kink velocity, and determination of flagellum tip motion are provided in the *SI Text*.

ACKNOWLEDGMENTS. We thank W. Shi, C. J. Brokaw, and L. Simpson for constructive comments, H. Jiang for assistance with the SEM images, as well as L. Bentolila and M. Schibler of the advanced light microscopy facility at the California NanoSystems Institute. This work was supported in part by the National Science Foundation (Grant DMR-0520894), National Institutes of Health/National Institute of Allergy and Infectious Diseases (Grant AI052348), the Alfred P. Sloan foundation, the Howard Hughes Medical Institute Gilliam fellowship for advanced studies, the Ruth L. Kirschstein National Research Service Award (GM07185), the Burroughs Wellcome Fund, and a University of California at Los Angeles Molecular Biology Interdepartmental Whitcome fellowship.

1. Legros D, et al. (2002) Treatment of human African trypanosomiasis—present situation and needs for research and development. *Lancet Infect Dis* 2:437–440.
2. Welburn SC, Odiit M (2002) Recent developments in human African trypanosomiasis. *Curr Opin Infect Dis* 15:477–484.
3. Van Den Abbeele J, Claes Y, van Bockstaele D, Le Ray D, Coosemans M (1999) *Trypanosoma brucei* spp. development in the tsetse fly: Characterization of the post-mesocyclic stages in the foregut and proboscis. *Parasitology* 118(Pt 5):469–478.
4. Vickerman K, Tetley L, Hendry KA, Turner CM (1988) Biology of African trypanosomes in the tsetse fly. *Biol Cell* 64:109–119.
5. Pepin J, Donelson JE (1999) *African Trypanosomiasis (Sleeping Sickness), in Tropical Infectious Diseases: Principles, Pathogens and Practice.* Guerrant R, Walker DH, Weller PF, Editors. (Churchill Livingstone: Philadelphia, PA).
6. Mulenga C, Mhlanga JD, Kristensson K, Robertson B (2001) *Trypanosoma brucei brucei* crosses the blood-brain barrier while tight junction proteins are preserved in a rat chronic disease model. *Neuropathol Appl Neurobiol* 27:77–85.
7. Engstler M, et al. (2007) Hydrodynamic flow-mediated protein sorting on the cell surface of trypanosomes. *Cell* 131:505–515.
8. Broadhead R, et al. (2006) Flagellar motility is required for the viability of the bloodstream trypanosome. *Nature* 440:224–227.
9. Ralston KS, Hill KL (2006) Trypanin, a component of the flagellar dynein regulatory complex, is essential in bloodstream form African trypanosomes. *PLoS Pathog* 2:e101.
10. Ralston KS, Lerner AG, Diener DR, Hill KL (2006) Flagellar motility contributes to cytokinesis in *Trypanosoma brucei* and is modulated by an evolutionarily conserved dynein regulatory system. *Eukaryot Cell* 5:696–711.
11. Kohl L, Robinson D, Bastin P (2003) Novel roles for the flagellum in cell morphogenesis and cytokinesis of trypanosomes. *EMBO J* 22:5336–5346.
12. Moreira-Leite FF, Sherwin T, Kohl L, Gull K (2001) A trypanosome structure involved in transmitting cytoplasmic information during cell division. *Science* 294:610–612.
13. Bastin P, Sherwin T, Gull K (1998) Paraflagellar rod is vital for trypanosome motility. *Nature* 391:548.
14. Ginger ML, Portman N, McKean PG (2008) Swimming with protists: Perception, motility and flagellum assembly. *Nat Rev Microbiol* 6:838–850.
15. Hill KL (2003) Biology and mechanism of trypanosome cell motility. *Eukaryot Cell* 2:200–208.
16. Kohl L, Bastin P (2005) The flagellum of trypanosomes. *Int Rev Cytol* 244:227–285.
17. Walker PJ (1961) Organization of function in trypanosome flagella. *Nature* 189:1017–1018.
18. Gruby M (1843) Analysis and observation of a novel hematozoan species, *Trypanosoma sanguinis*. *C R Hebd Seances Acad Sci* 17:1134–1136.
19. Turner L, Ryu WS, Berg HC (2000) Real-time imaging of fluorescent flagellar filaments. *J Bacteriol* 182:2793–2801.
20. Darnton NC, Turner L, Rojevsky S, Berg HC (2007) On torque and tumbling in swimming *Escherichia coli*. *J Bacteriol* 189:1756–1764.
21. Shaevitz JW, Lee JY, Fletcher DA (2005) Spiroplasma swim by a processive change in body helicity. *Cell* 122:941–945.
22. Yang J, Wolgemuth CW, Huber G (2009) Kinematics of the swimming of spiroplasma. *Phys Rev Lett* 102:218102.
23. Mitchell DR (2003) Orientation of the central pair complex during flagellar bend formation in *Chlamydomonas*. *Cell Motil Cytoskeleton* 56:120–129.
24. Ralston KS, Hill KL (2006) The flagellum of *Trypanosoma brucei*: New tricks from an old dog. *Int J Parasitol* 36:869–884.
25. Purcell EM (1977) Life at low Reynolds number. *Am J Phys* 45:3–11.
26. Bray D (2001) *Cell Movements: From Molecules to Motility* (Garland Pub., New York) 2nd Ed pp. xiv, 372.
27. Satir P, Christensen ST (2007) Overview of structure and function of mammalian cilia. *Annu Rev Physiol* 69:377–400.
28. Brokaw CJ (2008) Thinking about flagellar oscillation. *Cell Motil Cytoskeleton* 66:425–436.
29. Berg HC (2003) The rotary motor of bacterial flagella. *Annu Rev Biochem* 72:19–54.
30. Heinrich V, Ourmazd C (2007) Force versus axial deflection of pipette-aspirated closed membranes. *Biophys J* 93:363–372.
31. Wada H, Netz RR (2007) Model for self-propulsive helical filaments: Kink-pair propagation. *Phys Rev Lett* 99:108102.
32. Gilad R, Porat A, Trachtenberg S (2003) Motility modes of Spiroplasma mellifera BC3: A helical, wall-less bacterium driven by a linear motor. *Mol Microbiol* 47:557–569.
33. Mitchell DR (2007) The evolution of eukaryotic cilia and flagella as motile and sensory organelles. *Adv Exp Med Biol* 607:130–140.
34. Lindemann CB (2007) The geometric clutch as a working hypothesis for future research on cilia and flagella. *Ann N Y Acad Sci* 1101:477–493.
35. Hines M, Blum JJ (1983) Three-dimensional mechanics of eukaryotic flagella. *Biophys J* 41:57–79.
36. Satir P, Sale WS (1977) Tails of tetrahymena. *J Protozool* 24:498–501.
37. Satir P, Matsuoka T (1989) Splitting the ciliary axoneme: Implications for a "switch-point" model of dynein arm activity in ciliary motion. *Cell Motil Cytoskeleton* 14:345–358.
38. Badoual M, Julicher F, Prost J (2002) Bidirectional cooperative motion of molecular motors. *Proc Natl Acad Sci USA* 99:6696–6701.
39. Hilfinger A, Julicher F (2008) The chirality of ciliary beats. *Phys Biol* 5:16003–16015.
40. Baron DM, Ralston KS, Kabututu ZP, Hill KL (2007) Functional genomics in *Trypanosoma brucei* identifies evolutionarily conserved components of motile flagella. *J Cell Sci* 120:478–491.
41. Wirtz E, Leal S, Ochatt C, Cross GA (1999) A tightly regulated inducible expression system for conditional gene knock-outs and dominant-negative genetics in *Trypanosoma brucei*. *Mol Biochem Parasitol* 99:89–101.
42. Hutchings NR, Donelson JE, Hill KL (2002) Trypanin is a cytoskeletal linker protein and is required for cell motility in African trypanosomes. *J Cell Biol* 156:867–877.
43. Hill KL, Hutchings NR, Grandgenett PM, Donelson JE (2000) T lymphocyte-triggering factor of African trypanosomes is associated with the flagellar fraction of the cytoskeleton and represents a new family of proteins that are present in several divergent eukaryotes. *J Biol Chem* 275:29369–29378.
44. Lumsden WH, Herbert WJ (1975) Pedigrees of the Edinburgh trypanosome (Trypanozoon) antigenic types (ETat). *Trans R Soc Trop Med Hyg* 69:205–208.

Appendix 2

Structure-Function Analysis of Dynein Light Chain 1 Identifies Viable Motility Mutants in Bloodstream-Form *Trypanosoma brucei*

EUKARYOTIC CELL, July 2011, p. 884–894 Vol. 10, No. 7
1535-9778/11/$12.00 doi:10.1128/EC.00298-10

Structure-Function Analysis of Dynein Light Chain 1 Identifies Viable Motility Mutants in Bloodstream-Form *Trypanosoma brucei*[▽]†

Katherine S. Ralston,[1]‡ Neville K. Kisalu,[1] and Kent L. Hill[1,2]*

Department of Microbiology, Immunology and Molecular Genetics, University of California, Los Angeles, California 90095,[1] and Molecular Biology Institute, University of California, Los Angeles, California 90095[2]

Received 30 November 2010/Accepted 23 February 2011

The flagellum of *Trypanosoma brucei* is an essential and multifunctional organelle that is receiving increasing attention as a potential drug target and as a system for studying flagellum biology. RNA interference (RNAi) knockdown is widely used to test the requirement for a protein in flagellar motility and has suggested that normal flagellar motility is essential for viability in bloodstream-form trypanosomes. However, RNAi knockdown alone provides limited functional information because the consequence is often loss of a multiprotein complex. We therefore developed an inducible system that allows functional analysis of point mutations in flagellar proteins in *T. brucei*. Using this system, we identified point mutations in the outer dynein light chain 1 (LC1) that allow stable assembly of outer dynein motors but do not support propulsive motility. In procyclic-form trypanosomes, the phenotype of LC1 mutants with point mutations differs from the motility and structural defects of LC1 knockdowns, which lack the outer-arm dynein motor. Thus, our results distinguish LC1-specific functions from broader functions of outer-arm dynein. In bloodstream-form trypanosomes, LC1 knockdown blocks cell division and is lethal. In contrast, LC1 point mutations cause severe motility defects without affecting viability, indicating that the lethal phenotype of LC1 RNAi knockdown is not due to defective motility. Our results demonstrate for the first time that normal motility is not essential in bloodstream-form *T. brucei* and that the presumed connection between motility and viability is more complex than might be interpreted from knockdown studies alone. These findings open new avenues for dissecting mechanisms of flagellar protein function and provide an important step in efforts to exploit the potential of the flagellum as a therapeutic target in African sleeping sickness.

African trypanosomes are protozoan parasites that cause significant human mortality and limit economic development in sub-Saharan Africa. Various subspecies of *Trypanosoma brucei* cause African sleeping sickness in humans and related trypanosomiases in wild and domestic animals. These parasites are transmitted between mammalian hosts through the bite of a tsetse fly vector. Parasite motility is thought to be important in both hosts (17); however, the role of motility has not been directly examined *in vivo* since it has not been possible to obtain a viable motility mutant in the life cycle stage that infects mammals. Trypanosome motility is driven by a single flagellum, which is laterally connected to the cell body and contains a canonical "9 + 2" axoneme that is the scaffold for assembly of molecular machinery that drives flagellar motility (35). Some features of the *T. brucei* flagellum are well-conserved among diverse taxa, while others are unique to trypanosomes. As such, the trypanosome flagellum has garnered increasing attention in recent years owing to its potential both as a target for therapeutic intervention in African trypanosomiasis and as an experimental system for studies of flagellum biology.

Recent work has revealed a fundamental role for the *T. brucei* flagellum in cell division and morphogenesis in both procyclic (insect midgut-form) and bloodstream-form (BSF) life cycle stages. African trypanosomes divide through binary fission, with a cleavage furrow between the new and old flagella that advances from anterior to posterior, producing two daughter cells that are oriented with their flagella facing in opposite directions just before final cell separation. In procyclic cells, RNA interference (RNAi) knockdown of intraflagellar transport (IFT) proteins blocks flagellum assembly, leading to shortened flagella and mispositioning of the cleavage furrow such that cell division gives rise to unequally sized daughter cells (25). Knockdown of axonemal proteins in procyclic cells causes a range of motility defects, and knockdowns with severe motility phenotypes exhibit defects in the final stages of cell separation, giving rise to multicellular clusters (8, 36). While the cell division defect was not observed in all knockdowns, it is generally correlated with severity of the motility defect and is rescued by physical agitation of the culture, suggesting that twisting and pulling forces derived from flagellum motility contribute to cell separation (4, 9, 36). A related phenomenon, termed rotokinesis, has been reported to drive cell separation in the protist *Tetrahymena* (10).

The role of the flagellum in the morphogenesis and division of bloodstream-form trypanosomes is less clear. In the bloodstream life cycle stage, RNAi knockdown of flagellum proteins induces a rapid and severe cytokinesis failure (8, 9, 33). There are significant differences between this phenotype and the phe-

* Corresponding author. Mailing address: Department of Microbiology, Immunology and Molecular Genetics, University of California, Los Angeles, 609 Charles E. Young Drive, Los Angeles, CA 90095. Phone: (310) 267-0546. Fax: (310) 206-5231. E-mail: kenthill@mednet.ucla.edu.

† Supplemental material for this article may be found at http://ec.asm.org/.

‡ Present address: Division of Infectious Diseases and International Health, University of Virginia, Charlottesville, VA 22908.

▽ Published ahead of print on 4 March 2011.

notype of procyclic knockdowns (33). For example, the terminal phenotype is different, since bloodstream-form cells fail to initiate cytokinesis, while procyclic cells fail at the end of cytokinesis. Additionally, a lethal phenotype is observed in most bloodstream-form flagellum protein knockdowns, while in procyclic cells the phenotype is correlated with severity of the motility defect (4, 36). Bloodstream cells are also more sensitive to perturbation of the flagellum, as knockdowns that produce little or no observable motility defect in procyclic cells are nonetheless lethal in the bloodstream stage (8, 9, 11, 33). In the one case where protein knockdown was directly examined, as little as 4-fold reduction in protein levels was lethal in bloodstream forms (33), while nearly complete ablation did not affect viability of procyclic-form cells (21). The reason for these life cycle stage-specific effects is not known.

The observation that lethal bloodstream-form flagellum protein knockdowns have in common a suspected motility defect has led to the hypothesis that flagellum motility itself might be essential (9, 15, 33). While attractive, this hypothesis has not been formally tested and there are significant reasons to consider alternative explanations (34). The question is more than an academic curiosity, as it impacts efforts to understand the role of motility in disease pathogenesis and efforts to exploit flagellar motility as a drug target. Notably, all knockdowns described retain some flagellar motility, and a direct correlation between lethality and a flagellar motility defect has not been established (34), suggesting that something other than defective motility underlies the lethal phenotype in the bloodstream form. So far, all flagellar mutants have been generated using RNAi to block target protein expression, rather than employing mutants with loss-of-function point mutations. Flagellar proteins are invariably part of large, multisubunit complexes, which are in turn connected to other complexes (30). It is therefore expected that loss of one protein within a complex may have pleiotropic consequences owing to loss of the whole complex. Numerous studies in *Chlamydomonas reinhardtii* have borne this idea out for a large number of flagellar proteins (1, 19, 20, 22, 24, 46). Most of the characterized *T. brucei* flagellar knockdowns have known or suspected structural defects that represent loss of more than just the targeted protein (34). As such, it is not possible to distinguish between phenotypes arising from defective motility and structural consequences of ablating target gene expression.

In an effort to distinguish between functional and structural requirements for flagellum proteins in *T. brucei*, we have adapted approaches for reverse genetics in *T. brucei* (2, 29, 39) to develop a system for inducibly perturbing flagellum protein function while retaining structural integrity. Our strategy was to replace an endogenous protein with a mutant protein with a loss-of-function point mutation that assembles like the wild-type protein. Simultaneous gene knockdown and complementation with wild-type genes has been successfully employed in *T. brucei*, either through transient RNAi directed against an endogenous untranslated region (UTR) combined with constitutive expression of a complementing construct with an alternate UTR (39) or by RNAi directed against an endogenous coding sequence and complementation with a heterologous coding sequence (39) or a synthetic gene carrying silent mutations throughout the coding sequence (2). In the present work, we built on these approaches to develop a facile system for structure-function analysis. The approach employs stably integrated, inducible constructs and does not require heterologous coding sequences or synthetic genes harboring silent mutations. The system offers advantages over traditional approaches that require gene deletions, particularly in a diploid organism such as *T. brucei*, and inducibility allows analysis of essential proteins. We have applied this system to identify amino acids that are required for function of dynein light chain 1 (LC1), a regulatory component of the outer-arm dynein motor (6). In procyclic-form cells, the phenotype of LC1 mutants with point mutations differs from that of LC1 knockdowns and distinguishes LC1-specific functions from outer-arm dynein functions. In bloodstream-form cells, LC1 mutants with point mutations have defective motility, yet are viable, in contrast to cells with LC1 knockdown, which is lethal. These results demonstrate that, counter to the prevailing notion based on RNAi studies alone, normal motility is not essential for viability in the bloodstream stage. As such, these findings open the door for investigations of the role of motility in disease pathogenesis. The facile nature of the system that we have developed also makes it broadly applicable to mechanistic studies of flagellar protein function.

MATERIALS AND METHODS

Cell culture and transfection. BSF single-marker (SM) cells and procyclic 29-13 cells (45), which stably express T7 polymerase and the tet repressor, were used for all experiments. Procyclic cells were cultured as described previously (33) in Cunningham's synthetic medium supplemented with 10% heat-inactivated fetal calf serum (HIFCS). Bloodstream-form cells were cultivated at 37°C and 5% CO_2 in HMI-9 medium supplemented with 15% HIFCS (33).

Transfections were performed using an adaptation of the method described previously (26). For procyclic trypanosomes, mid-log-phase cells (5×10^6 cells/ml) were washed once in electroporation medium (EM), a 3:1 mixture of cytomix (120 mM KCl, 0.15 mM $CaCl_2$, 10 mM K_2HPO_4, 25 mM HEPES, 2 mM EDTA, and 5 mM $MgCl_2$ brought to pH 7.6 with KOH) and phosphate-buffered sucrose (7 mM K_2HPO_4-KH_2PO_4, pH 7.4, 277 mM sucrose, and 1 mM $MgCl_2$ brought to pH 7.4 with K_2HPO_4). Washed cells were resuspended to 5×10^7 cells/ml in EM, and 0.45 ml was added to an electroporation cuvette (0.4 cm) together with 0.1 ml of linearized plasmid DNA (5 to 10 μg). Electroporation was performed using a Bio-Rad Gene Pulser set at 1,500 V and 25 μF; cells were subjected to two pulses with 10 s between pulses. Cells were then transferred to 5 ml of fresh medium and incubated overnight. Drug selection was initiated at 18 to 24 h posttransfection. Transfection of bloodstream-form trypanosomes was the same as for procyclic trypanosomes, except mid-log-phase cells (1×10^6 cells/ml) were resuspended to 2×10^7 cells/ml in EM after washing, 20 μg of DNA was used, and cells were subjected to only one pulse. Following electroporation, bloodstream-form cells were transferred to 10 ml of fresh medium and aliquoted into a 24-well culture plate (0.5 ml/well). The concentrations used for drug selection were as follows: G418, 15 μg/ml (procyclic) or 15 μg/ml (bloodstream form); hygromycin, 50 μg/ml (procyclic); phleomycin, 2.5 μg/ml (procyclic) or 5 μg/ml (bloodstream form); and puromycin, 1 μg/ml (procyclic) or 0.1 μg/ml (bloodstream form).

Following transfection and drug selection, clonal cell lines were obtained by limiting dilution. For tetracycline induction, cells were split into two flasks, cultured with or without 1 μg/ml tetracycline (−Tet and +Tet, respectively), and diluted as necessary to maintain exponential growth. For growth curves, cell densities were measured using a Coulter counter, and averages of two independent counts are reported.

DNA constructs. All RNAi plasmids were constructed in $p2T7^{TA}B$, which contains opposing, tetracycline-inducible T7 promoters such that tetracycline-induced transcription generates an intermolecular double-stranded RNA (dsRNA) (26). To choose 3′ UTR sequences to serve as RNAi targets, the parameters described previously (7) were used to select sequence beginning immediately downstream of the stop codon of the target open reading frame (ORF) and ending upstream of predicted polyadenylation sites. To create $p2T7^{TA}B$/trypanin-UTR, a 322-bp fragment corresponding to nucleotides 1 to 322 of the trypanin (*T. brucei* 10.70.0480 [Tb10.70.0480]) 3′ UTR was PCR amplified

from 29-13 cell genomic DNA and cloned into pZT7^{TB}. To create pZT7^{TB}/LC1-UTR, a 246-bp fragment corresponding to nucleotides 1 to 246 of the LC1 (Tb11.02.3390) 3′ UTR was PCR amplified from 29-13 cell genomic DNA and cloned into pZT7^{TB}.

To create pKR10, the puromycin (puro) resistance cassette from pHD1342 (C. Clayton, ZMBH, Heidelberg, Germany) was subcloned into pKH12 (also known as pLew100-HX-GFP) (4). Briefly, The puro resistance cassette ORF, together with 5′ and 3′ UTR sequences, was PCR amplified, with the 5′ primer designed to include a T7 promoter and an upstream KpnI site and the 3′ primer designed to add a SalI site. This PCR product was subcloned into KpnI/SalI in pKH12, replacing the phleomycin resistance cassette. To create the 3× HA tag and multicloning sites for N- and C-terminal tagging, PCR primers were designed to amplify the 3× HA tag sequence, with the 5′ primer designed to add HindIII, AflII, and a start codon (ATG) and the 3′ primer designed to add XhoI, MfeI, a stop codon (TGA), and BamHI. Following PCR with these primers, nested PCR was performed with shorter primers corresponding to the termini of the original primers. The resulting PCR product was subcloned into HindIII/BamHI in the puro-resistant version of pKH12, to generate the final plasmid, pKR10.

Full-length wild-type trypanin (Tb10.70.0480) and LC1 (Tb11.02.3390) were each subcloned into pCR-Blunt-II-TOPO (Invitrogen). Site-directed mutagenesis was performed using a QuikChange II kit (Stratagene). The full-length open reading frames of the wild-type gene or gene with a point mutation were then subcloned into pKR10. Trypanin and trypanin point mutants were cloned into the unique MfeI site in pKR10, while LC1 and LC1 point mutants were cloned into XhoI/MfeI. All DNA constructs and point mutations were verified by direct sequencing. Plasmids were linearized at the unique NotI or EcoRV site for transfection.

RNA preparation and real-time RT-PCR. Cells were incubated with or without tetracycline (1 μg/ml) for 24 h, and total RNA samples were prepared using an RNeasy kit (Qiagen) according to the manufacturer's instructions. RNA samples (1 μg) were treated with DNase I (Invitrogen), and reverse transcription (RT) was performed using oligo(dT) primers (Invitrogen) and a SuperScript reverse transcriptase II kit (Invitrogen). Real-time PCR was performed using SYBR master mix (Bio-Rad) and gene-specific primers. PCR specificity was verified by melt curve analysis of the resulting PCR products. All primer sets were calibrated against a standard curve of *T. brucei* genomic DNA. The housekeeping genes glyceraldehyde-3-phosphate dehydrogenase (GAPDH; Tb927.6.4280/Tb927.6.4300) and RPS23 (Tb10.70.7020/Tb10.70.7030) were used as normalization controls. Relative gene expression was determined using the $2^{-\Delta\Delta CT}$ (where C_T is the threshold cycle) method (28). For each cell line, two independent sets of −Tet and +Tet cultures were used for RNA preparation and real-time RT-PCR. Data presented in Fig. 1C and Fig. S1A in the supplemental material represent averages from the two independent sets of −Tet and +Tet cultures, with standard deviations indicated by error bars. Primers used were as follows: GAPDH, 5′ GGC TGA TGT CTC TGT GGT GGA 3′ and 5′ GGC TGT CGC TGA TGA AGT CG 3′; RPS23, 5′ AGA TTG GCG TTG GAG CGA AA 3′ and 5′ GAC CGA AAC CAG AGA CCA GCA 3′; trypanin, 5′ GCA ATG AGG TTC TCC AGC AAA 3′ and 5′ GCG ATG AGT TCC AGC GTC TT 3′; LC1, 5′ GGA CGG AGA TTG ACA GGT TGG 3′ and 5′ TTC TGA TGG GGG GTT ATT GTG A 3′; Tb10.70.0470, 5′ GGC GAG TGA AGC GTG GTT ACA 3′ and 5′ GCC CCG AGA ACT GTG CCT AA; and Tb11.02.3400, 5′ CTC TCT CAG CCG CCC CAT T 3′ and 5′ AAC CCG ATA CCA CCC GCT TT 3′.

Protein preparation and Western blotting. Cells were grown in the presence or absence of 1 μg/ml tetracycline for 72 h. Flagellum skeleton protein extracts were prepared essentially as described previously (37). Briefly, cells were extracted with PEME buffer containing 1% NP-40 [1% NP-40, 100 mM piperazine-*N*,*N*′-bis(2-ethanesulfonic acid), pH 6.9, 2 mM EGTA, 0.1 mM EDTA, 1 mM $MgSO_4$, 25 μg/ml aprotinin, 25 μg/ml leupeptin] for 5 min at room temperature. Insoluble cytoskeletons were sedimented at 2,000 × *g* and then washed in PMN buffer (1% NP-40, 10 mM Na_2HPO_4-NaH_2PO_4, pH 7.4, 150 mM NaCl, 1 mM $MgCl_2$, 25 μg/ml aprotinin, 25 μg/ml leupeptin). Washed cytoskeletons were resuspended in PMN buffer containing 500 mM NaCl (final concentration) and 0.25 mg/ml protease-free DNase I (Worthington) and incubated on ice for 30 min. Insoluble flagellar skeletons were washed twice in the extraction buffer and then resuspended in Laemmli sample buffer for Western blotting as described previously (18). Trypanin was detected with a monoclonal antibody directed against a synthetic peptide corresponding to the last 13 amino acids of trypanin (33). HA-LC1 was detected with an anti-HA monoclonal antibody (Cowance). Blots were probed with an anti-β-tubulin monoclonal antibody (Developmental Studies Hybridoma Bank, University of Iowa) as a control for protein loading.

Electron microscopy. Procyclic cells were grown in the presence or absence of 1 μg/ml tetracycline for 72 h, washed twice with PBS, and then prepared for electron microscopy as described previously (21). Briefly, cells were fixed for 60 min in half-strength Karnovsky's solution (1% paraformaldehyde, 1% glutaraldehyde, 0.1 M sodium cacodylate, pH 7.2) containing 1% (wt/vol) tannic acid. Fixed cells were washed in fixative without tannic acid and then rinsed and postfixed with 1% osmium tetroxide plus 1.5% potassium ferrocyanide. Dehydration through an acetone gradient was performed, followed by infiltration and embedment in Eponate 12 (Ted Pella, Co.). Sections were cut on a Reichert Ultracut E ultramicrotome, poststained with uranyl acetate and lead citrate, and imaged using an Hitachi H-7000 or a 20 Philips CM 120 transmission electron microscope.

Bloodstream-form cells were grown in the presence or absence of 1 μg/ml tetracycline for 42 h, and flagellar skeletons were isolated using modifications of the standard procedure (37) to better preserve flagellum ultrastructure. We modified the procedure by using one-step instead of two-step fractionation, 150 mM instead of 1 M NaCl, additional protease inhibitors, and protease-free DNase. Briefly, log-phase cell cultures were collected by centrifugation at 2,000 × *g* and washed three times with 1× PBS. Cells were resuspended to 2 × 10^8 cells/ml in PMN buffer (1% NP-40, 10 mM Na_2HPO_4-NaH_2PO_4, pH 7.4, 150 mM NaCl, 1 mM $MgCl_2$, 25 μg/ml aprotinin, 25 μg/ml leupeptin, and protease inhibitor cocktail). Protease-free DNase I (Worthington) was added at 0.25 mg/ml. Samples were incubated at room temperature for 10 min and then on ice for 30 min to destabilize the subpellicular microtubules, and flagellar skeletons were collected by centrifugation at 16,000 × *g* for 10 min. Flagellar skeleton pellets were subsequently transferred to a fresh tube and washed twice with PMN buffer. Samples were then fixed and stained as described above for procyclic cells.

Motility assays. Sedimentation assays were performed as described previously (5). Briefly, cells were incubated with or without tetracycline for 72 h and then resuspended to 5 × 10^6 cells/ml in fresh medium. Each culture was aliquoted into four cuvettes (1 ml per cuvette) and incubated under standard growth conditions. The optical density at 600 nm (OD_{600}) was measured every 2 h. At each time point, two cuvettes from each culture were left undisturbed to monitor sedimentation, while the other two cuvettes were resuspended to monitor growth. The change in the OD_{600} (ΔOD_{600}) for each sample was calculated by subtracting the OD_{600} of resuspended samples from that of undisturbed samples.

For motility traces, all procyclic and bloodstream-form knockdowns and mutants with point mutations were incubated with or without tetracycline for 72 h; however, bloodstream-form knockdowns were incubated for 24 h to minimize the contribution of cell division defects to the assay readout. Cells were observed using a ×10 objective on a Zeiss Axiskop II compound microscope in polyglutamate-coated slide chambers (14). Cells were viewed under dark-field illumination for 45 s for procyclic cells or 60 s for bloodstream-form cells. Metamorph software (Molecular Devices) was used to track cell movement and generate motility traces. Cells that were not tracked for the full time period, such as cells that moved out of the focal plane, were not used for analysis. For quantification of total distance traveled by individual cells, data from at least 100 cells ($N > 100$) were used. The mean of each data set was calculated, and for statistical analysis, the results for the data sets were compared to those for RNAi −Tet using the Student unpaired two-tailed *t* test.

Live videos (30 frames per second) were obtained after cells were incubated for 72 h with or without tetracycline, except bloodstream-form knockdowns, which were incubated for 24 h, using differential interference contrast (DIC) optics on a Zeiss Axiovert 200 M inverted microscope with a ×63 Plan-Neofluor oil-immersion objective. Cells were visualized in polyglutamate-coated slide chambers (14). Slides were inverted and examined through the coverslip. Videos were imaged by using a COHU charge-coupled-device analog video camera and converted to digital format with an ADVC-300 digital video converter (Canopus, Co., Ltd.). Digital clips were captured at 30 frames per s and converted to AVI movies with Adobe Premiere Elements software (Adobe Systems).

RESULTS

Two-plasmid system for RNAi-based structure-function studies and selection of target gene. We set out to develop a system in which an endogenous protein is replaced with a mutant protein with a loss-of-function point mutation that assembles like the wild-type protein. To achieve this, we took advantage of robust systems for inducible RNAi and protein expression in *T. brucei* to direct tetracycline-inducible RNAi against a target mRNA 3′ UTR, with concurrent inducible expression of an epitope-tagged copy of the targeted gene. Any desired mutation may be introduced into the epitope-tagged

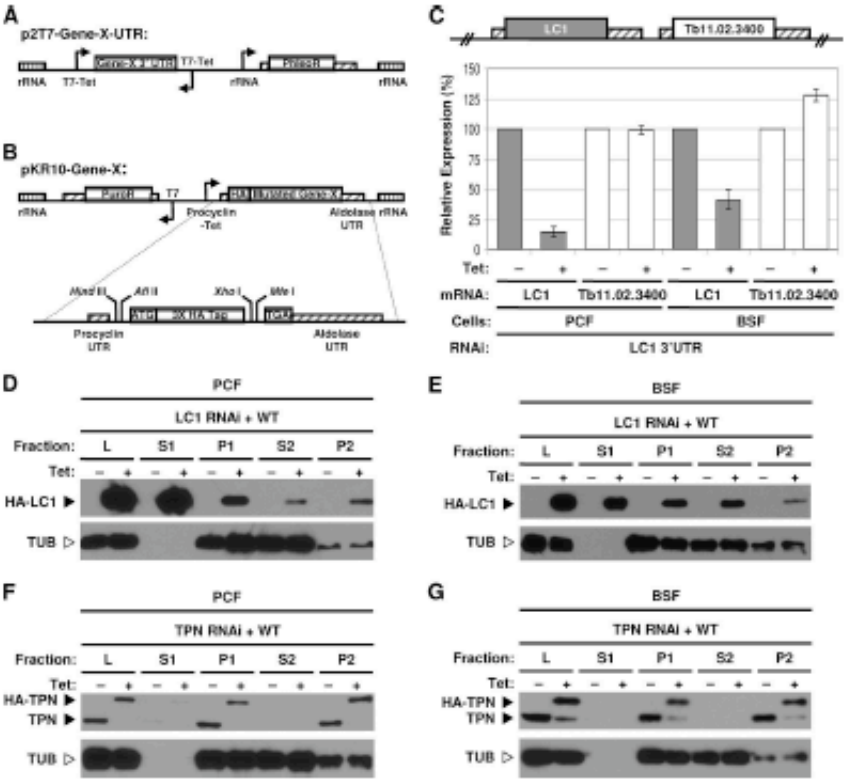

FIG. 1. Two-plasmid system for structure-function studies. (A) Schematic representation of the p2T7^{Ti}B vector (26) used for RNAi of the target gene (Gene-X) 3′ UTR. Opposing tetracycline-inducible T7 promoters (T7-Tet) drive the expression of dsRNA. The rRNA regions (rRNA, vertically lined boxes) direct stable, homologous integration into the genome. A phleomycin resistance cassette (PhleoR) is used for selection. (B) The pKR10 vector for inducible expression of mutants with HA-tagged point mutations with an aldolase 3′ UTR. A tetracycline-inducible procyclin promoter (Procyclin-Tet) drives inducible expression, and a puromycin resistance cassette (PuroR) is used for selection of stable integrants. The vector is shown with an N-terminal HA tag but is designed for convenient N terminus or C terminus tagging. A detailed view of the multicloning site is shown below the vector. Boxes with diagonal lines indicate UTRs. (C) Real-time RT-PCR analysis of LC1 expression in LC1 3′ UTR RNAi procyclic-form (PCF) and BSF cell lines. Both the targeted gene (LC1) and the gene immediately downstream (Tb11.02.3400) were assayed. Data represent averages from two independent sets of −Tet and +Tet cultures, with standard deviations indicated by error bars. (D to G) Flagellum fractionation and Western blot analysis of cell extracts from procyclic-form (D and F) and BSF (E and G) cells grown with or without tetracycline as indicated. Individual blots were probed with an anti-HA monoclonal antibody to detect HA-tagged LC1 or an anti-trypanin monoclonal antibody to detect endogenous trypanin and HA-trypanin, or an anti-β-tubulin monoclonal antibody was used as a loading and fractionation control. The positions of HA-tagged LC1 (HA-LC1), HA-tagged trypanin (HA-TPN), endogenous trypanin (TPN), and β-tubulin (TUB) are indicated. Fractions are as follows: L, total cell lysate; S1, detergent soluble fraction; P1, detergent-insoluble cytoskeleton; S2, NaCl-soluble fraction; P2, NaCl-insoluble flagellar skeleton. WT, wild type.

copy, enabling systematic structure-function analyses in a background where the endogenous protein has been removed and allowing identification of recessive as well as dominant mutations. Integrative plasmids used for simultaneous knockdown and replacement of target gene expression are shown in Fig. 1A and B. The p2T7^{Ti}B RNAi vector (26) drives tetracycline-inducible expression of target dsRNA, while pKR10 drives tetracycline-inducible expression of a wild-type or mutagenized copy of the target gene's ORF fused to an epitope tag. For knockdown, RNAi is directed against the 3′ UTR, rather than the ORF, to allow expression of the tagged copy with a different 3′ UTR.

To test the system, we wanted to target a flagellar protein for which data were available to inform selection of amino acids to alter. Surprisingly, despite the fact that several hundred flagellar proteins are known, there is very little information about which amino acids in these proteins are required for function. An exception is the outer-arm dynein light chain 1 (LC1),

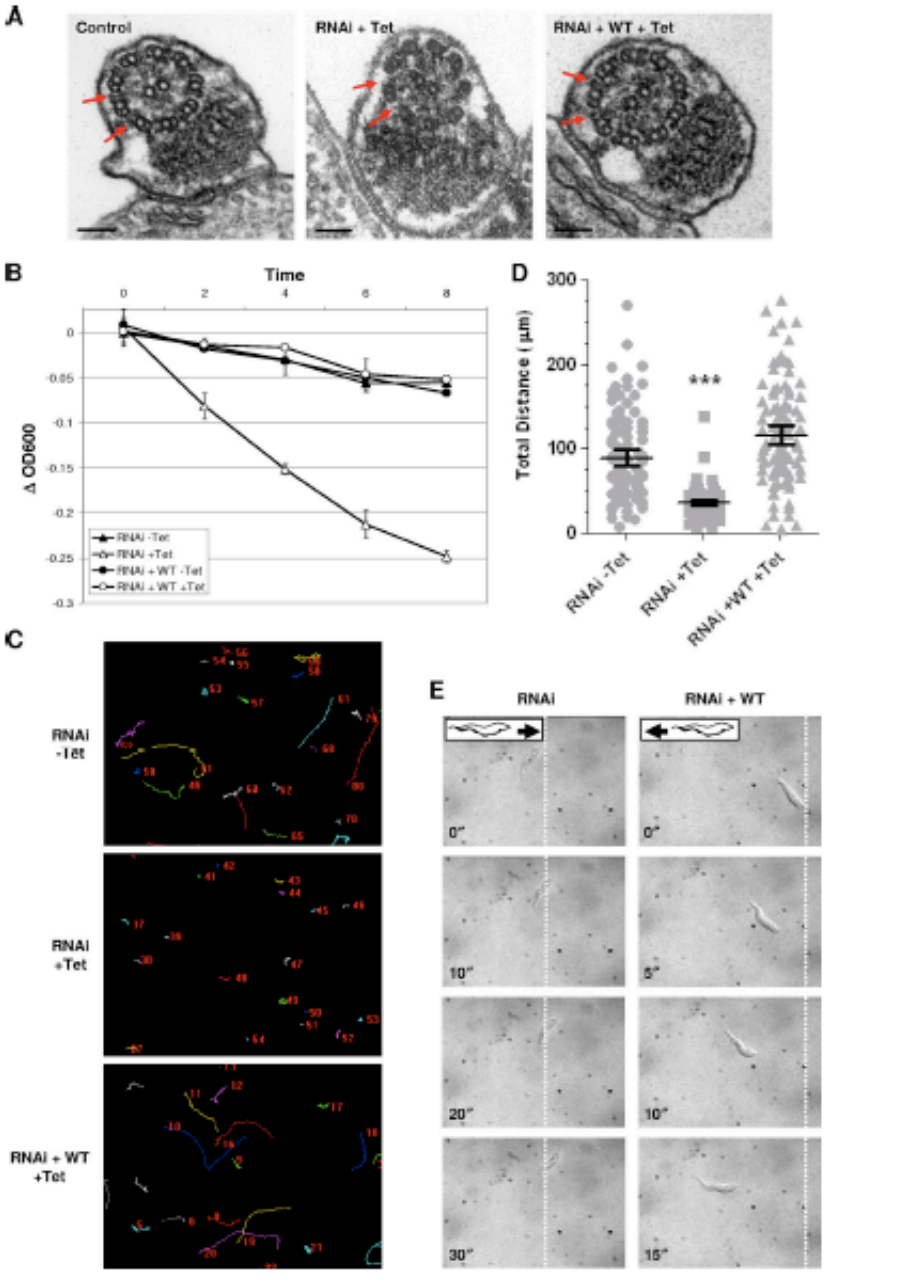
A
Control
RNAi + Tet
RNAi + WT + Tet
B
Time
Δ OD600
RNAi -Tet
RNAi +Tet
RNAi + WT -Tet
RNAi + WT +Tet
D
Total Distance (μm)
***
RNAi -Tet
RNAi +Tet
RNAi +WT +Tet
C
RNAi -Tet
RNAi +Tet
RNAi + WT +Tet
E
RNAi
RNAi + WT
0"
10"
20"
30"
5"
10"
15"

which binds the motor domain of the outer dynein γ heavy chain (6). At the time that we initiated our study, no LC1 mutants with point mutations were available, but a solution structure and extensive biochemical data on the LC1 protein from *C. reinhardtii* provided clear indications for amino acids expected to be important for function (48). Since that time, amino acid substitutions at these positions in the *C. reinhardtii* protein have been demonstrated to exert dominant negative effects on flagellum beating and cell motility in *C. reinhardtii* (32). We previously showed that RNAi knockdown of LC1 in procyclic-form parasites caused loss of outer-arm dyneins, reversal of flagellum beat direction, and backward cell propulsion (3). Therefore, with information on critical amino acids and a spectrum of assays to assess function, LC1 was selected as the target for mutational analysis.

3′ UTR RNAi knockdown and rescue with epitope-tagged wild-type protein. For RNAi, a DNA fragment corresponding to the first 246 bp of the LC1 3′ UTR was cloned into p2T7^{TI}B, and the resulting plasmid was stably transfected into procyclic and bloodstream-form parasites. Tetracycline-inducible knockdown directed against the 3′ UTR was highly effective, and the downstream gene was not affected (Fig. 1C). As an independent test, a 322-bp fragment of the 3′ UTR from the trypanin gene (21) gave potent and specific knockdown of trypanin expression in procyclic and bloodstream-from trypanosomes (see Fig S1A in the supplemental material). Therefore, RNAi directed against the 3′ UTR provides potent and specific knockdown of target gene expression.

For expression of wild type HA-tagged protein, the open reading frame was cloned in frame with the HA epitope tag in pKR10, which was then stably transfected into the corresponding 3′ UTR-knockdown cell line. Tetracycline-inducible expression was tightly controlled for both HA-LC1 and HA-trypanin in procyclic and bloodstream-form trypanosomes (Fig. 1D to G). Antibodies to *T. brucei* LC1 were not available for direct comparison with endogenous protein, but fractionation of HA-LC1 (Fig. 1D and E) was the same that as reported previously for green fluorescent protein (GFP)-tagged LC1 and was consistent with that expected on the basis of analogy with *C. reinhardtii* LC1 (3, 12). HA-trypanin was expressed at approximately the same level as the endogenous protein and fractionated exactly as seen for the endogenous protein (Fig. 1F and G) (18, 33). Therefore, the system provides simultaneous, tightly controlled tetracycline-inducible knockdown of an endogenous target gene and inducible expression of an epitope-tagged copy of the target gene in procyclic and bloodstream-form trypanosomes.

We next asked whether expression of wild-type, HA-tagged protein rescued the phenotype of procyclic knockdowns. RNAi directed against the LC1 open reading frame causes loss of outer-arm dyneins, reversal of flagellum beat direction, and reverse cell propulsion (3). RNAi against the LC1 3′ UTR phenocopied the outer-arm deficiency and motility defect of the open reading frame knockdown (Fig. 2; see Videos S1 to S3 in the supplemental material). Expression of wild-type HA-LC1 rescued the outer-arm deficiency (Fig. 2A) and the motility defect, as shown by sedimentation assay (Fig. 2B), motility trace analysis (Fig. 2C and D), and high-resolution video analysis of individual cells (Fig. 2E; see Video S4 in the supplemental material). Trypanin UTR knockdown likewise phenocopied the motility defect of trypanin ORF knockdowns, and the defect was rescued by wild-type HA-trypanin (see Fig S1D in the supplemental material).

LC1 mutants with point mutations show defective motility without disrupting outer-arm dynein. LC1 amino acids targeted for mutational analysis were selected on the basis of the solution structure of *C. reinhardtii* LC1 (47, 48) and cross-linking studies (6). These studies predicted that a C-terminal alpha helix, α9, regulates motor activity of the outer dynein γ heavy chain and that two C-terminal residues, R189 and R196, contact the ATP-hydrolyzing P1 AAA+ domain of the dynein motor (Fig. 3A and B) (48). Nearby residues, M182 and D189, were predicted to control positioning of the C-terminal α9 helix (48). Strong support for this model came from recent work using mutant forms of the *C. reinhardtii* LC1 protein, showing that amino acid substitutions at R189, R196, M182, and D185 exert dominant negative effects on flagellar motility (32). Therefore, the homologous residues, K203, R210, V196, and D199, in the *T. brucei* LC1 protein (Fig. 3A and B; see Fig. S2A in the supplemental material) were chosen for mutational analysis. Amino acids were changed individually or in pairs, as indicated in Table S1 in the supplemental material.

Procyclic cell lines harboring tetracycline-inducible constructs for each mutant with a point mutation in combination with tetracycline-inducible RNAi against the endogenous LC1 3′ UTR were induced with tetracycline. All mutant proteins exhibited the same expression and fractionation patterns seen for wild-type protein (see Fig. S2B and C in the supplemental material; data not shown), indicating that the mutant proteins were targeted to the flagellum and assembled normally. None

FIG. 2. HA-tagged LC1 rescues the LC1 RNAi phenotype in procyclic cells. (A) Transmission electron microscopy analysis of flagellum ultrastructure in uninduced control cells (control), LC1 UTR RNAi cells (RNAi + Tet), and LC1 UTR RNAi cells rescued with wild-type LC1 (RNAi + WT + Tet). Expression of HA-LC1 rescues loss of outer dynein (red arrows) caused by LC1 knockdown. Bars, 100 nm. (B) Sedimentation assay of cells with LC1 3′ UTR RNAi alone (RNAi) or LC1 3′ UTR RNAi plus HA-LC1 (RNAi + WT) grown with or without Tet, as indicated. Sedimentation curves represent the averages of two independent experiments, and error bars indicate the standard deviations. (C) Motility trace analysis of cells with LC1 3′ UTR RNAi alone (RNAi) or LC1 3′ UTR RNAi plus HA-LC1 (RNAi + WT) grown in the presence or absence of Tet, as indicated. Lines trace the movement of individual cells, and numbers in each panel are randomly generated by the software and represent individual cells. (D) Quantification of total distance traveled by individual cells in motility traces ($N > 150$ for each culture). Horizontal lines indicate the mean of each data set, with bars indicating the 95% confidence interval. Results for the data sets were compared to those for RNAi without Tet. ***, significant difference ($P < 0.0001$). (E) Time-lapse images taken from Videos S3 and S4 in the supplemental material demonstrate the backward translocation of LC1 knockdowns (RNAi) and the wild-type forward translocation of cells rescued with HA-LC1 (RNAi + WT). Dashed lines indicate the starting position of the posterior end of each cell, and time stamps (in seconds) are indicated.

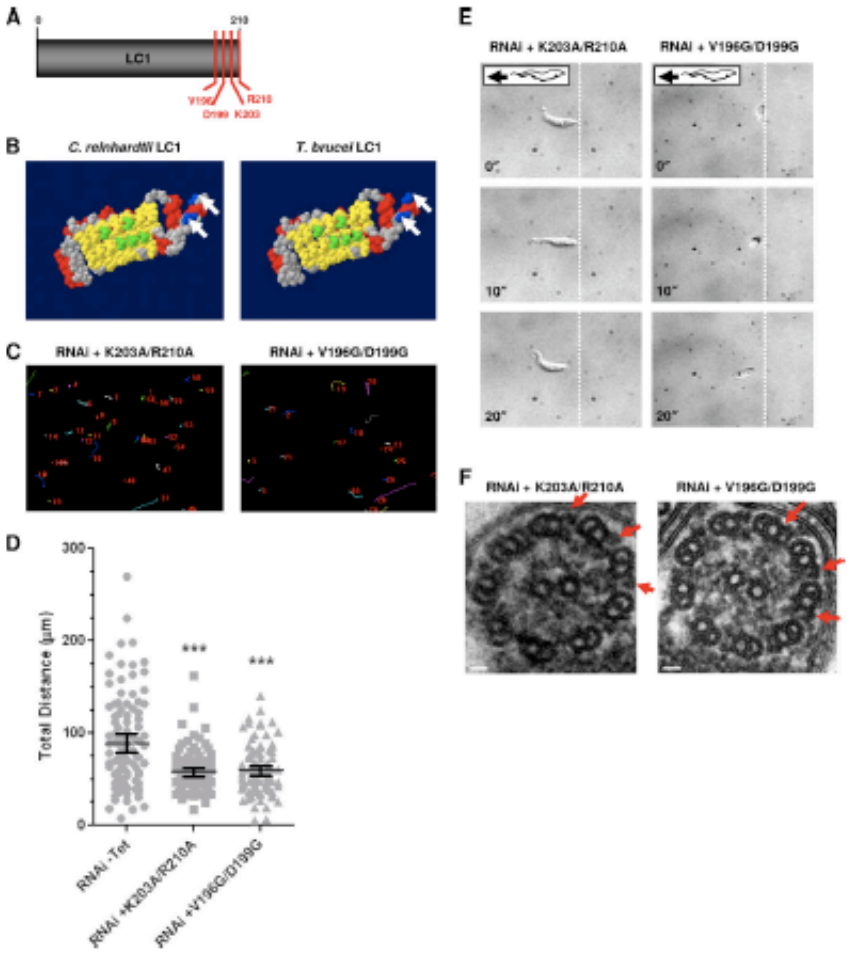

FIG. 3. Identification of LC1 mutants with loss-of-function point mutations in procyclic cells. (A) LC1 schematic showing residues selected for mutational analysis (V196, D199, K203, and R210). (B) Space-filling model of *C. reinhardtii* LC1 (48) compared with predicted *T. brucei* LC1 (3). *C. reinhardtii* LC1 residues that are predicted to bind to the outer dynein γ heavy-chain (green) and basic residues in the C terminus (blue, arrows) are conserved in the *T. brucei* protein. Red, α helices; yellow, β sheets; gray, residues with no functional predictions. Reprinted from reference 3, with permission. (C) Motility traces of LC1 mutants with K203A/R210A and V196G/D199G point mutations in procyclic cells, demonstrating motility defects in both mutants. Cells were incubated in the presence or absence of tetracycline, and motility traces were carried out as described in the legend to Fig. 2C. (D) Quantification of total distance traveled by individual cells in motility traces was carried out as described in the legend to Fig. 2D. Horizontal lines indicate the mean of each data set, with bars indicating the 95% confidence interval. Results for the data sets were compared to those for RNAi without Tet. ***, significant difference ($P < 0.0001$). (E) Time-lapse images taken from Videos S5 and S6 in the supplemental material demonstrate that the K203A/R210A and V196G/D199G mutants do not move backward. Dashed lines indicate the starting position of the posterior end of the cell, and time stamps (in seconds) are indicated. (F) Transmission electron microscopy analysis of flagellum ultrastructure in procyclic LC1 mutants with point mutations (K203A/R210A and V196G/D199G) shows that outer dynein arms are present (arrows). Images are oriented with the PFR at the bottom of the frame. Bars, 30 nm.

of the single mutants exhibited significant motility defects (see Table S1 in the supplemental material; data not shown), indicating that these individual amino acids are not essential for LC1 function and supporting the conclusion that the proteins were assembled normally. Both double mutants (K203A/R210A and V196G/D199G) exhibited severely defective motility, as demonstrated by motility trace analysis (Fig. 3C and D) and high-resolution video microscopy (Fig. 3E; see Videos S5 and S6 in the supplemental material).

The K203A/R210A and V196G/D199G mutants with point mutations moved more slowly than wild-type trypanosomes, but when they translocated, they did so in the forward direction (Fig. 3E; see Videos S5 and S6 in the supplemental material). This differs from LC1 knockdown cells, which exhibit reverse flagellum beating and translocate backward (see Video S3 in the supplemental material) (3). Reverse flagellum beating was also observed upon knockdown of the outer-arm dynein subunit DNAI1 (8). Both LC1 and DNAI1 knockdowns lack the outer-arm dynein complex, indicating that reverse flagellum beating is caused by loss of outer-arm dyneins (3, 8). Axoneme ultrastructure was therefore examined in the mutants with point mutations by transmission electron microscopy. In contrast to LC1 knockdowns (Fig. 2A) (3), the LC1 mutants with K203A/R210A and V196G/D199G point mutations retained outer-arm dyneins (Fig. 3F). Therefore, the phenotype of these mutants specifically reflects loss of LC1 function rather than simply being the consequence of losing outer-arm dyneins.

Motility mutants are viable in the bloodstream life cycle stage. Bloodstream-form *T. brucei* cells are exquisitely sensitive to perturbation of the flagellum, as RNAi knockdown of several different individual flagellar proteins produces a rapid and dramatic block in cell division that is lethal (8, 9, 33). These results have led to speculation that normal motility itself might be essential in bloodstream-form *T. brucei* (9, 15, 33). However, while such experiments demonstrate an essential requirement for the protein in question, they do not demonstrate an essential requirement for motility. For example, it is not possible to distinguish between functional and structural consequences, and all knockdowns examined have known or suspected structural defects (34). The LC1 mutants with K203A/R210A and V196G/D199G point mutations offer a unique opportunity to address this issue, because they exhibit defective motility, but the targeted protein and associated structures remain intact (Fig. 3F).

RNAi knockdown of LC1 in bloodstream-form cells was lethal (Fig. 4A and B). The phenotype was qualitatively the same as that reported for other bloodstream-form flagellum knockdowns (8, 9, 33), with cells accumulating as large amorphous masses that failed to divide (Fig. 4A). The phenotype was apparent within approximately 20 to 24 h postinduction and became progressively worse over time (data not shown). Motility was also defective (Fig. 4C and D; see Videos S7 and S8b in the supplemental material), although quantitation of motility traces must be considered with the caveat that cell division defects exacerbate the reduced cell translocation measured in the assay. The rapid and severe cell division phenotype of bloodstream-form LC1 knockdowns offered a sensitive test for rescue with mutant proteins. Each of the LC1 double mutants, K203A/R210A and V196G/D199G, rescued the cell division phenotype (Fig. 4A and B) yet showed severe motility defects (Fig. 4C and D; see Videos S9 and S10 in the supplemental material). Therefore, normal motility is not essential for viability of bloodstream-form trypanosomes.

DISCUSSION

We have developed an inducible system for structure-function analysis of flagellar proteins in *T. brucei*, which builds on and extends earlier important work showing complementation of RNAi knockdowns in *T. brucei* (2, 39). Using this system, we identified point mutations in the *T. brucei* axonemal dynein subunit LC1 that disrupt function while leaving the dynein motor intact, therefore discriminating between structural and functional requirements for LC1 in flagellar motility. Moreover, we identified two independent LC1 mutants with point mutations with defective motility that are viable in the bloodstream life cycle stage. These point mutants are the first such mutants to ever be isolated. Our results demonstrate that normal motility is not essential in the bloodstream life cycle stage in culture and make it possible for the first time to directly investigate the influence of motility on disease pathogenesis.

LC1 amino acid pairs K203/R210 and V196/D199 are required for normal flagellar motility in *T. brucei*. Expression of LC1 harboring mutations at the homologous amino acids in *C. reinhardtii* causes dominant negative effects on flagellar beating and swimming velocity (32). Thus, our results support and extend the conclusions of Patel-King and King (32) that LC1 is essential for normal function of the outer dynein motor. Notably, the phenotype of LC1 mutants with point mutations in procyclic *T. brucei* cells differs significantly from the phenotype caused by LC1 knockdowns. Backward flagellum beating is observed in the knockdowns (3) but not in the mutants with point mutations. Backward flagellum beating is also observed in DNAI1 knockdowns, which, like the LC1 knockdowns, lack outer-arm dyneins (8). The phenotype of LC1 or DNAI1 knockdown thus reflects a requirement for the outer-arm dynein motor, which is a massive structure with multiple heavy-chain motor domains and several light and intermediate chains (40), rather than individual contributions of LC1 or DNAI1 to flagellar motility. In contrast, the LC1 mutants with K203A/R210A and V196G/D199G point mutations retain outer-arm dyneins, and therefore, the motility phenotype of these mutants reflects loss of LC1 function. As such, our results discriminate between a requirement for LC1 in outer-arm dynein assembly and a functional requirement for LC1 in flagellar motility.

Our studies highlight a general caveat that is often overlooked in RNAi and knockout studies, namely, that complete loss of a protein of interest can have structural as well as functional consequences, thereby complicating phenotypic interpretation (23). This concern is particularly relevant for a biological machine such as the flagellum, in which thousands of interconnected protein complexes must operate in concerted fashion and disrupting one protein subunit generally has deleterious effects on other parts of the structure (23). In such instances, it is not possible to distinguish contributions of individual subunits, nor is it possible to readily distinguish between primary and pleiotropic phenotypes, and phenotypes must be interpreted in this context.

The flagellum is required for cell division in both procyclic

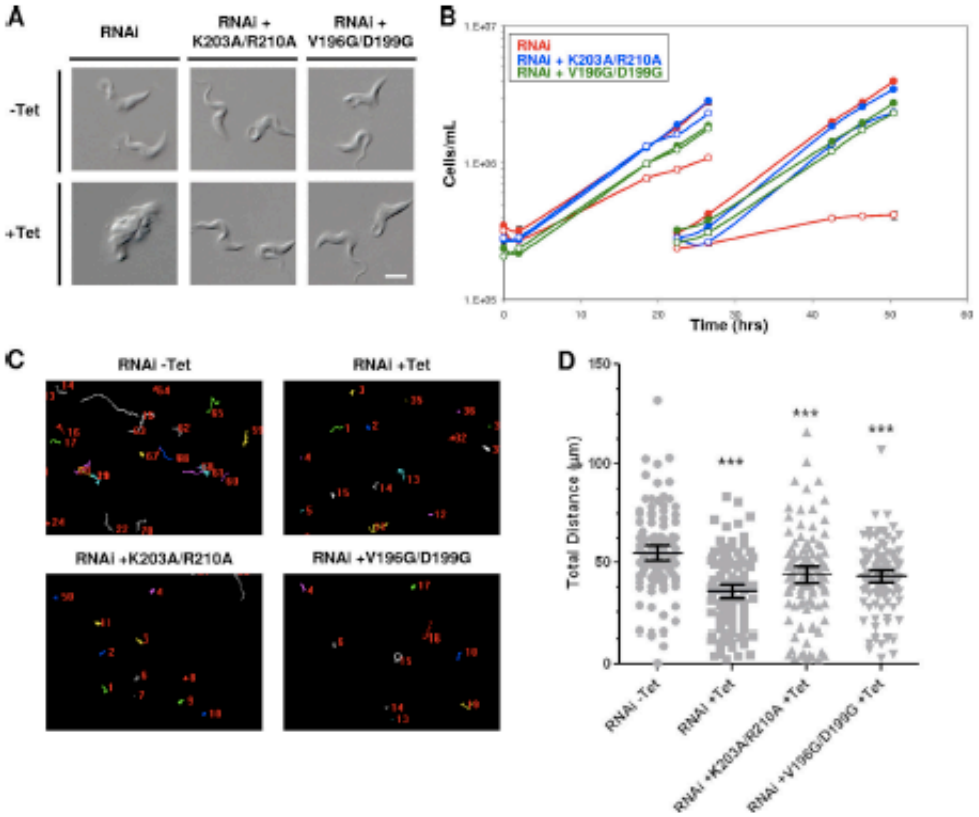

FIG. 4. Bloodstream-form motility mutants are viable. (A) DIC images of live BSF cells grown with or without Tet for 48 h, as indicated. Tet-induced LC1 3′ UTR RNAi cells (RNAi) are inviable and accumulate as amorphous masses with multiple flagella, indicating cytokinesis failure. LC1 mutants with point mutations (RNAi + K203A/R210A and RNAi + V196D/D199G) are viable and have normal morphology. Bar, 5 μm. (B) Growth curves of bloodstream-form LC1 3′ UTR RNAi knockdowns (RNAi, red lines) or LC1 mutants with point mutations (blue lines, K203A/R210A; green lines, V196D/D199G), demonstrating that LC1 mutants with point mutations rescue the lethal phenotype caused by LC1 knockdown. Cultures were incubated with (open symbols) or without (closed symbols) tetracycline added at time zero, and cells were diluted back to the starting density at 25 h. (C) Motility traces of control cells (RNAi − Tet), LC1 UTR knockdowns (RNAi + Tet), and LC1 mutants with point mutations (RNAi + K203A/R210A and RNAi + V196G/D199G) were carried out as described in the legend to Fig. 2C (the motility of mutants with point mutations in the absence of Tet was like that of the wild type and is not shown). (D) Quantification of total distance traveled by individual cells in motility traces from panel C ($N > 100$ for each culture) was carried out as described in the legend to Fig. 2D. Horizontal lines indicate the mean of each data set, with bars indicating the 95% confidence interval. Results for the data sets were compared to those for RNAi without Tet. ***, significant difference ($P < 0.0002$).

and bloodstream-form *T. brucei* (3, 4, 8, 9, 33, 36). This requirement is particularly acute in the bloodstream life cycle stage, where RNAi knockdown of flagellar proteins causes a rapid and dramatic cytokinesis failure (8, 9, 33). The phenotype is observed following independent knockdown of several different proteins that have a known or suspected role in flagellum motility, leading to the hypothesis that flagellar motility is required for viability of bloodstream-form cells (9, 15, 33). However, there are caveats to this interpretation, as detailed in the introduction (34, 35), and we therefore tested the hypothesis using mutants with loss-of-function LC1 K203A/R210A and V196G/D199G point mutations. Both mutants exhibit defective motility and are viable in the bloodstream life cycle stage, demonstrating unequivocally that normal motility is not essential in bloodstream-form trypanosomes.

If normal motility is not essential, further consideration must be given to understand why flagellum protein knockdown is often lethal (8, 9, 33) in bloodstream-form trypanosomes.

This question is of broad importance because it impacts efforts to understand the role of trypanosome motility in disease pathogenesis, as well as efforts to exploit the flagellum as a drug target. The lethal phenotype is not due to complete loss of flagellar motility because LC1-knockdown mutants have a beating flagellum. Indeed, to our knowledge, no bloodstream-form knockdowns that completely lack flagellar motility have ever been described. Notice that even in the large amorphous cell masses that result from LC1 knockdown, the flagella continue to beat vigorously (see Video S8a in the supplemental material). Likewise, the lethal event is not loss of cell propulsion, because LC1 mutants with point mutations lack cell propulsion and are viable. We considered the possibility that the lethal event is a flagellum beat defect that is more severe in knockdowns than in mutants with point mutations. To directly address this, high-resolution video analysis of individual cells was used to compare LC1 mutants with point mutations and knockdowns (see Videos S8a to 10 in the supplemental material). In these analyses, the motility defects of knockdowns and mutants with point mutations were indistinguishable. Future in-depth high-speed video microscopy analysis (38) of these mutants will be of great interest. We did not observe reverse cell translocation or reverse flagellum beating in bloodstream-form knockdowns or mutants, nor did we observe loss of outer-arm dyneins (see Fig. S3 in the supplemental material). This differs from what is observed in procyclic-form LC1 knockdowns and might reflect stage-specific differences or might simply reflect the rapid onset of the lethal phenotype in bloodstream cells, which prevents accumulation of flagellum ultrastructure defects at later time points when defects would become apparent. Therefore, direct analysis of viable motility mutants (LC1 mutants with point mutations) and inviable motility mutants (LC1 knockdowns) did not reveal a correlation between severity of the flagellum beat defect and lethality.

It is possible that the lethal event in bloodstream-form flagellum protein knockdowns is a subtle change in flagellum motility that is shared among all knockdowns but not LC1 mutants with point mutations and was not picked up in our analysis. We cannot formally rule out this possibility but consider it unlikely, since lethal knockdowns target a wide range of flagellum subcomplexes, e.g., outer dyneins, inner dyneins, the dynein regulatory complex, and the paraflagellar rod (PFR) (8, 9, 33), each of which has a separate role in flagellum motility. Flagellum protein knockdowns exhibit a range of flagellum beat defects. For example, some appear to have more severe beat defects, e.g., PFR knockdowns that disrupt the PFR structure, while others have subtle or imperceptible beat defects (e.g., LC1, trypanin, and PACRGA knockdowns), yet all of these are lethal. Hence, there is no clear correlation between the severity of knockdown and lethality.

With evidence lacking for a direct role of abnormal flagellum motility in the lethal phenotype of bloodstream-form flagellum protein knockdowns, we must consider alternate explanations. In other organisms, the flagellum participates in cell cycle regulation (31), and in *T. brucei*, aurora and polo kinases important for cell cycle control are dynamically associated with flagellum structures (27, 43). The *T. brucei* flagellum is an essential structure, and it is possible that fidelity of the flagellum might be subject to cell cycle monitoring, such that perturbation of flagellum integrity caused by flagellum protein knockdown induces a cell division block. In any case, our discovery of motility mutants that are viable in the bloodstream life cycle stage will now make it possible to test these ideas and facilitate a more complete understanding of the connection between the flagellum and cell division in these pathogens.

Several human diseases are caused by defects in flagellar motility, and numerous disease genes and disease gene candidates have been identified (13). However, knowledge of specific functions for these proteins remains limited, and scant information is available on molecular mechanisms or specific amino acids required for function. One barrier to studies of flagellum protein structure-function is a lack of facile systems for systematic mutational analysis of a given gene. As noted above, null mutants and RNAi knockdowns are valuable but provide limited information about molecular mechanisms. Recent elegant studies on inner-arm and outer-arm dynein subunits in *Chlamydomonas* have made important steps toward addressing this issue (16, 32, 41, 44), but investigating specific functions and molecular mechanisms of flagellum proteins remains a major challenge. The inducible system that we have developed in *T. brucei* offers an opportunity for systematic mutational analysis of virtually any flagellar protein in a background where the endogenous protein is reduced or absent. This minimizes potential deleterious effects of altering subunit stoichiometry, allows analysis of essential proteins, and enables identification of recessive mutations. Therefore, the approach is complementary to existing systems (2, 39) and offers unique advantages that should be broadly applicable for closing an important gap in our understanding of flagellum biology.

Summary. We have developed a system for structure-function analysis of flagellar proteins in *T. brucei* and identified amino acids required for function of the dynein light chain LC1. Our results represent the first time that viable motility mutants have been identified in the mammalian-infectious life cycle stage of these deadly pathogens. These findings will now make it possible to directly investigate the role of trypanosome motility in disease pathogenesis. Finally, the system that we have developed should find broad utility in studies of trypanosome biology, as well as flagellum protein dysfunctions that underlie ciliopathies in humans.

ACKNOWLEDGMENTS

Funding for the work was provided by grants to K.L.H. from the NIH-NIAID (AI052348) and Burroughs Wellcome Fund. K.S.R. is the recipient of a USPHS National Research Service Award (GM07104) and a Dissertation Year Fellowship from the UCLA graduate division.

We thank Randy Nessler (University of Iowa) for assistance with electron microscopy. We thank Hope E. Shaffer and Miguel A. Lopez for excellent technical assistance. We thank George Cross for the 29-13 and BSF-SM cell lines, John Donelson for the p2T7^{TB}B plasmid, and Christine Clayton for the pHD1342 plasmid. We thank Stephen King for sharing data prior to publication and are grateful to colleagues and members of our laboratory for critical reading of the manuscript and thoughtful comments on the work.

REFERENCES

1. **Adams, G. M., B. Huang, G. Piperno, and D. J. Luck.** 1981. Central-pair microtubular complex of Chlamydomonas flagella: polypeptide composition as revealed by analysis of mutants. J. Cell Biol. 91:69–76.
2. **Aphasizheva, I., et al.** 2009. Novel TUTase associates with an editosome-like complex in mitochondria of Trypanosoma brucei. RNA 15:1322–1337.
3. **Baron, D. M., Z. P. Kabututu, and K. L. Hill.** 2007. Stuck in reverse: loss of LC1 in Trypanosoma brucei disrupts outer dynein arms and leads to reverse flagellar beat and backward movement. J. Cell Sci. 120:1513–1520.

4. **Baron, D. M., K. S. Ralston, Z. P. Kabututu, and K. L. Hill.** 2007. Functional genomics in Trypanosoma brucei identifies evolutionarily conserved components of motile flagella. J. Cell Sci. 120:478–491.
5. **Bastin, P., T. J. Pullen, T. Sherwin, and K. Gull.** 1999. Protein transport and flagellum assembly dynamics revealed by analysis of the paralysed trypanosome mutant snl-1. J. Cell Sci. 112:3769–3777.
6. **Benashski, S. E., R. S. Patel-King, and S. M. King.** 1999. Light chain 1 from the Chlamydomonas outer dynein arm is a leucine-rich repeat protein associated with the motor domain of the gamma heavy chain. Biochemistry 38:7253–7264.
7. **Benz, C., D. Nilsson, B. Andersson, C. Clayton, and D. L. Guilbride.** 2005. Messenger RNA processing sites in Trypanosoma brucei. Mol. Biochem. Parasitol. 143:125–134.
8. **Branche, C., et al.** 2006. Conserved and specific functions of axoneme components in trypanosome motility. J. Cell Sci. 119:3443–3455.
9. **Broadhead, R., et al.** 2006. Flagellar motility is required for the viability of the bloodstream trypanosome. Nature 440:224–227.
10. **Brown, J. M., C. Hardin, and J. Gaertig.** 1999. Rotokinesis, a novel phenomenon of cell locomotion-assisted cytokinesis in the ciliate Tetrahymena thermophila. Cell Biol. Int. 23:841–848.
11. **Dawe, H. R., H. Farr, N. Portman, M. K. Shaw, and K. Gull.** 2005. The Parkin co-regulated gene product, PACRG, is an evolutionarily conserved axonemal protein that functions in outer-doublet microtubule morphogenesis. J. Cell Sci. 118:5421–5430.
12. **DiBella, L. M., et al.** 2005. Differential light chain assembly influences outer arm dynein motor function. Mol. Biol. Cell 16:5661–5674.
13. **Fliegauf, M., T. Benzing, and H. Omran.** 2007. When cilia go bad: cilia defects and ciliopathies. Nat. Rev. Mol. Cell Biol. 8:880–893.
14. **Gadelha, C., B. Wickstead, W. de Souza, K. Gull, and N. Cunha-e-Silva.** 2005. Cryptic paraflagellar rod in endosymbiont-containing kinetoplastid protozoa. Eukaryot. Cell 4:516–525.
15. **Ginger, M. L., N. Portman, and P. G. McKean.** 2008. Swimming with protists: perception, motility and flagellum assembly. Nat. Rev. Microbiol. 6:838–850.
16. **Gokhale, A., M. Wirschell, and W. S. Sale.** 2009. Regulation of dynein-driven microtubule sliding by the axonemal protein kinase CK1 in Chlamydomonas flagella. J. Cell Biol. 186:817–824.
17. **Hill, K. L.** 2003. Mechanisms and biology of trypanosome cell motility. Eukaryot. Cell 2:200–208.
18. **Hill, K. L., N. R. Hutchings, P. M. Grandgenett, and J. E. Donelson.** 2000. T Lymphocyte triggering factor of African trypanosomes is associated with the flagellar fraction of the cytoskeleton and represents a new family of proteins that are present in several divergent eukaryotes. J. Biol. Chem. 275:39369–39378.
19. **Huang, B., G. Piperno, and D. J. Luck.** 1979. Paralyzed flagella mutants of Chlamydomonas reinhardtii. Defective for axonemal doublet microtubule arms. J. Biol. Chem. 254:3091–3099.
20. **Huang, B., G. Piperno, Z. Ramanis, and D. J. Luck.** 1981. Radial spokes of Chlamydomonas flagella: genetic analysis of assembly and function. J. Cell Biol. 88:80–88.
21. **Hutchings, N. R., J. E. Donelson, and K. L. Hill.** 2002. Trypanin is a cytoskeletal linker protein and is required for cell motility in African trypanosomes. J. Cell Biol. 156:867–877.
22. **Kamiya, R.** 1988. Mutations at twelve independent loci result in absence of outer dynein arms in Chlamydomonas reinhardtii. J. Cell Biol. 107:2253–2258.
23. **Kamiya, R.** 2002. Functional diversity of axonemal dyneins as studied in Chlamydomonas mutants. Int. Rev. Cytol. 219:115–155.
24. **Kamiya, R., E. Kurimoto, and E. Muto.** 1991. Two types of Chlamydomonas flagellar mutants missing different components of inner-arm dynein. J. Cell Biol. 112:441–447.
25. **Kohl, L., D. Robinson, and P. Bastin.** 2003. Novel roles for the flagellum in cell morphogenesis and cytokinesis of trypanosomes. EMBO J. 22:5336–5346.
26. **LaCount, D. J., B. Barrett, and J. E. Donelson.** 2002. Trypanosoma brucei FLA1 is required for flagellum attachment and cytokinesis. J. Biol. Chem. 277:17580–17588.
27. **Li, Z., T. Umeyama, and C. C. Wang.** 2009. The aurora kinase in Trypanosoma brucei plays distinctive roles in metaphase-anaphase transition and cytokinetic initiation. PLoS Pathog. 5:e1000575.
28. **Livak, K. J., and T. D. Schmittgen.** 2001. Analysis of relative gene expression data using real-time quantitative PCR and the 2(−delta delta C(T)) method. Methods 25:402–408.
29. **Morris, J. C., Z. Wang, M. E. Drew, and P. T. England.** 2002. Glycolysis modulates trypanosome glycoprotein expression as revealed by an RNAi library. EMBO J. 21:4429–4438.
30. **Nicastro, D., et al.** 2006. The molecular architecture of axonemes revealed by cryoelectron tomography. Science 313:944–948.
31. **Pan, J., and W. Snell.** 2007. The primary cilium: keeper of the key to cell division. Cell 129:1255–1257.
32. **Patel-King, R. S., and S. M. King.** 2009. An outer arm dynein light chain acts in a conformational switch for flagellar motility. J. Cell Biol. 186:283–295.
33. **Ralston, K. S., and K. L. Hill.** 2006. Trypanin, a component of the flagellar dynein regulatory complex, is essential in bloodstream form African trypanosomes. PLoS Pathog. 2:e101.
34. **Ralston, K. S., and K. L. Hill.** 2008. The flagellum of Trypanosoma brucei: new tricks from an old dog. Int. J. Parasitol. 38:869–884.
35. **Ralston, K. S., Z. P. Kabututu, J. H. Melehani, M. Oberholzer, and K. L. Hill.** 2009. The Trypanosoma brucei flagellum: moving parasites in new directions. Annu. Rev. Microbiol. 63:335–362.
36. **Ralston, K. S., A. G. Lerner, D. R. Diener, and K. L. Hill.** 2006. Flagellar motility contributes to cytokinesis in Trypanosoma brucei and is modulated by an evolutionarily conserved dynein regulatory system. Eukaryot. Cell 5:696–711.
37. **Robinson, D., P. Beattie, T. Sherwin, and K. Gull.** 1991. Microtubules, tubulin, and microtubule-associated proteins of trypanosomes. Methods Enzymol. 196:285–299.
38. **Rodriguez, J. A., et al.** 2009. Propulsion of African trypanosomes is driven by bihelical waves with alternating chirality separated by kinks. Proc. Natl. Acad. Sci. U. S. A. 106:19322–19327.
39. **Rusconi, F., M. Durand-Dubief, and P. Bastin.** 2005. Functional complementation of RNA interference mutants in trypanosomes. BMC Biotechnol. 5:6.
40. **Sakato, M., and S. M. King.** 2004. Design and regulation of the AAA+ microtubule motor dynein. J. Struct. Biol. 146:58–71.
41. **Takazaki, H., Z. Liu, M. Jin, R. Kamiya, and T. Yasunaga.** 2010. Three outer arm dynein heavy chains of Chlamydomonas reinhardtii operate in a coordinated fashion both in vitro and in vivo. Cytoskeleton (Hoboken, N.J.) 67:466–476.
42. Reference deleted.
43. **Umeyama, T., and C. C. Wang.** 2008. Polo-like kinase is expressed in S/G2/M phase and associated with the flagellum attachment zone in both procyclic and bloodstream forms of Trypanosoma brucei. Eukaryot. Cell 7:1582–1590.
44. **Wirschell, M., et al.** 2009. IC97 is a novel intermediate chain of I1 dynein that interacts with tubulin and regulates interdoublet sliding. Mol. Biol. Cell 20:3044–3054.
45. **Wirtz, E., S. Leal, C. Ochatt, and G. A. Cross.** 1999. A tightly regulated inducible expression system for conditional gene knock-outs and dominant-negative genetics in *Trypanosoma brucei*. Mol. Biochem. Parasitol. 99:89–101.
46. **Witman, G. B., J. Plummer, and G. Sander.** 1978. Chlamydomonas flagellar mutants lacking radial spokes and central tubules. Structure, composition, and function of specific axonemal components. J. Cell Biol. 76:729–747.
47. **Wu, H., M. Blackledge, M. W. Maciejewski, G. P. Mullen, and S. M. King.** 2003. Relaxation-based structure refinement and backbone molecular dynamics of the dynein motor domain-associated light chain. Biochemistry 42:57–71.
48. **Wu, H., et al.** 2000. Solution structure of a dynein motor domain associated light chain. Nat. Struct. Biol. 7:575–579.